

“What distinguishes a mathematical model from, say, a poem, a song, a portrait or any other kind of ‘model’, is that the mathematical model is an image or picture of reality painted with logical symbols instead of with words, sounds or watercolors.”

- J. Casti

University of Alberta

**OPTIMIZATION OF BIOMASS AND LIPID PRODUCTION IN
HETEROTROPHIC MICROALGAL CULTURES**

by

Hector Jr. De la Hoz Siegler

A thesis submitted to the Faculty of Graduate Studies and Research
in partial fulfillment of the requirements for the degree of

Doctor of Philosophy

in

Chemical Engineering

Department of Chemical and Materials Engineering

©Hector Jr. De la Hoz Siegler

Spring 2012

Edmonton, Alberta

Permission is hereby granted to the University of Alberta Libraries to reproduce single copies of this thesis and to lend or sell such copies for private, scholarly or scientific research purposes only. Where the thesis is converted to, or otherwise made available in digital form, the University of Alberta will advise potential users of the thesis of these terms.

The author reserves all other publication and other rights in association with the copyright in the thesis and, except as herein before provided, neither the thesis nor any substantial portion thereof may be printed or otherwise reproduced in any material form whatsoever without the author's prior written permission.

Abstract

Microalgae are a promising source of biofuels and other valuable chemicals. The low cell density and slow growth rate that have traditionally characterized microalgal cultures, however, have resulted in a reduced economical feasibility. To develop a sustainable microalgal process it is required to increase culture productivity, maximize production yield, and reduce production costs. To achieve these goals it is necessary to improve the current understanding of the dynamic behaviour of microalgal cultures.

In this thesis, growth and oil production rates in heterotrophic cultures of *Auxenochlorella protothecoides* were evaluated as a function of the carbon and nitrogen source concentration. It was found that nitrogen plays a major role in controlling the productivity of microalgae. It was also shown that there exists a nitrogen source concentration at which biomass and oil production can be maximized. A mathematical model that describes the effect of nitrogen and carbon source on growth and oil production was proposed, considering the uncoupling between nitrogen uptake and growth, the possibility of luxurious uptake of nitrogen, and the time-delayed inhibitory effects caused by the transient spike in the intracellular nitrogen concentration.

Using a non-linear model-based optimization approach, biomass and oil

productivities were substantially increased. The use of an adaptive model predictive control strategy resulted in a 10-fold increase in the average biomass productivity and a 16-fold increase in the maximum productivity compared to batch experiments. The final cell density in the optimized culture was 144 g/L (dry weight), with 49.4 % w/w oil content. The maximum lipid productivity was 20.2 g/Ld, achieved during the exponential growth phase at an average cell density of 86 g/L. The lipid productivity in the optimized microalgal culture was higher than any previously reported productivity value for other oleaginous microorganisms.

Application of the adaptive optimization strategy to a two-stage glycerol/glucose culture resulted in an increased production yield (glucose to oil), from 0.267 g/g in the optimized single-stage culture to 0.347 g/g in the two-stage culture. The increased yield and productivity of the optimized cultures resulted in a largely improved economic feasibility.

Composition analysis of the algal oil produced in the optimized cultures shows that the oil has a high quality as biodiesel precursor, in terms of the expected cetane number, iodine value, and cold filter plug point temperature. The higher productivity and excellent lipid profile of the optimized microalgal culture make *A. protothecoides* an exceptional source for biodiesel production and a potential source of single cell oil for other applications.

Acknowledgements

Over the last five years, I have had the opportunity to discuss my thoughts and research ideas with many friends and colleagues. In this short sentences, I want to express my sincere gratitude to all then, as well as to all those persons that have guide me through different moments in my life.

I am in debt with my research advisors: Dr. Amos Ben-Zvi, Dr. William C. McCaffrey, and Dr. Robert E. Burrell. They provided valuable orientation and rewarding discussions regarding many aspects of the engineering and scientific research career. They gave me the opportunity to define the scope of my doctoral research and offered me the support and encouragement to successfully conduct my studies.

Several students worked with me at different stages of this research. Their assistance was not limited to conduct or assist me in some of the experiments, but they also served for me to practice and hone managerial and supervision skills. Marina Joseph, Kristen Kavich, Chantelle Tatum, Chelsie Ralph, Jacquie Cream, and Brittany Lissina conducted several of the exploratory experiments that allowed further understanding of the behaviour of microalgae; William Weng helped to develop the communication interface between the bioreactor control unit and Matlab; Kartik Surisetty assisted me running some

of the fed-batch cultures and improved the code for parameter estimation; Natasha Remtulla and Wendy Lang conducted some of the experimental work that supported the standardization of the lipid extraction protocol; Nadadoor Venkat developed the support vector regression algorithm for correlating the Raman spectra with the chemical composition of the bioreactor.

Special thanks are due to my friends, with whom we shared many memorable moments both inside and outside the university. It has been a wonderful experience to share time with you, learning, travelling, and talking.

My deepest gratitude goes to my family for their support, patience, love, and understanding. To my mom, Ada, who always encourage me to go one step further in my education, and to Hua who discussed with me about research and beyond, she has not only help me proof-reading the thesis, but has also give me the love, support, and company that have make my life happier.

This research was possible thanks to the financial support provided by Alberta Innovates Technology Futures (formerly Alberta Ingenuity Fund), the National Science and Engineering Research Council (NSERC), Avac Ltd., and the Department of Chemical and Materials Engineering at the University of Alberta. I am also thankful for the travel and professional development grants awarded by the Faculty of Graduate Studies and Research (FGSR) and the Graduate Student Association (GSA) at the University of Alberta.

Contents

Nomenclature	xxi
1 Introduction	1
1.1 Problem statement	1
1.2 Research Objectives	4
1.3 Thesis overview	4
2 Background	9
2.1 Microalgal biotechnology	9
2.1.1 Applications of microalgae	11
2.1.2 Microalgal production systems	14
2.2 The improvement of bioprocesses	16
2.2.1 Bioprocess Modelling	17
2.2.2 Bioprocess Monitoring	19
2.3 Modelling of microalgal systems	23
2.3.1 Physiological characteristics relevant for modelling of microalgal processes	23
2.3.2 Kinetic models of microalgal growth	25
3 Methodology	29
3.1 Microalgal cultures	29
3.1.1 Batch cultures	31
3.1.2 Fed-batch cultures	33
3.2 Analytical methods	35
3.2.1 Biomass measurement	36
3.2.2 Glucose quantification	37

3.2.3	Nitrogen quantification	37
3.2.4	Lipid characterization	39
3.3	Reagents	41
3.4	Model evaluation	43
3.4.1	Parameter estimation	43
3.4.2	Confidence analysis	44
3.4.3	Model selection	45
4	Measuring the bioprocess performance	47
4.1	Oil content in cells	48
4.1.1	Gravimetric method	50
4.1.2	Fluorometric method	56
4.2	On-line monitoring using Raman spectroscopy	71
4.2.1	Spectra of algal Biomass	71
4.2.2	Oil spectra	74
4.2.3	Spectra of media components	75
4.2.4	Multivariate model building	76
4.2.5	On-line estimation of bioreactor composition	84
5	The physiology of microalgal growth	89
5.1	Growth in mixotrophic and heterotrophic conditions	90
5.1.1	Photoheterotrophic growth	90
5.1.2	Heterotrophic growth	97
5.2	The effect of nutrients on growth	99
5.2.1	Selection of the nitrogen source	99
5.2.2	The response of growth and oil production to varying nutrient concentrations	102
5.3	Compositional changes in microalgae	107
5.4	Metabolites accumulation in the culture	109
5.5	Effect of antifoam agents	111
6	A model for algal metabolism	117
6.1	The compartmentalized cell	119
6.1.1	Kinetics of nutrient uptake	122

6.1.2	Growth kinetics	123
6.1.3	Product formation kinetics	126
6.2	Model selection	127
6.2.1	Experimental data	128
6.2.2	Nitrogen uptake	134
6.2.3	Effect of nitrogen concentration on growth	134
6.2.4	Effect of carbon concentration on growth	139
6.2.5	Lipid production	139
6.2.6	Summary of kinetic expressions	140
6.3	Model limitations	141
6.4	Model validation	143
7	The optimization of microalgal cultures	147
7.1	Evaluating the performance of microalgal cultures	148
7.1.1	Continuous cultures	151
7.1.2	Fed-batch cultures	155
7.2	Optimal feeding strategy for glucose-fed microalgal fed-batch cultures	156
7.2.1	Problem formulation	156
7.2.2	Implementation	157
7.2.3	Comparison	163
7.3	Optimization of glycerol-fed cultures	173
7.3.1	Culture conditions	173
7.3.2	Effect of glycerol on growth and oil production	175
7.3.3	A second stage to boost oil production	177
7.3.4	The yield of glucose and glycerol cultures	180
7.4	Characterization of algal oil as a source for biodiesel production	182
8	Feasibility evaluation of microalgal oil production	187
8.1	Land requirement for biodiesel production from microalgae	188
8.1.1	Substrates for heterotrophic microalgal growth	188
8.1.2	Substrate to product yield scenarios	194
8.1.3	Algal oil yield per hectare of sugar crop	194
8.1.4	Land requirements for biodiesel production	194

8.2	Estimation of production and capital costs	197
8.2.1	Organic carbon substrate cost	197
8.2.2	Other nutrients cost	198
8.2.3	Oil extraction	198
8.2.4	Capital cost	198
8.2.5	Labour cost	199
8.3	Valuation of algal byproducts	200
8.4	Economic evaluation	201
9	Conclusions and Recommendations	209
9.1	Conclusions	209
9.2	Future research directions	212
9.2.1	Adaptive optimization with Raman-enabled feedback control	212
9.2.2	Optimization of process conditions	213
9.2.3	Controlling the fatty acid profile	213
9.2.4	Population based modelling	214
9.2.5	Optimization of culture conditions for harvesting	216
	References	217
	Appendix A Experimental Protocols	237
A.1	Fluorometric Quantification of Neutral Lipids	237
A.2	Gravimetric Quantification of Neutral Lipids	241
	Appendix B Fed-batch cultures of <i>A. protothecoides</i>	245
B.1	Open-loop optimal run	245
B.1.1	Results	246
B.1.2	Important observations	253
B.2	Adaptive model predictive control run for maximum biomass	254
B.2.1	Results	254
B.3	Two-stage culture with glycerol/glucose feeding	260
B.3.1	Results	260
B.3.2	Important observations	268

Appendix C Matlab scripts	269
C.1 Simulation of batch and fed-batch cultures	269
C.2 Estimation of model parameter values and confidence analysis	272
C.2.1 Optimization of model parameter values	274
C.2.2 Numerical estimation of the covariance matrix of parameter estimates	277
C.2.3 Confidence intervals and confidence regions	281
C.3 Determination of optimal feeding profiles to fed-batch cultures	285
C.4 Cell count	289
 Appendix D Routines and functions for OPC in Visual Basic	 291

This page intentionally left blank

List of Tables

2.1	Comparison of different biodiesel sources in terms of oil yield and required land to partially replace current transportation fuel demand.	13
3.1	Composition of base culture media	32
4.1	Polarity index (PI) and boiling point (BP) for several solvents commonly used for extraction of lipids.	51
4.2	Effect of mixing on the inter-sample variability of oil concentration estimates based on the Nile Red fluorescence measurements.	66
4.3	Characterization of the datasets used for building and validating a Raman chemometric model for algal culture composition	82
4.4	Coefficient of determination of the support vector regression model for the calibration (R_C^2) and testing (R_T^2) datasets.	83
5.1	Box-Behnken experimental design to evaluate the influence of carbon, nitrogen, phosphorus, and iron substrate concentrations on the growth rate and oil productivity of microalgae	103
5.2	Elemental analysis of algal biomass	109
5.3	Variation in the concentration of nitrogen-containing compounds in the culture media during a single batch experiment	110
6.1	Initial and final conditions, after 150 h of heterotrophic cultivation, for batch experiments.	129
6.2	Comparison among kinetic expressions to model the nitrogen uptake rate.	137

6.3	Performance of kinetic functions evaluated to model \tilde{r}_N , the normalized growth rate based on the intracellular nitrogen content.	137
6.4	Performance of kinetic functions evaluated to model \tilde{r}_C , the normalized growth rate based on the glucose concentration in the media.	139
6.5	Performance of kinetic functions evaluated to model the oil production rate (π)	140
6.6	Estimated model parameter values and 95 % confidence bounds.	142
7.1	Biomass concentration (x_B), biomass productivity (\mathbb{P}_B), lipid productivity (\mathbb{P}_L), and specific lipid production rate (\mathcal{P}) for several microalgae species cultured under different conditions.	150
7.2	Lipid content and lipid productivity, \mathbb{P} , of <i>A. protothecoides</i> and other selected oleaginous microorganisms growing on glucose.	172
7.3	Composition of glycerol-rich feed.	175
7.4	Fatty acid profile, % w, of <i>A. protothecoides</i> for different fed-batch cultures of <i>A. protothecoides</i>	184
8.1	Annual yield of sugar crops in North-America, and expected oil yield for the heterotrophic cultivation of microalgae	195
8.2	Oil yield, cost, and required land to satisfy the biodiesel demand to comply with a B2 (2% biodiesel) target, for different oleaginous crops.	196
8.3	Estimated production cost of microalgal oil	202
B.1	Flow rate and process conditions for the Open-Loop MPC culture	246
B.2	Biomass concentration for the Open-Loop MPC culture	253
B.3	Flow rate and process conditions for the Adaptive MPC culture	255
B.4	Experimental measurements for the Adaptive MPC culture	259
B.5	Flow rate and process conditions for the two-stage culture	261
B.6	Experimental measurements for the two-stage culture	266

List of Figures

1.1	Flow diagram of the methodology followed for bioprocess optimization	5
2.1	Phylogenic tree of microalgae based on the photosynthetic plastic genealogy	10
3.1	Microphotograph of <i>Auxenochlorella protothecoides</i> observed in a light microscope	30
3.2	Diagrammatic representation of the Bioreactor and control system network	35
3.3	Standard calibration curve for glucose in aqueous solutions	38
3.4	Standard calibration curve between the absorbance of the Ninhydrin complex and the concentration of glycine in aqueous solutions.	40
3.5	Determination of optimal step size for the numerical estimation of the Hessian matrix	45
4.1	The effect of the solvent extraction system on the measured oil content and the recovery efficiency	52
4.2	The effect of the cell disruption method on the measured oil content of a dry sample of <i>A. protothecoides</i>	54
4.3	Microphotographies of <i>A. protothecoides</i> cells subjected to sonication.	55

4.4	The effect of the sample size on the measured oil content and the lipid recovery efficiency, using the single solvent (hexane) extraction procedure.	57
4.5	Excitation and emission spectra of <i>Auxenochlorella protothecoides</i> cells stained with an ethanolic solution of Nile-Red. . .	59
4.6	Effect of the intracellular oil content on the excitation and emission spectra of <i>A. protothecoides</i> cells stained with an ethanolic solution of Nile Red.	60
4.7	Effect of the concentration of the carrier solvent on the fluorescence count of <i>A. protothecoides</i> cells stained with Nile Red as a function of the biomass concentration.	62
4.8	Correlation between the fluorescence count of Nile Red stained cells and the neutral lipid content of the algal cells determined gravimetrically, after hexane extraction.	63
4.9	Effect of the Nile Red concentration and the incubation time on the relative standard error of fluorescence measurements. .	65
4.10	Microphotographs of <i>A. protothecoides</i> stained with the lipid probe Bodipy 505/515	69
4.11	Emission spectra of <i>A. protothecoides</i> cells stained with Bodipy 505/515.	70
4.12	Unprocessed Raman spectra of algal biomass powder	72
4.13	Raman spectra of algal biomass powder after piecewise linear baseline removal.	73
4.14	Raman spectra of algal biomass powders with varying oil content after piecewise linear baseline removal.	73
4.15	Raman spectra of different vegetable oils after piecewise linear baseline removal. Spectra of algal cells is included for reference.	74
4.16	Raman spectra of glucose and glycine solutions in water . . .	77
4.17	Raman spectra of MgSO ₄ and FeSO ₄ solutions in water	78
4.18	Raman spectra of K ₂ HPO ₄ and KH ₂ PO ₄ solutions in water . .	79
4.19	Raman spectra of Thiamine HCl and Arnon 5 solutions in water	80
4.20	Biomass concentration profile for an algal culture estimated through Raman spectroscopy	85

4.21	Glucose concentration profile for an algal culture estimated through Raman spectroscopy	86
4.22	Profile for the oil content in the algal cells estimated through Raman spectroscopy	86
5.1	Biomass concentration profile for photoheterotrophic microalgal cultures at varying concentrations of glycine for B1 medium	91
5.2	Uptake of glycine in <i>A. protothecoides</i> cultures	93
5.3	Biomass concentration profile for photoheterotrophic microalgal cultures at varying concentrations of glycine for B4 medium	94
5.4	Uptake of glycine in <i>A. protothecoides</i> cultures using B4 medium	95
5.5	Biomass to nitrogen yield in mixotrophic cultures of <i>A. protothecoides</i>	96
5.6	Biomass concentration profile for photoheterotrophic and heterotrophic batch cultures	98
5.7	Effect of the nitrogen source on the growth of microalgae	101
5.8	Effect of the initial nutrient concentrations on the initial growth rate of <i>A. protothecoides</i>	104
5.9	Effect of the initial concentration of nutrients on the intracellular neutral lipid content after 200 h of culture	106
5.10	Effect of the initial nutrient concentrations on the algal lipid productivity	108
5.11	The inhibitory effect of accumulated metabolites on the heterotrophic growth of <i>A. protothecoides</i>	112
5.12	The effect of antifoam agents on the growth of <i>A. protothecoides</i>	114
5.13	The effect of the organic, fatty acid ester type, O-30 antifoam concentration on the growth profile of <i>A. protothecoides</i>	115
6.1	Schematic representation of the algal cell	120
6.2	Specific biomass growth rate and intracellular nitrogen concentration for a batch culture.	124
6.3	Biomass concentration profiles of all batch runs used for model calibration	131

6.4	Specific growth rate of <i>A. protothecoides</i> at exponential growth	132
6.5	Glucose concentration profiles of all batch runs used for model calibration	133
6.6	Biomass concentration profiles of all batch runs used for model calibration	135
6.7	Oil content profiles for all batch runs used for model calibration	136
6.8	Feeding flow-rate profiles of the fed-batch run used for model validation	144
6.9	Measured and predicted concentration profiles for the fed-batch validation run	145
7.1	Predicted biomass productivity in continuous cultures of <i>A. protothecoides</i>	153
7.2	Predicted lipid productivity in continuous cultures of <i>A. protothecoides</i>	154
7.3	Flow diagram for the Adaptive Model Predictive Control optimization approach used.	158
7.4	Feeding flowrates for the pseudo-random binary sequence (PRBS) fed-batch culture of <i>A. protothecoides</i>	160
7.5	Feeding flowrates for the open-loop optimal feeding trajectory (OFT) fed-batch culture of <i>A. protothecoides</i>	161
7.6	Feeding flowrates for the adaptive MPC fed-batch culture of <i>A. protothecoides</i>	164
7.7	Increased biomass concentration as a result of the proposed optimization strategy.	165
7.8	Biomass productivity and growth rate for different culture strategies.	166
7.9	Lipid content and apparent lipid production rate in an Adaptive MPC fed-batch culture of <i>A. protothecoides</i>	168
7.10	Carbon to nitrogen molar ratio during the Adaptive MPC fed-batch culture.	169
7.11	Maximum lipid productivity and specific lipid production rate for different <i>A. protothecoides</i> cultures.	170

7.12	Feeding flowrates for the glycerol-fed culture of <i>A. protothecoides</i>	174
7.13	Biomass and oil content profiles of a glycerol-fed culture of <i>A. protothecoides</i>	176
7.14	Glucose feeding flowrate for the two-stages culture of <i>A. protothecoides</i>	178
7.15	Biomass and oil content profiles of the two-stages culture of <i>A. protothecoides</i>	179
8.1	Historical yield and production cost of sugar beet crops in U.S.	190
8.2	Historical yield and production cost of sugar cane crops in U.S.	191
8.3	Historical yield and production cost of maize crops in U.S.	192
8.4	Historical yield and average farm price of soft red winter wheat crop in U.S.	193
8.5	Historical FOB price of fish meal and soybean meal	201
8.6	Sensitivity of the return on assets (ROA) and return on equity (ROE) indicators to the cost of the sugar feedstock	204
8.7	Sensitivity of the return on assets (ROA) and return on equity (ROE) indicators to the extraction cost of algal oil	205
8.8	Sensitivity of the return on assets (ROA) and return on equity (ROE) indicators to the selling price of algal meal	206
8.9	Sensitivity of the return on assets (ROA) and return on equity (ROE) indicators to the selling price of algal oil	207
9.1	Size distribution of a microalgal population in a heterotrophic culture	215

This page intentionally left blank

Code listings

C.1	Dynamic model of microalgal batch cultures	269
C.2	Dynamic model of microalgal fedbatch cultures	271
C.3	Residual error for a given set of model parameters	272
C.4	BFGS method for optimization	274
C.5	Numerical estimation of the gradient	276
C.6	Pattern search function call for parameter estimation	276
C.7	Numerical approximation of the Hessian matrix	277
C.8	Second derivative for symmetric elements	278
C.9	Second derivative for asymmetric elements	279
C.10	Preparation of matrices for generating confidence regions	281
C.11	Generation of an ellipse from a symmetric 2x2 matrix	282
C.12	Generation of a plot from any implicit function	284
C.13	Pattern search calling function	285
C.14	Determination of culture productivity	285
C.15	Feeding rate and set points to implement in the culture	287
C.16	Data reading from .Z2 file	289
D.1	Main routine for the OPC client	291
D.2	Class definition for OPC data access	294
D.3	Functions for saving OPC readings in historian database	300
D.4	General functions for handling client files	302
D.5	Interface between Matlab and the OPC client	305

This page intentionally left blank

Nomenclature

Greek symbols

α	Confidence level for statistical tests
ϵ	Threshold parameter for the support vector regression algorithm
γ	Radial basis function kernel parameter
μ	Biomass growth rate
μ_m	Maximum specific biomass growth rate
π	Oil production rate
π_m	Maximum oil production rate
ρ	Nitrogen uptake rate
ρ_m	Maximum uptake rate
ξ	Vector of state variables

Roman symbols

AIC	Akaike information criterion
BIC	Bayesian information criterion
C	Soft margin for the support vector regression cost function
D	Dilution rate

$E(\mathbf{p})$	Weighted sum of square errors for a given set of model parameters, \mathbf{p}
F	Fisher-Snedecor probability distribution
f_1^i	Nitrogen-rich inlet flowrate
f_2^i	Carbon-rich inlet flowrate
f_o	Bioreactor outlet flowrate
H	Hessian matrix to approximate the model covariance matrix
k	Set of model parameters
k_m	Maintenance constant
K_ρ	Half saturation constant for glycine uptake
$K_{\bar{q}}$	Half saturation constant for growth in terms of the intracellular nitrogen concentration
K_{i1}	Growth inhibition constant in terms of the nitrogen concentration in the cells
K_{i2}	Growth inhibition constant in terms of the carbon source concentration
K_{ip}	Lipid production inhibition constant in terms of the intracellular nitrogen concentration
K_{ps2}	Half saturation constant for oil production in terms of the carbon source concentration
K_{s1}	Half saturation constant for nitrogen uptake
K_{s2}	Half saturation for biomass growth in terms of the carbon source concentration
M	Number of samples removed from the reactor at some specified time point t

m	Number of measured states used for parameter estimation
N	Hill allosteric regulation coefficient
N_d	Number of experimental data points
n_p	Number of model parameters being estimated
\mathbb{P}_B	Biomass volumetric productivity
\mathbb{P}_L	Lipid volumetric productivity
\mathbf{p}	Vector of model's parameter values
p	Lipid concentration
$\hat{\mathbf{p}}$	Estimated model parameter values
PRESS	Predicted residual sum of squares
q	Intracellular nitrogen concentration
\tilde{q}	Mass fraction, or cell quota, of nitrogen in the cells
\tilde{q}_M	Maximum cell quota
\tilde{q}_m	Minimum cell quota
\tilde{r}_C	Normalized growth rate based on the carbon substrate
\tilde{r}_N	Normalized growth rate based on the nitrogen substrate
R^2	Coefficient of determination
s_0	Threshold substrate concentration
s_1	Nitrogen source concentration in culture media
s_1^i	Nitrogen concentration in the nitrogen-rich feed
s_2	Carbon source concentration in culture media

s_2^i	Carbon concentration in the carbon-rich feed
t	Reaction time
u	Set of input variables
V	Reactor volume
w	weight factor for parameter estimation, variance of experimental measurements
WSSE	Weighted sum of square errors
x	metabolically active biomass concentration
y	Estimated state value
\hat{y}	Measured state value
$Y_{p/s}$	Product to carbon substrate yield
$Y_{x/p}$	Biomass to lipid yield
$Y_{x/q}$	Biomass to nitrogen source yield
$Y_{x/s}$	Biomass to carbon substrate yield

1

Introduction

This chapter provides the general overview of the thesis. First, the research problem and motivation are introduced together with the general and the specific objectives pursued in this research project. The reader will also find a description of the thesis structure and an anticipation of the contents of each of the subsequent chapters that make the body of the thesis.

1.1 Problem statement

The increasing evidence of global climate change, associated with a surge in the concentration of green-house gases in the atmosphere, and the declining reserves of fossil fuels have motivated a growing interest in the research of renewables sources of energy (Sørensen et al., 2011; Bessou et al., 2011). Biofuels are considered a viable alternative to partially replace our energy requirements in term of liquid fuels (Sørensen et al., 2011). Ethanol and

biodiesel derived from agricultural food-based crops are considered the first generation of biofuels (Naik et al., 2010). A second generation of biofuels are those derived from lignocelulosic materials (Antizar-Ladislao and Turrion-Gomez, 2008), which are more abundant and have a lower commercial value than agricultural food-based crops. Algal derived biofuels have emerged on the recent past as the third generation biofuels (Demirbas, 2011).

Several microalgal species are able to accumulate large amounts of oil, which can be later converted into biodiesel by transesterification (Li et al., 2007a; Xu et al., 2006). Microalgae also have the ability to produce several valuable chemicals, which could improve the economic performance of algal biofuels by integrating the production of chemicals and biofuels in a biorefinery approach (Singh and Gu, 2010). Microalgae can be grown directly on CO₂ and light, or on organic carbon substrates. The first growth mode is called photoautotrophic, as the algal cells derive their energy and carbon from photosynthesis. The second growth mode is called heterotrophic. The combined use of light as the source of energy and organic substrates as the carbon source is called photoheterotrophy or mixotrophy. Third generation biofuels are biofuels derived from photoautotrophically-grown algae. A fourth biofuels generation has been proposed by combining the use of highly efficient microorganisms and crop plants (Masarovicova et al., 2009). In this case, optimized heterotrophic or mixotrophic microalgae can play a fundamental role in the development of the fourth generation biofuels.

Currently, a limitation to the large-scale implementation of algal biodiesel is its high production cost compared with fossil fuels (Chisti, 2007). The reduced economic feasibility is due to the low densities and meagre productivities that have traditionally characterized algal cultures. Optimization of microalgal cultures is hindered by the reduced understanding of algal metabolism, the lack

of appropriate sensors to measure relevant biological variables in the reactor, and the non-linear complex nature of biological processes.

It is well known that microalgae are capable of storing high amounts of oil when subjected to nitrogen deficiency (Chen and Johns, 1991; Sheehan et al., 1998; Hu et al., 2008). The mechanisms controlling oil production and accumulation, however, are not clearly understood, and neither is the relationship between growth and oil production. There is a need for a comprehensive, quantitative or semiquantitative description of microalgal dynamics. A mathematical model, suitable for engineering applications, will facilitate the design, control, and optimization of algal processes.

Additionally, it is necessary to develop fast and reliable methods for lipid quantification in algal cells. Such measurements are required to gauge the performance of the bioprocess in terms of productivity and for on-line control. Ideally, an on-line, *in situ*, sensor for measuring one or more relevant variables in the reactor will allow the implementation of feedback control methods. Process analytical technologies (PAT) have been proposed for monitoring and optimization of bioprocesses (Clementschi and Bayer, 2006; Junker and Wang, 2006). PAT are, ideally, real time sensors that guarantee quality in the production of bioproducts. An ideal PAT provides a rapid, precise, and accurate analysis of the reaction broth biochemical composition, and allows the characterization of the organisms it contains (McGovern et al., 2002). Spectroscopy methods satisfy most of the criteria outlined above, and allow a non-invasive, non-destructive and continuous monitoring of the bioprocess (Clementschi and Bayer, 2006). The application of spectroscopic PAT, however, is so far restricted to processes in which the sample matrix is simple enough or have an unusual characteristic that facilitates the correlation of spectral information to chemical composition.

1.2 Research Objectives

The overall focus of the research project presented in this thesis was the optimization of the productivity of microalgal cultures, with the final goal of producing a cost-effective, high-quality, microalgal biodiesel. The specific objectives of this study were as follows:

1. Study the effect of nutrient availability on growth and oil production in microalgae.
2. Develop an experimental technique for fast quantification of key process variables in microalgal cultures.
3. Formulate and evaluate a mathematical model to describe the algal bioreactor dynamics.
4. Develop a high cell density, heterotrophic culture of microalgae.
5. Determine the optimal feeding profiles in fed-batch bioreactors in order to maximize culture productivity.

1.3 Thesis overview

In this thesis, an optimized process for the heterotrophic production of microalgae was developed. The methodology followed for the development and optimization of the aforementioned process is summarized in Fig. 1.1.

As can be seen in Fig. 1.1, the development of the thesis did not follow a linear path, but as with any optimization activity the repeated iteration through several steps was required. The results presented in this document are those at the final iteration performed, though they are still amenable for further improvement.

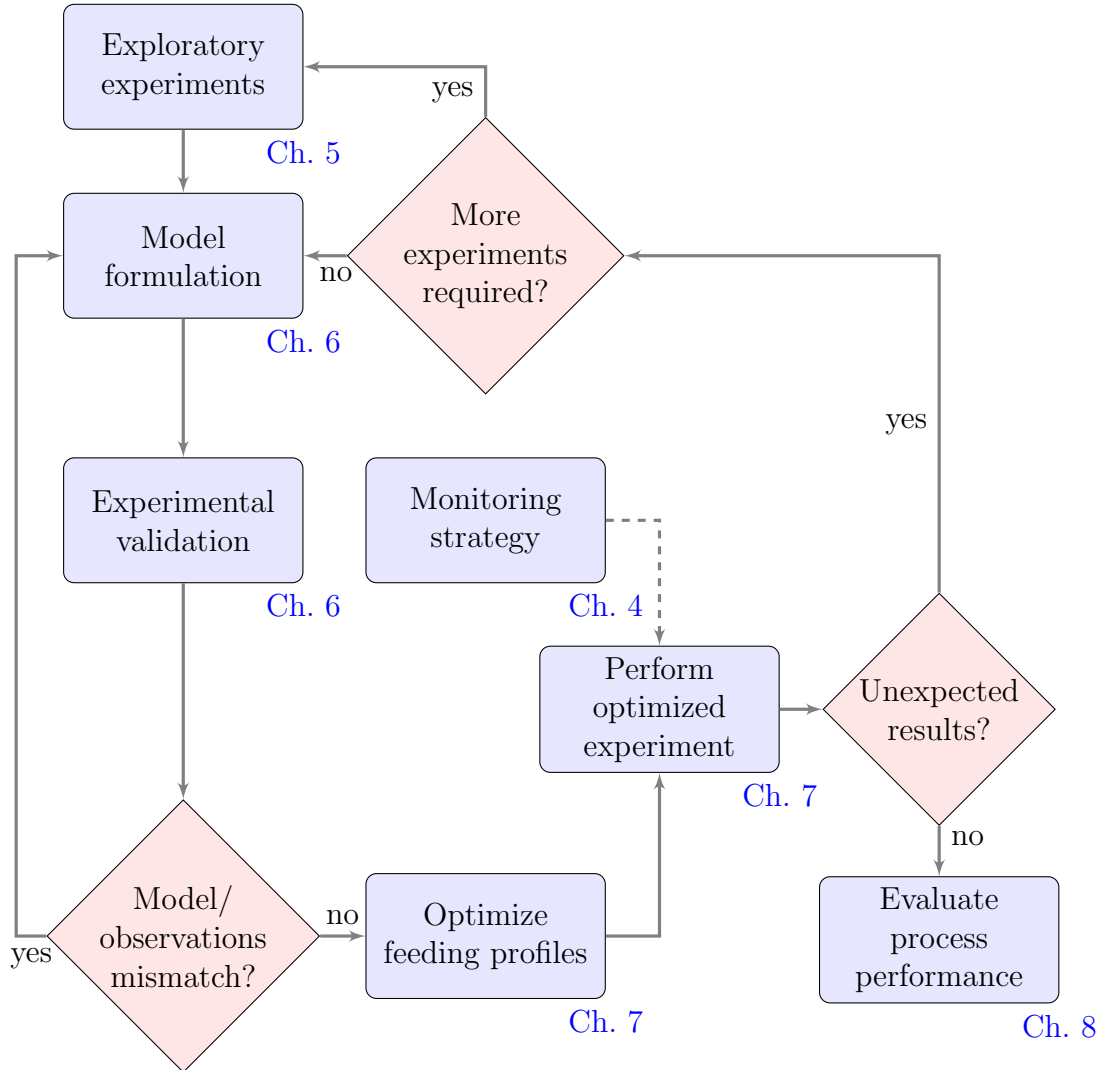


Figure 1.1: Flow diagram of the methodology followed for bioprocess optimization. The number under each process block specifies the chapter that provides the details and final results of the activities performed. The broken line is used to indicate an activity that was not integrated in the final optimization presented in this thesis, but nonetheless was developed and whose integration is part of the recommended future work.

Chapter 2 provides the background information for this thesis. First, a general description of microalgae and microalgal biotechnology is presented. The methods for culturing microalgae as well as relevant biotechnological applications are reviewed. Second, a discussion of the necessary steps for bioprocess optimization is presented. A review of the current trends in process analytical technologies, as applied to bioprocess monitoring, and a description of the different approaches for bioprocess modelling is included in this discussion. A brief review of the current understanding of microalgal growth kinetics finalizes the chapter.

Succinct descriptions of the experimental apparatuses, microalgal cultures, standard analytical methods, and numerical methods used in this research are presented in Chapter 3.

The results and discussion are presented in Chapters 4 to 8. In Chapter 4, two different approaches to quantify the neutral lipid content in algal cells are presented. The first approach involves the extraction of the neutral lipids and further gravimetric quantification. The second approach considers the quantitation through a fluorescence marker and correlation of the fluorescence intensity of the stained cells with their internal lipid content. Also in Chapter 4, a spectroscopic based multivariate technique is developed to simultaneously estimate the intracellular oil content, the biomass, and the glucose concentration in the bioreactor.

Several interesting findings regarding microalgal metabolism, and their behaviour in photoheterotrophic and heterotrophic cultures, are presented in Chapter 5. These findings, together with those previously reported and summarized in Chapter 2, constitute the support for the model developed in Chapter 6.

In Chapter 6, a mathematical model of the dynamic behaviour of heterotrophic

cultures of microalgae is reported. The model considers the effect of both carbon and nitrogen sources on the growth rate and oil production rate. The model was calibrated using experimental observations from batch cultures, and validated in fed-batch cultures.

In Chapter 7, the proposed dynamic model is used to optimize the biomass and lipid productivity in fed-batch cultures of *Auxenochlorella protothecoides*. It is shown that by using the proposed model, the productivity of glucose-fed cultures can be increased by a factor of 20. The model is further used to optimize the productivity in glycerol-fed cultures. The characterization of the oil extracted from *A. protothecoides* is also presented, together with a discussion of the properties of a biodiesel obtained using this oil as feedstock.

The economic aspects of interest to the large scale cultivation of microalgae are reported in Chapter 8. An estimate of the production cost of microalgae, based on the results reported in Chapter 7, is also reported.

Chapter 9 provides the conclusions of this thesis, as well as a series of recommendations for future work. Some of the recommendations are directly related to the objective of this thesis, and aim to further improve or enhance the productivity of microalgal cultures. Other recommendations are potential lines of exploratory research, that are related to algal biotechnology and which came from observations done during the course of this research project, but that do not form part of the core of this thesis.

This page intentionally left blank

2

Background

2.1 Microalgal biotechnology

Microalgae comprise a diverse, polyphyletic, group of organisms whose common characteristic is the ability to carry out photosynthesis (Andersen, 1992). The diversity of the organisms covered by the term microalgae is illustrated in Fig. 2.1, where their phylogenetic tree is shown. For each taxonomic group in Fig. 2.1, a representative microalgal genus of biotechnological interest has been indicated.

As photosynthetic organisms, microalgae are at the base of the food chain in most of the environments in which they are present. Microalgae are found in such dissimilar biomes as soil, seawater, freshwater, decaying matter, and living plants and animals, which highlights the success of microalgae as a group to adapt to environmental conditions. It is important to mention

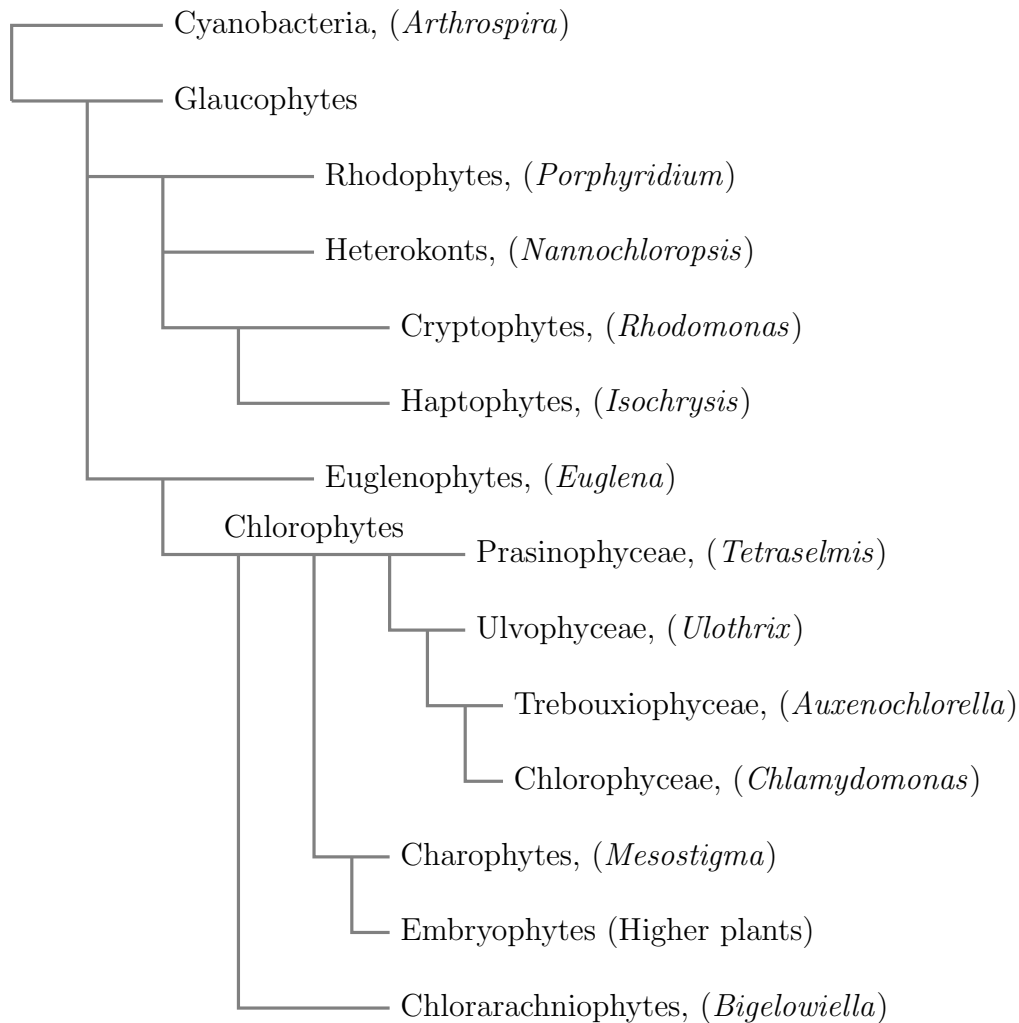


Figure 2.1: Phylogenetic tree of microalgae based on the photosynthetic plastid genealogy, adapted from Bhattacharya et al. (1998) and Lewis and McCourt (2004). In parenthesis, is indicated a representative genus of biotechnological interest. In the past, cyanobacteria were included among the algae, but currently they are regarded as quite distinct organisms, belonging to a different kingdom, and are excluded from the strict definition of algae. In the discussion of microalgae as a source of biofuels and other products, however, several cyanobacteria species are usually used as examples.

that even though microalgae are characterized by being photosynthetic, most microalgal groups contain members that have lost their plastid and therefore are obligate heterotrophs, while an increasing number of species are being recently identified as mixotrophs.

2.1.1 Applications of microalgae

Thanks to their genetic diversity, their adaptability to different and sometimes extreme environmental conditions, and their flexibility to use different sources of energy and carbon to fuel their metabolism, microalgae have a great potential as a source of biotechnological products (Carlsson et al., 2007). Microalgae are being used for the production of animal food, human food supplements (nutraceuticals), pigments, and for wastewater treatment and soil reclamation (Aaronson and Dubinsky, 1982; Spolaore et al., 2006). Potential future applications of microalgae include their use as a source of biofuels, the production of pharmaceutical products, and for capturing carbon dioxide at the point of emission (Carlsson et al., 2007; Olaizola, 2003).

The methods and results presented in this thesis are directly applicable to two microalgal applications: biomass and biodiesel production. With further research and development they can also impact the production of nutraceuticals, pigments, and other fine chemicals and pharmaceutical products from microalgae.

Microalgae as a biomass source

The dried biomass is by large the main biotechnological product derived from microalgae. Whole microalgal biomass is sold for human consumption as a food supplement rich in carotenoids, docosahexaenoic acid (DHA), and eicosapentaenoic acid (EPA). It is commercialized as a powder or in compressed

form in the health market, or as an additive in functional foods (Spolaore et al., 2006).

Microalgal biomass is also used directly as animal food, as it is rich in proteins, essential fatty acids, and carotenoids. The feeding of *Chlorella* and *Scenedesmus* has been reported to provide a better weight control, improved fertility, a healthier skin and lustrous coat in test animals (Pulz and Gross, 2004). In aquaculture, microalgae are fed to shrimps and mollusc larvae, and are used for colouring of salmonoids (Brennan and Owende, 2010).

The direct pyrolysis of algal biomass has been shown to produce diesel quality hydrocarbons. The pyrolysis also left a solid charcoal-like residue, biochar, that can potentially be used as fertilizer or as an adsorption material for carbon sequestration or other applications (Brennan and Owende, 2010).

Biodiesel production

Due to their capacity to accumulate large amounts of intracellular lipids in the form of triacylglycerols, microalgae were early identified as a source of biodiesel (Sheehan et al., 1998). Biodiesel is a proven alternative to traditional fossil fuel diesel (Ma and Hanna, 1999; Kinast, 2003; Gerpen et al., 2004; Chisti, 2007). Its advantages in terms of environmental and health effects, fuel quality, and economic diversification, have been previously documented (USEPA, 2002; McCormick et al., 2006). Commercially, biodiesel is currently produced from oilseed crops (Ma and Hanna, 1999; Chisti, 2007). However, replacement of current diesel fuel demand with biodiesel from oil crops is unfeasible, as it requires unrealistic or unsustainable large cultivation areas (Chisti, 2007) as shown in Table 2.1.

Microalgae, with their high efficiency and ability to produce and store high amounts of lipids that can be converted into biodiesel, is to date the only

Table 2.1: Comparison of different biodiesel sources in terms of oil yield and required land to partially replace current transportation fuel demand (Chisti, 2007)

Crop	Oil yield (L/Ha)	Required land area ^a (MHa)	(%) ^b
Corn	172	1540	846
Soybean	446	594	326
Canola	1190	223	122
Oil Palm	5950	45	24
Microalgae ^c	136900	2	1.1
Microalgae ^d	58700	4.5	2.5

^a For meeting 50% of all transport fuel needs of U.S.

^b Percentage of existing U.S. cropping area.

^c 70% oil(w/w) in biomass.

^d 30% oil(w/w) in biomass.

source of biofuels that could potentially meet the required demand for liquid fuels. In Table 2.1, the corresponding oil yield and land area needed for two possible scenarios of phototrophic microalgal production is reported. As can be observed, there is a dramatic difference between microalgae and other alternatives for biodiesel production.

Even though it is theoretically possible to produce enough biodiesel from phototrophic microalgae without an excessive land requirement, the unfavourable financial cost and energy ratio of current production technologies have hindered the large-scale implementation of microalgal based biofuels. Heterotrophic microalgal cultures can be used to increase the culture productivity and to reduce the high cost associated with the operation and recovery of biomass in phototrophic systems.

2.1.2 Microalgal production systems

As previously indicated, in their natural habitat most microalgae use sunlight and carbon dioxide to fuel their metabolism. Several microalgal species, on the other hand, have lost the capacity to perform photosynthesis and are therefore obligate heterotrophs. In addition a growing number of microalgal species are being identified as mixotrophs, that is they have the capability of thriving either phototrophically or heterotrophically. This flexibility in terms of the basic cellular metabolism offers the possibility of using a wide arrangement of cultivation technologies.

Reactor design

Large-scale culturing of microalgae has been traditionally done in natural uncontrolled systems, such as lakes, lagoons, and ponds. In these systems, microalgal cells grow using the light and nutrients freely available in nature, with the advantage that there is no cost associated with media preparation or illumination. Clearly, the disadvantages of these natural systems are the large variability in the culture conditions and the possibility of contamination by other microalgal species or by predators. Furthermore, biomass recovery cost is usually high due to the low culture cell density in these systems.

To overcome some of the aforementioned disadvantages, several alternative culture systems has been proposed and implemented. Microalgal culturing techniques can be classified as open or closed. The first case includes both unstirred and raceways ponds. Unstirred ponds are essentially equal in operation to natural uncontrolled systems, while raceway ponds provide an improvement in terms of better mixing and circulation, which stabilize microalgal productivity. The application of open systems, however, is restricted in practice to extremophile microalgae due to the potential contamination risk.

Closed culture reactors allow for single-species cultures, reducing or eliminating the risk of contamination. They are in general more efficient in terms of productivity, due to reduced evaporation losses, better temperature control, and better mixing that translate into improved mass transfer. Closed systems include tubular, flat-plate, stirred tank, and airlift column bioreactors.

Operation mode

Microalgae can be produced in several distinctive reactor operation modes, i.e. batch, fed-batch, perfusion, semicontinuous, and continuous. The operation mode determines the maximum achievable productivity and the control strategies that are feasible to optimize the bioreactor performance.

In **batch** cultures, all nutrients are loaded in the reactor at the start of the culture and cells are harvested after a predefined period of time, or when the nutrients are exhausted. Growth, therefore, is limited by the maximum amount of nutrients that can be loaded in the reactor without causing excessive inhibition.

In **fed-batch** mode, nutrients are continuously added to the culture and therefore growth can be extended with respect to the batch case, as nutrient inhibition is not an issue anymore. Cells are harvested once the culture reaches stationary conditions or when the maximum operating volume of the reactor is reached.

In **continuous** systems, cells are harvested as fresh medium is added to the reactor, keeping the total operating volume constant. An intermediate operating mode between batch and continuous are the **semicontinuous** cultures, where only a fraction of the reactor volume is harvested at any given time and then the culture volume is replenished with fresh medium. Continuous and semicontinuous culture might experience wash-out, if cells are harvested at a

higher pace than the growth rate. Additionally, the cell cultures might be too diluted, increasing the cost of product recovery.

Perfusion cultures have been proposed to overcome the low density of continuous systems. In this case, the spent medium is removed from the culture as fresh medium is added, while algal cells are retained in the reactor.

2.2 The improvement of bioprocesses

Bioprocesses are widely used for the production of biofuels, chemicals, pharmaceuticals, and food products. The advantages of bioprocesses, as opposed to classical chemical processes, are their greater specificity, desirable reaction kinetics, and their reduced environmental impact (McGovern et al., 2002). A large number of commercial bioprocesses, however, still rely on the life-long experience of operators (Blanco et al., 2006) and are operated at conditions far from the optimal ones (Clementschitsch and Bayer, 2006).

In order to improve production processes, or to achieve optimal conditions, appropriate control strategies must be implemented. To implement an optimal control strategy, it is necessary to have a quantitative description of the system, that is a mathematical model that relates the controlled variables to the process outputs. It is also required to have the capability to monitor, at a relatively high frequency, the system outputs. Both areas, modelling and monitoring of bioprocesses, still poses several challenges due to the complexities and particularities of biological systems.

2.2.1 Bioprocess Modelling

Process modelling is a central element to the task of process control and optimization. The function of a model is twofold: first, it provides a measure of order to the experimental observations and the tools to make specific predictions about the system under study; second, it can be used to determine the structure of the system and to improve our understanding of it (Becker et al., 2009).

Depending of the available knowledge of the biosystem of interest and the intended application of the model, different approaches to modelling can be followed. In a white-box modelling strategy, the mathematical relations are strictly derived from mechanistic, first-principles, considerations. White-box models possess good extrapolation properties, and provide the engineer or scientist with a reliable tool to inquire about the nature of the system. The formulation of white box models, however, is restricted due to our limited knowledge of the structure and properties of biological systems. Furthermore, due to the complex nature of biological materials, to achieve a tractable model structure, extensive simplification is required when deriving models from mechanistic considerations. The resulting mechanistic models tend to resemble black-box models, more than white-box ones (Becker et al., 2009).

In a black-box modelling approach, on the other hand, the model formulation is purely driven by the available data, without regards to any biological explanation of the model structure. Black-box models are based on different probabilistic or artificial intelligence approaches. This category of models does not have any reliable extrapolation properties and provides little understanding of the underlying nature of the system. They are useful, however, for control of processes operating inside the operating region in which the model was built. Models that take into account both statistical approaches and the

existing knowledge of the system are termed grey-box models.

Models of biological processes can be further categorized with respect to the assumptions made on the identities of the cell and the cell population. Models can be either unstructured, in which cells are assumed to be a single chemical component with a fixed composition, or structured where cells are regarded as composed of two or more interacting compartments. Models can also be classified as unsegregated or segregated. In unsegregated models all the cells in the system are assumed to behave equally and to have the same properties, while segregated models account for the variability in the cell population.

By definition, a model should be kept as simple as possible. The complexity in a model is determined by the intended application of the model or the question that the model is expected to help to answer. Unstructured-unsegregated models are the simplest and represent an ideal case, in which the population acts as a single solute in the bioreaction. Despite and because of this simplicity, unstructured-unsegregated models are of widespread use in bioprocess engineering. This category of models successfully describes many bioprocesses characterized by pseudo-steady state and balanced growth.

For bioprocess control and optimization, the vast majority of documented applications use unstructured-unsegregated models (Mandenius, 2004), even though these models are known to fail in describing dynamic systems.

The most complex, and closest to reality, category of bioprocess models are structured-segregated models. The use of these models is, however, restricted due to the intractability of the systems of multiple partial differential and integro-differential equations that are present in them. The use of a higher complexity model is determined by the inability of simpler models to provide a satisfactory result.

2.2.2 Bioprocess Monitoring

Due to the reduced availability of appropriate sensors to measure key state variables, e.g. biomass and product concentrations (Macaloney et al., 1996), bioprocesses are largely performed without any type of control and quality is only tested on final products (Junker and Wang, 2006). The introduction of the Process Analytical Technology (PAT) initiative by the FDA (2004) has increased the interest in the research and development of optimal bioprocesses in the pharmaceutical and food fields. According to the PAT initiative, quality cannot be tested in products, but should be built-in or should be achieved by design (Clementsich and Bayer, 2006; Junker and Wang, 2006). The PAT initiative, in contrast to the previous FDA's Good Manufacturing Practices standard, promoted the use of real time sensors to guarantee quality in the bioprocesses.

Process monitoring approaches can be classified as on-line, at-line, or off-line (Vaidyanathan et al., 1999). Off-line measures have been the standard in bioprocess industries. Conventional off-line analysis is performed daily or at the end of the culture, resulting in a rather unreliable and inefficient analysis procedure (Arnold et al., 2002). Even in the cases when analyses are performed more frequently during a fermentation, several labor-intensive analytical techniques are required for the measurement of biomass and products concentration (Macaloney et al., 1996).

At-line monitoring represents an improvement over the conventional approach. In this case the analyzer is within the vicinity of the bioreactor and samples taken from it are analyzed quickly (Vaidyanathan et al., 1999; Arnold et al., 2002). In an ideal monitoring strategy, measurements are taken in real-time; therefore, on-line monitoring is the desirable approach. On-line monitoring can be performed *in situ* or *ex situ*. In the first case, the analyzer is in direct

contact with the process stream or is immersed in the bioreactor. In the second case, a flow device allows for the passage of the process stream through the analyzer. According to Arnold et al. (2002) and Macaloney et al. (1996) a process monitor located *ex situ*, such as an external loop, is non-ideal since there is a potential for major operating faults.

The increased robustness and reliability of process spectrometers has made spectroscopy a realistic alternative to off-line laboratory analysis as a source of chemical information. The main advantage of spectroscopy over other monitoring techniques is that multivariate chemical information is obtained, in contrast to standard univariate process measurements of temperature, pressure, pH, DO, flow rate, and levels (Gurden et al., 2002). An ideal monitoring method should provide a rapid, precise, and accurate analysis of the reaction broth biochemical composition; should allow the characterization of the organisms it contains; should have minimum, or no sample preparation; and should be automated and inexpensive (McGovern et al., 2002). Spectroscopy methods satisfy most of the criteria outlined above, and allow a non-invasive, non-destructive and continuous monitoring of a bioprocess (Clementschitsch and Bayer, 2006).

Raman spectroscopy is a physicochemical method that measures the fundamental vibrational modes of bonds within functional groups (Sivakesava et al., 2001; McGovern et al., 2002), allowing for the quantification of the biochemical species present in the culture broth. Moreover, it has been reported that each microorganism has a distinctive fingerprint spectra (Naumann et al., 1991), allowing for monitoring of biomass as well. Raman spectroscopy is based on the inelastic scattering of monochromatic light. In an elastic scattering process, light photons interact with the electron cloud of a molecule, raising the electrons to a virtual energy state; electrons quickly drop back to their ground

energy state releasing a photon of equal energy to the incident photon. In a Raman or inelastic scattering, on the other hand, the electrons do not return to their ground energy state but to a vibrational state, causing the interacting photons to gain or lose energy during the scattering process, shifting their wavelength.

Shope et al. (1987) reported the first application of Raman spectroscopy to a bioprocess, namely the analysis of ethanol fermentation products. They collected the spectra off-line for several samples removed at different fermentation times, and showed that the Raman spectra can be used for the simultaneous quantification of biochemical species in aqueous solutions. Gomy et al. (1988) reported the use of a fibre optic in combination with a Raman spectrometer for the off-line monitoring of an alcoholic fermentation; they reported an average error of 10-15% for their fibre optic measures. Xu et al. (1997) simultaneously measured the concentration of glucose, glutamine, lactate and ammonia in a fermentation broth. Cells were removed from the samples before measuring the spectra. Spectra were measured by using two different laser sources (Argon ion at 514.5 nm and solid state diode laser at 785 nm). The background fluorescence was substantially eliminated by using the 785 nm laser, and the limit of detection was improved up to a factor of 5. Using a 785 nm laser, Giles et al. (1999) showed that high quality quantitative analysis can be performed using Raman spectroscopy without requiring spectral standardization for a chemical system. They conclude that the quantitative information available from the Raman spectra is comparable to that from IR spectra, but avoid the requirement for complicated sample preparation procedures. Shaw et al. (1999) followed the fermentation of glucose to ethanol on-line by using a flow-through cell (*ex situ*), concluding that Raman spectroscopy is an ideal method for following the biotransformation in a nondestructive noninvasive way. They used a 780 nm diode laser, and pointed out that even though

an Nd:YAG (neodymium-doped yttrium aluminium garnet) at 1064 nm laser could further reduce the background fluorescence, the quantum efficiency of the CCD detectors was very low at 1064 nm photons, making the 780 nm laser an optimum selection.

The first on-line and *in situ* application of Raman spectroscopy to monitoring a bioprocess was reported by Cannizzaro et al. (2003). They used a 785 nm laser, and a 12.5 mm immersion Raman probe inserted in a side port of the bioreactor. The probe was connected to the control unit with a fibre optic. They quantified the carotenoids production in *Phaffia rhodozyma*. Taking advantage of the unique enhanced Raman signal of carotenoids, caused by a resonance effect, no chemometric tools were required for signal deconvolution. Quantification of carotenoids using Raman spectroscopy has also been reported in the microalgae *Dunaliella* and *Phaedactylum* (Abbas et al., 2011).

Lee et al. (2004) monitored *Escherichia coli* bioreactions using Raman both *in situ* and off-line. Limited accuracy of on-line measures was reported, associated with a change in the Raman spectrum of the sapphire window probe after steam-sterilization. A chemometric model was built using data from pure components spectra measured off-line and before probe sterilization. Lee et al. (2004) suggested that better results could be obtained by modifying the probe design to allow the measurement of the sapphire spectra after steam sterilization or by building the chemometric model in such a way that sapphire spectra do not affect it.

More recently, Huang et al. (2010) and Wu et al. (2010) have shown the feasibility of using confocal Raman spectroscopy for the characterization and quantification of lipids at the cellular level in microalgae.

2.3 Modelling of microalgal systems

The research effort for modelling microalgal systems has been largely done from an ecological perspective. Due to the importance of microalgae for both marine and freshwater biomes, ecologists have been interested in the productivity of microalgae, the population cycles and succession, and the effect of eutrophication on microalgal populations.

Phosphorus and nitrogen are usually regarded as the key factors in most eutrophication processes. Given that they are usually present in limiting quantities in the aquatic environments, whenever there is an oversupply of nitrogen or phosphorus algal blooms occur. The research on eutrophic environments have provided a wealth of information regarding the kinetics and mechanisms of nutrient uptake, nutrient accumulation, and nutrient limitation.

2.3.1 Physiological characteristics relevant for modelling of microalgal processes

From a biotechnological perspective, several of the findings in ecological research are relevant. In particular, the kinetics of nitrogen uptake and its regulating effect on algal growth is of prime interest, as nitrogen deficiency has been previously identified as the key to achieve a high oil content in algal cultures (Chen and Johns, 1991; Hu et al., 2008). The so called ‘trigger effect’ that nitrogen deficiency has over oil accumulation has consequently attracted research interest. Empirical evidence suggests that there are clear differences between nitrogen-sufficient and nitrogen-deficient cultures. These differences include changes in the content of chlorophyll, protein, and lipids, as well as variation in cells pigmentation, (Shihira-Ishikawa and Hase, 1964; Piorreck et al., 1984). As a major cellular nutrient, nitrogen is required for the

assembly of nucleic acids and proteins, and its availability plays a major role in cell growth and division and affects many intracellular processes (Ahmad and Hellebust, 1990; Huppe and Turpin, 1994). Therefore, a nitrogen deficient culture is expected to grow at a slower rate than a nitrogen sufficient one.

Consequently, the effect nitrogen has in promoting a higher oil content in algal cells has been considered the result of a slower growth rate, and not due to the activation of a high oil producing metabolic pathway (Sheehan et al., 1998). Research on autotrophic systems has found that the increase in oil accumulation in algae due to nitrogen limitation is inversely proportional to oil productivity (Sheehan et al., 1998; Brennan and Owende, 2010), which has led to the conclusion that lipid content in microalgae is less important than the maximization of growth rates (Weldy and Huesemann, 2007).

Previous studies have revealed several characteristics of algal nitrogen uptake and metabolism:

- i. Nitrogen uptake is not linear (Ricketts, 1988; Hein et al., 1995; Inokuchia et al., 2002);
- ii. Transport is feedback regulated, although regulation is either not performed at the nuclear level or transport enzymes have long persistence in the cell (Hein et al., 1995; Inokuchia et al., 2002; Chaudhuri and Spencer, 1968);
- iii. Free amino acids are stored in the cytosol;
- iv. The glycine uptake system is induced by glucose and by nitrogen starvation (Tyler et al., 2005; Cho and Komor, 1985);
- v. Respiration and nitrogen assimilation are interacting processes that involve the activation of several metabolic pathways that share common

metabolites and enzymes (Inokuchia et al., 2002).

Most of the ecological studies on nitrogen uptake and metabolism have focused on dissolved inorganic nitrogen (DIN) uptake and limitation, while few studies have dealt with dissolved organic nitrogen (DON) uptake (Piedras et al., 1998; Tyler et al., 2005). DON includes compounds such as amino acids, urea, purines and ureides, among others (Piedras et al., 1998). There are no studies, however, on DON uptake kinetics under heterotrophic conditions in high cell density algal cultures. Whether or not the findings on dilute algal communities are applicable to single-species, high density cultures needs to be investigated.

2.3.2 Kinetic models of microalgal growth

Extensive research has been done in the field of microbial kinetic modelling, as it is an important tool in physiology, genetics, ecology and biotechnology (Janasch and Egli, 1993). The aim of kinetic modelling is to relate the growth or production rate of microalgae to one or more process variables. The specific growth rate, μ , expresses the change in the cellular biomass per unit of time:

$$\frac{dx}{dt} = \mu x \quad (2.1)$$

from where, after integrating from time t_1 to time t_2 , it is obtained the expression for determining the growth rate:

$$\mu = \frac{1}{t_2 - t_1} \ln \frac{x_2}{x_1} \quad (2.2)$$

where x_1 and x_2 are the biomass concentrations at time t_1 and t_2 , respectively.

Several unstructured and structured models has been proposed to represent the growth rate of microalgae in terms of the concentration of the limiting

nutrient. Wu et al. (2007) used a kinetic expression based on the unstructured Aiba’s model to describe the heterotrophic growth of *Chlorella* with glucose as the carbon source and KNO_3 as the nitrogen source.

Unstructured models fail to describe the relationship between growth rate and the concentration of the limiting nutrient whenever the limiting nutrient can be assimilated in excess by the cells. The luxurious uptake of several nutrients was early observed in microalgae by Droop (1968) in the study of vitamin B12 limited cultures of *Monochrysis lutheri*. Droop introduced the concept of nutrient quota, \tilde{q} , to account for the time scale differences between nutrient uptake, and growth. In essence, this is equivalent to introducing a second compartment in the model, making the Droop’s quota model a structured model. Droop (1973) proposed the following empirical correlation between the cell quota, \tilde{q} , and growth rate:

$$\mu = \max \left\{ 0, \mu_m \left(1 - \frac{\tilde{q}_m}{\tilde{q}} \right) \right\} \quad (2.3)$$

where \tilde{q}_m is the minimum cell quota required for growth. The max function above implies that the growth rate cannot be negative.

Caperon and Meyer (1972) proposed to use a Michaelis-Menten type expression as an alternative to Eq. (2.3):

$$\mu = \frac{\mu_m(\tilde{q} - \tilde{q}_m)}{K_{\tilde{q}} + (\tilde{q} - \tilde{q}_m)} \quad (2.4)$$

It must be noted that Eq. (2.3) is a special case of Eq. (2.4) with $K_{\tilde{q}} \approx \tilde{q}_m$.

In Droop (1973), the substrate uptake was assumed to obey a Michaelis-Menten type kinetics:

$$\rho = \frac{\rho_m s_1}{K_{\rho} + s_1} \quad (2.5)$$

with ρ being the substrate uptake rate, ρ_m the maximum uptake rate, and K_ρ the uptake half-saturation constant.

The applicability of a Michaelis-Menten type kinetic to the uptake of nutrients in algae is widely accepted, though several modifications to it have been suggested to improve the fitting of experimental data. Lehman et al. (1975) introduced a saturation term in the Michaelis-Menten expression that considers the effect of an upper limit, or finite cellular storage, of a specific nutrient:

$$\rho = \frac{\rho_m s}{K_\rho + s_1} \left(\frac{\tilde{q}_M - \tilde{q}}{\tilde{q}_M - \tilde{q}_m} \right) \quad (2.6)$$

in which \tilde{q}_M is the maximum internal quota.

To account for the presence of a lower threshold concentration, s_0 , below which no substrate is assimilated, Caperon and Meyer (1972) replaced s_1 in Eq. (2.5) by $(s_1 - s_0)$:

$$\rho = \frac{\rho_m (s_1 - s_0)}{K_\rho + s_1 - s_0} \quad (2.7)$$

Several modifications to the quota model have been proposed to account for a higher degree of realism and to consider the simultaneous multiple nutrient limitation (Flynn, 2001, 2003).

This page intentionally left blank

3

Methodology

This chapter describes the experimental set-up used to conduct the experiments, the analytical methods used to quantify important process variables, as well as the numerical methods used for parameter estimation, model selection, and confidence analysis.

3.1 Microalgal cultures

Among the different groups of microalgae, *Chlorophyceae* and *Trebouxiophyceae* (green algae) have attracted considerable research attention due to the similarity of their members with higher plants. Fatty acid composition in green microalgae resembles those seen in higher plants and oleaginous yeasts (Behrens and Kyle, 1996; Sheehan et al., 1998), and for this reason lipids from green algae are expected to be converted into biodiesel using the same processes developed for oilseed crops (Chisti, 2007).

In this study, the fresh-water green microalga *Auxenochlorella protothecoides*, shown in Fig. 3.1, was used as a model organism. *A. protothecoides* is a green microalga that has the ability to grow under phototrophic or heterotrophic conditions. Biodiesel production from *A. protothecoides* has been previously reported (Miao et al., 2004; Miao and Wu, 2006; Xu et al., 2006; Li et al., 2007a). When grown heterotrophically in fed-batch mode, *A. protothecoides* have reached cell densities as high as 15.5 g/L (dry weight), with an oil content close to 45 % (Xu et al., 2006; Li et al., 2007a).

The microalgal culture was obtained from the UTEX Culture Collection of Algae at the University of Texas. Hereinafter it is referred as *A. protothecoides*. Its basionym is *Chlorella protothecoides* (Kruger), and it is catalogued as SAG 211-7a, and UTEX B 25 (previously catalogued as UTEX 25). *A. protothe-*

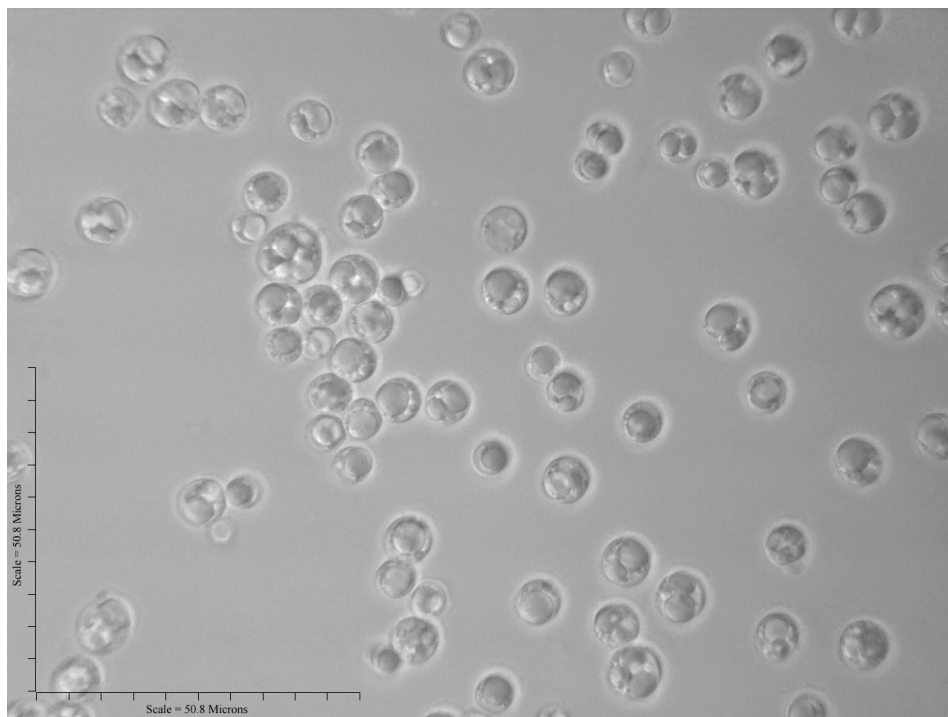


Figure 3.1: Microphotograph of *Auxenochlorella protothecoides* observed in a light microscope, 100x.

coides are unicellular microscopic algae with globose or broadly ellipsoid cells. Cells contain a single eccentric nucleus and a single and parietal chloroplast. Reproduction is by autospores, with 2, 4, 8, or 16 per sporangium, released by rupture of the parental cell walls (Guiry and Guiry, 2005).

Cultures of *A. protothecoides* were kept axenically in agar plates for long term storage, at 4 °C. Agar plates were prepared according to the sporulation agar formulation, ATCC Medium 5. Sporulation agar contains: yeast extract (1.0 g), beef extract (1.0 g), tryptose (2.0 g), FeSO₄ (0.002 g), dextrose (10.0 g), technical agar (15.0 g), and deionized water (1000 mL).

For continuous use, liquid cultures were maintained at 25 °C, in a shaker incubator at 100 rpm. Liquid cultures were periodically tested for contamination by visual inspection under the microscope and by streaking an aliquot of the liquid culture in an agar plate and subsequent incubation of the plate. The liquid cultures were periodically transferred to fresh media every two or three weeks.

3.1.1 Batch cultures

Batch experiments were conducted in a shaker incubator at 100 rpm using wide-mouth culture flasks (1 L) with 250 mL working volume. All materials were thoroughly cleaned, with soap and hot water in a labware washing machine, and sterilized before use. Sterilization was conducted in a steam autoclave, holding the temperature at 121 °C for 20 minutes.

Three different media formulation were used for batch cultures as reported in Table 3.1. Culture media composition was defined in such away that it provided a balanced source of all trace elements according to the elemental composition of algae (Mandalam and Palsson, 1998).

Working stock solutions were prepared using deionized water and autoclaved with steam at 121 °C for 20 minutes. A single stock solution containing most trace elements was prepared according to the A5 solution reported by Arnon (1938). Iron sulfate stock solution was prepared by complexation with EDTA. The Fe-EDTA complex was prepared by dissolving 1.2 g of $\text{FeSO}_4 \cdot 7 \text{H}_2\text{O}$ and 1.6 g of disodium-salt of EDTA in 80 mL of deionized boiling water. After the solution has cooled down to room temperature it was made up to 100 mL. Stock solutions were let to cool down at room temperature before preparing the culture media. It must be noted that, a precipitate is formed when stock solutions are mixed at warm or high temperature. Stock solutions were stable for an extended period of time (> 1 year), with no precipitate, when kept unmixed. Unmixed stock solutions could also undergo repetitive autoclaving without loss of stability.

Photoheterotrophic experiments were conducted at room temperature (approximately 20 °C), with continuous illumination at a photosynthetic photon

Table 3.1: Composition of base culture media

Component	Concentration			
	B1	B4	B4-Fe	Units
KH_2PO_4	0.7	2.8	2.8	g/L
K_2HPO_4	0.3	1.2	1.2	g/L
$\text{MgSO}_4 \cdot 7 \text{H}_2\text{O}$	0.3	1.2	1.2	g/L
$\text{FeSO}_4 \cdot 7 \text{H}_2\text{O}$	3.0	12	48	mg/L
$\text{CaCl}_2 \cdot 2 \text{H}_2\text{O}$	25	100	10	mg/L
H_3BO_3	2.9	11.6	11.6	mg/L
$\text{MnCl}_2 \cdot 4 \text{H}_2\text{O}$	1.8	7.2	7.2	mg/L
$\text{ZnSO}_4 \cdot 7 \text{H}_2\text{O}$	0.22	0.88	0.88	mg/L
$\text{CuSO}_4 \cdot 5 \text{H}_2\text{O}$	0.08	0.32	0.32	mg/L
$\text{Na}_2\text{MoO}_4 \cdot 5 \text{H}_2\text{O}$	0.04	0.12	0.12	mg/L
Thiamine hydrochloride	10	40	40	$\mu\text{g/L}$

flux (PPF) of $29.9 \pm 1.4 \mu\text{mol m}^{-2}\text{s}^{-1}$, using four Philips F40T12/Plant & Aquarium fluorescent tubes positioned 60 cm above of the orbital shaker surface. Heterotrophic experiments were conducted at 25 °C in a refrigerated shaker incubator (Innova 4300). All cultures were inoculated with 10 mL of algal suspension taken from a liquid culture at the end of the log-phase.

3.1.2 Fed-batch cultures

Experiments were conducted in a 2 L stirred-tank bioreactor (Sartorius Biostat A plus). The bioreactor unit consisted of a 2 L glass vessel, with a total volume of 3 L, with a stainless steel cover.

Instrumentation

The bioreactor temperature was kept constant using an electrical heating blanket, and an external water-cooling system. Temperature was measured with a platinum electrode Pt-100 (Sartorius BBI Systems, Type 200-4).

An EasyFerm Plus K8 (Hamilton Bonaduz AG) electrode was used to measure the pH. Aqueous solutions of KH_2PO_4 (acid) and K_2HPO_4 (base) were used as required to control the pH.

Dissolved oxygen was measured with an Oxyferm FDA (Hamilton Bonaduz AG) electrochemical sensor. Agitation rate was kept constant at 300 rpm, while varying aeration rate to control the dissolved oxygen at a predefined set-point.

Spectroscopic sensors

Raman spectra were measured using a solid-state fibre Bragg grating stabilized laser, with an excitation wavelength of 785 nm and output power equal to

300 mW. The spectrometer (RSI QEB0049, Ocean Optics Inc.) consisted of an f/4 symmetrical crossed Czerny-Turner monochromator, with a 50 μm wide slit, and a 1024 \times 58 pixels (2D array) Hamamatsu detector.

Spectra were acquired using an immersion probe inserted into one of the upper ports of the bioreactor. The stainless steel immersion probe was chemically sterilized by submerging it into an 800 ppm solution of benzalkonium chlorides (Roccal-D) for at least 15 minutes prior to its installation in the bioreactor.

Sampling system

An automatic sampler system was set-up in order to withdraw a fixed amount of culture broth every four hours and store it in a fridge at 4 °C for further analysis. The sampling system consisted of a set of solenoid pinch-valves, a peristaltic pump, and systems for cleaning and drying of the fluid path.

Data acquisition and Supervisory control system

The bioreactor digital control unit (DCU) and the peripheral instrumentation was interconnected using a local ethernet network. The network setup allowed for any computer connected in the network to access process data, as well as to send setpoints to the reactor DCU.

Communication between the network clients (computers), and the DCU was regulated using an OPC server. OPC, Object linking and embedding for Process Control, is an open standard that allows open connectivity among different process equipment and instrumentation with Windows[®] based networks.

A client application in Visual Basic 6.0 was developed to act as a manager among the optimization and control algorithms (implemented in Matlab[®]), the spectral and process databases and the OPC server. The source code

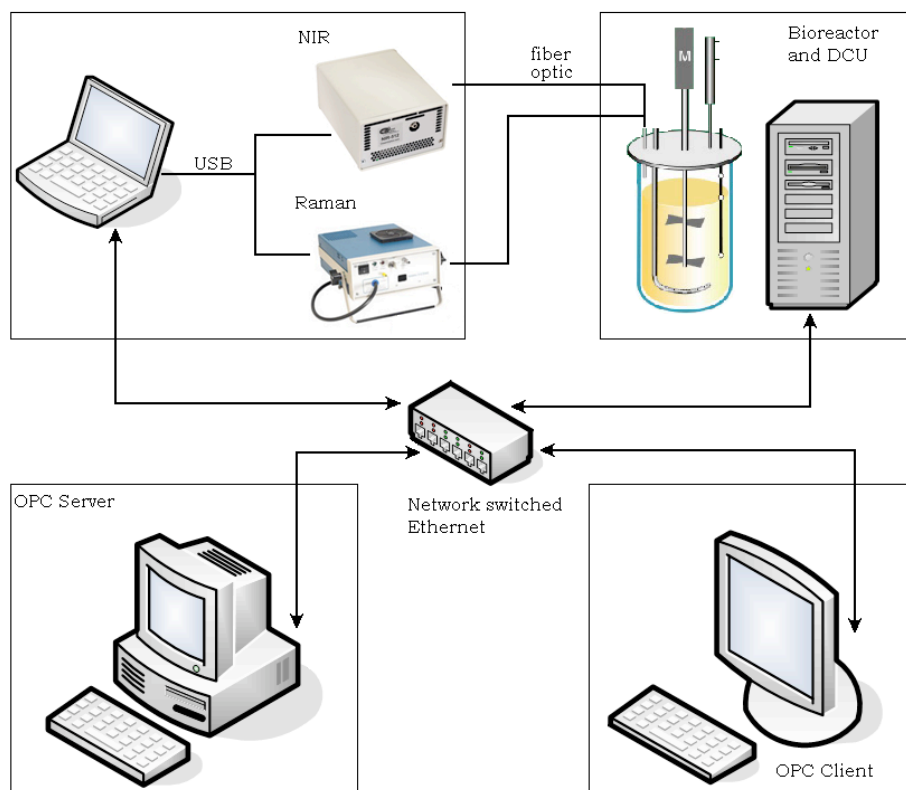


Figure 3.2: Diagrammatic representation of the Bioreactor and control system network. The bioreactor digital control unit (DCU) was connected to a desktop computer, that acted as the data acquisition and control server (OPC server) using an Ethernet connection. The spectroscopic instrumentation and the OPC clients were interfaced to the reactor through the Ethernet network.

of this OPC client is presented in Appendix D. A diagram of the network architecture is presented in Fig. 3.2.

3.2 Analytical methods

In this section, the methods used to determine the concentration of biomass, carbon substrate, and nitrogen substrate are presented. Also included in this section are the methods used for characterization of the lipids extracted from

algal cells. The methods used for lipid quantification are not included here, but instead are presented in Chapter 4 as their development is part of the contributions this research project.

3.2.1 Biomass measurement

The biomass content in the culture is usually quantified in terms of total cell material weight or as total cell count. In this work, the primary method for biomass quantification was total cell dry weight. In a few instances, cell numbers were also counted and the cell size distribution was determined.

Determination of total cell dry weight

Biomass concentration was determined as total suspended solids (TSS) by centrifuging 1.4 mL of cell suspension at 10000 rpm (RCF = 9335 *g*) for 10 minutes. Pellets were washed twice with a saline phosphate buffer solution (pH 6.2) and re-centrifuged. Final precipitate was vacuum dried at 50 °C and 0.1 bar until constant weight. These measurements were checked against vacuum filtration of 10 mL of the culture broth with a 0.22 μm filter paper. The average relative standard deviation in dry biomass measurements was 3.8 %.

Cell count and cell size distribution

Cell count was performed on a Beckman Coulter Z2 particle counter and size analyzer. *A. protothecoides* is a unicellular microscopic algae with globose or broadly ellipsoid cells ranging in diameter from 1.5 – 9.0 μm , with typical cells being 3.0 – 6.0 μm . The instrument was set up to cover this broad range, by using two different configurations. In the first configuration the gain was adjusted at 32 and the current intensity at 500 mA, providing a measurement range from 3.5 μm to 12.73 μm . The second configuration used a gain equal to

256 and current intensity at 2000 mA, given an operating range from 1.2 μm up to 4.0 μm .

Samples were prepared in the safety cabinet in order to avoid contamination with dust particles, which increased the particle count or introduced other artifacts in the measurements. Samples were diluted with Isoton[®] solution to achieve a final particle count around 5 – 10 % of the saturation level.

3.2.2 Glucose quantification

Algal culture samples were centrifuged at 10000 rpm ($\text{RCF} = 9335 g$) for 10 minutes, and the clear supernatant was filtered using a 0.22 μm syringe filter in order to remove any residual cells. Glucose concentration in this filtered supernatant was measured by high performance liquid chromatography (Agilent 1200 Series HPLC), using a SupelcoGel Pb carbohydrate column at 70 °C (Internal diameter 7.8 mm, length 30 cm) with guard column. The sample injection volume was 10 μL ; the eluent was deionized, sterile water (MilliQ, MilliPore); the elution flow-rate was set at 0.5 mL/min, and a refractive index detector (RID) at 35 °C was used. Glucose solution standards with concentrations ranging from 0.1 g/L to 100 g/L were prepared and analyzed by HPLC. A calibration curve was generated based on standard results. The relative standard deviation in HPLC measurements was 0.32 %.

3.2.3 Nitrogen quantification

Total nitrogen

Total nitrogen, in both filtered supernatant and dry cells, was determined by pyro-chemiluminescence using an Antek 9000NS nitrogen analyzer. The total sample injection volume used was 20 μL , with the furnace set up to operate at

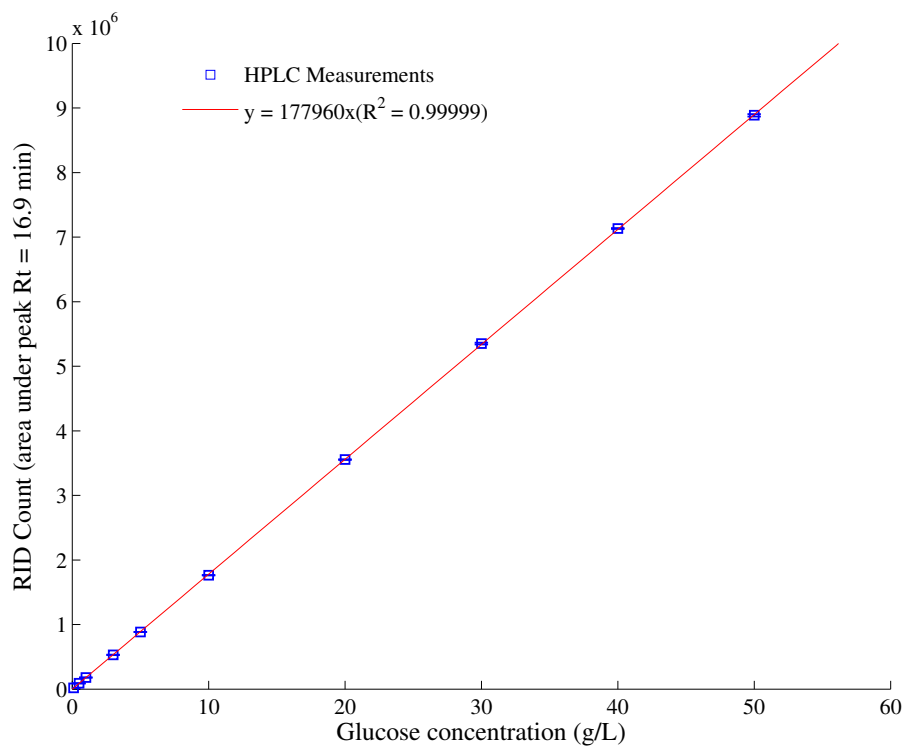


Figure 3.3: Standard calibration curve for glucose in aqueous solutions with respect to high performance liquid chromatography measurements, using a refractive index detector.

1050 °C, helium flowing at 140 mL/min, and oxygen flowing at 450 mL/min. Glycine was used as standard for calibration. The average relative standard deviation of the measurements was 2.2 %.

Amino-nitrogen

The concentration of chemical species containing amino groups in the media was measured using the Ninhydrin method (Meyer, 1957; Friedman, 2004). For this, 200 μL of sample were diluted in 1800 μL of deionized water, and mixed with 500 μL of Ninhydrin reagent. The resulting mixture was put in boiling water for 10 minutes, and later let to cool down to room temperature. Ninhydrin reacts with amino-containing compounds to give an intense purple colour. To measure the absorbance at 570 nm, samples were diluted by adding 5.0 mL of ethanol. A calibration curve between the measured absorbance and glycine concentration is reported in Fig. 3.4.

3.2.4 Lipid characterization

Total lipids analysis

Total lipid classes were analyzed by high performance liquid chromatography. For this, 5.0 μL of a 1:10 dilution of the oil sample was added to 200 μL of phosphatidyl N,N-dimethylaminoethanol (PDME) in chloroform (1.0 $\mu\text{g}/\mu\text{L}$). 1.0 μL of the resulting solution was injected into the HPLC, and PDME was used as internal standard for quantification.

Fatty acid analysis

Fatty acid chain length and saturation analysis was performed by gas chromatography after derivatization to fatty acid methyl esters (FAME).

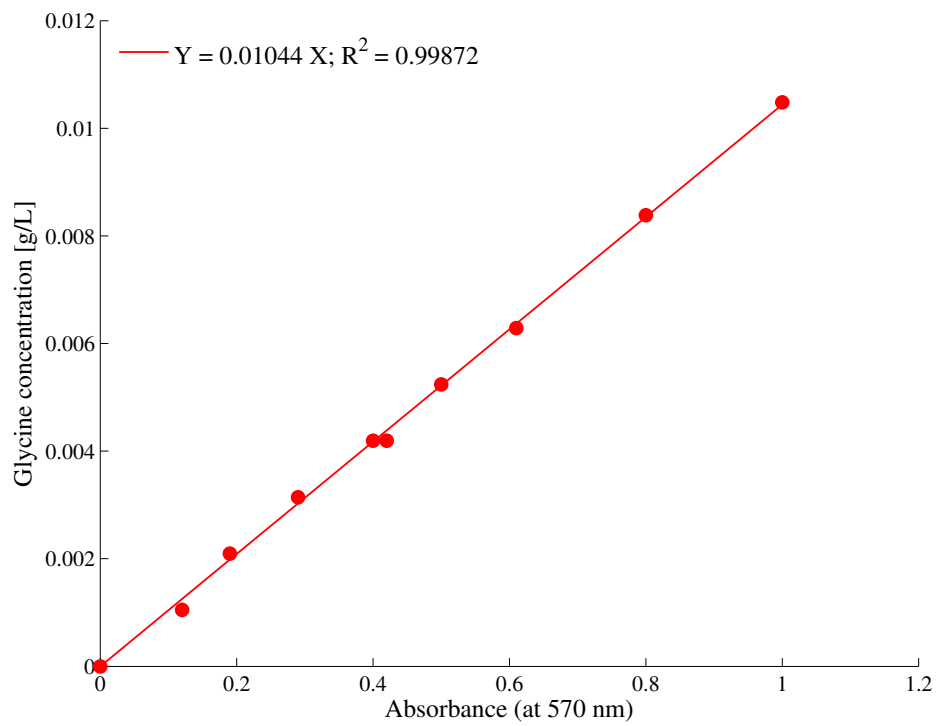


Figure 3.4: Standard calibration curve between the absorbance of the Ninhydrin complex and the concentration of glycine in aqueous solutions.

FAMEs derivatives were prepared by adding 1.5 mL of a 6.0% sulphuric acid solution in methanol to a known volume of the extracted oil in a 15 mL glass screw-cap tube. This mixture was vortexed and incubated at 80 °C for 2 hours, after which it was let to cool down at room temperature. Subsequently, 2.0 mL of ammonium hydroxide:water (1:3) were added to the glass tube and vortexed. Finally, 5.0 mL of HPLC-grade hexane were added to the mixture, vortexed, and centrifuged at 1000 rpm for 1 minute. The upper hexane layer was removed and passed through a sodium sulphate column into another clean glass tube. The sodium sulphate column consisted of a Pasteur pipette with a glass wool plug at the bottom, and approximately 2 cm of granular sodium sulphate on top of it. The eluent was dried under inert gas, and redissolved in 200 μ L of HPLC-grade hexane for injection into the gas chromatograph.

Different FAMEs were separated by gas chromatography, and quantification was done by using C17:0 as internal standard.

3.3 Reagents

The list of reagents used in this work together with its specified grade or quality, the manufacturer, and the catalog number is presented below.

1. Reagents used for culture media preparation:
 - Calcium Chloride, $\text{CaCl}_2 \cdot 2\text{H}_2\text{O}$, ACS, Fisher, C79
 - Sodium Molybdate, $\text{MoNa}_2\text{O}_4 \cdot 2\text{H}_2\text{O}$, > 99%, Acros, 20637-1000
 - Boric acid, H_3BO_3 , > 99%, Acros, 18057-0010
 - Copper Sulfate, $\text{CuSO}_4 \cdot 5\text{H}_2\text{O}$, Sigma-Aldrich, 209198
 - Ferrous Sulfate, $\text{FeSO}_4 \cdot 7\text{H}_2\text{O}$, ACS, Fisher, I146
 - Manganese Chloride, $\text{MnCl}_2 \cdot 4\text{H}_2\text{O}$, ACS, Fisher, M87

-
- Magnesium Sulfate, $\text{MgSO}_4 \cdot 7 \text{H}_2\text{O}$, Plant Cell Culture, Sigma, M7774
Magnesium Sulfate, $\text{MgSO}_4 \cdot 7 \text{H}_2\text{O}$, ACS, Fisher, M63
 - Potassium Phosphate monobasic, KH_2PO_4 , ACS, Fisher, P285
 - Potassium Phosphate dibasic, K_2HPO_4 , ACS, Fisher, P288
 - Zinc Sulfate, $\text{ZnSO}_4 \cdot 7 \text{H}_2\text{O}$, USP/FCC grade, Fisher, Z76
 - D-(+)-Glucose, 99.5%, Sigma, G8270
 - Glycerol, VWR Intl, BDH1172
 - EDTA Disodium salt dihydrate, ACS, Fisher, S311
 - Glycine, $\text{NH}_2\text{CH}_2\text{COOH}$, Reagent grade, Fisher, G46
 - Urea, NH_2CONH_2 , ACS, Fisher, U15
 - Thiamine Hydrochloride, $\text{C}_{12}\text{H}_{17}\text{ClN}_4\text{OS} \cdot \text{HCl}$, Biotech research grade, Fisher, BP892
 - Yeast Extract: Oxoid Ltd., LP0021
 - Technical Agar: Becton and Dickinson Company, 281230.
 - Tryptose, Sigma, T2813
 - Beef extract

2. Reagents used for oil extraction / quantification:

- Hexanes, technical grade, Fisher, N3
- iso-Propanol, histological, Fisher, A426
- Acetone, certified ACS, Fisher, A18
- Nile Red, $\text{C}_{20}\text{H}_{18}\text{N}_2\text{O}_2$, Sigma, N3013
- Sudan Red 7B, $\text{C}_{24}\text{H}_{21}\text{N}_5$, Sigma, 46290
- Bodipy 505/515, 4,4-difluoro-1,3,5,7-tetramethyl-4-bora-3a,4a-diazas-indacene, Invitrogen, D3921

- Dimethyl Sulfoxide (DMSO), for molecular Biology, Sigma, D8418

3. Other reagents:

- Sodium Azide, NaN_3 , > 99.5%, Sigma-Aldrich, S2002
- Antifoam O30, Sigma, A8082
- Antifoam SE-15, Sigma, A8582
- Isoton II Diluent, Beckman Coulter,
- Ostro San (Roccal), n-alkyl dimethyl benzyl ammonium chloride, Ostrem Chemical Co.

3.4 Model evaluation

In Chapter 6 a mathematical model is proposed to describe the dynamic behaviour of heterotrophic algal cultures. This model is later used in Chapter 7 to optimize the productivity of the culture. In this section the methods used for parameter estimation and for evaluating the performance of the different models considered are presented.

3.4.1 Parameter estimation

Parameters involved in the models are estimated by minimizing the weighted sum of squared errors (WSSE). The WSSE for a set \mathbf{p} of model parameters, $E(\mathbf{p})$, is calculated as:

$$E(\mathbf{p}) = \sum_{i=1}^m \sum_{j=1}^{N_d} (y_{ij} - \hat{y}_{ij})^T w_{ij}^{-1} (y_{ij} - \hat{y}_{ij}) \quad (3.1)$$

where N_d is the number of experimental data points, m is the number of measurable states ($y_{1j} = x_j$ and $y_{2j} = s_j$), \hat{y}_{ij} is the measured value of state i at

time j , and y_{ij} is the value of the state i at time j as calculated from the model. The weight factor w_{ij} was set equal to the variance of the experimental data. The ODE system and the non-linear regression problem stated in Eq. (3.1) were solved using Matlab R2006a (The Mathworks, Inc.).

3.4.2 Confidence analysis

Confidence regions are valuable as they permit the quantification of the uncertainty associated with the model parameters estimation, providing a way to judge the validity of each calculated parameter value. Marsili-Libelli et al. (2003) proposed a procedure to estimate the covariance matrix of the solution to Eq. (3.1) and used it to approximate the confidence regions. The covariance matrix is estimated through the Hessian matrix of the objective function:

$$H(\hat{\mathbf{p}}) = \left. \frac{\partial^2 E(\mathbf{p})}{\partial \mathbf{p} \partial \mathbf{p}^T} \right|_{\hat{\mathbf{p}}} \quad (3.2)$$

The Hessian was computed numerically, with a global error $O(h^6)$, using the algorithm proposed by Marsili-Libelli et al. (2003). The step size in the numerical approximation of the Hessian matrix was optimized to reduce the error associated with numerical round-off and data noise. At each iteration, the step size was reduced, following a predefined step-sequence, until the infinite norm of the difference between two consecutive estimations of the Hessian started to increase, as illustrated in Fig. 3.5.

Confidence ellipsoids are calculated as:

$$\left\{ \mathbf{p} : (\mathbf{p} - \hat{\mathbf{p}})^T \left[\frac{N_d - n_p}{2E(\hat{\mathbf{p}})} H(\hat{\mathbf{p}}) \right] (\mathbf{p} - \hat{\mathbf{p}}) \leq n_p F_{n_p, N_d - n_p}^{1-\alpha} \right\} \quad (3.3)$$

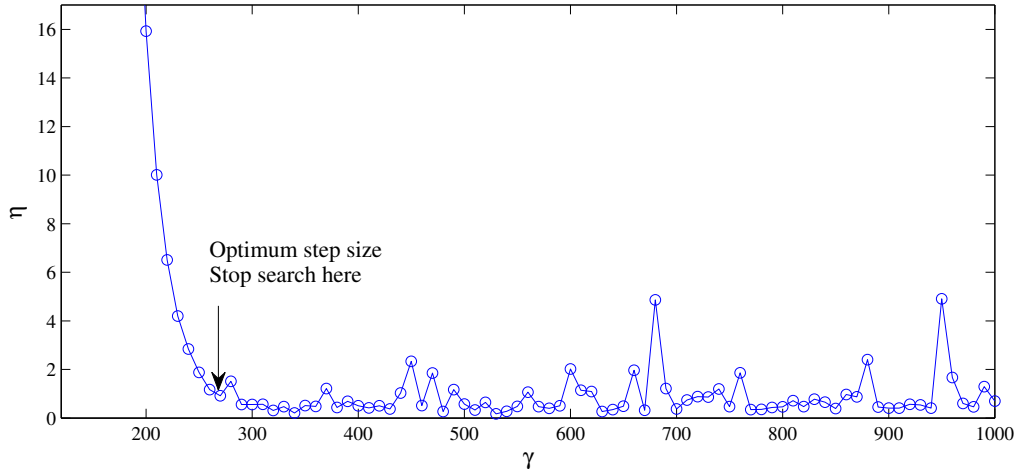


Figure 3.5: Determination of optimal step size for the numerical estimation of the Hessian matrix

with n_p being the number of parameters to be estimated, α the desired confidence level, and $F_{n_p, N_d - n_p}^{1-\alpha}$ the Fisher-Snedecor probability distribution. To quantify the confidence of the parameter estimation, the 2-norms of the semi-axes (eigenvalues) of the confidence hyper-ellipsoids (SACHE) are calculated.

3.4.3 Model selection

In order to balance model complexity and data fitting, and to prevent overfitting, two information criteria are used to select a parsimonious model. The best model will be the one able to explain the experimental data with the minimum number of parameters. The first criterion used is the Akaike information criterion (*AIC*):

$$AIC = 2n_p + N_d \left\{ \ln \left(\frac{2\pi E(\hat{\mathbf{p}})}{N_d} \right) + 1 \right\} \quad (3.4)$$

A second criterion used is the Bayesian information criterion (*BIC*), which is

evaluated as:

$$BIC = N_d \ln \left(\frac{E(\hat{\mathbf{p}})}{N_d} \right) + n_p \ln(N_d) \quad (3.5)$$

When comparing two models, the best is the one with the lowest numerical value of the information criteria calculated for the same data-set. It must also be noted that in *BIC* free parameters are more strongly penalized than in *AIC*.

4

Measuring the bioprocess performance

Critical to the task of optimizing the performance of a given process is the ability to measure such performance. In algal processes in which the main product is the stored oil, it is necessary to have the ability to perform a fast and reliable measurement of both oil content and biomass concentration in the culture broth. There are several well-known and reliable methods to measure biomass concentration in algal cultures, including total cell dry weight, either by filtration or by centrifugation, and total cell count as presented in Chapter 3. For oil content determination, on the other hand, there is not a widely accepted standard method. Furthermore, all methods for either biomass or lipid content quantification are highly elaborate and time consuming and, therefore, unsuitable for control and real-time optimization purposes.

In this chapter, two different approaches for the off-line determination of the total neutral lipid content are considered. The first involves the extraction

and gravimetric quantification of total lipids, while the second relies on the labelling of neutral lipid with a fluorophore. Procedures for both approaches are developed and optimized in order to reduce measurement variability, sample size, and analysis time.

Raman spectroscopy is evaluated as a technique for the on-line determination of both biomass and oil content. The second part of this chapter covers the fundamentals on Raman spectroscopy as applied to bioprocess analysis, and the statistical and machine learning techniques used to develop a multivariate model for the on-line monitoring of algal growth.

4.1 Oil content in cells

Oil production and storage by microalgae is of increasing interest as several microalgae species are able to accumulate large amounts of oil, and because growth rate and productivity are higher in algae than in plants. As a result, microalgae are seen as an alternative source of oils for both biofuel production (i.e. biodiesel) and for nutritional purposes.

Neutral lipids in *Auxenochlorella protothecoides* can be accumulated at very high levels, representing more than 50% the dry weight of algal cells. Such accumulation is a response to changes in the cells environment including nitrogen limitation, alkaline pH, and changes in light. Oil is stored intracellularly in lipid bodies, which are involved in several metabolic processes. Variations in the external environment of the cell result in quick changes of the lipid content and composition of lipid bodies.

In order to identify those conditions that better induce lipid production and accumulation, as well as to measure the lipid productivity of algal cultures, it is necessary to have an accurate and reliable method to measure neutral lipid

content. Methods to quantify neutral lipids can be broadly divided into direct and indirect methods. Direct methods are those in which lipids are separated from the cellular matrix and then are quantified by either direct gravimetry, a quantitative chemical reaction, or chromatography. Indirect methods rely on measuring a physical or chemical property of the matrix containing the lipids, and correlating this property to the lipid content of the sample. For proper interpretation of the results obtained by indirect methods, they must be compared to direct measurements of the lipid content on representative samples in order to build a calibration model.

Direct methods for quantification of neutral lipids include: gravimetry, gas chromatography, and high performance liquid chromatography. These methods require as a first step the extraction and purification of the lipid classes of interest. Extraction can be performed by mechanical press, solvents, or a combination of these. Mechanical press is not a quantitative method of lipid extraction as the cell debris will remain saturated with lipids. Therefore, the use of solvent-only or solvent assisted extraction is required for analytical techniques. The selection of the extraction solvent is controlled by the polarity of lipid class of interest. When total lipid quantification is required a mixture of solvents, ranging from low to high polarity, is frequently used. In this work, however, we are concerned mainly with non-polar lipids, particularly triacylglycerol lipids (TAGs). TAGs are non-polar lipids with a glycerol backbone and fatty-acid side chains ranging in length from C12 to C24 (though shorter and longer chains are not forbidden). Therefore extraction solvent must be non-polar or very-weakly polar.

Indirect methods of lipid content quantification aim to reduce the complexity of lipid measurement by measuring a property of the sample that correlates to the oil content, but whose measurement is easier to carry out. Ideally

the indirect method will require little or no sample preparation, will be fast, cheap, and will not produce toxic residues. Spectroscopic methods usually satisfy most of these conditions. The use of fluorescence spectrometry for neutral lipid quantification is explored in Section 4.1.2, while in Section 4.2 Raman spectroscopy is proposed as a multivariate technique for quantifying algal cultures, including the quantification of neutral lipids. In a multivariate technique several characteristics of the culture are measured simultaneously as opposed to traditional univariate techniques in which only one variable is being measured.

As previously mentioned, indirect methods have to be calibrated using representative samples for which neutral lipid content has been previously determined. Therefore, it is necessary to develop a direct quantitation tool prior to the development and calibration of indirect methods. In Section 4.1.1, a protocol for the gravimetric quantitation of neutral lipids in *A. protothecoides* is given.

4.1.1 Gravimetric method

Gravimetric determination of neutral lipids in microalgal cells requires the extraction of the lipids from the cells, the removal of any possible contaminants from the extract, and the concentration of the lipids by removing the solvent. The oil content is then determined by comparing the initial weight of the sample with the weight of the lipid fraction recovered. The efficiency of each of these steps will affect the accuracy and precision of the lipid measurement. In this section the effect of solvent selection, cell disruption method, solvent extraction method, and sample size is studied. The recommended protocol for *Quantitation of Neutral Lipid in Microalgae* is presented in Appendix A.2.

Table 4.1: Polarity index (PI) and boiling point (BP) for several solvents commonly used for extraction of lipids.

Solvent	PI	BP, °C
1,1,2 Trichlorotrifluoroethane	0.0	48
Pentane	0.0	36
Hexane	0.1	69
Ethyl Ether	2.8	35
Dichloromethane	3.1	40
Isopropanol	3.9	82
Chloroform	4.1	61
Acetone	5.1	56
Methanol	5.1	65
Dimethyl Sulfoxide (DMSO)	7.2	189
Water	10.2	100

Selection of solvent for extraction

Solvent selection is mandated by the polarity of the target lipid class. Common solvent systems for lipid extraction include hexane, chloroform/methanol, ethanol/tri-chloroacetic acid, isopropanol, and hexane/isopropanol. The polarity index of a solvent, shown in Table 4.1, is a relative measurement of the strength of interaction between the solvent and a reference polar solute. The higher the polarity index is, the less neutral the solvent is.

Hexane and hexane/isopropanol mixtures are considered here as they are neutral or weakly polar, and therefore only non-polar lipids will be extracted. Furthermore, both hexane and isopropanol have low toxicity and their use in the food-oil industry is accepted and generally regarded as safe.

To evaluate the effect of the solvent type on lipid quantitation, a known mass of freeze-dried algal cells (approximately 1.0 g) was ground for 15 minutes using a mortar and pestle system, and later extracted using either a technical mixture

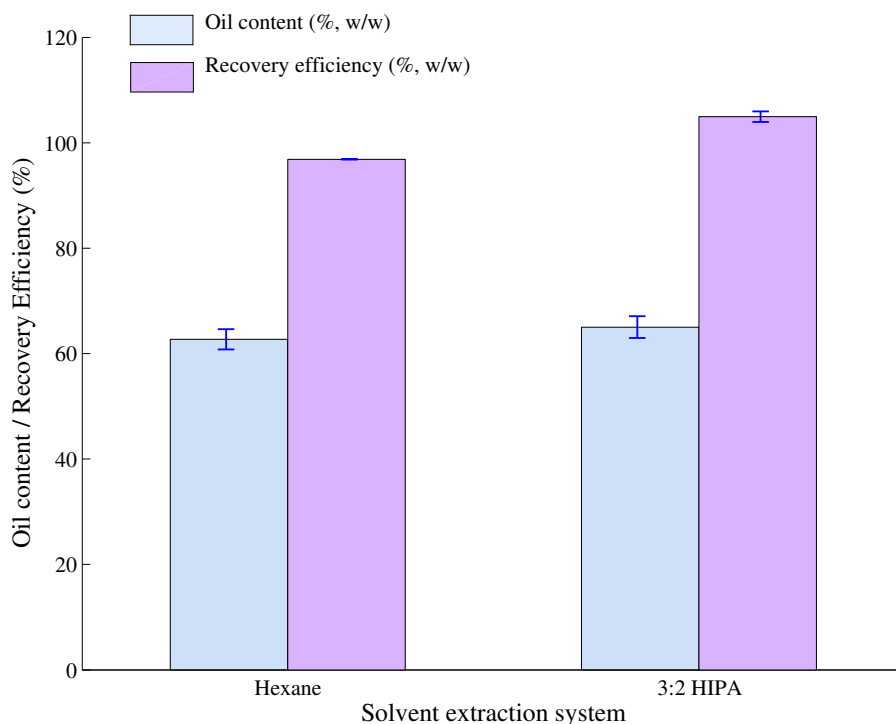


Figure 4.1: The effect of the solvent extraction system on the measured oil content and the recovery efficiency. 3:2 HIPA contained 3 volumes of hexane per each 2 volumes of iso-propanol.

of hexanes, or a solution of 3 parts in volume of hexane and 2 parts of iso-propanol (3:2 HIPA). The solvent was separated by vacuum filtration from the cell debris and left to evaporate until constant weight was reached. Measured oil content is shown in Fig. 4.1, as well as the total recovery efficiency. That is the sum of the oil and the cell debris fraction divided by the initial sample weight, and expressed as percentage.

The selection of solvent for extraction does not appear to have a significant effect on the amount of oil recovered nor the recovery efficiency. The higher total recovery for the 3:2 HIPA system, greater than 100%, may be due to the lower volatility of iso-propanol, which can cause it to remain as a contaminant.

Cell disruption

To evaluate the effect mechanical techniques of cell disruption have on the efficiency of the oil extraction, six different methods were used:

- i. No cell disruption (control), cells were mixed with a solution of 3:2 HIPA and mixed on an orbital shaker, at 100 rpm for 24 hours;
- ii. Heating, cells were mixed with 5 mL of IPA, boiled at 80 °C, and volume was completed to 10 mL by adding 3:2 HIPA, and vigorously shaken by hand for 6 minutes, at intervals of 1 minute;
- iii. Grinding, cells were ground using a mortar and pestle for 15 minutes;
- iv. Homogenizing, Cells were homogenized at 30000 rpm using a Polytron 1300D mixing unit (Kinematica AG);
- v. Sonication, an aqueous suspension of algal cells was sonicated on a Branson B-52 ultrasonic bath with 240 W input power;
- vi. Microwaving, cells were suspended on a 1:5 v/v solution of water and isopropanol and microwaved for 2 minutes with a 20 W input power.

The measured oil content obtained by using different cell disruption methods is shown in Fig. 4.2. Among the different disruption methods compared, homogenization of the cells produced the highest average oil recovery. The variability between repeated measurements in this case, however, was much higher than for the other methods, and consequently the measured oil content when the homogenizer was used was not statistically different than for the mortar and pestle system. The high variability associated with the use of the homogenizer is likely due to the difficulty in recovering the cell debris (and associated oil) from the internal mechanism of the homogenizer. Cell

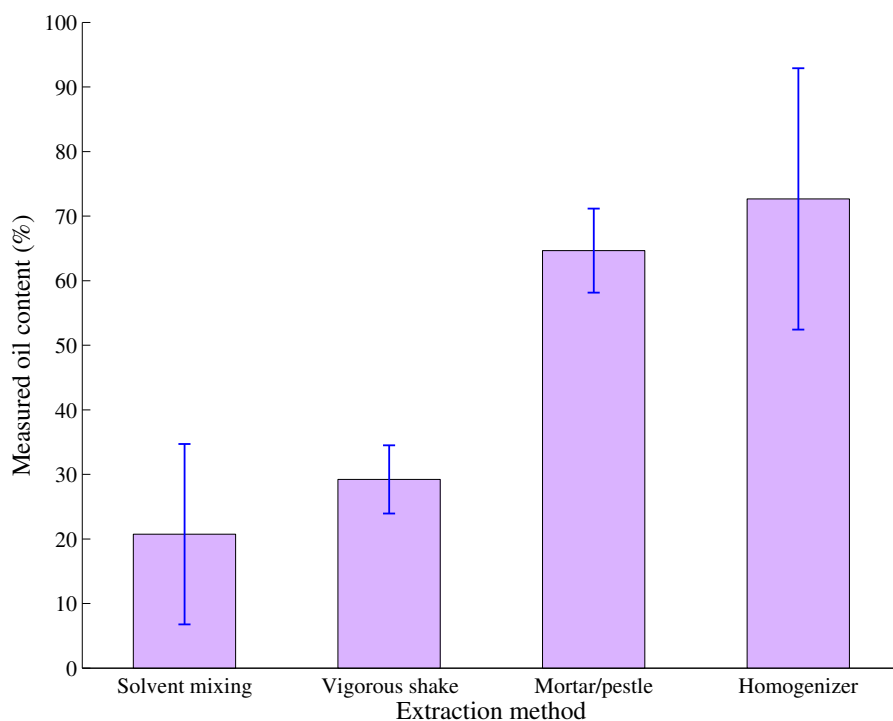


Figure 4.2: The effect of the cell disruption method on the measured oil content of a dry sample of *A. protothecoides*.

disruption by using the mortar and pestle also achieved a high recovery of oil, with a considerably lower variability in the results. The other methods have a lower recovery efficiency.

Sonication failed at generating any significant disruption of the cells, as observed in Fig. 4.3. A cell suspension was subjected to sonication for 10 min, 30 min, and 60 min. However, even after 60 min cells appeared intact in the microscope. Previously, Pernet and Tremblay (2003) found that the effect of sonication on the oil extraction in the diatom *Chaetoceros gracilis* was somehow obscure and contradicting, while Lee et al. (1998) observed an slight increase in oil recovery when sonication was used for disrupting the cells of

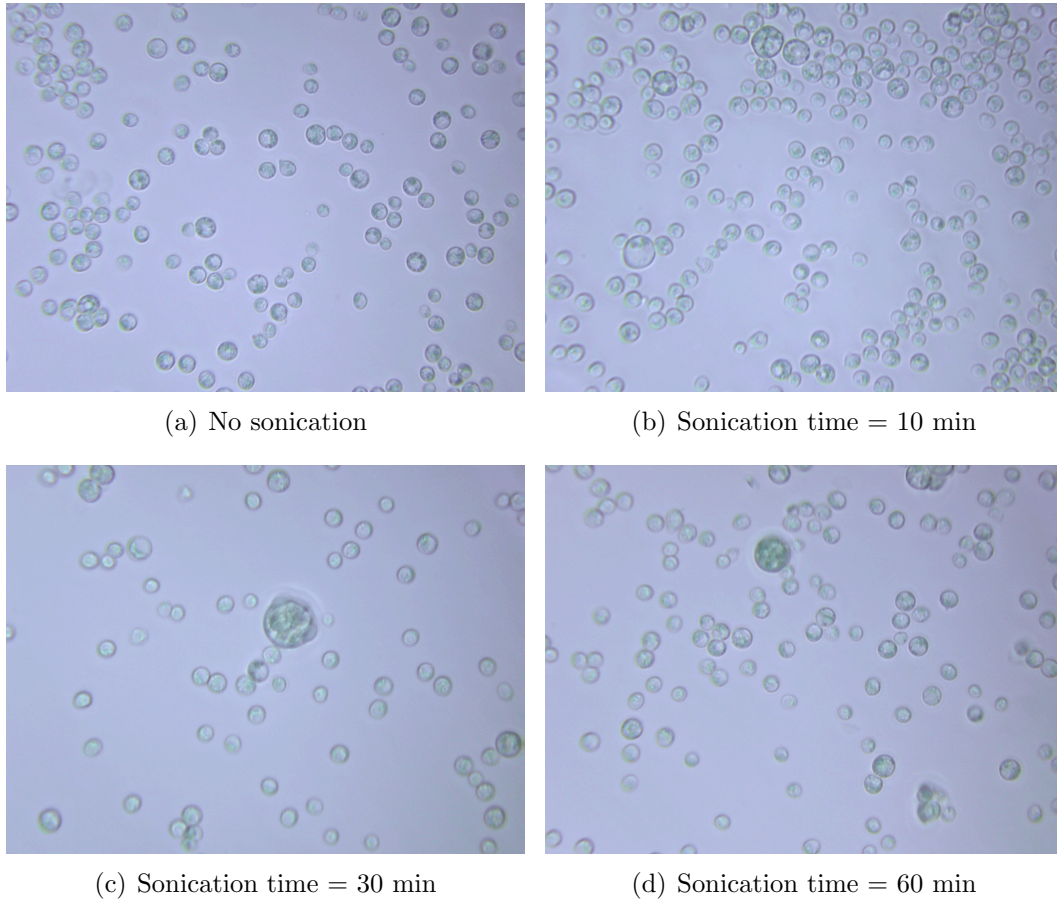


Figure 4.3: Microphotographies of *A. protothecoides* cells subjected to sonication. There were not observable differences between sonicated, and unsonicated cells.

Botryococcus braunii. The sonication nominal input power used by Pernet and Tremblay (2003) was 50 W, while Lee et al. (1998) did not report the conditions used. Alga cell wall has in general a high elasticity module, while cells are essentially incompressible (Miyoshi, 1972). This translates in a high energy requirement to achieve cell disruption, which given the results in Fig. 4.3 were higher than the input power (20 W) used here.

The effect of microwaving on cell disruption was not quantified due to the poor recovery of cells after microwave treatment. When the container was kept closed intensive evaporation caused the container to break, and when the container was kept open algal cells were splattered around. To evaluate the feasibility of using microwaves for disrupting the cell wall it is suggested that future research should initially focus on the design of a tight and safe container for holding the cells while they undergo the microwave treatment.

Sample size

The effect of sample size on the quantitation of oil in algal samples was evaluated for the single solvent (hexane) extraction method. From Fig. 4.4 it can be seen that for the larger sample size (1.0 g) there was a significant variability between replicates, while variability was minimum for the intermediate sample size (0.5 g). The larger variability in the larger sample size can be due to improper grinding of the sample, which might be reduced by increasing the grinding time. In general the estimated oil content is not significantly affected by the sample size, though it will be necessary to optimize the grinding step to ensure samples are homogeneously ground.

4.1.2 Fluorometric method

Quantitation of neutral lipids using the previously discussed gravimetric method is labor and time intensive. Fluorescence spectroscopy offers an alternative way to quantify the lipid content, provided that an appropriate fluorescence marker is available. Nile Red (9-diethylamino-5H-benzo[α]-phenoxazine-5-one) has been proposed as an *in-situ* lipid marker with the advantage of having a strong fluorescence in non-polar environments, while its fluorescence is quenched in water (Greenspan and Fowler, 1985; Fowler et al., 1987). It has been used,

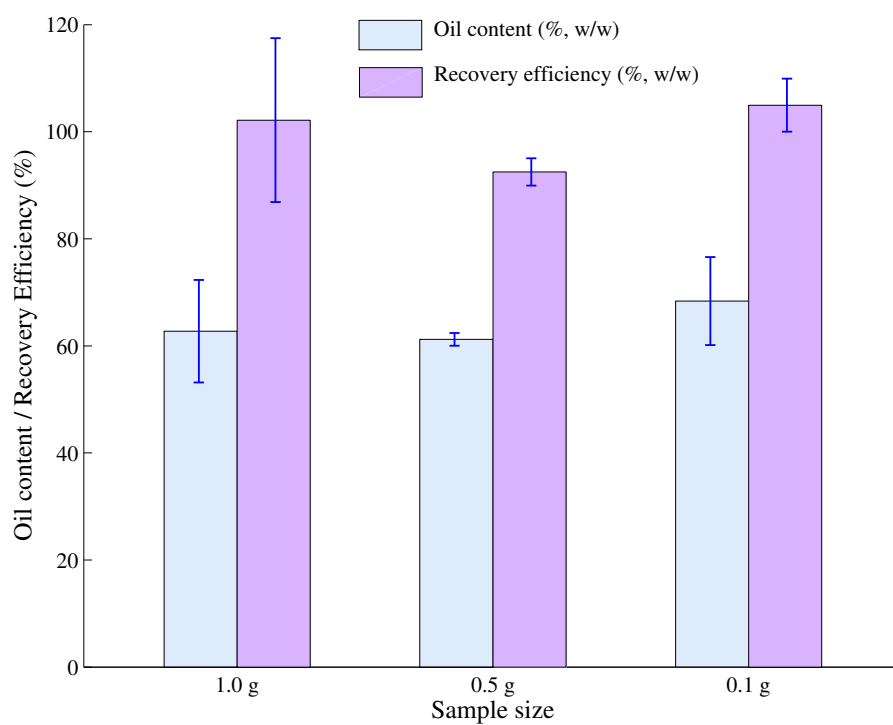


Figure 4.4: The effect of the sample size on the measured oil content and the lipid recovery efficiency, using the single solvent (hexane) extraction procedure.

with relative success, for measuring the lipid content in microalgae (Lee et al., 1998; Elsey et al., 2007; Huang et al., 2009), while Chen et al. (2009) proposed a protocol to use it as a high-throughput method for quantitation of neutral lipids in microalgae.

Staining of algal cells with Nile Red

The excitation and emission spectra of *A. protothecoides* cells stained with an ethanolic solution of Nile Red ($10\mu\text{g}/\text{mL}$) are shown in Fig. 4.5. The maximum fluorescence count happens at an excitation of 530 nm and emission of 580 nm. The reported spectrum is noisy and there are some extra peaks in the excitation spectra. The noisy signal can be explained by the particulate nature of the sample, and the heterogeneity of cell structures, while the extra peaks can correspond to differences in the absorption properties of different lipids classes in the cells. The average standard deviation among five spectra replicates was 0.78%, with a maximum variation of 3.8% with respect to the mean count.

The different peaks observed in the spectra correspond to differences in the absorption properties of different lipids classes, or other structures, in the cells. Elsey et al. (2007) reported that Nile Red fluorescence maximum emission shifts to higher wavelengths as polarity of the medium increases, being 576 nm for hexane, 600 nm for chloroform, and 632 nm for ethanol. Therefore, it is expected to observe different absorption bands in a cellular sample as it will contain different lipid classes of varying polarity.

Fig. 4.6 presents the average fluorescence emission and excitation spectra for two algal samples with different oil content. It can be seen that for the oil-lean sample there are two peaks on emission spectra, the one at around 590 nm corresponds to the expected emission band for Nile Red in a non-

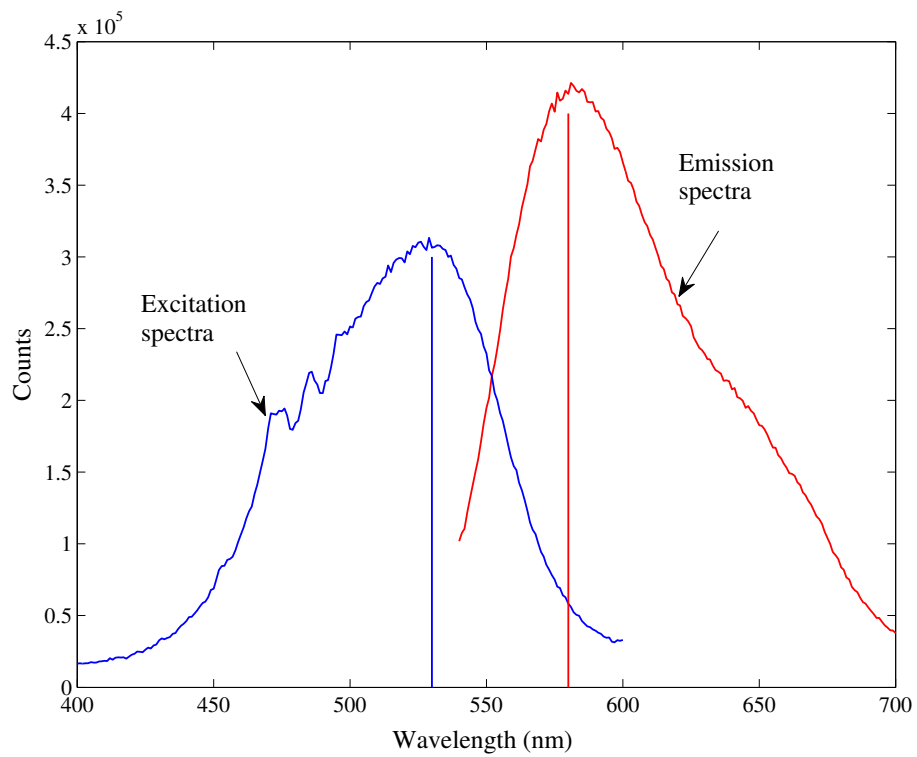


Figure 4.5: Excitation and emission spectra of *Auxenochlorella protothecoides* cells stained with an ethanolic solution of Nile-Red.

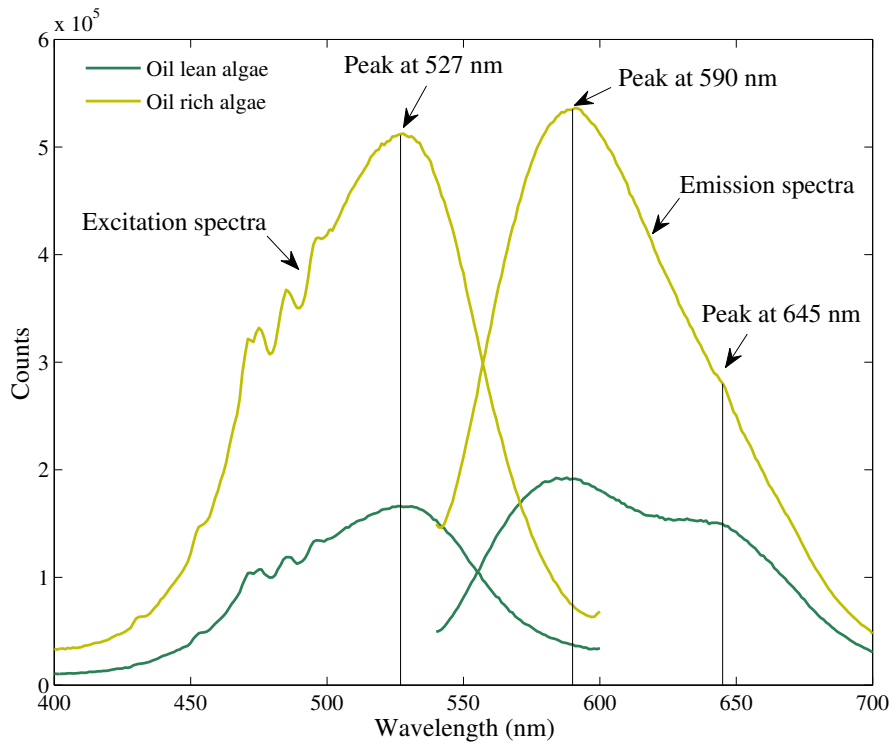


Figure 4.6: Effect of the intracellular oil content on the excitation and emission spectra of *A. protothecoides* cells stained with an ethanolic solution of Nile Red.

polar environment, while the one at around 645 nm indicates the presence of a more polar lipid environment. This indicates that Nile Red could be used to selectively quantify neutral lipids in algal samples. Moreover, it can be seen that the fluorescence intensity increases with increasing oil content.

Chen et al. (2009) proposed a staining procedure for use in microplates, requiring small sample volumes and with a relatively short total analysis time, as several samples can be analyzed at the same time in a multiwell microplate. This staining procedure is modified here, substituting DMSO with ethanol as the carrier solvent. The reason for this change is that there is not a significant difference in the fluorescence intensity of stained cells using either ethanol or

DMSO, as shown by Chen et al. (2009), while ethanol poses a lower health risk for routine use than DMSO does. The basic procedure is as follows:

1. 10 μL of an algal suspension of known biomass concentration was added to the measurement well of the microplate. Algal suspensions were prepared at a concentration of 10 g/L (dry weight), unless stated otherwise.
2. A 10 μL aliquot of a 10 $\mu\text{g}/\text{mL}$ Nile Red solution in ethanol was added to each well of a 96-microplate;
3. The volume in each well was completed to 200 μL by adding an aqueous ethanol solution;
4. Samples were incubated at 40 °C for 10 min; and,
5. Fluorescence emissions were recorded at excitation and emission wavelengths of 530 nm and 604 nm, respectively.

To determine the dependance of the fluorescence intensity with respect to the biomass and the carrier-solvent concentrations, aliquots of a suspension containing algal cells with an oil content of $50.2 \pm 0.9\%$ (w/w), as determined gravimetrically after hexane extraction, were diluted to a variable biomass concentration and stained using a carrier solution with a varying concentration of ethanol. Fluorescence measurements were performed in triplicate, and the results are reported in Fig. 4.7.

From Fig. 4.7, it is observed that fluorescence intensity increases non-linearly with increasing biomass concentration. Therefore, it is advisable to perform the fluorescence measurements at a constant biomass concentration, or to include the effect of biomass concentration in the calibration model. Furthermore, there is a continuous decrease on the fluorescence intensity as ethanol

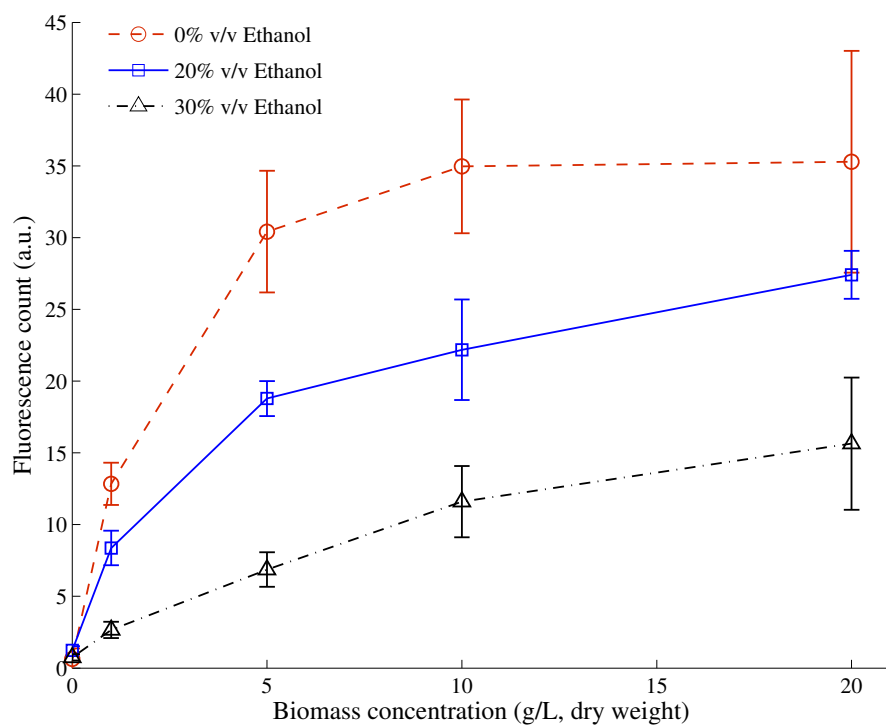


Figure 4.7: Effect of the concentration of the carrier solvent on the fluorescence count of *A. protothecoides* cells stained with Nile Red as a function of the biomass concentration.

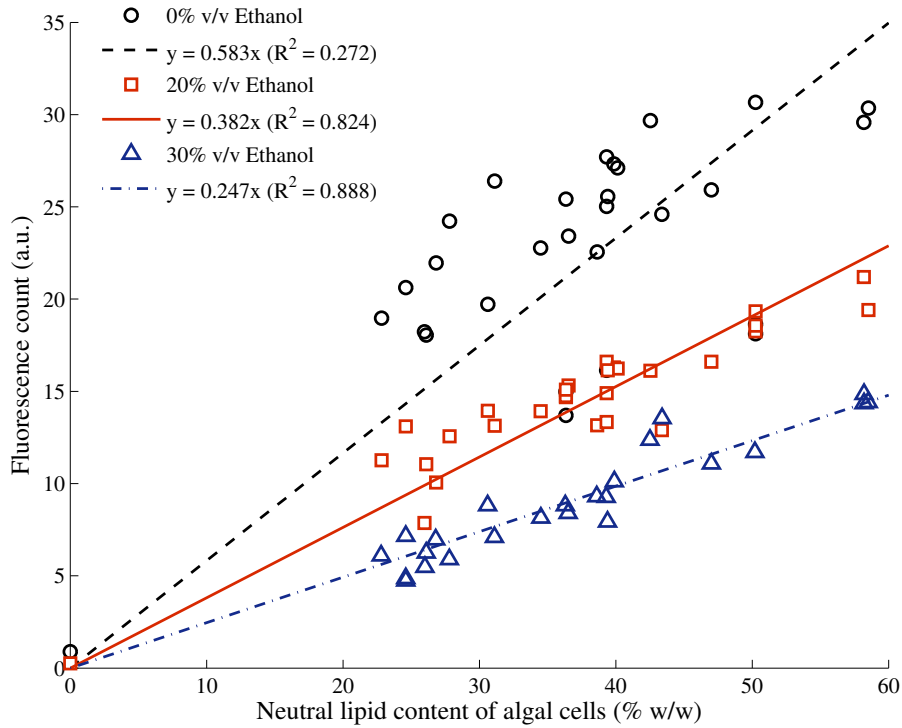


Figure 4.8: Correlation between the fluorescence count of Nile Red stained cells and the neutral lipid content of the algal cells determined gravimetrically, after hexane extraction.

concentration increases, which is different from the results for DMSO reported by Chen et al. (2009).

The effect of solvent addition on the correlation between neutral lipid content and fluorescence intensity is examined by preparing algal samples of varying oil content and staining them as per the basic procedure. Fig. 4.8 shows that the use of ethanol improved the correlation between fluorescence measurements and neutral lipid content. Consequently, hereinafter fluorescence measurements are performed at a constant biomass concentration of 5 g/L (dry-weight basis), using a solution of 30% v/v of ethanol in water.

Reducing the variability in fluorescence measurements

The measurement of fluorescence in algal suspensions is subject to significant variability, as can be concluded from the large error bars in Fig. 4.7, which corresponds to two times the sample standard deviation or approximately a 95% confidence limit. It is necessary to reduce this variability before using Nile Red fluorescence as a quantitative tool to estimate the oil content in algal cells.

The effect of the staining agent concentration, as well as the effect of the incubation time given for staining, on the relative standard error was calculated at two different Nile Red concentrations, and for incubation times of 0, 10, 20, and 30 minutes. Incubation was done at 40°C.

As shown in Fig. 4.9, for incubation times shorter than 20 minutes there was significantly more error on the measurements done with the lower concentration of Nile Red, which can be due to an excess of biomass with respect to the staining agent, causing an inhomogeneous staining of the cells. Staining time did not considerably affected measurement error, except for the longest incubation time.

The inter-sample variation in fluorescence count was determined by preparing either a full or a half 96-well microplate with replicates of the same algal sample and measuring the fluorescence count. In Table 4.2 several statistics for the inter-sample variability are presented. Statistically, the variation in a population is quantified by the standard sample deviation, or by its robust counterpart the median absolute standard deviation (MAD). Another measured of variability is the range, which is the length of the smallest interval containing all the measurements. Given that the range is highly influenced by the presence of an outlier, a robust estimation of the spread is the interquartile

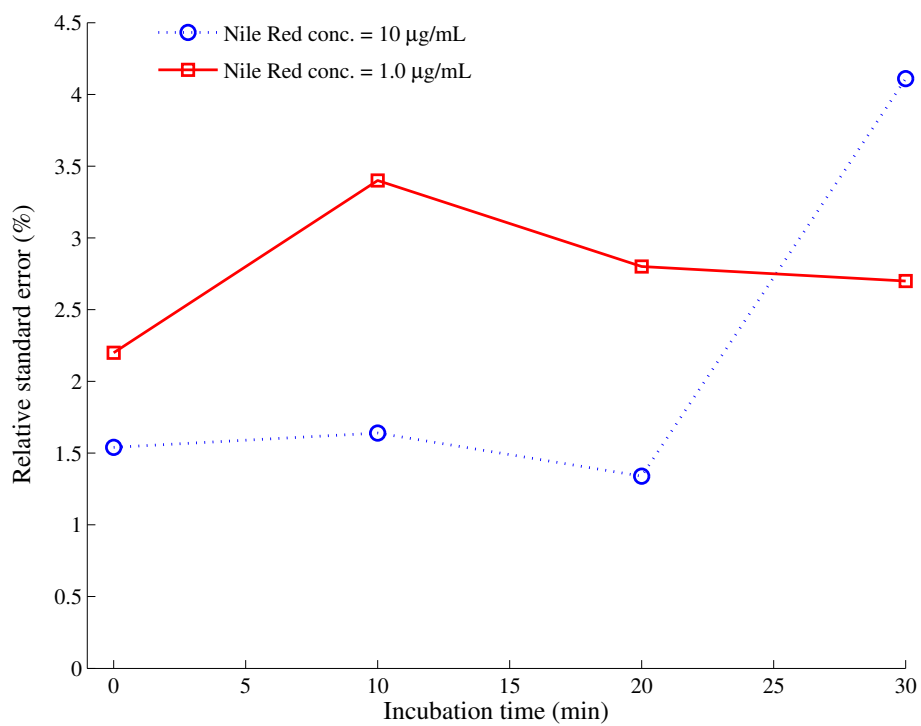


Figure 4.9: Effect of the Nile Red concentration and the incubation time on the relative standard error of fluorescence measurements.

Table 4.2: Effect of mixing on the inter-sample variability of oil concentration estimates based on the Nile Red fluorescence measurements for an algal sample containing $50.2 \pm 0.9\%$ (w/w) oil content, as determined gravimetrically with hexane extraction.

Treatment	STD	RSD	MAD	Range	IQR	N
Mix-in-well, 600 rpm, $v_w = 200\mu L$	4.1	8.2	3.2	24.2	5.2	96
Premixed, $v_w = 200\mu L$	2.4	4.9	1.9	12.3	3.3	96
Mix-in-well, 1200 rpm, $v_w = 200\mu L$	3.2	6.4	2.0	21.7	2.7	47
Mix-in-well, 1200 rpm, $v_w = 120\mu L$	2.2	4.4	1.6	12.2	2.3	47

Reported values are percentage (%) on weight basis.

All measurements were done on a sample containing 10 g/L of biomass.

STD: sample standard deviation; RSD: relative standard deviation (%); MAD: median absolute deviation is a robust measure of the variability of quantitative data; IQR: interquartile range or midspread is a robust measurement of the statistical dispersion; N: number of replicates; v_w : total volume of sample in the well.

range (IQR).

Variations in the fluorescence count were found to be due to both mixing effects, as well as inherent variability of fluorescence readings. Improvement in sample mixing, either by premixing or by modifying mixing parameters reduced measurement variability. Sample standard deviation was reduced by 56% when mixing all the reagents before distributing the sample in the microwells, as shown in Table 4.2. This implies that 56% of the inter-sample variation is due to volumetric measurement error or mixing effects. By modifying mixing parameters (doubling the rpm) a reduction in both sample standard deviation and spread range is observed, as presented in Table 4.2.

When the mixing rate was increased to 1200 rpm, spillover of the content of the microwells was observed. A reduction in the total well volume, from $200\mu L$ to $120\mu L$, prevented this spillover. The variability for these two datasets was

comparable in terms of the fluorescence count. However, given that the volume reduction results in a larger fluorescence count due to a lower dilution, it is beneficial as it translates into a reduced relative error in the oil measurements, as shown in Table 4.2.

The reduction in the measurements variability achieved by modifying the analysis volume and mixing parameters represents a significant improvement with respect to previous protocols for lipid quantification using Nile Red. For instance, Chen et al. (2009) reported a relative standard deviation of 8.5% for the Nile Red quantification among replicate measurements using a triolein standard. The relative standard deviation of the measurements performed here on a microalgal suspension sample was reduced from 8.2% to 4.4%, which represents a 48% reduction in the relative variability between replicates with respect to the original measurement protocol as presented by Chen et al. (2009).

Repeated resampling of the replicate fluorescence measurements, followed by a t-test hypothesis test, showed that when five measurements were selected at random, the mean and variance of the selected five measurements were statistically equal to the mean and variance of the full dataset containing the 47 measurements, more than 96% of the time. Therefore, by performing only five replicate measurements, it is expected to achieve the error bounds presented in Table 4.2.

After reducing the sources of variability, a correlation between Nile Red fluorescence measurements and oil content determined gravimetrically after hexane extraction gave a correlation coefficient R^2 greater than 0.99. Due to variations in the excitation light intensity, due to lamp aging, as well as other sources of day to day variation in the fluorometer, the use of an internal standard for recalibration is required with each plate that is run.

Use of Bodipy as an alternative fluorophore

Gocze and Freeman (1994) previously studied the variability of fluorescence measurements of lipid droplets in tumor cells, using Nile Red as staining agent. They reported that the variability in measurements was due to the Nile Red itself. By using a different dye (4,4-Difluoro-1,3,5,7,8-pentamethyl-4-bora-3A-4A-diaza-S-indacene, aka Bodipy) variability was reduced 44%. More recently, Cooper et al. (2010) used Bodipy for *in-vivo* visualization of lipid bodies in algal cells, and as a dye of choice for fluorescence activated cell sorting aimed at selecting cells with high neutral-lipid content. Given the superiority of Bodipy in visualization applications, compared to Nile Red, it is of interest to evaluate the potential use of Bodipy as a quantitative stain as an alternative to Nile Red in microplate fluorometry.

Algal suspensions were stained with a solution of the lipid probe Bodipy 505/515 in DMSO, following the procedure outlined by Cooper et al. (2010). Fluorescence microscopy shows that the Bodipy probe is highly selective for neutral lipids, with a strong fluorescence of the liposomes and a very low signal from other cellular structures, as presented in Fig. 4.10.

However, when the excitation and emission spectra were recorded for cells with different oil content, in a similar way as presented in Fig. 4.6 for Nile Red, no significant differences were observed, as shown in Fig. 4.11. Furthermore, when algal suspensions varying in biomass concentration were stained with equal amounts of Bodipy, no significant differences in fluorescence count were observed. These results imply that even though Bodipy preferentially binds to neutral lipids, the binding is not proportional to the amount of lipid in the cells and therefore Bodipy is unsuitable as a quantitative probe for neutral lipids.

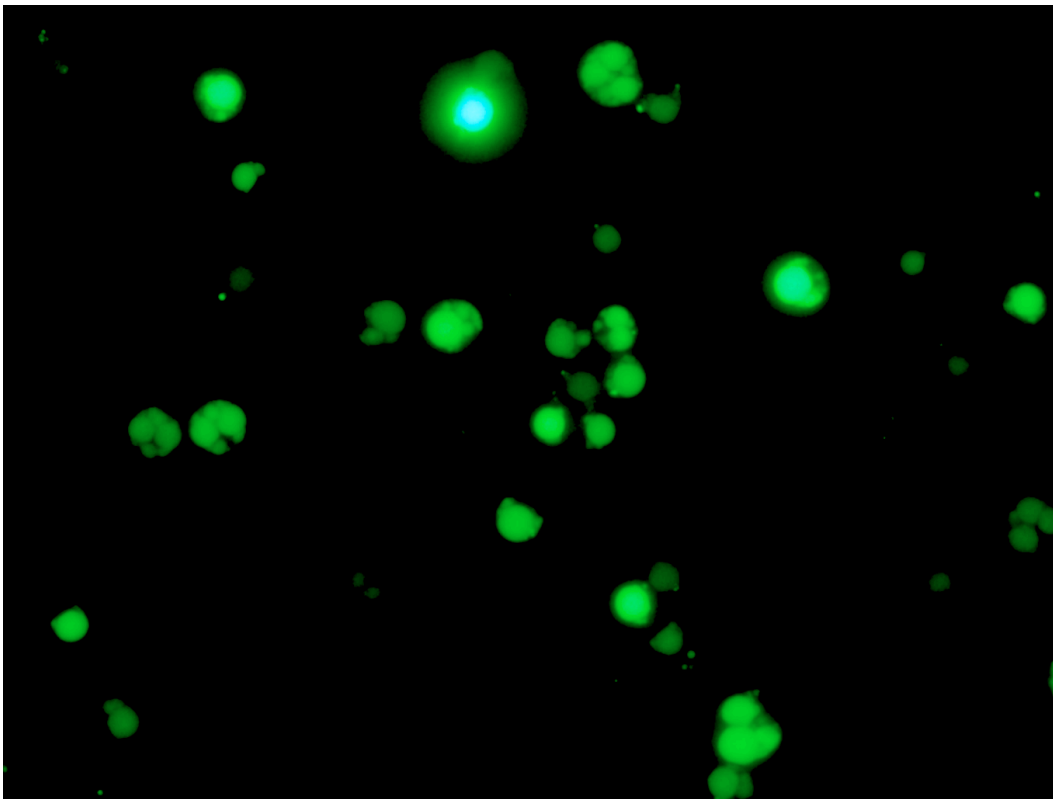


Figure 4.10: Microphotographs of *A. protothecoides* stained with the lipid probe Bodipy 505/515

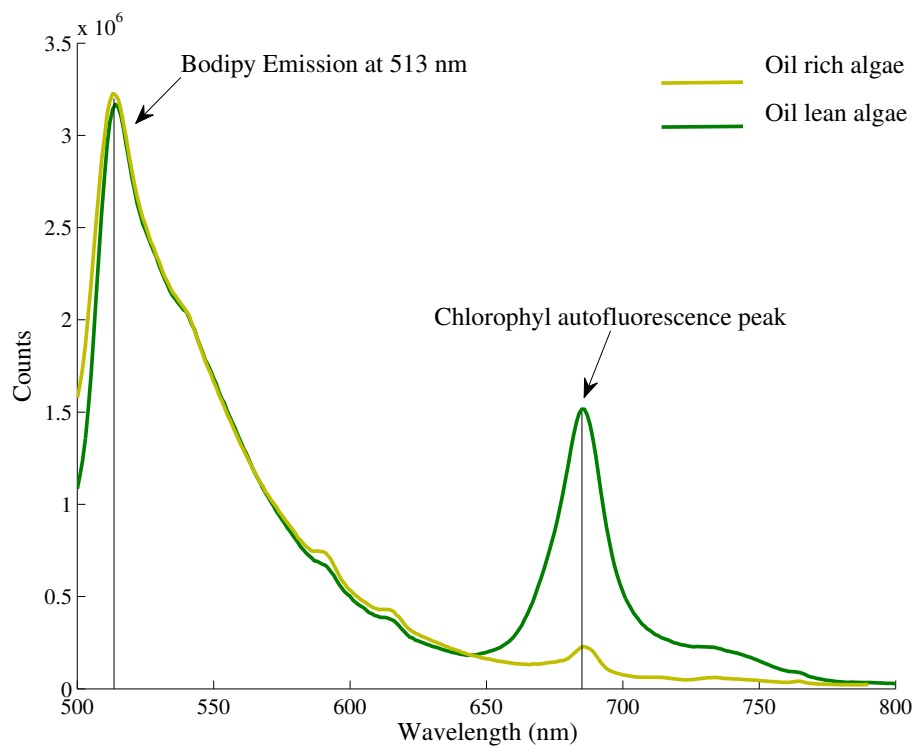


Figure 4.11: Emission spectra of *A. protothecoides* cells stained with Bodipy 505/515, with excitation at 485 nm. Note that there was no significant difference between the emission counts for the two algal samples, except for the autofluorescence peak at 685 nm corresponding to chlorophyll.

4.2 On-line monitoring of microalgal cultures using Raman spectroscopy¹

Raman spectroscopy is a technique used to study the vibrational, rotational, and other low-frequency modes in a molecular system. It is based on the inelastic scattering of a monochromatic excitation source. Akin to infrared spectroscopy, it is useful to identify the molecular structure of an unknown compound or can be used as a chemical fingerprint. Raman spectroscopy has been proposed as a multivariate process analytical technique for several chemical and biochemical systems.

In this section, we study the spectral characteristics of microalgae, medium components, and microalgal cultures in general. A chemometric model is then developed to correlate the spectra of culture samples to their chemical composition.

4.2.1 Spectra of algal Biomass

The spectra of biological samples is rather complex due to the presence of several thousands of chemical components in the sample. Furthermore, some of these components can have a fluorescent effect.

The spectra of freeze-dried cells of *A. protothecoides* is shown in Fig. 4.12. In this case, the spectra were collected ten times, at regular intervals. After each collected spectra, the total exposure time of the sample to the laser source was consequently higher. In Fig. 4.12, it can be seen that total Raman count decreased as exposure time to the laser increased. This result indicates that

¹Some parts of this section were developed in collaboration with N.S. Venkat Raghavan, and have been accepted for publication. N.S.V. Raghavan *et al.* 2011. Chemometrics and Intelligent Laboratory Systems, DOI: 10.1016/j.chemolab.2011.09.007.

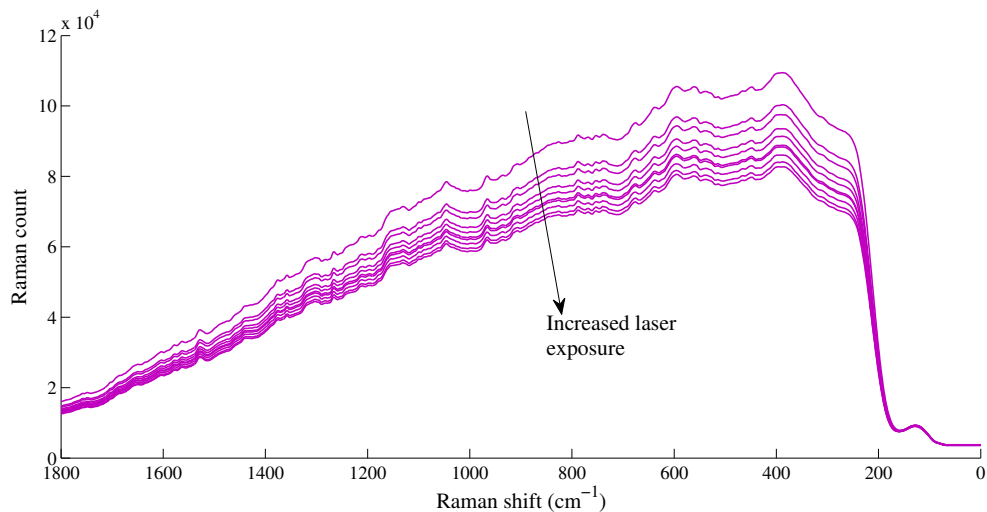


Figure 4.12: Unprocessed (raw) Raman spectra of algal biomass powder. Spectra were collected one after the other, increasing at each collection the total exposure time to the laser. Background fluorescence decreases with increasing exposure time.

there was background fluorescence coming from the sample, as photo-bleaching usually results in a significant reduction in the intensity of the fluorescent background.

To eliminate the effect of background fluorescence a piecewise linear baseline removal algorithm was implemented. In Fig. 4.13, the same ten spectra previously presented in Fig. 4.12 are shown after baseline removal. It can be seen that the effect of background fluorescence has been almost completely eliminated.

The same baseline removal algorithm was applied to a set of spectra collected from algal samples cultured under different conditions. These baseline-corrected spectra are shown in Fig. 4.14. Two of the algal samples were cultured using glucose as the carbon substrate, while the third sample was grown on glycerol.

4.2. On-line monitoring using Raman spectroscopy

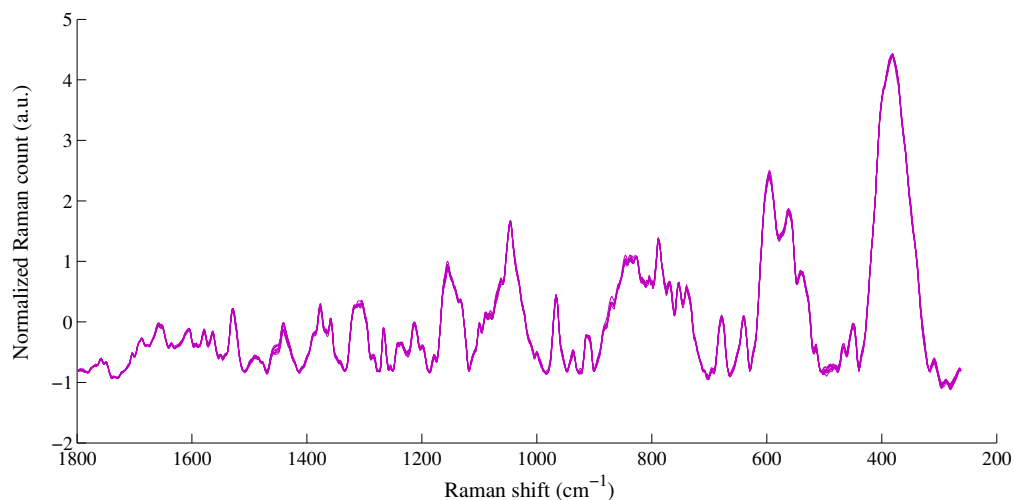


Figure 4.13: Raman spectra of algal biomass powder after piecewise linear baseline removal.

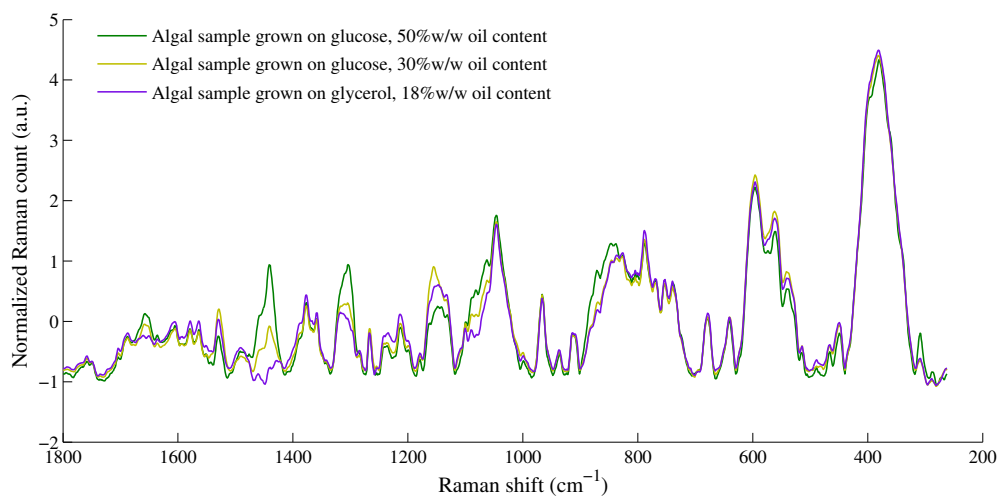


Figure 4.14: Raman spectra of algal biomass powders with varying oil content after piecewise linear baseline removal.

From Fig. 4.14, it can be seen that there are three peaks that are clearly dependent on the algal composition, these are in the regions around 1440, 1655, and 1305 cm^{-1} . The algal sample grown on glycerol has the lower oil content (approximately 18% w/w) among the samples reported in the figure. For this sample, the peaks at 1440 cm^{-1} and 1655 cm^{-1} are almost inexistent, indicating that these two peaks are related to the oil content in the cells.

4.2.2 Oil spectra

To further explore the regions in the Raman spectra that are related to the oil content and composition, oil samples derived from oil palm, flaxseed, and sunflower were analyzed and their spectra were processed as previously shown. The baseline-corrected spectra of the three oil samples and that of algal cells are shown in Fig. 4.15.

The three peaks previously identified as composition dependent in the dry

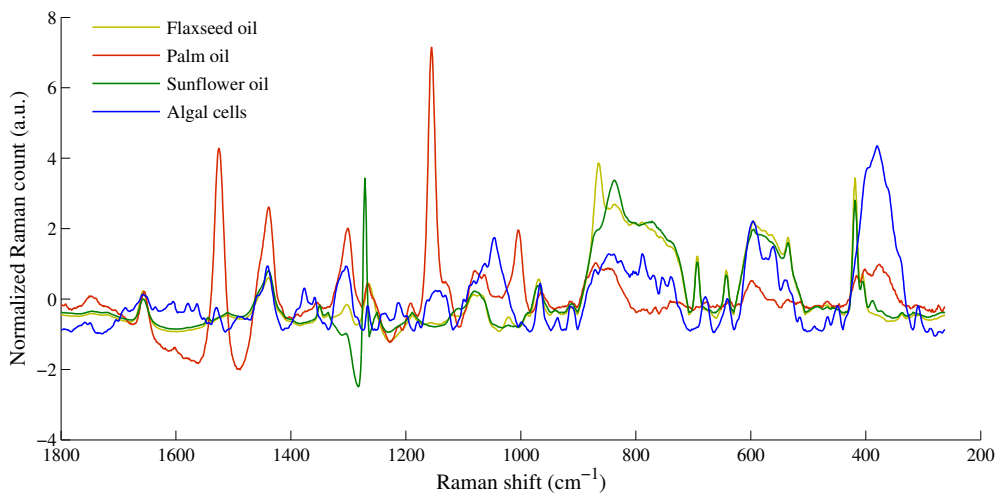


Figure 4.15: Raman spectra of different vegetable oils after piecewise linear baseline removal. Spectra of algal cells is included for reference.

algal spectra, were also present and clearly defined in the Raman spectra of the vegetable oil samples examined. The peak at 1440 cm^{-1} , that extended from $1410 - 1480\text{ cm}^{-1}$, is in the region normally associated to saturated carboxylic acids and carboxylate groups; the peak at 1655 cm^{-1} , with a range from $1640 - 1670\text{ cm}^{-1}$, corresponds to a characteristic absorption band of double bonds (C=C); and the peak at 1305 cm^{-1} , from $1280 - 1330\text{ cm}^{-1}$, is a characteristic absorption frequency of unsaturated esters (Ning, 2005).

There are some peaks present in the spectra of the algal and palm oil sample, but not in the spectra of the sunflower or the flaxseed oil. These are in the region from $1120 - 1180\text{ cm}^{-1}$ and the region from $320 - 440\text{ cm}^{-1}$. Even though it is difficult to associate these peaks to specific functional groups, it is expected that these regions will be related to the carotenoid content that causes the red colour in both palm oil and algal cells. Carotenoids are complex molecules with multiple functional groups (alcohols, ketones, phenyl groups, etc), several of which have characteristic absorption bands in the indicated frequencies.

4.2.3 Spectra of media components

To determine if Raman spectroscopy is sensitive enough to detect the compounds present in the culture media, aqueous solutions containing the analytes of interest were prepared at concentrations typically found in the cultures. For each solution, Raman spectra was measured 5 to 10 times, and compared with the spectra of pure water. In order to determine if there are significant characteristics in the spectra, the average spectra of each solution was subtracted from the average spectra of water and the difference was plotted together with the noise of the instrument. Peaks that fall outside the noise region are significant at the 95% confidence level, as the plotted noise area corresponds

to $\pm 2\sigma$, with σ being the noise standard deviation at each wavenumber. These results are shown in Figs. 4.16 to 4.19

In Fig. 4.16(a) it can be seen that the glucose fingerprint is significant in several regions of the Raman spectra. In total eight Raman modes are detected with a significance at 95%: 423, 445, 516, 900, 915, 1063, 1125, and 1360 cm^{-1} . Another two modes are present below the 95% confidence level: 1462 and 840 cm^{-1} . Among the other main media constituents, only magnesium sulphate has a detectable Raman mode (at 980 cm^{-1}). Therefore, it is expected that in complex media only glucose and magnesium sulphate will have a detectable fingerprint on the Raman spectra.

4.2.4 Multivariate model building

The wealth of data generated by Raman spectroscopy would be useless without the proper means to extract the desired information (Shaw et al., 2000). Multivariate mathematical and statistical modelling techniques, namely chemometrics, are used to extract meaningful information from the spectral data (McGovern et al., 2002; Jarvis and Goodacre, 2005). The final goal of the chemometric process is to find a model or mapping that will correctly associate the inputs, i.e. spectral data, with the outputs, i.e. composition values (Goodacre, 2003).

Chemometrics methods are powerful, but special care must be given to the interpretation of the results obtained, as statistical analysis might appear more impressive than what they really are (Shaw et al., 2000). In order to develop a robust model, three independent datasets are usually recommended: one to build the model, one to validate it, and one for testing the model performance (Shaw et al., 2000). This last dataset should contain observations that are not used during the modelling process.

4.2. On-line monitoring using Raman spectroscopy

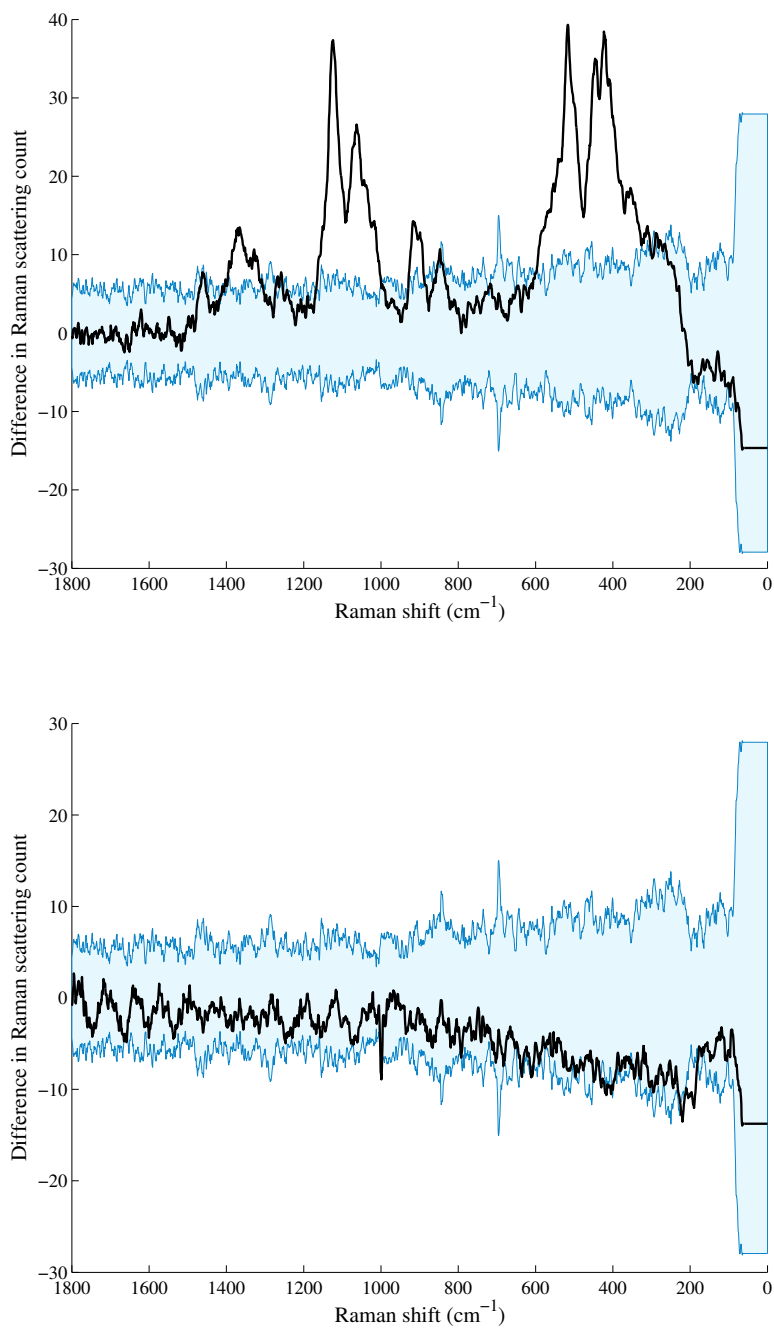


Figure 4.16: Raman spectra of (a) glucose (40 g/L) and (b) glycine (1 g/L) solutions in water. Water spectra was subtracted from raw solution spectra. Shaded blue area corresponds to $\pm 2\sigma$, with σ being the noise standard deviation at each wavenumber.

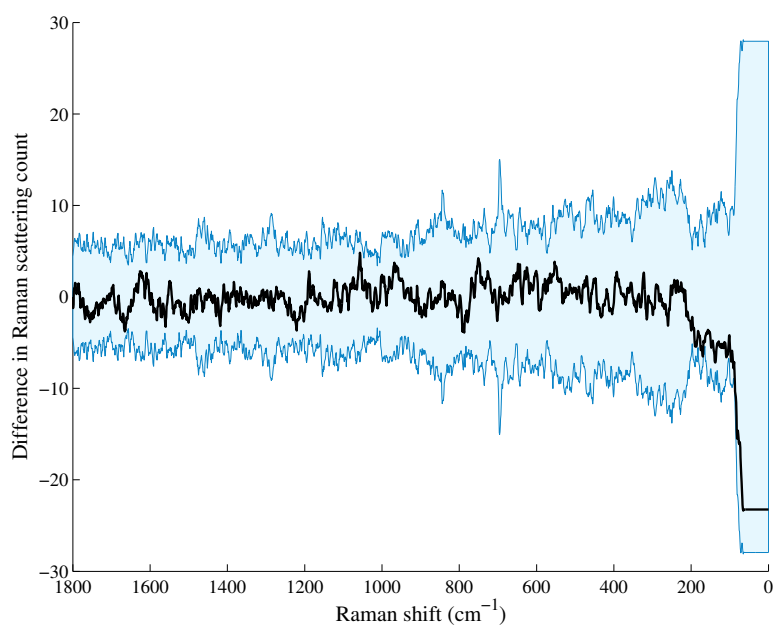
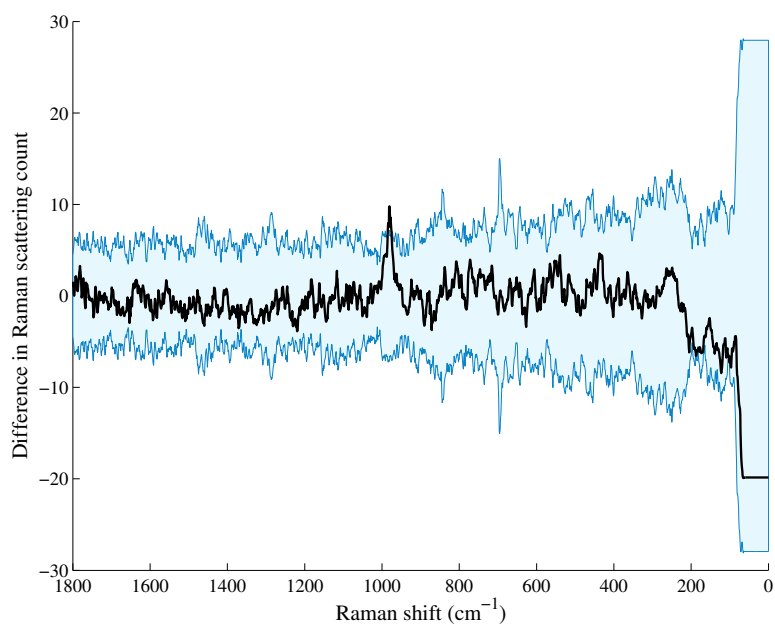


Figure 4.17: Raman spectra of (a) MgSO₄ (1.2 g/L) and (b) FeSO₄ (0.048 g/L) solutions in water. Water spectra was subtracted from raw solution spectra. Shaded blue area corresponds to $\pm 2\sigma$, with σ being the noise standard deviation at each wavenumber.

4.2. On-line monitoring using Raman spectroscopy

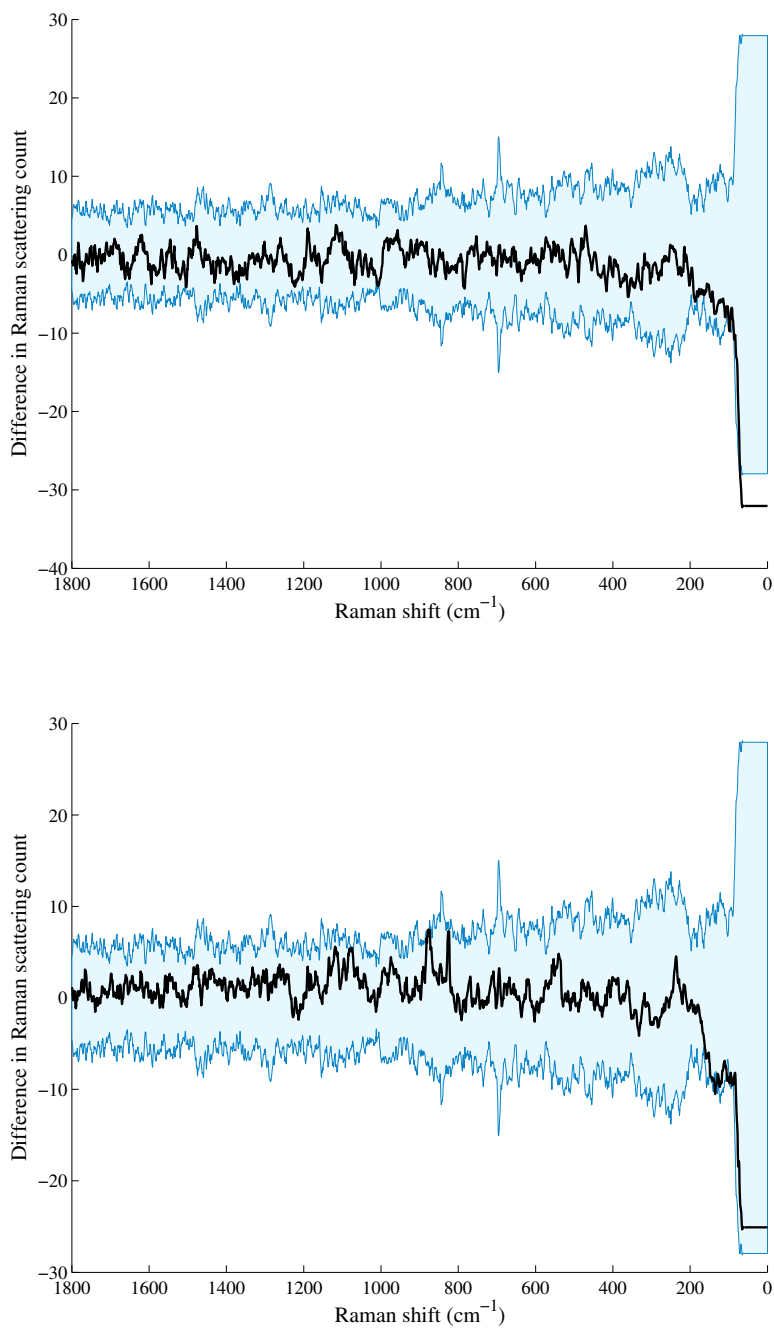


Figure 4.18: Raman spectra of (a) K_2HPO_4 (1.2 g/L) and (b) KH_2PO_4 (2.8 g/L) solutions in water. Water spectra was subtracted from raw solution spectra. Shaded blue area corresponds to $\pm 2\sigma$, with σ being the noise standard deviation at each wavenumber.

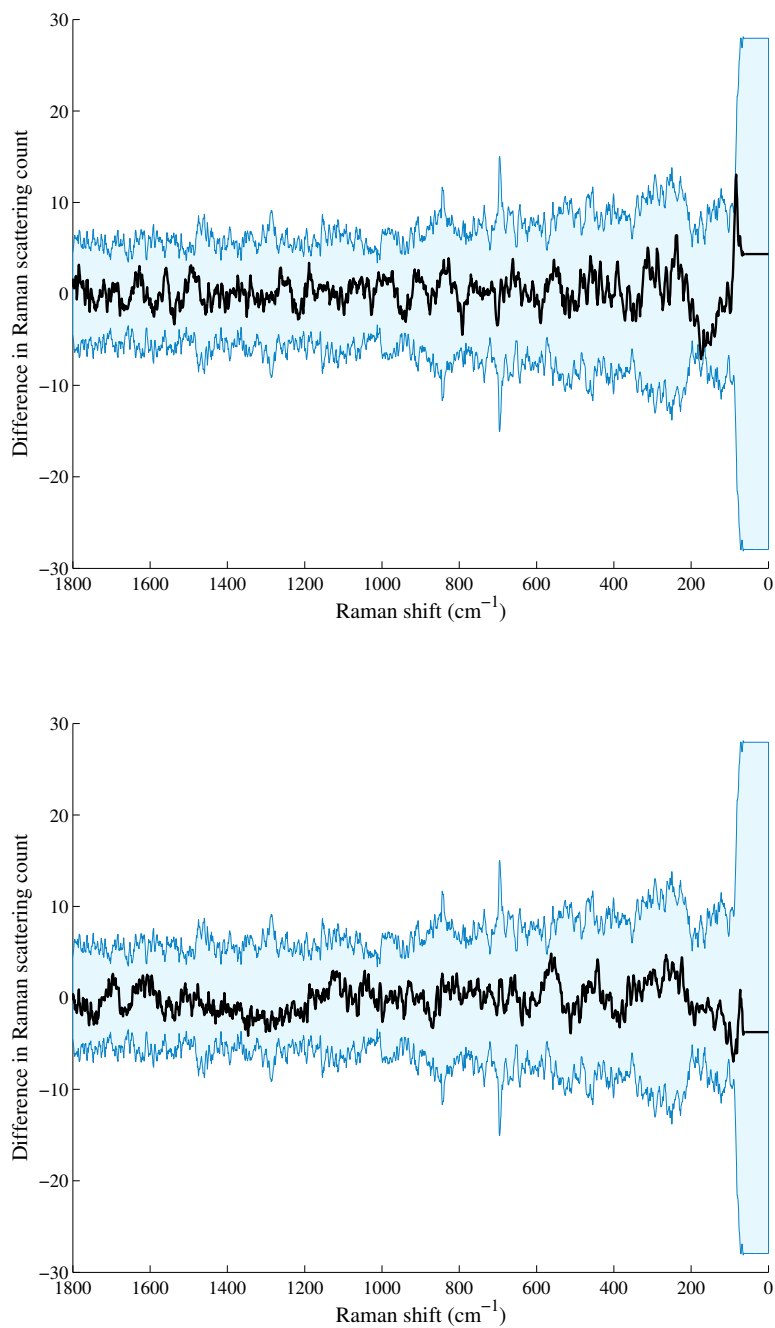


Figure 4.19: Raman spectra of (a) Thiamine HCl (40 ug/L) and (b) Arnon 5 solutions in water. Water spectra was subtracted from raw solution spectra. Shaded blue area corresponds to $\pm 2\sigma$, with σ being the noise standard deviation at each wavenumber.

In this section, the development of a multivariate support vector machine learning based model is presented. The model is developed to correlate the Raman spectra to the concentration of biomass, glucose, and oil content in the bioreaction system.

Experimental datasets used for model building

For building the model, as well as for validation and testing, the Raman spectra was collected in fed-batch cultures. Samples were withdrawn from the bioreactor at four hour intervals and analyzed to determine the total biomass concentration, oil content in the cells, and glucose concentration in the broth media. The spectral data was paired to compositional data based on the time at which the spectra was recorded and the time at which the sample was withdrawn.

Three datasets were generated by growing the green microalga *A. protothecoides* in fed-batch mode starting at different initial conditions and by varying the feed flowrates. The first dataset corresponds to a D-Optimal run, as reported in Surisetty et al. (2010). In this case, algae were cultured over a period of 360 h, and glucose, glycine, and minerals were supplemented to the reactor in order to generate significant perturbations in the bioreactor response. For the second dataset, the feed flow-rate followed a pseudo-random binary profile (PRBS), as presented in Fig. 6.8. In the third dataset, the culture conditions were modified in order to maximize biomass production as reported for the adaptive MPC run in Section 7.2.2. The minimum and maximum biomass concentration, oil content, and carbon substrate concentration (glucose), are presented in Table 4.3.

Table 4.3: Characterization of the datasets used for building and validating a Raman chemometric model for algal culture composition: Number of samples (N) and concentration range (min and max) of samples in each dataset for biomass, glucose, and oil content

Dataset	N	Biomass (g/L, dry weight)	Glucose (g/L)	Oil content (%w/w, dry basis)
D-Optimal	79	0.8 – 39.4	0.00 – 101.9	14.3 – 65.1
PRBS	78	0.5 – 38.2	0.01 – 52.3	19.4 – 79.1
Adaptive MPC	57	2.4 – 144.3	0.05 – 45.6	32.9 – 82.1
Combined	214	0.50 – 144.3	0.00 – 45.6	14.3 – 82.1

Spectra preprocessing

Preprocessing of the spectra is required before model building in order to reduce the noise associated with the spectral measurements. Preprocessing is also useful to enhance the information content of the spectra. Several techniques are available for spectra preprocessing as reviewed by Afseth et al. (2006). In this work, the Savitzky-Golay filter and the Standard Normal Variate (SNV) transformation were used to preprocess the Raman spectra. The Savitzky-Golay filter is a smoothing filter based on local polynomial regression; for this, a third order polynomial with a section size of 7 points was used. In the SNV transformation, the Raman spectra is scaled such that the resulting spectra has mean equal to zero and unitary variance. The aim of this transformation is to give equal weight to all the spectral features.

Building and validating a support vector regression model

In order to build a chemometric model that relates Raman spectra to biomass concentration, the three datasets reported in Table 4.3 were combined to generate a combined dataset containing 214 observations. From this dataset, 60 data points were selected at random for model calibration and the remaining

data points were used for model testing.

The non-linear radial basis function support vector regression algorithm used in this work posses three adjustable parameters: the soft margin (C) for the regression cost function, the threshold parameter (ϵ), and the radial basis function kernel parameter (γ). To determine the optimal value of these parameters, a systematic grid search was performed in combination with a 10-fold cross-validation method using the predicted residual sum of squares (PRESS) statistic.

In the 10-fold cross-validation method, the calibration dataset is divided in 10 subsets. The regression model is calibrated using 9 of these subsets and the resulting model is evaluated in the remaining subset. The calibration is repeated 10 times, leaving out at each iteration a different subset. The PRESS statistic is computed for each one of the 10 regression models constructed, and the average PRESS value is used as a measure of the goodness of fitting provided by the combination of C , ϵ , and γ values. This procedure was performed for every value in the parameter space, to determine the parameter combination that reduces the average PRESS.

In Table 4.4, the coefficient of determination of the optimized support vector regression model is presented for both the dataset used for model calibration and for the remaining dataset (testing).

Table 4.4: Coefficient of determination of the support vector regression model for the calibration (R_C^2) and testing (R_T^2) datasets.

Predicted variable	R_C^2	R_T^2
Biomass concentration	0.9975	0.9822
Glucose concentration	0.9978	0.8947
Oil content	0.8312	0.4389

From Table 4.4, it can be seen that there is a good correlation between the values predicted by the support vector regression model and the experimental observations in the calibration dataset. The coefficient of determination is also close to the unity for the prediction of the biomass concentration in the testing dataset, which indicates that the model has indeed the capabilities to predict the biomass concentration in the culture broth.

The calibrated support vector regression model, however, failed to satisfactorily transform the Raman spectral data into glucose concentration and oil content for the testing dataset. The failure of the model to predict glucose and oil concentration could be due to the cross-correlation that exists in two of the three datasets (D-Optimal and PRBS datasets) between glucose and biomass concentration, as well as between oil content and biomass concentration, and the strong effect that biomass concentration has on the Raman spectra. For this reason, a new model was built using only observations from the Adaptive MPC dataset. In this case, 30 observations were used for calibration and cross-validation of the model, and the remaining 27 observations were used for testing the performance of the model. The procedure used for model building was the same as the one previously described.

4.2.5 On-line estimation of bioreactor composition

In Section 4.2.4, the Raman spectra of microalgal cultures were successfully correlated with the concentrations of biomass, glucose, and oil content in the cells. In this section, the use of Raman spectroscopy as an on-line, real-time multivariate sensor is evaluated.

The Raman spectrum of a heterotrophic culture of *A. protothecoides* was collected every ten minutes with an integration time equal to 20 seconds. The average time required for transforming the spectra to chemical composition,

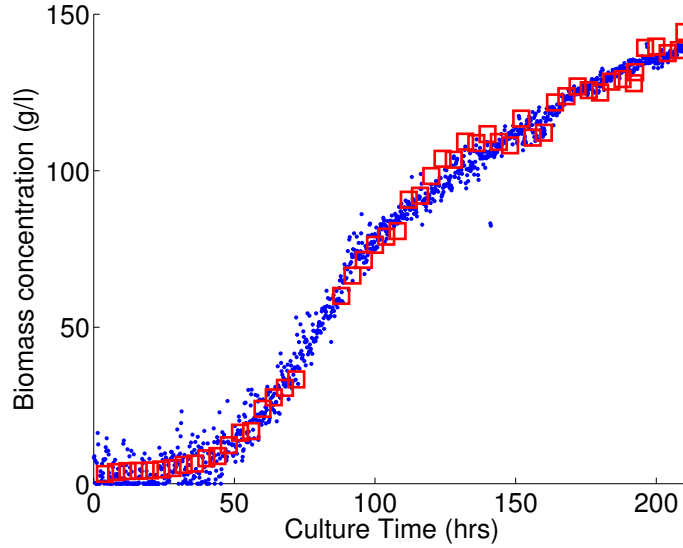


Figure 4.20: Biomass concentration profile for an algal culture: (\cdot) support vector Raman spectroscopy -based measurement; (\square) Off-line experimental measure.

using the SVR sensor developed in Section 4.2.4, was 0.058 seconds. The average total time, including spectra collection, was around 20 seconds with the prediction of the composition taking an insignificant amount of time compared to the spectral integration time. The estimation of the chemical properties of an algal culture is, therefore, solely determined by the spectral integration time. Compared to the algal culture dynamics, which can range from several minutes to days, the prediction time (around 20 seconds) is insignificant. Therefore, Raman spectra can be used for the real time on-line estimation of the composition in algal bioreactors.

The predicted profiles for biomass, glucose, and oil content are shown in Figs. 4.20, 4.21, and 4.22 respectively. For comparison purposes, the off-line experimental measurements are also included in the plots. A good match between the Raman spectra based predictions and the experimental measurements for the full range of concentrations is observed.

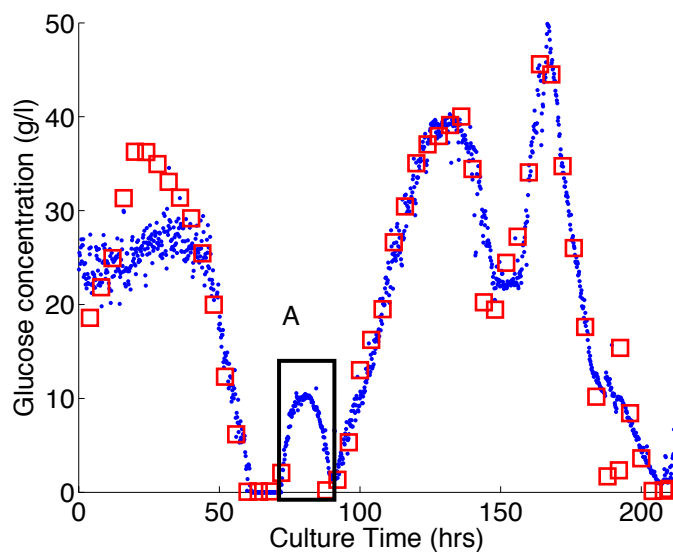


Figure 4.21: Glucose concentration profile for an algal culture: (·) support vector Raman spectroscopy-based measurement; (□) Off-line experimental measure. The higher measuring frequency possible with Raman spectroscopy allows to identify variations in the culture that are normally missed by traditional off-line measurements, as highlighted in Box A.

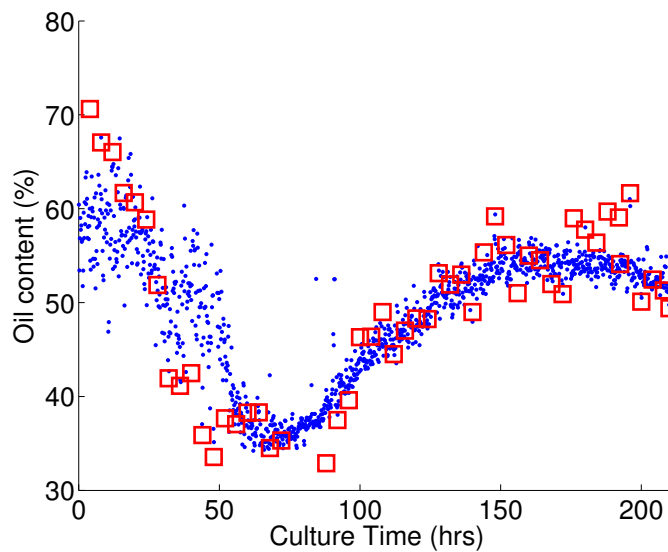


Figure 4.22: Profile for the oil content in the algal cells: (·) support vector Raman spectroscopy-based measurement; (□) Off-line experimental measure.

During the initial 50 hours of culture time, the variance between contiguous Raman based predictions was higher than in the subsequent culture times. This indicates that there were significant interferences from the sample matrix at the start-up of the culture. At the start of the culture (lag phase), several important changes in both the chemical composition of the culture media and the biochemical composition of the algal cells occurs. Rapid changes in cell size and morphology, cell pigmentation, and composition of the culture medium -due to uptake of nutrient and excretion of trace compounds, proteins, or extracellular polymers- could be responsible for the high variance observed in the initial spectral measurements. Therefore, the spectral based estimations should be used with utmost precaution during the lag phase. It is suggested that a moving average window be used to reduce the fluctuation in the predictions.

From Figure 4.21, it can be seen that glucose estimates (after lag phase) based on Raman spectroscopy have a smoother profile than the experimental measurements. Although, experimental measurements for glucose based on HPLC have, in general, a high precision, the samples drawn from the reactor and analyzed in the HPLC might not be representative of the bioreactor contents. This is because, the conditions in the sampling line may not be the same as the conditions in the reactor. Furthermore, the sample obtained from the reactor might undergo changes during the time lapsed for preparing the sample for HPLC and other analysis. These could lead to reduced accuracy and reliability of the off-line measurements.

An additional advantage of the on-line Raman based method is that the composition measurements can be taken at a considerably higher frequency compared to the off-line experimental measurements, given that the Raman based method does not require the removal of a sample from the reactor. The

reduced frequency for the removal of a sample, in turn, reduces the chance of contamination from faster growing bacteria and fungi. A higher measurement frequency helps in observing the changes in the composition that will otherwise be overlooked. For example, the variation in the glucose concentration between approximately 75 and 90 hours (enclosed in box ‘A’ in Figure 4.21) is not readily apparent from the off-line experimental measurements. Whereas, the Raman spectroscopic method is able to clearly identify these changes.

From Figure 4.22, it can be seen that the variance of contiguous oil estimates using the Raman spectra is lower compared to the one obtained using off-line measurements. This implies that the estimates provided by the Raman spectra are more reliable than the off-line experimental measurements.

5

The physiology of microalgal growth

A clear understanding of the factors that determine algal growth rate and product yield is required before proceeding to formulate a mathematical model that describes algal growth or to optimize algal lipid production. In this chapter, the growth of the fresh-water microalga *A. protothecoides* is studied in both photoheterotrophic and heterotrophic conditions. The effect of the carbon to nitrogen ratio, as well as the effect of the total nutrient availability on growth rate and product yield is examined. The influence of other nutrients and media components on growth is evaluated, as well as the potential inhibitory effects of secondary algal metabolites and other media additives. Finally, the compositional changes that algal biomass undergoes as a consequence of the imbalance between growth rate and nutrient uptake rate are appraised.

5.1 Growth in mixotrophic and heterotrophic conditions

Microalgae are characterized for being photosynthetic unicellular eukaryotes. Most microalgae species are photoautotrophs, though several species are known for being photoheterotrophs or mixotrophs. That is, they can either oxidize organic substrates or fix CO₂ to support their energy and carbon requirements. There are even some microphytes that have completely lost their photosynthetic apparatus and therefore are obligate heterotrophs. In this section, the growth profiles and biomass yields in mixotrophic and heterotrophic conditions are studied and compared.

5.1.1 Photoheterotrophic growth

A first series of experiments was conducted by growing *A. protothecoides* in B1 Medium, supplemented with glucose (10 g/L) and glycine (at varying concentrations), with continuous illumination at a photosynthetic photon flux (PPF) of $29.9 \pm 1.4 \mu\text{mol m}^{-2}\text{s}^{-1}$ as described in Section 3.1.1. Cultures were severely nitrogen limited with a high carbon to nitrogen molar ratio (500:1, 250:1, and 167:1). For comparison, it should be noted that the typical carbon to nitrogen ratio, given by the Redfield ratio, is 106:16, or roughly 6:1.

The growth curves for these first experiments are plotted in Fig. 5.1, where both the exponential and stationary growth phases can be seen. There is a clear trend of increased biomass production with increasing nitrogen source availability, which is consistent with the severe nitrogen limitation in the culture media.

The concentration of glycine in the filtered culture media was measured using the Ninhydrin method, as described in Section 3.2.3. Fig. 5.2 shows the

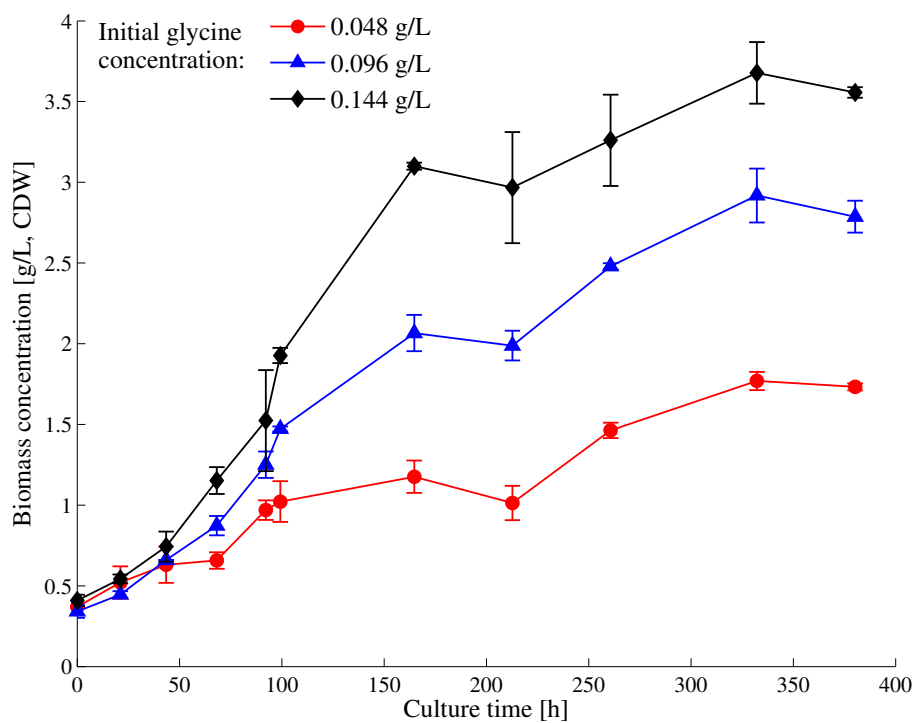


Figure 5.1: Biomass concentration profile for photoheterotrophic microalgal cultures at varying concentrations of glycine, using B1 medium with an initial glucose concentration of 10 g/L. Cultures were continuously illuminated at a $\text{PPF} = 29.9 \pm 1.4 \mu\text{mol m}^{-2}\text{s}^{-1}$. The experiments were performed in duplicate, as well as the biomass measurements.

rapid depletion of glycine observed in the culture. After 68 hours, glycine concentrations were 1–5 % of their initial values. In this same period, biomass concentrations had only reached 31–37 % of their final values. This highlights that there is a definite uncoupling between nutrient uptake and growth, at least in terms of nitrogen uptake.

A second series of experiments were performed increasing the concentration of all nutrients by a factor of 4 (Medium B4). The resulting carbon to nitrogen ratio, on a molar basis, were 400:1, 200:1, and 100:1, having again a strong nitrogen limitation in the formulated media. Fig. 5.3 presents the growth curves for these series of experiments. There was a proportional rise in the total biomass production with respect to the higher total nutrient availability, with a five fold average increase in biomass concentration for all runs between medium B1 and B4.

The effect of nitrogen availability on biomass production, however, did not follow the same linear trend as in the previous experiments. At the highest nitrogen availability (lower C:N ratio = 100:1), biomass production was lower than at the intermediate value. That is, growth was maximized at a moderate level of nitrogen availability. The concentration profile of glycine in the filtered culture media is shown in Fig. 5.4. As previously, there was a rapid uptake of nutrients that was uncoupled from biomass production.

The results in Figs. 5.3 and 5.1 indicate that the carbon to nitrogen ratio and the total nutrient availability had a combined effect on growth. This combined effect can be seen in terms of biomass yield in Fig. 5.5. The yield of biomass to nitrogen was evaluated by taking the ratio between the total biomass produced and the total nitrogen consumed by the cells.

5.1. Growth in mixotrophic and heterotrophic conditions

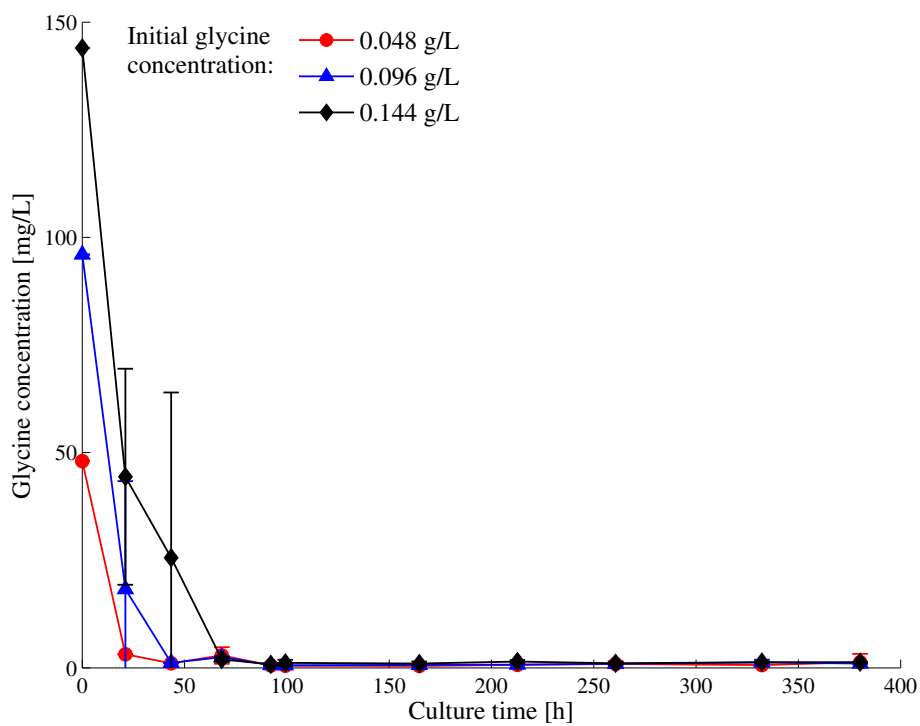


Figure 5.2: Uptake of glycine in *A. protothecoides* cultures, using B1 medium with an initial glucose concentration of 10 g/L. Cultures were continuously illuminated at a PPF = $29.9 \pm 1.4 \mu\text{mol m}^{-2}\text{s}^{-1}$. Experiments were performed in duplicate and glycine measurements were done in triplicate.

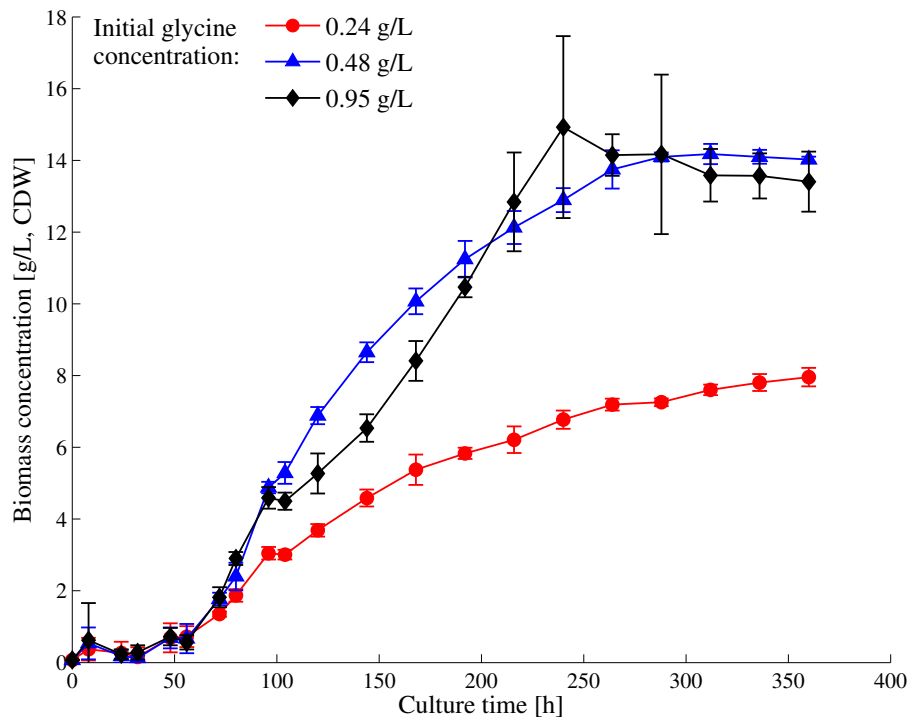


Figure 5.3: Biomass concentration profile for photoheterotrophic microalgal cultures at varying concentrations of glycine, using B4 medium with an initial glucose concentration of 40 g/L. Cultures were continuously illuminated at a PPF = $29.9 \pm 1.4 \mu\text{mol m}^{-2}\text{s}^{-1}$. Experiments were performed in duplicate, as well as biomass measurements.

5.1. Growth in mixotrophic and heterotrophic conditions

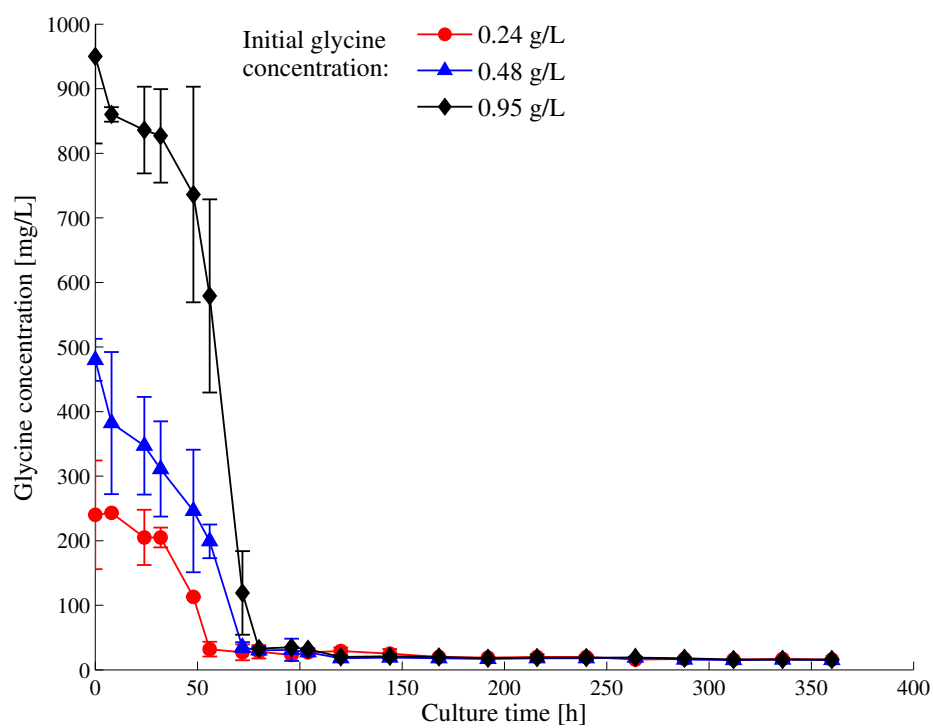


Figure 5.4: Uptake of glycine in *A. protothecoides* cultures, using B4 medium with an initial glucose concentration of 40 g/L. Cultures were continuously illuminated at a PPF = $29.9 \pm 1.4 \mu\text{mol m}^{-2}\text{s}^{-1}$. Experiments were performed in duplicate and glycine measurements were done in triplicate.

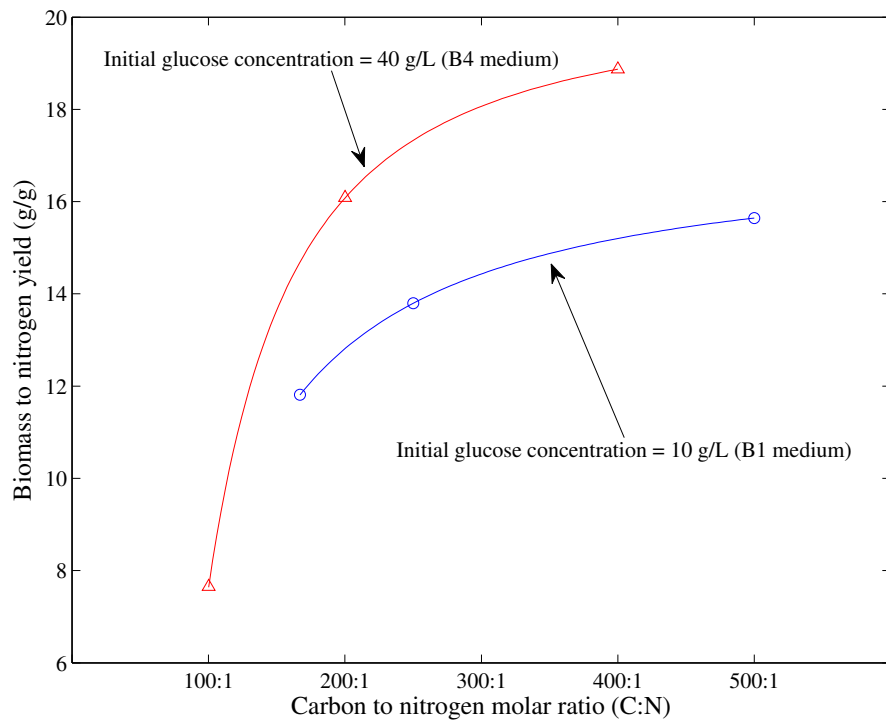


Figure 5.5: Biomass to nitrogen yield in mixotrophic cultures of *A. protothecoides*. All cultures were continuously illuminated at a PPF = $29.9 \pm 1.4 \mu\text{mol m}^{-2}\text{s}^{-1}$. Yield is a function of both C:N ratio and total nutrient availability.

5.1.2 Heterotrophic growth

The effect of total nutrient concentration and C:N ratio in algal growth was studied in the previous section for photoheterotrophic conditions. To evaluate the differences between photoheterotrophic and purely heterotrophic growth, a comparative experiment was performed. Four flasks were prepared with 190 mL of B4 medium and a 10 mL inoculum; two of these flasks were incubated in the dark, while the remaining two were put under continuous illumination with an average photosynthetic photon flux (PPF) at the liquid surface of $29.9 \pm 1.4 \mu\text{mol m}^{-2}\text{s}^{-1}$. The corresponding growth curves are plotted in Fig. 5.6.

The initial growth rate was greater for the photoheterotrophic culture than for the purely heterotrophic one. The observed differences in the biomass concentrations between the two cultures is marginally significant, with a p-value equal to 0.045. This indicates that even though the growth rate for the cultures was significantly different at the 95 % confidence level, there is a 4.5 % probability that the observed differences occurred at random. The final biomass concentration, on the other hand, was the same for both types of cultures. These results suggests that the photosynthetic pathway plays a significant role during the first part of the culture, but the increased initial growth rate had no measurable effect on the final biomass production and product yield.

To understand this behaviour, it is necessary to recall that several factors may limit the growth under phototrophic conditions, including CO_2 limitation and mutual shading. Mutual shading is a relevant limiting factor for high density cultures in phototrophic systems. Mutual shading impedes the use of light by the bulk of the cells in the culture, and only the cells at the surface can effectively behave phototrophically. As culture density increases, mutual shad-

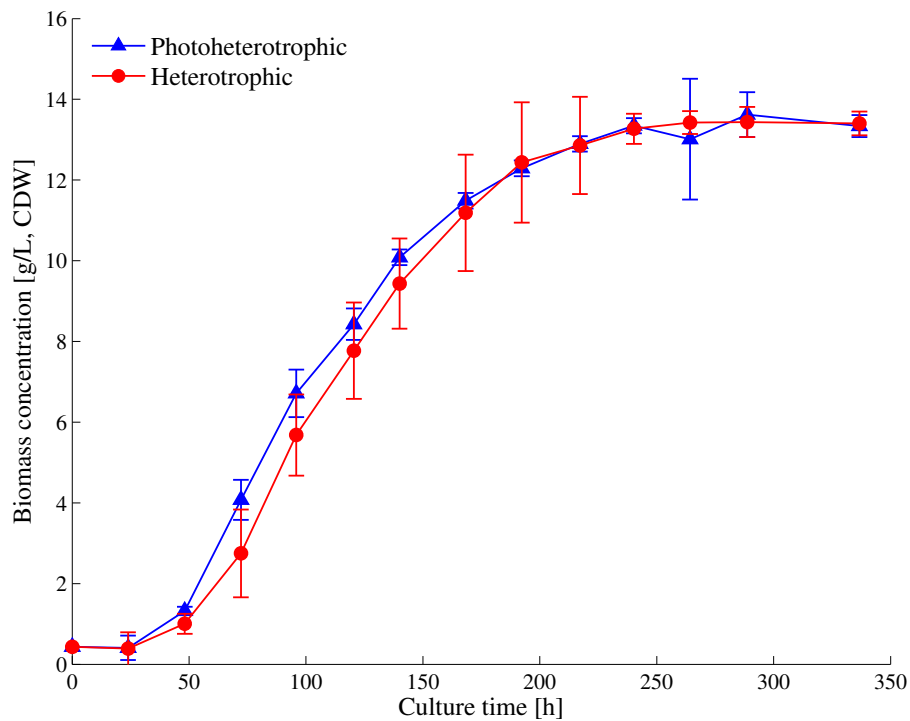


Figure 5.6: Biomass concentration profile for photoheterotrophic and heterotrophic batch cultures. Media used was B4 with and initial glycine concentration of 0.4 g/L an initial glucose concentration of 40 g/L. Cell dry weight measurements were corrected for evaporation losses in the cultures. Photoheterotrophic cultures were continuously illuminated at a PPF = $29.9 \pm 1.4 \mu\text{mol m}^{-2}\text{s}^{-1}$. Experiments were performed in duplicate.

ing is exacerbated. Considering that most photoautotrophic bioalgal cultures operate at cell densities below 2 g/L, it is clear that the culture conditions in this report are just marginally photoheterotrophic. That is, only at the initial stage of the culture, can the system be considered photoheterotrophic, and for most of the culture, the conditions for the average algal cell are just heterotrophic.

5.2 The effect of nutrients on growth

The carbon to nitrogen ratio (C:N) plays a critical role in the physiology of algal cultures as shown in the previous section. There are, however, other nutrients and factors affecting growth and lipid production. This section covers the effect of different nitrogen substrates on growth and the relative influence other nutrients have in both growth rate and oil accumulation.

5.2.1 Selection of the nitrogen source

Microalgae are able to assimilate nitrogen from several different substrates, including NH_4^+ , NO_3^- , urea, amino acids, and purine and pyrimidines bases. The bioavailability of each nitrogen substrate differs markedly and affects in turn the growth rate of algae. Previously, it has been reported that glycine and urea are excellent nitrogen sources (Shi et al., 2000) for the heterotrophic growth of *Chlorella* species. In this thesis, most experiments were conducted using glycine as the sole nitrogen source. The reader should be aware, however, that due to its high cost glycine will not be the preferred nitrogen substrate for the industrial large-scale production of microalgae.

In this section, an experiment was conducted to compare the effect on growth when glycine is replaced with urea as the nitrogen substrate. For this experi-

ment, B1 medium was supplemented with glucose at a concentration of 10 g/L, and urea was added at a concentration of 0.1 g/L and 1.0 g/L. Six flasks were prepared, with two of them at the lower level of urea (C:N = 100, molar ratio), two at the higher level of urea (C:N = 10), and the other two at a concentration of 0.1 g/L of glycine (C:N = 250). In Fig. 5.7, the average growth curves are reported for each of the nitrogen substrate/concentration pairs evaluated.

As seen in Fig. 5.7, there is a significant difference between the growth curves of algae growing on glycine and algae growing on urea. At the same mass concentration (0.1 g/L) of the nitrogen substrate, which corresponds to a molar concentration of nitrogen in the urea culture 2.5 times higher than in the glycine culture, the algae growing on urea exhibit a much lower growth rate and yield, with a final concentration equal to 1.2 g/L, or 32% of the final concentration of the culture growing on glycine. For urea cultures to achieve a similar growth profile and yield to that of glycine cultures, the concentration of urea has to be increased by a factor of 10. This is equivalent to a 25 times increase, in molar basis, in the nitrogen availability.

For the range of concentrations explored for the growth of *A. protothecoides* in urea, it seems like the bioavailability of the nitrogen contained in urea is significantly lower than that of the nitrogen contained in glycine. It will be necessary, however, to conduct further experimentation expanding the range of urea concentration to verify if this is a general characteristic valid for a broader range of the C:N ratios. It must also be noticed that both glycine and urea can potentially serve as a carbon source. For very high carbon to nitrogen ratios (C:N > 100), however, the contribution of the nitrogen substrate to the total available carbon in the culture is negligible.

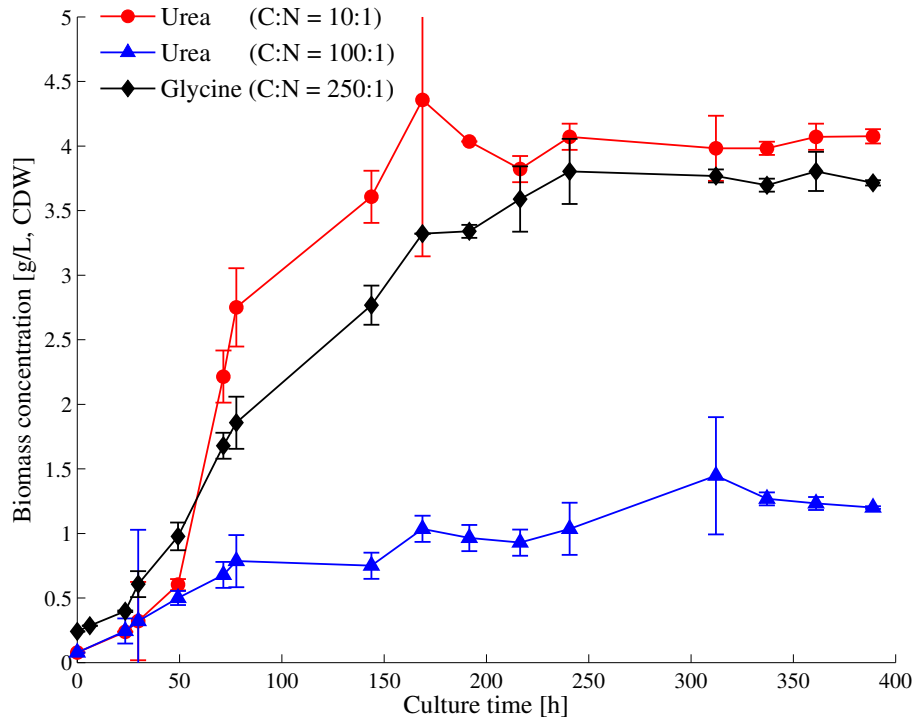


Figure 5.7: Effect of the nitrogen source on the growth of microalgae. Cells were grown photoheterotrophically in medium B1 supplemented with either urea or glycine as the nitrogen source and glucose (10 g/L) as the carbon source. Cultures were continuously illuminated at a PPF = $29.9 \pm 1.4 \mu\text{mol m}^{-2}\text{s}^{-1}$.

5.2.2 The response of growth and oil production to varying nutrient concentrations

A four factor Box-Behnken experimental design, with three concentration levels, was performed to qualitatively study the influence that different media components have over the growth rate and oil accumulation in *A. protothecoides*. The four factors selected were the initial concentration of carbon, nitrogen, phosphorus, and iron substrates in the media.

The summary of the experimental design is presented in Table 5.1. Glucose was used as the carbon source with the three concentration levels at 15 g/L (−1), 30 g/L (0), and 45 g/L (+1). Glycine was used as the nitrogen source with the concentration levels at 0.2 g/L (−1), 0.4 g/L (0), and 0.6 g/L (+1). A mixture of potassium phosphates was used as the phosphorus source, with K_2HPO_4 representing 30 % (mass basis) of the total and KH_2PO_4 being the other 70 %; the concentration levels, as total phosphates, were 2 g/L (−1), 4 g/L (0), and 6 g/L (+1). Heptahydrate ferric sulphate ($FeSO_4 \cdot 7H_2O$) was used as iron source, with the three concentration levels at 24 mg/L (−1), 36 mg/L (0), and 48 mg/L (+1).

The observed initial growth rate, i.e. average for the first 48 h, for each experiment was calculated based on biomass measurements performed in duplicate. The results are summarized in Fig. 5.8 as box-plots for each of the factors considered in the experimental design.

The box-plot presents the median of the growth rate for each factor-level (red horizontal line), and the interquartile range of all observations (blue rectangle), as well as the total range of observed growth rates (dashed lines between whiskers). Observations considered as outliers, that is falling beyond the 99.3 % confidence interval, are represented as crosses in the diagram. From this representation of the data it is possible to qualitatively compare the effect

Table 5.1: Box-Behnken experimental design to evaluate the influence of carbon, nitrogen, phosphorus, and iron substrate concentrations on the growth rate and oil productivity of microalgae.

Experiment	Glycine	Glucose	Phosphates	Iron sulphate
1	-1	-1	0	0
2	-1	+1	0	0
3	+1	-1	0	0
4	+1	+1	0	0
5	0	0	-1	-1
6	0	0	-1	+1
7	0	0	+1	-1
8	0	0	+1	+1
9	-1	0	0	-1
10	-1	0	0	+1
11	+1	0	0	-1
12	+1	0	0	+1
13	0	-1	-1	0
14	0	-1	+1	0
15	0	+1	-1	0
16	0	+1	+1	0
17	-1	0	-1	0
18	-1	0	+1	0
19	+1	0	-1	0
20	+1	0	+1	0
21	0	-1	0	-1
22	0	-1	0	+1
23	0	+1	0	-1
24	0	+1	0	+1
25	0	0	0	0
26	0	0	0	0
27	0	0	0	0

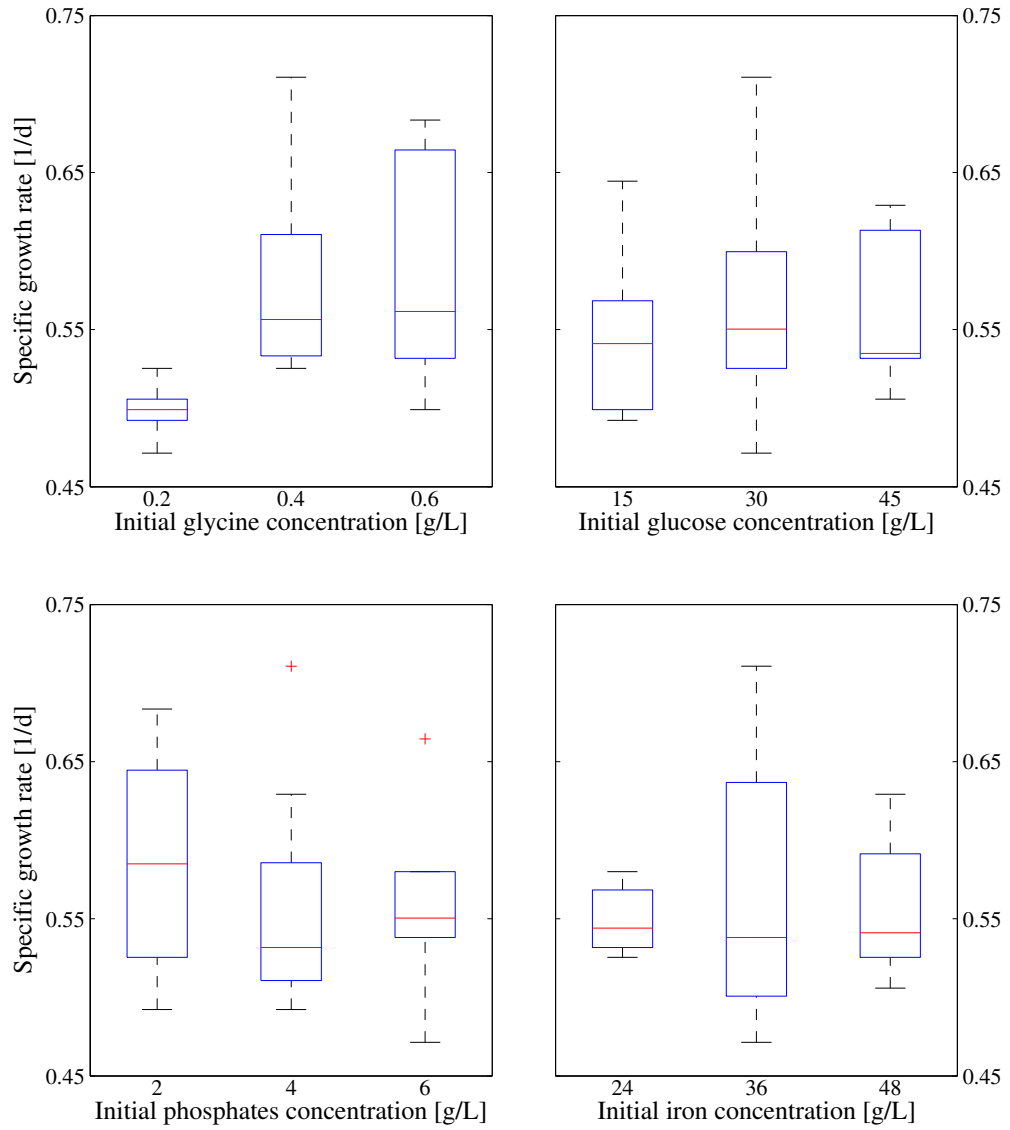


Figure 5.8: Effect of the initial nutrient concentrations on the initial growth rate of *A. protothecoides*.

of each nutrient on the initial growth rate.

From Fig. 5.8, glycine and phosphate concentration have a greater effect on growth rate than either glucose or iron. The influence of glycine on the median and the interquartile range of the growth rate shows a monotonous trend, with increased growth rate as glycine increases. The total range shows, however, a maximum at the intermediate glycine level. Phosphate concentrations, on the other hand, had an inverse effect on growth rate, with a minimum observed in the median growth rate at 4 g/L and with the maximum median growth rate at the lower phosphate concentration. Iron concentration seems not to have any significant effect on growth, except that at the lower concentration value the spread of the observations (full range between whiskers) was substantially minimized.

After 200 h, each experiment was stopped and cells harvested and freeze-dried. Oil was extracted from freeze dried cells and quantified following the procedure described in Appendix A.2. The box-plots in Fig. 5.9 summarize the effect each nutrient has over the final oil content of the cells.

As with growth rate, only glycine and phosphates seem to have a clear and marked effect on the final oil content in the cells. Glycine had a negative effect on oil accumulation, with decreasing oil content as glycine concentration increases. The initial phosphate concentration had a positive effect on oil accumulation, with a monotonously increasing trend in oil content with increased phosphate concentration. Surprisingly, a higher carbon source availability, i.e. higher glucose concentration, did not translate into a higher accumulation of lipids. Moreover, there was a slight decreasing trend in lipid accumulation with increased glucose concentration.

Similar results were observed in terms of lipid productivity, i.e. the total amount of oil accumulated per unit of time and unit of culture volume, as

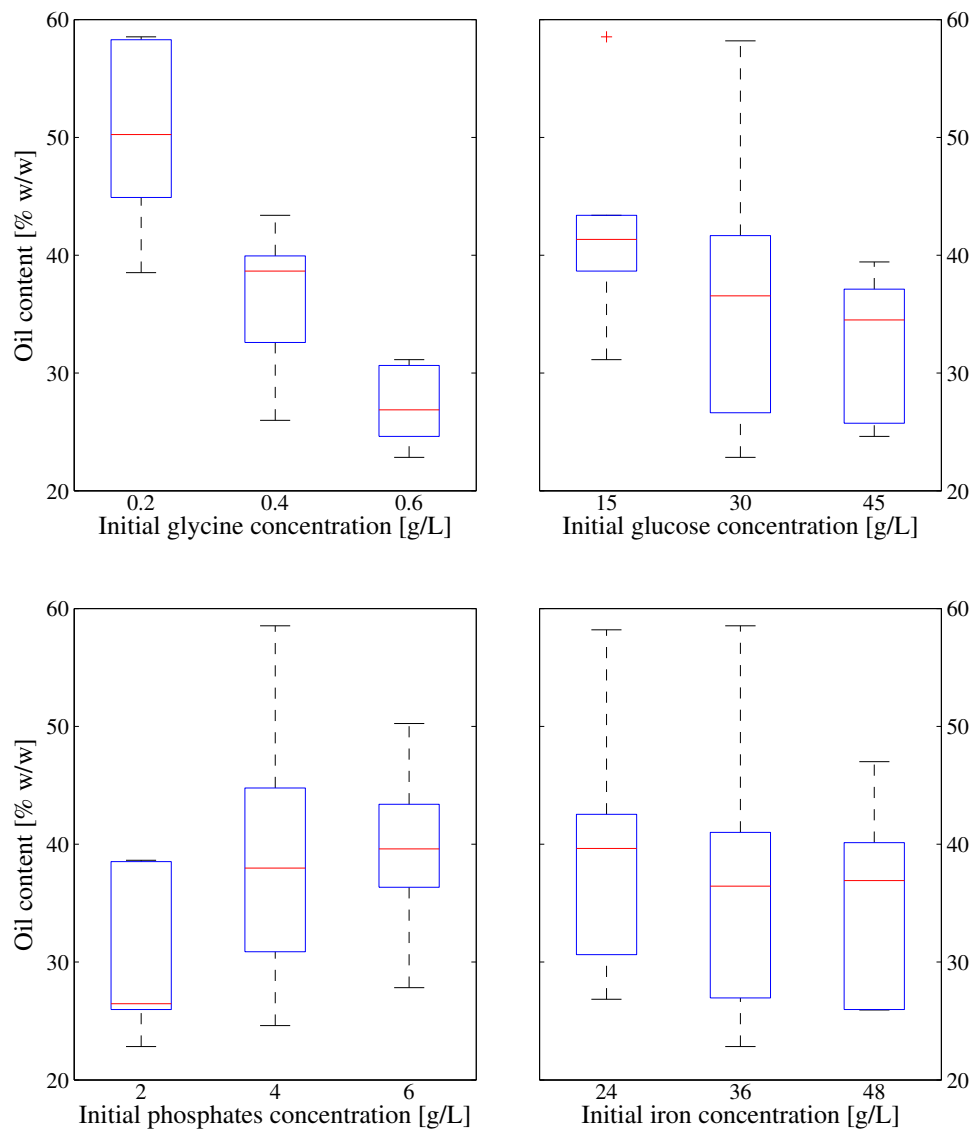


Figure 5.9: Effect of the initial concentration of nutrients on the intracellular neutral lipid content after 200 h of culture.

shown in Fig. 5.10. Clearly a lower concentration of glycine resulted in a higher accumulation of oil in the culture; an opposite effect was observed in terms of phosphate concentration. For the range of concentrations covered in this study, glucose and iron did not appear to have a major effect on either growth rate or lipid accumulation in algae. The reader must recall, however, that it was previously shown that the carbon to nitrogen molar ratio had an effect on growth that was as significant as the total nutrient concentration.

5.3 Compositional changes in microalgae

Chemical engineers usually treat biomass as a pseudo-chemical component with a defined, more or less constant, empirical chemical formula. This assumption is normally valid for many microorganisms, but it cannot be applied for algal systems. In Section 5.1.1 it has been shown that algae consume nutrients from the medium at a rate that is faster than the growth rate. Furthermore, algae tend to accumulate large amounts of lipids intracellularly, with the chemical composition of these lipids being significantly different to the rest of the algal biomass.

Changes in the chemical composition of algal biomass were reported in Table 5.2. In this case, algae was grown on B1 medium supplemented with glucose (10 g/L) and glycine (0.15 g/L). Samples were withdrawn at different times for the first 100 hours of the culture, and composition was determined using a Carlo Erba EA 1108 elemental analyzer.

A surge in the nitrogen content of the cells was observed at 20 h, while there was a continuous reduction in the carbon and hydrogen content in the biomass. The surge in the cellular nitrogen content can be explained by the transient accumulation and subsequent consumption of nitrogen compounds that results

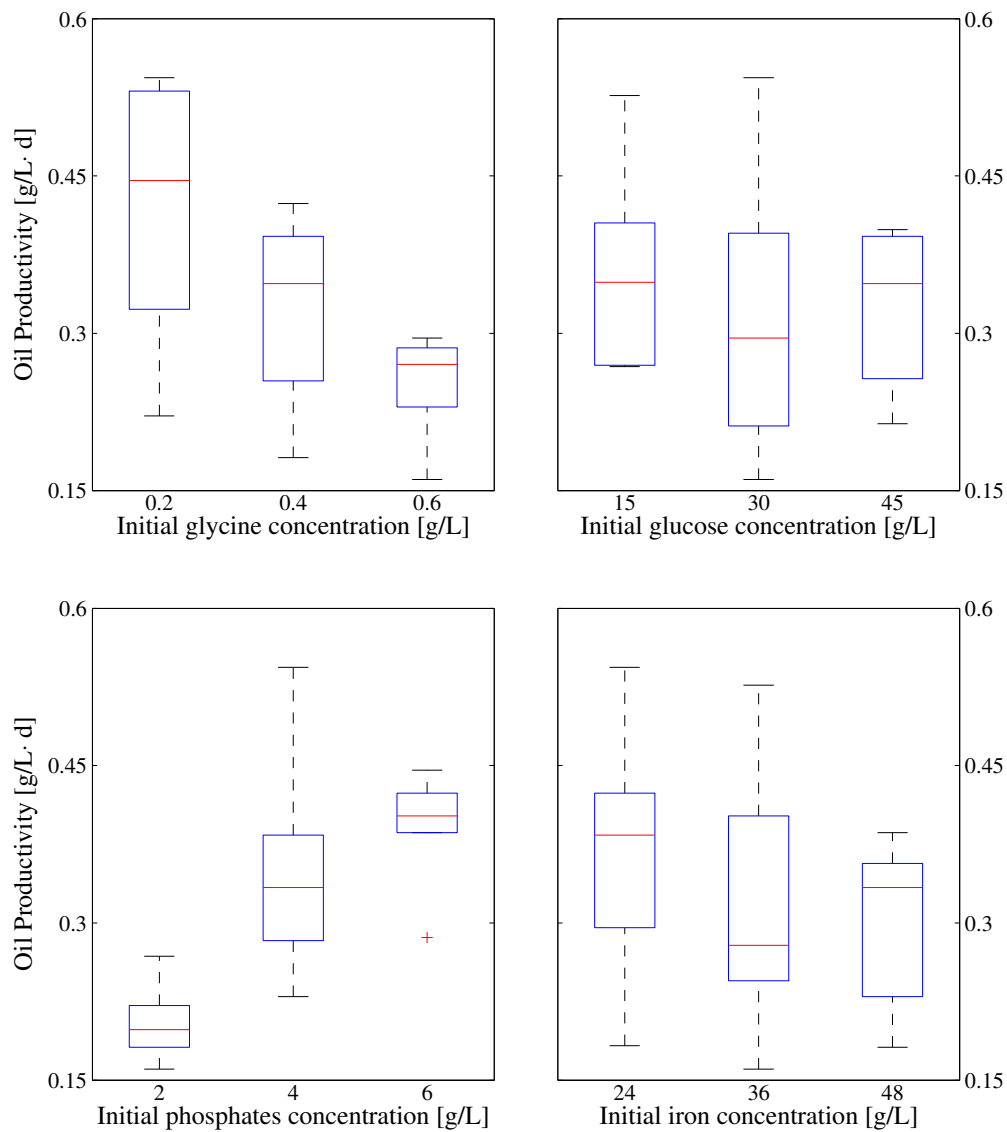


Figure 5.10: Effect of the initial nutrient concentration on the algal lipid productivity.

from the imbalance between nitrogen uptake rate and growth rate. The decrease in the carbon and hydrogen content could be the result in a reduction in lipid content, as lipids are highly reduced compounds with a relatively higher content of carbon and hydrogen than other cell metabolites.

5.4 Metabolites accumulation in the culture

In Figs. 5.2 and 5.4 it can be observed that there was a final positive concentration of nitrogen in the media. Further experimentation revealed, that there was indeed an accumulation of nitrogen compounds in the media as culture progressed. This was an indication that algal cells export nitrogen compounds into the media. Analysis of the culture media by HPLC showed an increase in amino-acid content as cultures progressed, as illustrated in Table 5.3. Results in Table 5.3 suggest that extracellular proteins and oligopeptides were being built up in the media.

Accumulation of metabolites in the culture media might have some effects on the growth and overall metabolism of algal cells. To test this hypothesis, an alga was cultured on a medium prepared using filtered spent media and the growth curves were compared against the alga growing on completely fresh

Table 5.2: Elemental analysis of algal biomass. Cell were withdrawn from the liquid culture at the indicated sample time, counted after inoculation.

Sample time h	Molar percentage		
	N	C	H
0	1.3	60.0	9.1
2	1.2	57.4	8.9
20	2.7	56.9	8.8
100	1.5	55.2	8.3

Table 5.3: Variation in the concentration of nitrogen-containing compounds in the culture medium during a single batch experiment. *A. protothecoides* exports several amino-compounds to the media including low molecular weight oligopeptides and proteins.

AA residue	Concentration ($\mu\text{mol/L}$)		
	Culture time	0 h	80 h
Ala	-	67	150
Arg	-	70	-
Asx	-	53	77
Glx	-	116	143
Gly	6660	155	212
Ile	-	-	87
Leu	-	-	108
Lys	-	28	35
Pro	-	-	73
Ser	-	-	70
Thr	-	-	66
Tyr	-	-	177
Val	-	-	80

medium. The spent medium was obtained from an axenic, two week old, high density culture of algae ($\sim 30 \text{ g/L}$, CDW). Culture broth was centrifuged, and the supernatant was filtered using a $0.22 \mu\text{m}$ PTFE membrane.

Four different flasks were prepared in duplicate (8 in total) from spent medium. The first flask contained only spent medium, with no added nutrients; the second flask was prepared by adding glycine to the spent medium to achieve a concentration of 0.4 g/L ; the third flask was prepared by combining equal volumes of spent medium and concentrated fresh medium in order to achieve a nutrient concentration equal to that of B4 medium, with supplemented glucose (40 g/L) and glycine (0.4 g/L); and the fourth flask contained 1 volume of spent medium for every 3 volumes of fresh medium, nutrient concentration was the same as for flask 3. Another two flasks were prepared as controls, containing

only fresh medium with the same nutrients concentration as in flask 3. Growth curves for all experiments are shown in Fig. 5.11.

As expected, the spent medium alone, or supplemented with only glycine, was not able to support algal growth. This confirms that the medium was indeed lacking the necessary nutrients for supporting algal metabolism. There was a slight reduction, significant at the 95 % confidence level (p-value = 0.006), in the biomass growth between the cultures prepared using spent media and the control, accounting for a 3.5 % to 4.0 % difference in the final biomass concentration. This reduction in yield could be due to either the presence of inhibitory metabolites in the spent media or due to a higher concentration of trace elements. Accumulation of trace elements in the culture can result in a higher osmotic pressure, increasing the maintenance energy of the cells. Because trace elements are fed in excess to the culture and their final concentration is not measured, it is not possible to exclude them as the reason for a lower yield in the cultures prepared from spent media.

5.5 Effect of antifoam agents

Algal cultures, particularly at cell densities greater than 20 g/L, can foam extensively. To avoid this problem, antifoam agents are normally added to the culture broth to modify its surface tension. Alternatively, mechanical devices can be used as foam breakers.

Before using an antifoam agent it is necessary to evaluate its effect on the culture, as some of the components in the antifoam mixture might have an inhibitory effect or may act as a substrate for growth. An experiment was conducted to evaluate the effect of two different antifoams on the growth of *A. protothecoides*: Antifoam SE-15 is a 10 % emulsion of an active silicon

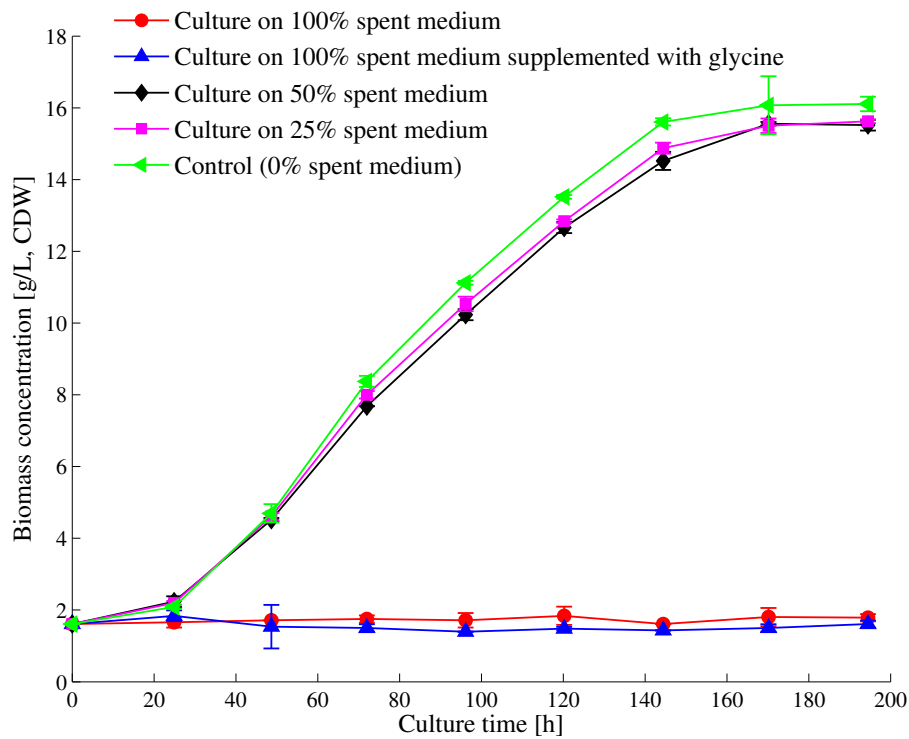


Figure 5.11: The inhibitory effect of accumulated metabolites on the heterotrophic growth of *A. protothecoides*. Culture media was prepared using spent media (two weeks old) from a high density culture. In the first experiment no nutrients were added to the spend media; for the second experiment spent media was supplemented with glycine at a concentration of 0.4 g/L, and for the remaining experiments nutrients were as added as per B4 Medium formulation, with an initial glycine concentration of 0.4 g/L and initial glucose concentration of 40 g/L.

antifoam and non-ionic emulsifiers, while Antifoam O-30 is an organic, fatty acid ester-type antifoam.

Usually, antifoams are added to the culture medium at a concentration ranging from 100 to 1000 ppm. In order to facilitate the evaluation of any potential inhibitory effect, antifoams were applied to the culture at two different concentrations, 1000 ppm (0.1 % v/v) and 10000 ppm (1 % v/v); higher values than would be expected during normal operation. Experiments were conducted with B4 medium, supplemented with glucose (40 g/L) and glycine (0.4 g/L). Two additional flasks were prepared as controls without any antifoam added to them. The growth curves for all the experiments are reported in Fig. 5.12.

At the higher concentration level, the silicon-based antifoam SE-15 caused a 10 % reduction in the final biomass concentration with respect to the control flask. The corresponding reduction at the lower level, however, was not significant. The organic antifoam, on the other hand, acted as a growth enhancer, boosting the initial growth rate by 28 %, with respect to the control.

A second series of experiments was performed using only the organic, fatty acid ester-type antifoam O-30. The antifoam concentrations were 0, 100, 500, and 1000 ppm. These values cover the concentration ranges that are expected during normal operation. The medium compositions were the same as in the previous experiments. Fig. 5.13 presents the growth curves for these experimental series.

As previously observed, the organic antifoam seemed to act as a growth enhancer. A *t*-test, however, shows that the observed variations are not significant at 95 % confidence levels for the two lower concentrations of the antifoam, with a *p*-value equal to 0.1. At the highest concentration examined in this experiment, 1000 ppm of O-30, the observed enhancement in growth becomes significant with a *p*-value equal to 0.017.

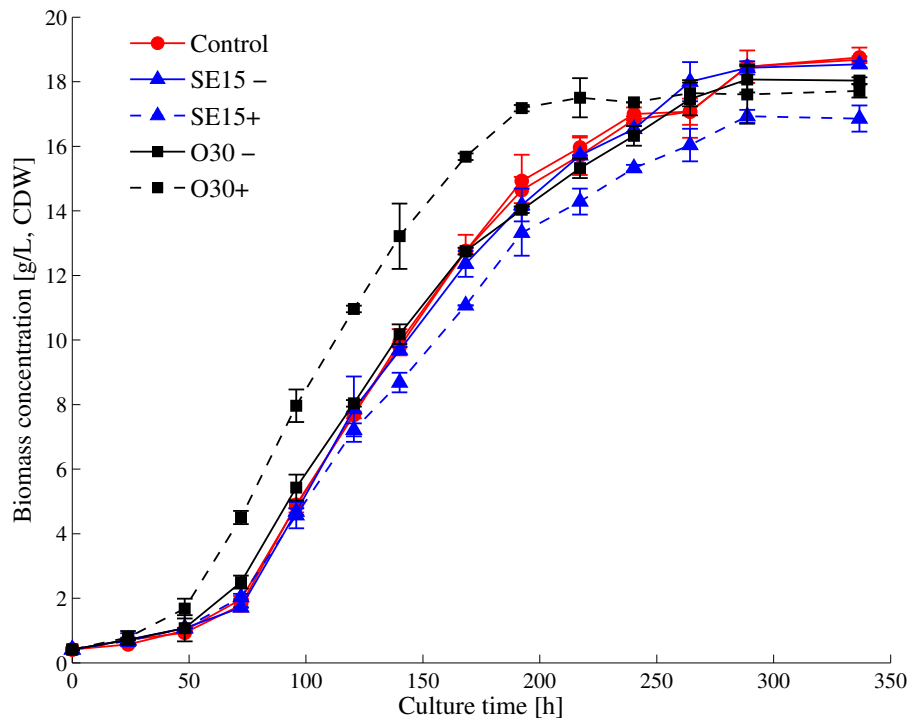


Figure 5.12: The effect of antifoam agents on the growth of *A. protothecoides*. B4 Medium was used with an initial glycine concentration of 0.4 g/L and an initial glucose concentration of 40 g/L. The lower level of antifoam (–) was set at 0.1 %, and the higher level (+) was set at 1 %.

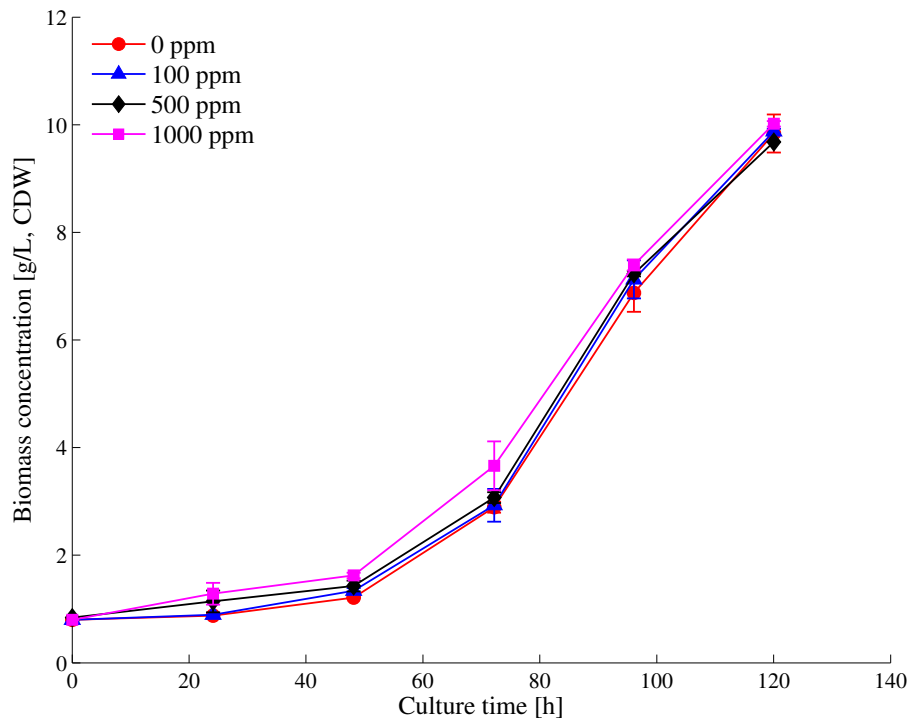


Figure 5.13: The effect of the organic, fatty acid ester type, O-30 antifoam concentration on the growth profile of *A. protothecoides*. B4 Medium was used with an initial glycine concentration of 0.4 g/L and an initial glucose concentration of 40 g/L.

The organic antifoam O-30 is preferred over the silicon based SE-15, as this last one has some minor inhibitory effect on growth, while O-30 shows a positive enhancement of growth. The drawback of this result is that the antifoam could be being consumed by algae and therefore would have to be replenished as the culture proceeds.

6

A model for algal metabolism¹

The task of modelling a biological process requires one to carefully consider the purpose that the model will serve, and the potential use others can make of that model. The objective of this study is to develop a model that successfully describes the macroscopic behaviour of microalgal cultures in heterotrophic reactors, but is still simple enough to be used for process optimization and control. In particular it is desirable to model the effect of nitrogen and carbon substrate concentration on biomass growth rate and oil production rate.

An additional and far-reaching goal of this modelling exercise is to gain insight in the behaviour of algae. For this reason, the use of black-box models, frequently used for control and optimization, was not considered. The understanding of algal physiology, gained through the formulation and use of

¹Some sections of this chapter have been published. De la Hoz Siegler *et al.* 2011. *Bioresource Technology*. 102(10): 5764–5774.

this model, will hopefully provide microbiologists and chemical engineers with better tools for developing algal biotechnology.

Algal cells are known for their capacity to assimilate nutrients much faster than what is required to support their metabolism (Droop, 1973; Sommer, 1991). In Chapter 5, it has been shown that there is a significant variation in the cellular composition along a single batch run, and that nitrogen uptake and growth are uncoupled processes. The implication of these facts is that biomass growth rate might not be directly related to the concentration of the limiting substrate in the medium; therefore, Monod-like models are, in general, not appropriate for modelling algal dynamics.

To model the uncoupling of nutrient uptake and growth it is possible to use the quota concept proposed by Droop (1973) or the structured compartmentalized cell approach. It should be noted that these are not opposite formulations, but rather equivalent ones (Tett and Droop, 1988). In the quota formulation, the content or quota of one or more nutrients inside the cells is variable, but the cell is still regarded as a unique compartment. In the structured model formulation, cells are considered to be formed by two or more compartments, with each compartment having a fixed chemical composition. The resulting mathematics of these two approaches are equivalent, and therefore either of them can be used to derive the model presented here. In this work, the model is derived using the compartmentalized cell approach, as it is a more familiar approach in engineering. It is important to highlight, however, that the quota approach is the preferred one in the physiological literature (Leadbeater, 2006).

This chapter provides the rationale followed in the development of the model and presents to the reader the different alternative kinetic expressions considered. A set of batch experiments, conducted to calibrate the model, as well as a fed-batch experiment used for model validation are also presented.

6.1 The compartmentalized cell

A compartmentalized model of the algal cells is proposed in order to incorporate the experimental observations presented in Chapter 5, and to satisfy the proposed modelling objectives, based on the following premises:

- Cells are composed of three main compartments: metabolically active biomass (x), lipid body (p), and a nitrogen pool (q).
- Nitrogen source is taken up into the nitrogen pool and later converted, at a constant yield $Y_{x/q}$, into active biomass.
- Carbon source is taken up by the cells and directly converted either into active biomass or oil, at constant yields $Y_{x/s}$ or $Y_{p/s}$, respectively.
- Oil stored in the lipid bodies is used to support growth at a constant yield $Y_{x/p}$.

The transformation from nutrients to the different cell compartments is represented in the schematic shown in Fig. 6.1. A fundamental assumption in the model is that the nitrogen source cannot be used directly to support growth but has to be first integrated into the nitrogen pool. The carbon source, on the other hand, can be stored into the lipid bodies or can be assimilated to sustain growth. Stored carbon in the lipid bodies, can be further used to support biomass growth.

The active biomass, x , acts as the catalyst for all the reactions in the cells, being responsible for taking nutrients up from the medium and for producing oil and biomass. The overall biochemical reactions can be written as:

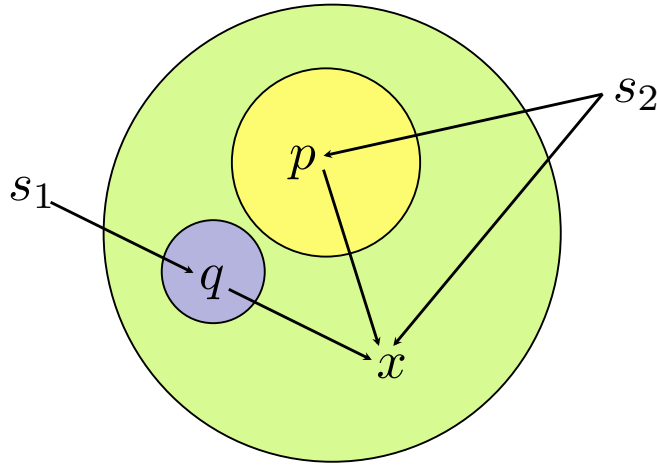
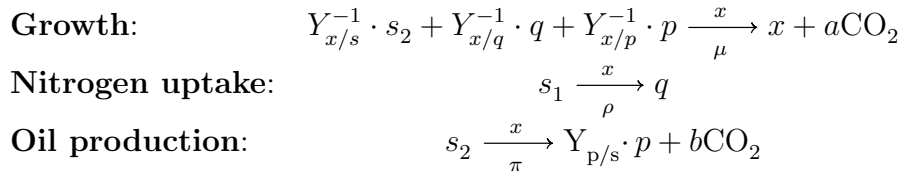


Figure 6.1: Schematic representation of the algal cell. Cells are considered to be formed by three main compartments: active biomass (x), lipid body (p), and nitrogen pool (q). The nitrogen source (s_1) is taken up by the cells into the nitrogen pool, while the carbon source (s_2) is used directly to support lipid production and biomass growth.



The three reaction rates (μ , ρ , and π) are specific reaction rates with respect to the active biomass concentration. This is a convenient convention given that all three reactions are catalyzed by the algal biomass.

A bioreaction system where the two main nutrients, carbon and nitrogen, are fed independently is assumed to write the non-steady state material balance. The nitrogen source is fed at a volumetric flow rate f_1^i and concentration s_1^i , while the carbon source is fed at f_2^i and concentration s_2^i . Consequently, the dilution rate is given by $D = (f_1^i + f_2^i)/V$, with V being the reaction volume. The dynamics of the algal bioreactor can be described using the following set of differential equations:

$$\frac{ds_1}{dt} = -\rho x + s_1^i \frac{f_1^i}{V} - s_1 D \quad (6.1a)$$

$$\frac{ds_2}{dt} = -\frac{1}{Y_{x/s}} \mu x + s_2^i \frac{f_2^i}{V} - k_m x - \frac{1}{Y_{p/s}} \pi x - s_2 D \quad (6.1b)$$

$$\frac{dx}{dt} = \mu x - x D \quad (6.1c)$$

$$\frac{dp}{dt} = \pi x - \frac{1}{Y_{x/p}} \mu x - p D \quad (6.1d)$$

$$\frac{dq}{dt} = \rho x - \frac{1}{Y_{x/q}} \mu x - q D \quad (6.1e)$$

$$\frac{dV}{dt} = V D - f_o \quad (6.1f)$$

where f_o is the flow rate of the outlet stream, if any. In Eq. 6.1b, k_m is the maintenance constant. Here, it is assumed that only the carbon substrate is consumed for supporting the maintenance of the cells, but no nitrogen is consumed. The rationale for this assumption is that even though cells do consume nitrogen compounds for supporting and repairing their metabolic machinery, they tend to optimize the use of naturally limiting nutrients and therefore recycle most of the nitrogenous compounds. Carbon substrates, on the other hand, are to be consumed to generate the ATP necessary to fuel the biochemical reactions in the cell.

In Eq. 6.1, the production of CO_2 was not included as the gas exhaust from the reactor was not analyzed in this project. It should be noted however, that a additional ordinary differential equations could be written for CO_2 production and O_2 consumption, whenever such data is available.

Several expressions have been previously proposed to model the three main reaction rates that appear in Eqs. 6.1. Experimental data from batch cultures are used to decide which kinetic expressions provide a better representation of

microalgal dynamic behaviour. The following subsections present the different alternative kinetic models considered, while in Section 6.2 the performance of these expressions is evaluated.

6.1.1 Kinetics of nutrient uptake

The uncoupling between nutrient uptake and growth is one of the most important characteristics of algal systems. This uncoupling proscribes the use of those growth models, such as Monod one, that assume a direct dependance between limiting nutrient concentration in the medium and growth rate.

For modelling the uptake of nitrogen-containing compounds by microalgae several expressions have been previously proposed, as summarized below:

- Michaelis-Menten:

$$\rho = \rho_m \frac{s_1}{K_{s_1} + s_1} \quad (6.2)$$

- Hill allosteric regulation model:

$$\rho = \rho_m \frac{s_1^N}{K_{s_1}^N + s_1^N} \quad (6.3)$$

- Lehman et al. (1975):

$$\rho = \rho_m \frac{s_1}{K_{s_1} + s_1} \left(\frac{\tilde{q}_M - \tilde{q}}{\tilde{q}_M - \tilde{q}_m} \right) \quad (6.4)$$

- Caperon and Meyer (1972):

$$\rho = \rho_m \frac{s_1 - s_0}{K_{s_1} + s_1 - s_0} \quad (6.5)$$

Eq. 6.2 corresponds to the conventional Michaelis-Menten kinetics, as proposed by Droop (1973) in his original quota model. Here, ρ_m is the maximum specific

nitrogen uptake rate and K_{s_1} is the half saturation constant for nitrogen uptake, in terms of the extracellular nitrogen concentration.

The Hill allosteric regulation model considers that the activity of the transporter enzymes is affected, either positively or negatively, by the concentration of the substrate being taken up. Allosteric regulation of nutrients uptake in algae has been proposed by Flynn (2003). In Eq. 6.3, N is the Hill allosteric regulation coefficient; if N is greater than one there is a positive regulation, and if N is less than one there is a negative regulation.

Eq. 6.4 was proposed by Lehman et al. (1975) to take into account the finite maximum storage capacity algal cells have, with \tilde{q}_M being the maximum fraction of nitrogen that can be stored by the cells, and \tilde{q}_m the minimum amount of nitrogen in the cells that will support growth. The current fraction of nitrogen stored in the cells is given by \tilde{q} . The final expression, proposed by Caperon and Meyer (1972), considers that there is a threshold nutrient concentration, s_0 , below which no nutrient can be taken up by the cells.

6.1.2 Growth kinetics

The growth rate, μ , for a system with two interacting substrates, carbon and nitrogen, can be expressed as:

$$\mu = \mu_m \tilde{r}_C \tilde{r}_N \tag{6.6}$$

where μ_m is the maximum growth rate and \tilde{r}_C and \tilde{r}_N are the normalized reaction rates based on the concentration of the carbon source and the nitrogen source, respectively. Each one of the normalized growth rates \tilde{r} is to be defined in such a way that they are bounded between 0 and 1 (Bellgardt, 2000).

Effect of nitrogen cell content on growth rate kinetics

To study the relationship between intracellular nitrogen content and growth rate, biomass concentration profiles were fitted to a smoothing spline and the instantaneous growth rate was calculated as per Eq. 2.2. The instantaneous growth rate and the intracellular nitrogen concentration for a batch run are shown in Fig. 6.2. It can be seen that growth rate closely follows the nitrogen content profile.

However, in Fig. 5.3, it has been previously shown that the growth rate was

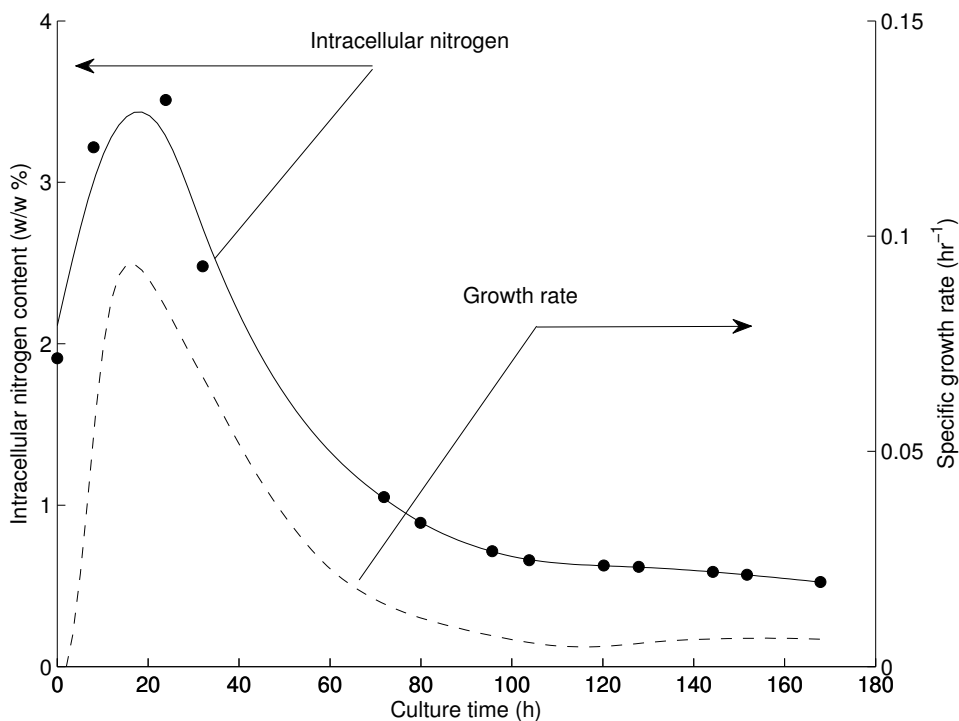


Figure 6.2: Specific biomass growth rate [---] and intracellular nitrogen concentration [- o -] for a batch culture with an initial glycine concentration = 0.19 g/L and initial glucose concentration = 19.8 g/L, other nutrients as in medium B4-Fe.

maximized at an intermediate level of the initial nitrogen availability. That is, growth rate increased as the initial nitrogen concentration increased, up to the point in which nitrogen started being inhibitory to algal growth. To model these two effects, the following kinetic expressions were evaluated:

- Haldane-like inhibition:

$$\tilde{r}_N = \frac{\tilde{q}}{K_{\tilde{q}} + \tilde{q} + \frac{\tilde{q}^2}{K_{i1}}} \quad (6.7)$$

- Cumulative inhibition:

$$\tilde{r}_N = \frac{\tilde{q}}{K_{\tilde{q}} + \tilde{q}} \exp\left(-\frac{\frac{1}{t}[\tilde{q}(t_0) + \int_0^t \tilde{q} dt]}{K_{i1}}\right) \quad (6.8)$$

In these two equations, \tilde{q} is the mass fraction of the nitrogen pool in the cells, $\tilde{q} = q/(q+p+x)$; $K_{\tilde{q}}$ is the half saturation constant in terms of the intracellular nitrogen concentration; and K_{i1} is the inhibition constant expressed as weight fraction of nitrogen in the biomass.

Eq. 6.7 corresponds to the classic Haldane uncompetitive inhibition model. In the kinetic expression presented in Eq. 6.8, it was considered that growth is inhibited by the historical average of the nitrogen content in the cells, instead of the instantaneous nitrogen concentration. The average was taken from the start of each culture. Eq. 6.8 aimed to incorporate the cumulative effect that previous events in the culture has over the instantaneous observed growth rate. In particular, it was desirable to capture the effect of changes in metabolic activity induced by variations in the nitrogen content (Xiong et al., 2010) and that resulted in an apparent inhibition of growth due to excessive luxurious nitrogen consumption.

Effect of glucose concentration on growth rate kinetics

To model the effect of the carbon source concentration on the growth rate of microalgae two alternative expressions were considered:

- Michaelis-Menten:

$$\tilde{r}_C = \frac{s_2}{K_{s_2} + s_2} \quad (6.9)$$

- Haldane-like inhibition:

$$\tilde{r}_C = \frac{s_2}{K_{s_2} + s_2 + \frac{s_2^2}{K_{i_2}}} \quad (6.10)$$

with K_{s_2} being the half saturation constant in terms of the glucose concentration in the media, and K_{i_2} being an inhibition constant.

6.1.3 Product formation kinetics

Algal cells are remarkable for their capacity to produce and store large amounts of oil. Oil assembly occurs in the endoplasmic reticulum, and it is stored in lipid bodies (liposomes), which are single membrane organelles in the cytoplasm. The size and number of liposomes varies as a function of cell age and nutritional status. In Fig. 4.10, it can be seen that liposomes can be as large as 90% of the cell's diameter, while in other cases multiple lipid bodies are present in the cells. Neutral lipids stored in lipid bodies are used as an energy supply or to build the membranes for the next cell generation; membrane lipids constitute about 5-20% of the algal dry cell weight (Hu et al., 2008).

To model the oil production rate in microalgae it was considered that the production rate is largely dependent on the availability of a carbon source. A sigmoidal (Michaelis-Menten like) dependance of the specific growth rate with respect to the glucose concentration was therefore assumed:

$$\pi = \pi_m \frac{s_2}{K_{ps_2} + s_2} \quad (6.11)$$

where π_m is the maximum oil production rate, and K_{ps_2} is the concentration of glucose at which the oil production rate is equal to half the maximum rate.

This expression was compared with two other alternative models. First, it was assumed that the oil production rate was a decreasing function of the oil content; as the lipid bodies occupied a larger fraction of the cell volume, the oil production rate decreased. With \tilde{p} being the mass fraction of oil in the cells, $\tilde{p} = p/(p + q + x)$, the resulting kinetic expression is:

$$\pi = \pi_m \frac{s_2}{K_{ps_2} + s_2} (1 - \tilde{p}) \quad (6.12)$$

In the second expression evaluated, it was considered that oil production rate was inhibited by the intracellular nitrogen concentration, with a kinetics of the following type:

$$\pi = \pi_m \frac{s_2}{K_{ps_2} + s_2} \left(1 - \frac{\tilde{q}}{K_{ip}} \right) \quad (6.13)$$

where K_{ip} corresponds to the inhibition constant in terms of the intracellular concentration of nitrogen.

6.2 Model selection

To select the kinetic expressions that better represent the growth of algae in heterotrophic conditions a series of batch experiments were conducted. Model parameters were estimated by minimizing the weighted sum of squared residuals between the predicted concentrations and the experimental measurements,

using the variance of the experimental measurements as the weighted factor. Several measurements of the goodness of fit for each model were subsequently evaluated.

The Michaelis-Menten rate equation was used as the base case in order to evaluate the effect of each individual kinetic expression on the goodness of fitting of the overall dynamic model presented in Eq. 6.1. That is, when evaluating the alternative kinetic expressions for one of the reaction rates in the model, all the other reaction rates were set to the base Michaelis-Menten case.

6.2.1 Experimental data

A three-level full-factorial design was used to conduct the experimentation to generate the data for model calibration. The green microalga *Auxenochlorella protothecoides* was cultured heterotrophically, in the dark, as described in Section 3.1.1. Glycine and glucose were the sole nitrogen and carbon sources, respectively. The initial and final conditions for each experiment are reported in Table 6.1.

As shown in Table 6.1, nine out of the eleven batch experiments were conducted with nitrogen limitation and thus had residual glucose at the end of the culture. For these nitrogen-limited cultures, the analysis of variance (ANOVA) shows that there was not a significant effect of the glucose initial concentration on the final biomass concentration (p-value = 0.542). For these same cultures, the final oil concentration was found to be not statistically significantly dependent on the initial glucose or glycine availability. Any observed variations in the oil content among different runs were within the measurement error. For the glucose-limited runs, however, the final oil content was the lowest among the batch experiments. This result was expected, given that glucose was exhausted

Table 6.1: Initial and final conditions, after 150h of heterotrophic cultivation, for batch experiments. *A. protothecoides* was grown axenically using glucose as the sole carbon source, and glycine as the sole nitrogen source.

Initial conditions		Final conditions			
Glucose g/L	Glycine g/L	Biomass g/L, dry basis	Oil Content %/w/w	Nitrogen content %/w/w	Glucose g/L
38.9	0.19	6.4 ± 0.03	61.9 ± 1.3	0.56 ± 0.02	23.5 ± 0.12
29.3	0.19	6.6 ± 0.05	52.0 ± 6.9	0.51 ± 0.02	12.5 ± 0.06
19.8	0.19	6.7 ± 0.08	62.9 ± 3.7	0.58 ± 0.01	2.8 ± 0.01
38.9	0.38	10.6 ± 0.05	51.8 ± 5.0	0.60 ± 0.01	11.2 ± 0.06
29.3	0.38	10.8 ± 0.10	54.9 ± 4.9	0.61 ± 0.01	1.2 ± 0.01
19.8	0.38	7.6 ± 0.20	48.1 ± 3.9	0.84 ± 0.04	0.0
38.8	0.57	8.5 ± 0.00	60.1 ± 9.3	0.99 ± 0.04	16.6 ± 0.08
29.3	0.57	8.5 ± 0.05	63.8 ± 2.9	0.92 ± 0.01	6.6 ± 0.03
19.8	0.57	7.2 ± 0.15	49.1 ± 4.2	1.13 ± 0.01	0.0
29.3	0.38	10.2 ± 0.08	60.7 ± 3.1	0.63 ± 0.01	2.3 ± 0.01
29.3	0.38	10.3 ± 0.05	61.1 ± 4.0	0.61 ± 0.02	2.1 ± 0.01

and there was no other carbon source available for further conversion into lipids.

Samples were taken, twice a day, from each flask and centrifuged to separate the algal cells from the culture broth. Algal cells were dried, and the supernatant was frozen for later analysis. Biomass cell concentration profiles, as cell dry weight, are presented in Fig. 6.3. Growth was maximized at the intermediate level of nitrogen availability: at low nitrogen concentrations growth was limited by the extreme nitrogen deficiency (final nitrogen content around 0.5 %); while at high nitrogen content growth was inhibited.

Cells double at their maximum rate during exponential phase. In all the experiments, exponential growth was observed between 20 h and 80 h. The calculated growth rates during the exponential phase are plotted in Fig. 6.4 as a function of the initial nitrogen and carbon sources concentration. The growth rate exhibits a non-linear dependence on the initial glycine concentration, while it is almost independent of the glucose concentration. The simpler model that was able to fit the dependence between growth rate at exponential phase and initial nutrients concentration was a pure quadratic model. The predicted surface response is plotted in Fig. 6.4 together with the observed growth rates, as calculated using Eq. 2.2.

Glucose concentrations in the filtered growth media were determined by high performance liquid chromatography. Glucose profile for each flask is presented in Fig. 6.5. Glucose consumption is directly related with algal growth, with a decreasing profile as more biomass is being produced, as can be seen by comparing Figs. 6.3 and 6.5.

The uncoupling between nitrogen uptake and growth has been shown in Chapter 5. It was also observed that such uncoupling results in a transient increase in the nitrogen content in the cells. Total nitrogen content in dry algal cells,

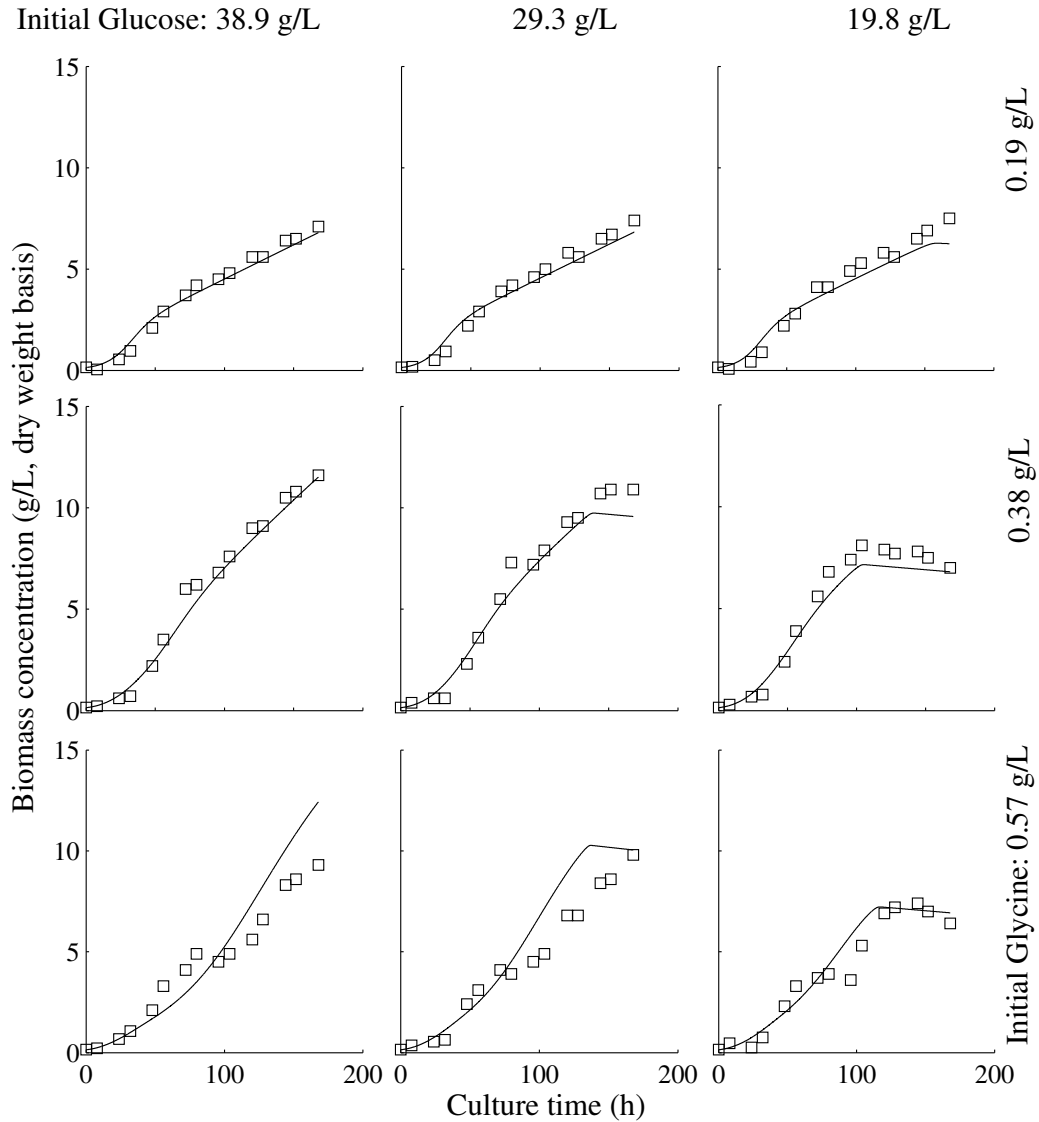


Figure 6.3: Biomass concentration profiles of all batch runs used for model calibration. Fitted lines correspond to the predicted profile by using the model presented in Eq. 6.1 and Section 6.2.6.

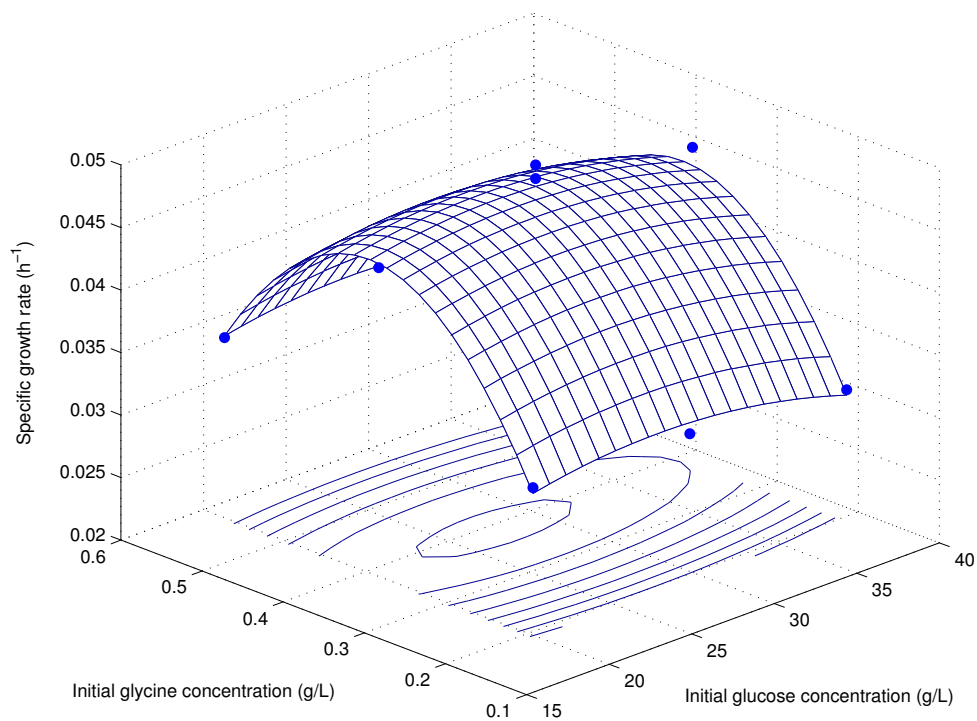


Figure 6.4: Specific growth rate of *A. protothecoides* at exponential growth. Observed data points [●] are plotted over the fitted response surface plot. The initial nitrogen concentration (as glycine) has a significant, inhibitory, effect on the growth rate, ANOVA p value = 0.0007.

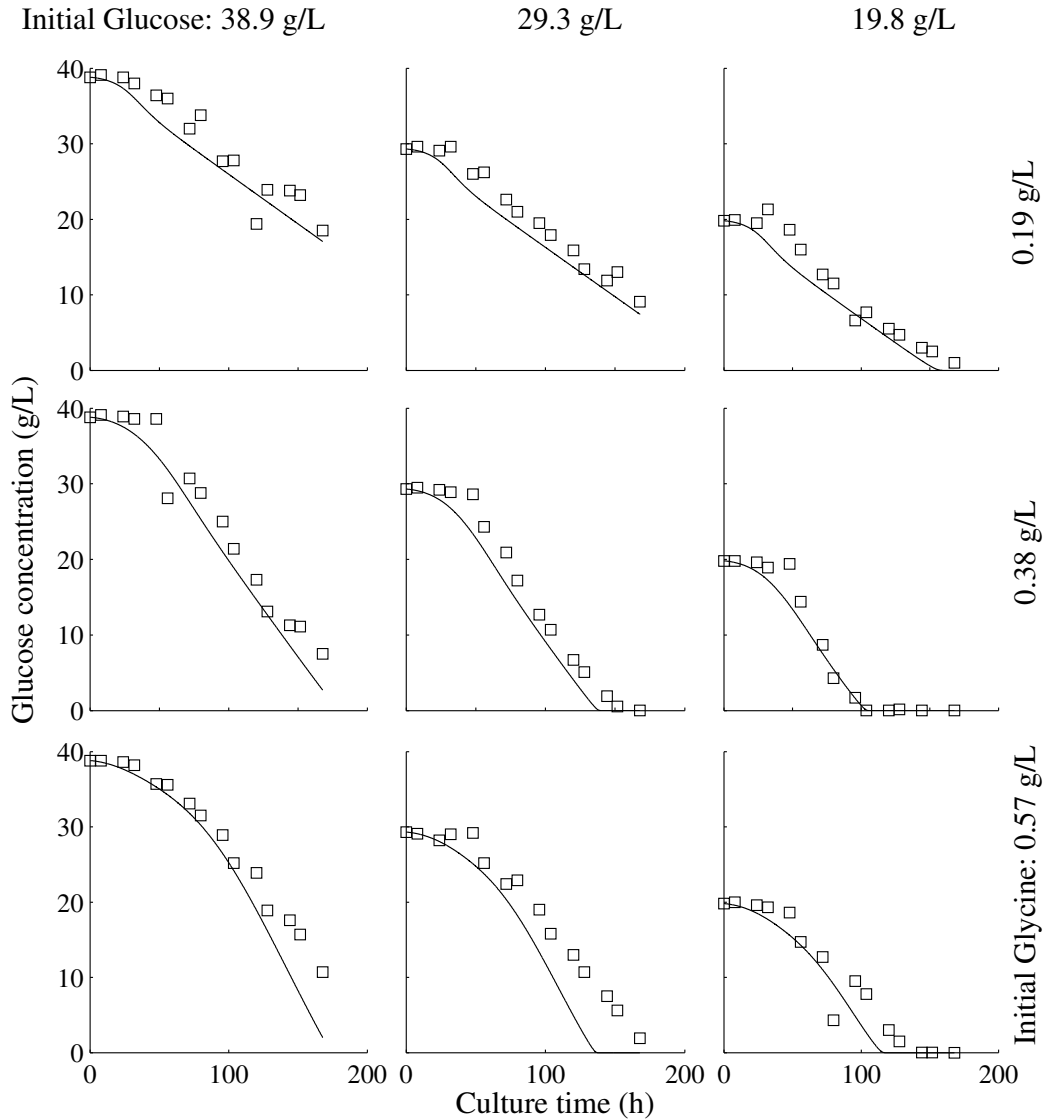


Figure 6.5: Glucose concentration profiles of all batch runs used for model calibration. Fitted lines correspond to the predicted profile by using the model presented in Eq. 6.1 and Section 6.2.6.

as measured by pyrochemiluminescence, is shown in Fig. 6.6. The maximum nitrogen content was measured at around 48 h after inoculation, with a rapid depletion afterwards. A two to five-fold increase in the nitrogen content of algal biomass was observed.

The total content of oil in algal cells varies as it is the result of the balance between growth and oil production. The variations in oil content of algal cells, as a function of culture time, are shown in Fig. 6.7. There was a significant decrease in the oil content, as percentage of cell dry weight, at the early stage of growth. Furthermore, total oil content (as grams of oil per litre of culture broth) decreased 22 % on average for all runs in the first 24 h of culture, which implies cells were consuming the oil reserves to support their metabolism.

6.2.2 Nitrogen uptake

The ability of the kinetic expressions presented in Section 6.1.1 to explain the experimental data was evaluated by computing several performance criteria, as summarized in Table 6.2. The weighted sum of squared errors (WSSE) for the Hill allosteric regulation model is slightly better than the one for the Michaelis-Menten base case; however, both the Akaike and the Bayesian information criteria show that these two models are equivalent, and therefore the simpler one should be selected. The other models evaluated have higher values for the WSSE and the information criteria, and therefore are worse than the Michaelis-Menten model.

6.2.3 Effect of nitrogen concentration on growth

To decide which of the kinetic expressions for modelling the effect of nitrogen on the growth rate provided a better representation of the experimental observations, the kinetic parameters were fitted in order to minimize the weighted

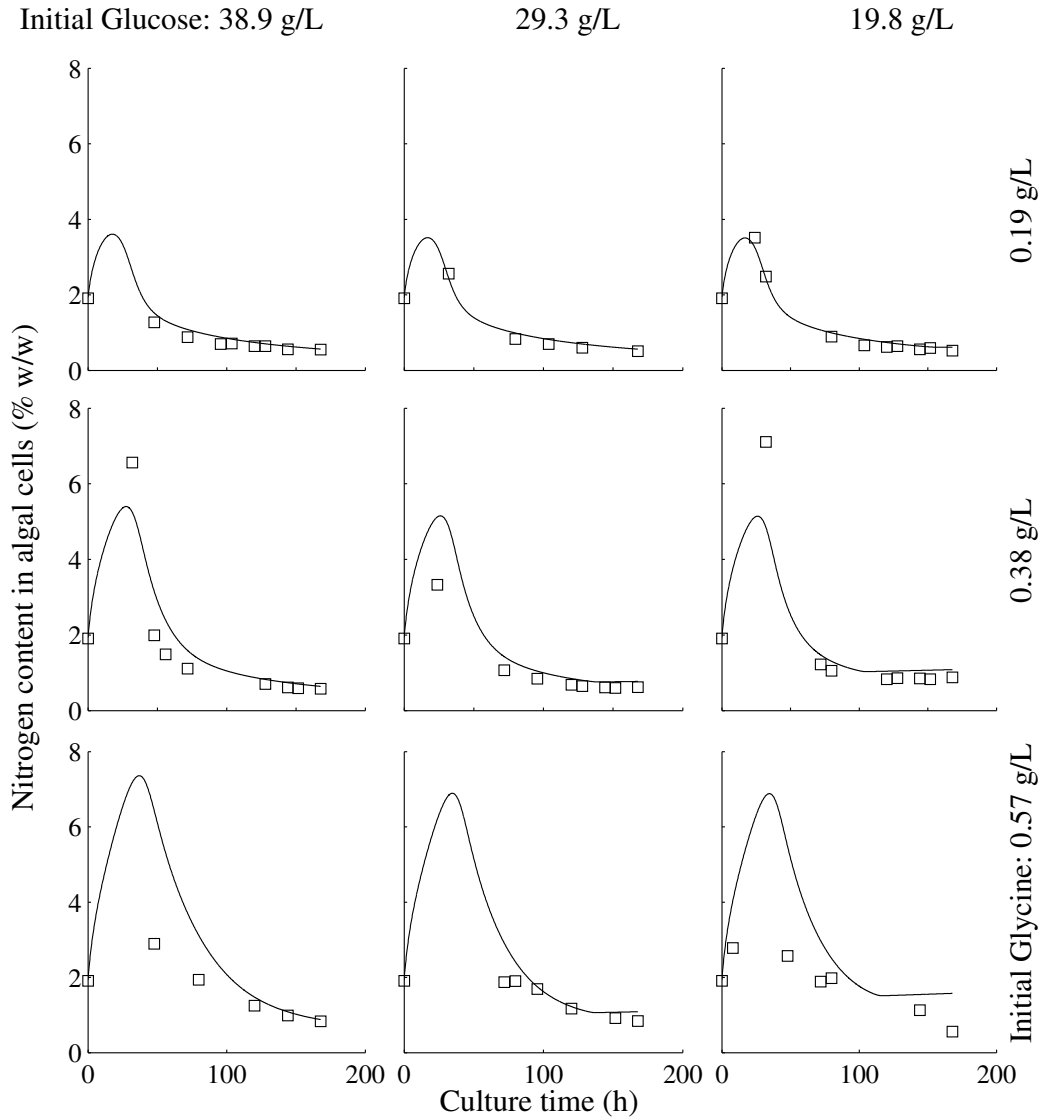


Figure 6.6: Biomass concentration profiles of all batch runs used for model calibration. Fitted lines correspond to the predicted profile by using the model presented in Eq. 6.1 and Section 6.2.6.

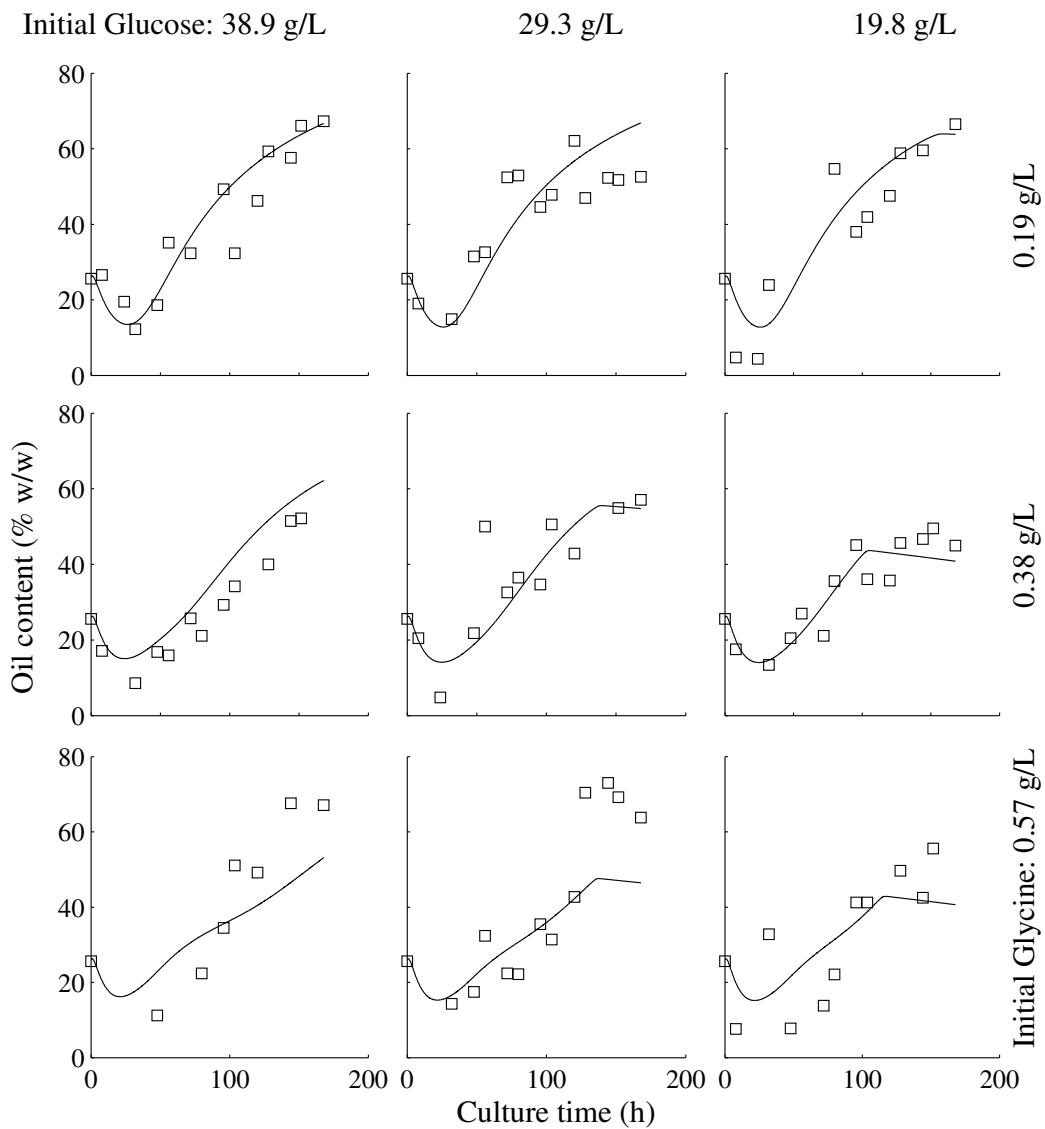


Figure 6.7: Oil content profiles for all batch runs used for model calibration. Fitted lines correspond to the predicted profile by using the model presented in Eq. 6.1 and Section 6.2.6.

Table 6.2: Comparison among kinetic expressions to model the nitrogen uptake rate.

Kinetic model for ρ	WSSE	AIC	BIC
Michaelis-Menten	74.7	-0.60	-3.41
Hill allosteric regulation, Eq. 6.3	74.2	-0.60	-3.41
Lehman et al, Eq. 6.4	80.7	-0.53	-3.33
Caperon-Meyer, Eq. 6.5	76.5	-0.58	-3.39

sum of squared errors (WSSE), and the Akaike and Bayesian information criteria were computed, as summarized in Table 6.3.

From Table 6.3, it can be seen that the best fitting of the experimental data is obtained when Eq. 6.8 is used to model the growth rate kinetics, as it provides significantly lower values for the two information criteria used (AIC and BIC), as well as a lower residual error (WSSE). This result supports the idea that the growth rate follows a hyperbolic profile with respect to the intracellular nitrogen concentration and is in turn affected by the past concentration of nitrogen in the cells. It must be noted that, the Michaelis-Menten and the Haldane inhibition models provided a reasonable fit when only the data from the low and medium initial nitrogen concentration runs were considered, but failed to model the full dataset that included all the runs (low, medium, and high nitrogen).

Table 6.3: Performance of kinetic functions evaluated to model \tilde{r}_N , the normalized growth rate based on the intracellular nitrogen content.

Kinetic model for \tilde{r}_N	WSSE	AIC	BIC
Michaelis-Menten	74.7	-0.60	-3.41
Haldane inhibition, Eq. 6.7	75.7	-0.59	-3.40
Cumulative inhibition, Eq. 6.8	16.3	-2.12	-4.93

Excessive nitrogen uptake starts a cascade of events that result in growth inhibition. When nitrogen deficient algal cells undergo a significant increase in their cellular pool of nitrogen compounds, their metabolism will adapt to the new condition shifting the concentration of enzymes and other intermediates; the larger the increase in the nitrogen pool, the larger the change in the metabolic machinery. Variations in the metabolic flux as a function of nitrogen nutrition status have been previously reported in *A. protothecoides* (Xiong et al., 2010).

For transient events, in which the nitrogen pool increases and then decreases, there was an observed residual inhibitory effect in the growth rate. Given that an observed variation in the metabolic flux in the cells was due to several other processes happening in a tightly regulated environment, it was expected that there would be a time delay between the event that activated the metabolic change and the observed change. For modelling, it is relevant to account for these time delays or processing times. Davidson and Cunningham (1996) considered that nutrients are subject to an average processing time, τ' , before it affects growth; and modified the mass balances and kinetic expressions accordingly, that is, changes at time t were assumed dependent on the nutrient concentrations at time $t - \tau'$. In this work, this idea was extended to consider the average intracellular nutrient concentration over the culture, instead of a single time point in the past. This approach considers that a large and sustained increase in the intracellular nitrogen concentration will have a larger inhibitory effect than a quick spike, even a large one.

For model fitting, it was found satisfactory to include the full history, from the start of the culture, of intracellular nitrogen concentration to model the observed growth rate inhibition. When only the previous 24 hours of nitrogen concentration were included in the integral term in Eq. 6.8, the fit of the model

decreased. It must be highlighted that, in general, events that happened long ago will influence current cell growth. Therefore, for repeated batches or continuous cultures with a long culture time, a finite time-window for considering nutrient history is expected to be a more appropriate approach. Further research is required in order to establish how far back in time it is necessary to integrate Eq. 6.8.

6.2.4 Effect of carbon concentration on growth

Table 6.4 summarizes the the weighted sum of squares (WSSE) and the two model information criteria used for model comparison. The values of the performance evaluation criteria for the Haldane inhibition model are comparatively lower than the corresponding values for the Michaelis-Menten model. Therefore, it is concluded that the Haldane inhibition model provides a superior representation of the experimental data.

Table 6.4: Performance of kinetic functions evaluated to model \tilde{r}_C , the normalized growth rate based on the glucose concentration in the media.

Kinetic model for \tilde{r}_C	WSSE	AIC	BIC
Michaelis-Menten	74.7	-0.60	-3.41
Haldane inhibition	67.4	-0.71	-3.51

6.2.5 Lipid production

The weighted sum of squared errors (WSSE) and the two information criteria (AIC and BIC) used to compare the model performance are reported in Table 6.5 for the three alternative expressions used to model oil production rate.

Table 6.5: Performance of kinetic functions evaluated to model the oil production rate (π)

Kinetic model for π	WSSE	AIC	BIC
Michaelis-Menten, Eq. 6.11	74.7	-0.60	-3.41
Saturation by lipid content, Eq. 6.12	69.0	-0.68	-3.49
Inhibition by nitrogen, Eq. 6.13	80.3	-0.53	-3.34

According to the results in Table 6.5, the saturation model presented in Eq. 6.12 provides the best representation of the experimental data. This implies that oil production does indeed follow a Michaelis-Menten kinetic, but as cell volume was getting filled by the oil body, oil production rate was turning down.

6.2.6 Summary of kinetic expressions

Overall, the best fitting is achieved by considering that the growth rate was a double sigmoidal function of the external glucose concentration and the internal nitrogen content:

$$\mu = \mu_m \frac{s_2}{K_{s_2} + s_2 + \frac{s_2^2}{K_{i_2}}} \frac{\tilde{q}}{K_{\tilde{q}} + \tilde{q}} \exp\left(-\frac{\frac{1}{t}[\tilde{q}(t_0) + \int_0^t \tilde{q} dt]}{K_{i_1}}\right) \quad (6.14)$$

By assuming this representation, the transient accumulation of nitrogen compounds in the cytoplasm, that occurs whenever nitrogen-deficient algal cells are exposed to a nitrogen source (Dortch et al., 1984), can be represented by the model. Furthermore, the inhibition terms from glucose and from the past history of the nitrogen content have a significant effect on model prediction, as shown by the lower values for both information criteria (AIC and BIC) and the lowest residual error.

The nitrogen uptake rate is best modelled by a simple Michaelis-Menten kinetics,

$$\rho = \rho_m \frac{s_1}{K_{s_1} + s_1} \quad (6.2)$$

while the oil production rate follows a Michaelis-Menten kinetics with an additional saturation term due to the finite storage capacity of the cells:

$$\pi = \pi_m \frac{s_2}{K_{ps_2} + s_2} (1 - \tilde{p}) \quad (6.12)$$

The use of these three kinetic expressions together with the system of ordinary differential equations presented in Eq. 6.1 provides the best representation of the batch experimental data. The predicted concentration profiles for biomass, glucose, intracellular nitrogen, and oil content for all the experimental dataset are shown in Figs. 6.3, 6.5, 6.6, and 6.7. For all four experimental measurements, there is a close agreement between the observed concentrations and the predicted ones. The mean absolute error was 0.72 g/L for biomass, 2.1 g/L for glucose, 0.53 % (w/w) for intracellular nitrogen, and 8.2 % (w/w) for oil content.

The optimal values of the model parameters are shown in Table 6.6, together with the 95 % confidence bounds estimated from a t-test. It must be notice, however, that usually model parameters are highly correlated and that the simple t-test does not provide reliable estimates of the confidence bounds of parameter estimates.

6.3 Model limitations

The dynamic model summarized in section 6.2.6 and Eq. 6.1 was calibrated using batch experimental data. In its formulation, however, the possibility of its use for fed-batch and continuous systems has been incorporated. When

Table 6.6: Estimated model parameter values and 95 % confidence bounds.

Parameter	Optimum value	Lower bound	Upper bound	Units
$Y_{x/s}$	0.5504	0.3897	0.9369	
$Y_{p/s}$	0.3401	0.2755	0.4444	
$Y_{x/q}$	56.67	53.83	59.84	
k_m	0.1940	-0.0116	0.3996	1/d
μ_m	14.18	10.22	18.13	1/d
K_{s_2}	8.453	6.557	10.349	g/L
$K_{\hat{q}}$	0.0041	0.0013	0.0068	
ρ_m	0.9340	0.7883	1.0797	1/d
K_{s_1}	0.1372	0.0485	0.2259	g/L
π_m	0.5045	0.4343	0.5747	1/d
$K_{s_2}^\pi$	0.0910	-0.6883	0.8703	g/L
$Y_{x/p}$	11.84	6.8102	45.3968	
K_{i_2}	49.50	42.26	56.75	g/L
K_{i_1}	0.016	0.0144	0.0178	

expanding the use of the model to extended batch or fed-batch cultures, or for continuous cultures, it would be necessary to modify the integral term in Eq. 6.14, so as to limit how far back in time it is necessary to take the average for the intracellular nitrogen concentration.

A limitation in the proposed model is that it does not account for the export of nitrogen compounds to the media. As shown in Table 5.3, microalgae excrete nitrogen-rich compounds to the media. Whether the exported compounds are metabolically relevant proteins, or waste by-products, was not investigated. However, it was observed that the exported nitrogen was not re-assimilated. For modelling purposes, the exported nitrogen was considered as non-existing, which is consistent with the fact that it is not re-assimilated by algae. Such an assumption, however, implies that the model is not able to accurately predict the external concentration of total nitrogen in the media.

6.4 Model validation

The proposed model was validated by comparing the model predictions using the parameter set estimated from batch experiments, with the experimental observations from a fed-batch culture. The fed-batch culture was started with 1 L of B4-Fe medium containing glycine (0.4 g/L) and glucose (40 g/L). A concentrated glycine stream (10 g/L) was fed into the reactor following the profile shown in Figs. 6.8(a); glucose was fed following the profile shown in Fig. 6.8(b). The concentrated glucose solution (200 g/L) also contained all the trace elements present in the original culture medium at a concentration 5 times the one in medium B4-Fe.

Model predictions and experimental observations are shown in Figs. 6.9(a) and 6.9(b). The model predictions were based on the set of parameters estimated from the batch culture data. The model was able to capture the underlying dynamics of algal cultures, keeping track, within experimental error, of the variations in oil content, nitrogen content, and biomass concentration in the culture media. The predictive capabilities of the model are significant considering that glucose and biomass concentrations are beyond the concentration range used in the model calibration.

The relatively higher deviation of the predicted oil concentration from the experimental measurements indicates that the model does not provide a completely accurate representation of the oil accumulation dynamics. The higher variability of lipid content experimental measurements, in both the calibration and the validation dataset, may be responsible for this relative lack of fit of the model. It is expected that a more accurate technique for measuring lipid content in the cells will allow for a better model discrimination and calibration.

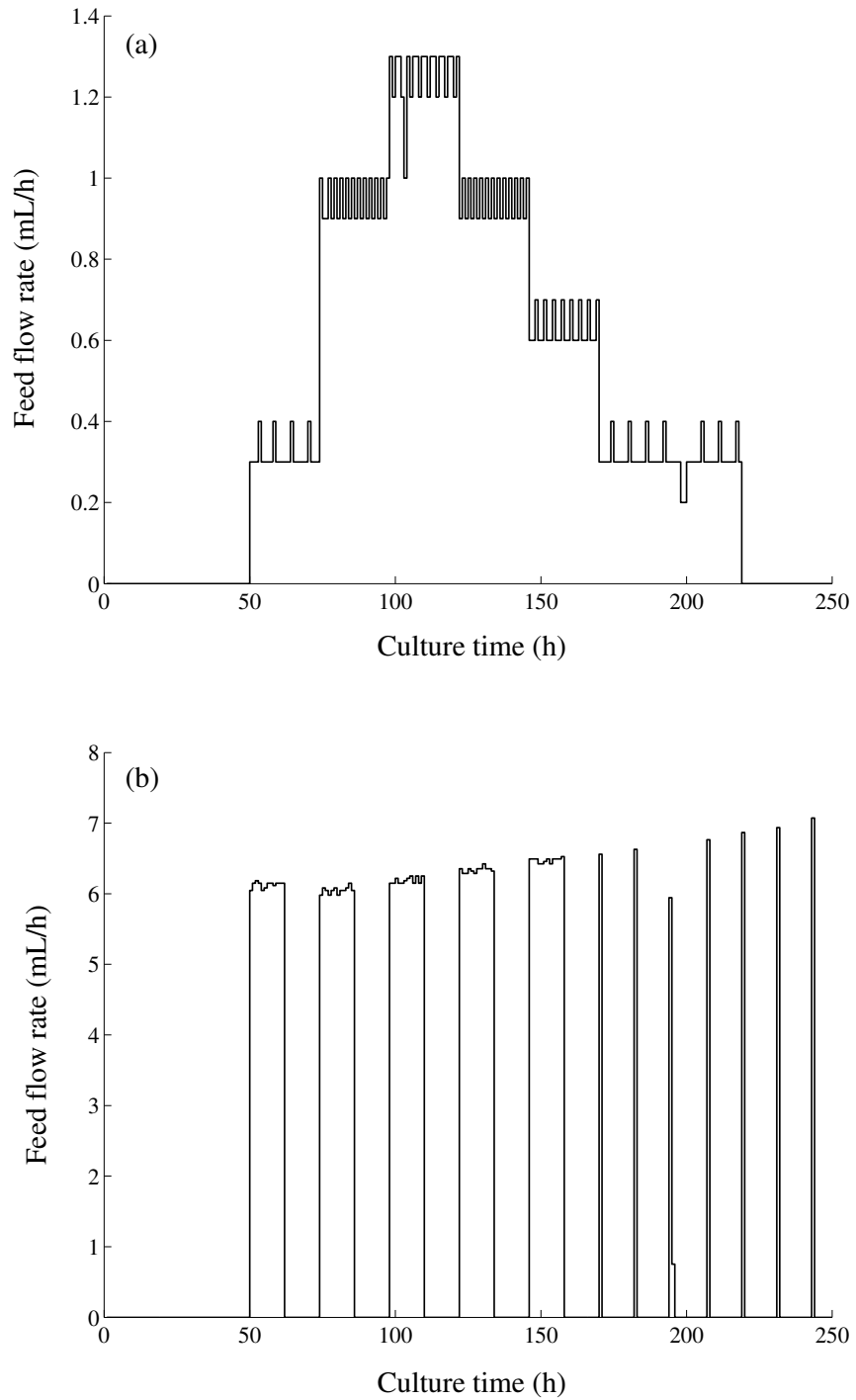


Figure 6.8: Feeding flow-rate profiles of the fed-batch run used for model validation. (a) Glycine rich feed; (b) Glucose rich feed.

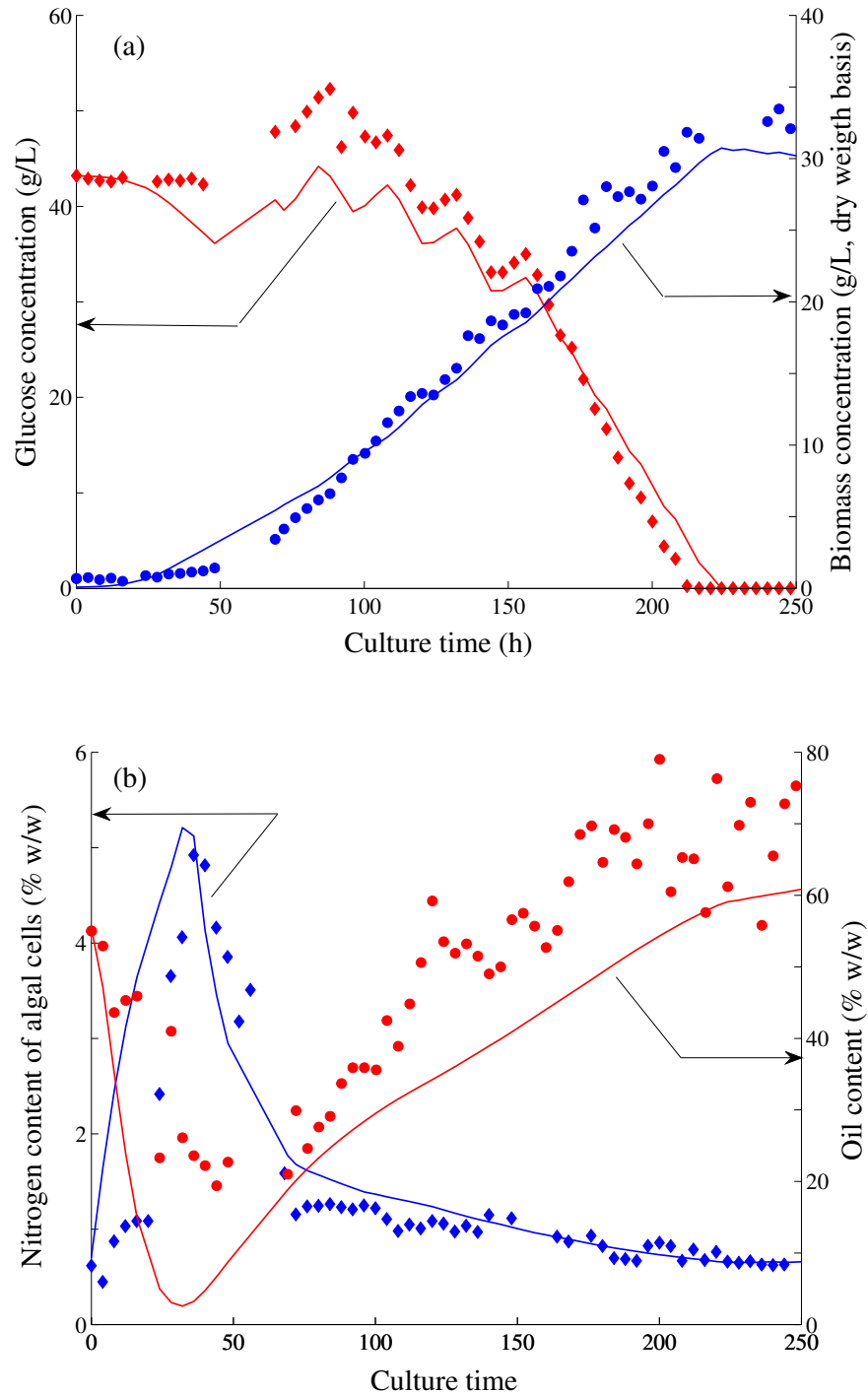


Figure 6.9: Measured and predicted concentration profiles for the fed-batch validation run. (a) Glucose and biomass concentration; (b) Nitrogen and oil content.

This page intentionally left blank

7

The optimization of microalgal cultures¹

The potential use of microalgae as a source of biofuels and bulk chemicals has generated an increasing interest in their industrial, large-scale, cultivation. Microalgae can also be used, and are being cultured, as a source of fine chemicals, pharmaceuticals, nutraceuticals, and food products. While the latter category of products can be produced at a high cost that is transferred to the consumers without significantly affecting their economic viability, production of bulk chemicals and biofuels requires greatly reduced production costs of microalgae.

An optimal process to cultivate microalgae will reduce production costs and will potentially enable the large-scale adoption of microalgal derived biofuels.

¹Some sections of this chapter have been accepted for publication. De la Hoz Siegler *et al.* 2011. Bioresource Technology, DOI: 10.1016/j.biortech.2011.10.029

Algal biofuels can be derived by pyrolysis or anaerobic digestion of the algal biomass, or by conversion of the oil contained in the algal cells into biodiesel. Therefore, algal culture optimization can be approached with either the goal of biomass or lipid production.

In this chapter, a model-based optimization approach is used to maximize the productivity of heterotrophic microalgal cultures. First, a key performance indicator (KPI) is selected as the optimization target. A theoretical interpretation of the model proposed in Chapter 6 is presented, evaluating the possibility of maximizing the selected KPI in both fed-batch and continuous cultures. Second, fed-batch cultures of *Auxenochorella protothecoides* are optimized, using glucose as the carbon source. Third, the possibility of reducing production costs by replacing the carbon source with a cheaper substrate (glycerol) is presented. Finally, the extracted algal oil is evaluated as a potential source of biodiesel.

7.1 Evaluating the performance of microalgal cultures

To properly define the optimization problem it is necessary to select the objective of the optimization. In principle, any measurable characteristic of the bioprocess can be optimized. Traditional targets in bioprocess optimization include growth rate, production rate, volumetric productivity, culture density, product yield, and production costs. The aim is to improve the selected key performance indicator by manipulating process conditions.

In general, the final goal of any process optimization strategy is to reduce total production cost. Other key performance indicators (KPI), however, are usually selected as the target of the optimization due to the complexity and

variability of costs estimates. The selection of the KPI to be used as the optimization target depends on the scale of the operation, the type of process, and the relative easiness to measure or estimate the proposed KPI.

Growth rate and production rate are desirable targets for optimization, as they are usually explicitly defined in the process model. The practical implementation of a control strategy based on keeping the reaction rate at a specified set point, however, is difficult and usually restricted to processes operating in quasi-steady state (i.e. continuous) conditions. In continuous processes, a maximum reaction rate translates into maximum productivity. For processes with time-varying behaviour (i.e. batch or fed-batch), the volumetric productivity is the default KPI, as it can be easily defined and measured.

Culture density and product yield affect the cost of processing and the cost of raw materials per unit of final product, and therefore its maximization is desirable. The effect of culture density and yield on total production cost, however, cannot be calculated in a straightforward way as increments in any of these two variables might have unexpected consequences in overall culture behaviour.

In this work, volumetric productivity was selected as the key performance indicator for the algal cultures. In Table 7.1, the maximum reported biomass and lipid productivities are presented for several microalgal species, cultured under different reactor configurations and media composition. The specific lipid production rate (\mathcal{P}), which corresponds to the oil produced per unit of algal biomass per unit of time, is also indicated.

From Table 7.1, it can be concluded that the productivity in heterotrophic systems is considerably higher than in phototrophic systems and that the use of perfusion or fed-batch reactors can further increase the productivity. Low productivity is partially the result of low cell density in the culture. In

Table 7.1: Biomass concentration (x_B), biomass productivity (\mathbb{P}_B), lipid productivity (\mathbb{P}_L), and specific lipid production rate (\mathcal{P}) for several microalgae species cultured under different conditions.

Species	Culture	Reactor type	x_B g/L	\mathbb{P}_B [mg/L.h]	\mathbb{P}_L [mg/L.h]	\mathcal{P}^a [1/d]	References ^e
<i>Ettlia oleabundans</i>	Phototrophic	Batch	2.9	26.3	6.8	0.056	1, 2
<i>Nannochloropsis sp.</i>	Phototrophic	Batch	2.1	12.5	8.5	0.097	3
<i>Amphora</i>	Phototrophic	Batch	—	—	24.7	—	4
<i>Chlorella sp.</i>	Phototrophic	Semicont.	1.1	12.8	5.8	0.126	5
<i>C. vulgaris</i>	Photoheterotrophic	Batch	1.7	10.6	2.3	0.032	6
<i>C. zofingiensis</i>	Phototrophic	Batch	1.9	5.7 ^a	1.5 ^a	0.018	7
<i>C. zofingiensis</i>	Heterotrophic	Batch	9.6	28.9 ^a	14.8 ^a	0.037	7
<i>Nitzschia laevis</i>	Heterotrophic	Perfusion	22.1	281	38.1 ^b	0.120	8, 9
<i>Schizochytrium limacinum</i>	Heterotrophic	Batch	37.9	158	27.3 ^c	0.018	10
<i>Aureochlorella protothecoides</i>	Heterotrophic	Batch	8.4	69.6	34.2	0.098	11
<i>A. protothecoides</i>	Heterotrophic	Fed-batch	51.1	275 ^a	138 ^a	0.065	12
<i>A. protothecoides</i>	Heterotrophic	Continuous	100	9320 ^d	1120 ^d	0.243	Predicted

^a Calculated from data presented in the original references.

^b Reference only reported EPA productivity, which accounted for 19.1% of total fatty acids.

^c Reported productivity includes only DHA.

^d Calculated maximum value. See Section 7.1.1 for details.

^e Reference key: 1. Griffiths and Harrison (2009); 2. Li et al. (2008); 3. Rodolff et al. (2009); 4. Sheehan et al. (1998); 5. Hsieh and Wu (2009); 6. Liang et al. (2009); 7. Liu et al. (2011); 8. Wen and Chen (2001); 9. Wen and Chen (2003); 10. Chi et al. (2009); 11. Cheng et al. (2009); 12. Xiong et al. (2008).

phototrophic microalgal cultures, typical cell density is about 1 g/L and, due to mutual shading effects, it is difficult to significantly increase it without causing a substantial drop in growth rate. In heterotrophic systems, where mutual shading does not play a role, growth limitation is caused by nutrient starvation or accumulation of inhibitory compounds in the growth media. The much higher productivities reported for fed-batch and perfusion cultures are due to the improved control in the feeding and bleeding strategies that are possible in these type of systems.

In the following sections, the model developed in Chapter 6 is used to assess the potential for optimizing the productivity of heterotrophic cultures of the green microalga *A. protothecoides* in continuous and fed-batch cultures.

7.1.1 Continuous cultures

In a continuous bioreactor, cells are harvested as fresh medium is added to the reactor, keeping the total operating volume constant. The outlet stream composition is representative of the reactor content at any given time, if ideal mixing is assumed. That is, the biomass concentration and the oil content in the harvested cells in the effluent stream are the same as inside the reactor. The productivity can therefore be written in terms of the reactor composition as $\mathbb{P}_B = xD$, for the biomass productivity, and $\mathbb{P}_L = pD$, for the lipid productivity; the dilution rate, D , is defined as the ratio of outlet flowrate to reactor volume ($D = f_o/V$).

A steady state analysis of the dynamic model presented in Eq. 6.1 shows that the maximum lipid productivity is achieved by maximizing the following term:

$$\mathbb{P}_L^* = \max \left\{ \pi x - \frac{\mu x}{Y_{x/p}} \right\} \quad (7.1)$$

Similarly, the maximum biomass productivity is given by:

$$\mathbb{P}_B^* = \max \{ \mu x \} \quad (7.2)$$

In both cases, the biomass concentration x acts as a scaling factor. That is, increasing the biomass concentration in the culture should result in a proportional increase in productivity. In practice, however, others factors will limit the achievable productivity in the culture. For instance, sustaining a high density culture requires the continuous feed of large amounts of substrate which might induce reactor wash-out, if the dilution rate exceeds the maximum growth rate.

To determine the theoretical maximum productivity in continuous cultures of *A. protothecoides*, the model presented in Eq. 6.1, in combination with the kinetic expressions presented Section 6.2.6, was implemented in SIMULINK[®]. In the model, it was considered that the bioreactor operates at steady state conditions with $D = f_1 + f_2/V$, where f_1 is the flowrate of the glycine-rich feed and f_2 is the flowrate of the glucose-rich feed. The predicted biomass productivity is plotted in Fig. 7.1. The maximum expected biomass productivity is 9.32 g/L·h, for a dilution rate equal to 0.088 1/h, a glycine feeding rate equal to 0.88 g/L·h, and a glucose feeding rate equal to 22 g/L·h. This maximum biomass productivity, however, occurs at the limit of wash-out and therefore it is impractical to operate at such condition, given that any disturbance in the reactor could cause a dramatic decrease in productivity.

The predicted lipid productivity in continuous cultures of *A. protothecoides* is shown in Fig. 7.2. In this case, the maximum ($\mathbb{P}_L = 1.12$ g/L·h) occurs at a dilution rate $D = 0.058$ 1/h, and with a glycine feeding rate equal to 0.54 g/L·h and glucose feeding rate equal to 15.5 g/L·h. As expected, the conditions

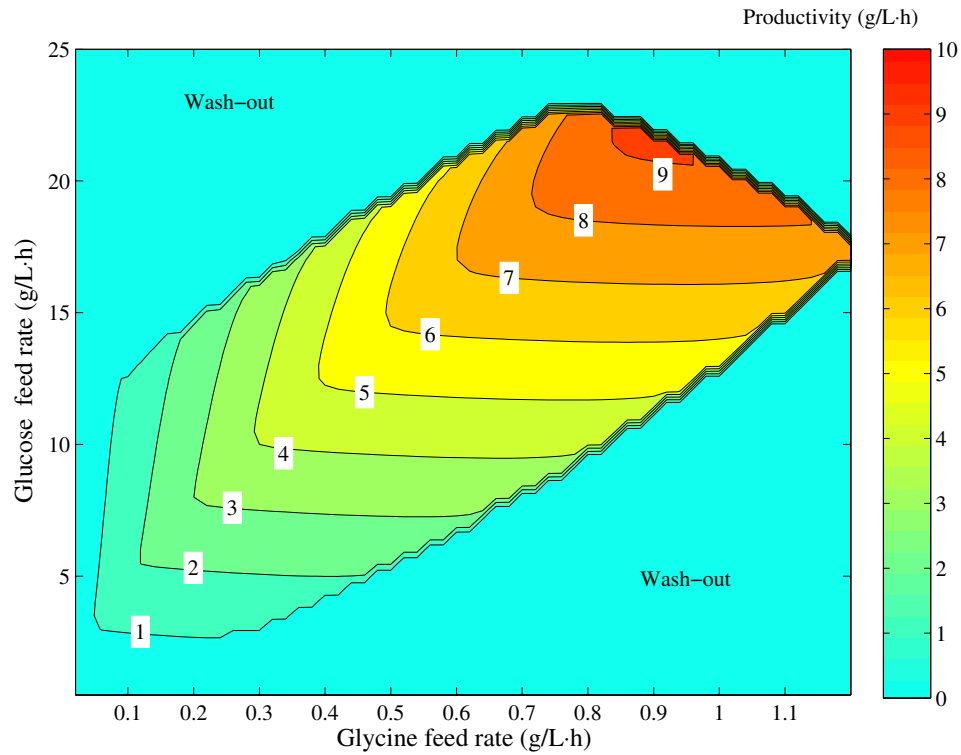


Figure 7.1: Predicted biomass productivity in continuous cultures of *A. protothecoides*, in g/L·h. Optimal productivity occurs near a wash-out point, making unfeasible the operation at this condition. Wash-out occurs whenever the dilution rate is greater than the growth rate.

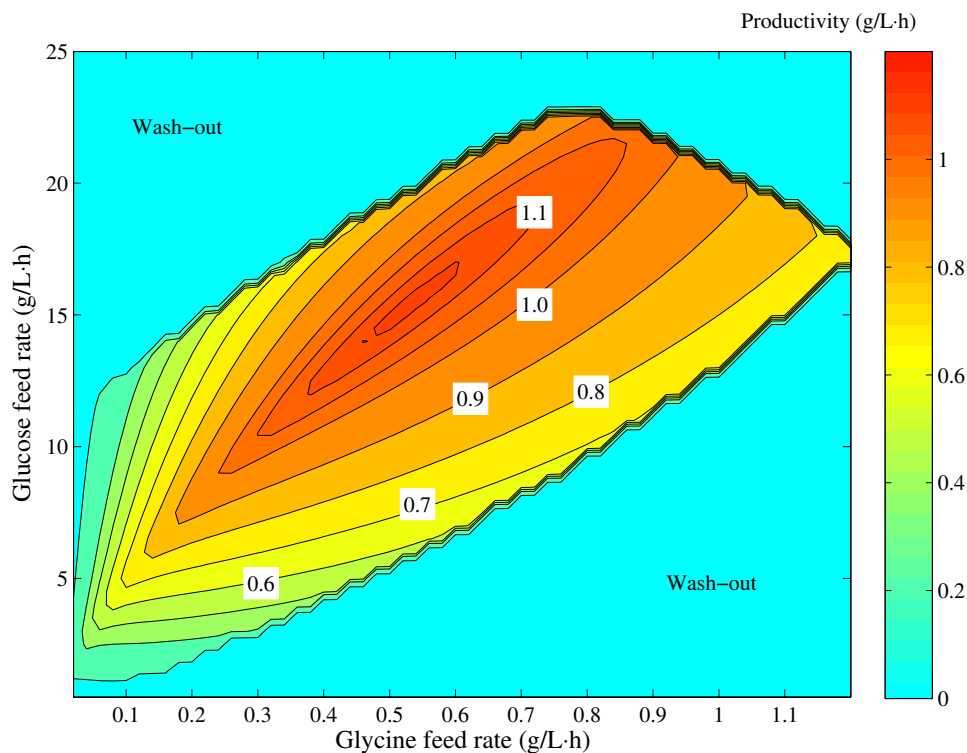


Figure 7.2: Predicted lipid productivity in continuous cultures of *A. protothecoides*, in g/L·h.

at which the maximum lipid productivity is achieved do not coincide with the conditions for maximizing biomass productivity. Furthermore, the lipid productivity is maximized at a condition that does not coincide with the wash-out dilution rate, which means that the bioreactor could be safely operated at the optimal conditions to maximize oil production.

For comparison purposes, the predicted maximum biomass and lipid productivities, as calculated from the proposed model, are shown in Table 7.1 together with reported experimental values. The highest reported specific lipid production rate is 0.120 d^{-1} for *Chlorella vulgaris*, which is about one half of the estimated maximum oil production rate for *A. protothecoides*.

7.1.2 Fed-batch cultures

In fed-batch cultures, cell concentration increases as nutrients in the medium are consumed. Fresh medium is continuously added to replenish the nutrients that are being exhausted. As such, reactor conditions are undergoing constant change, and there is not a point of steady operation. Under this set of operating conditions, it is convenient to evaluate the productivity in terms of the total concentration of the desired product at two different time points. The biomass productivity can be calculated as:

$$\mathbb{P}_B = \frac{x(t_2) - x(t_1)}{t_2 - t_1} \quad (7.3)$$

while the lipid productivity is given by:

$$\mathbb{P}_L = \frac{p(t_2) - p(t_1)}{t_2 - t_1} \quad (7.4)$$

The average productivity for the full fed-batch duration is simply evaluated with t_2 equal to the total culture time, and t_1 equal to zero.

Because process conditions are in a permanent drift in a fed-batch culture, it is not possible to calculate a single point, as in the case of continuous cultures, at which productivity will be maximized. Instead, the optimal input is a set of flow-rates in a time dependent trajectory or profile.

7.2 Optimal feeding strategy for glucose-fed microalgal fed-batch cultures

In the previous section it has been shown, through simulation studies, that there exist a set of operating conditions at which the productivity of microalgal cultures is maximized. In this section, the experimental improvement in the biomass productivity of heterotrophic fed-batch cultures of *A. protothecoides* is reported.

First, the general mathematical framework of the optimization problem is presented. The problem is formulated as a model-based optimization, in which it is assumed that the model provides a satisfactory representation of the real biosystem. The optimized feeding strategy is later implemented experimentally. Two different approaches are followed for the optimization, i.e. open-loop model predictive control and adaptive model predictive control. For reference, an additional run was performed without any optimization.

7.2.1 Problem formulation

A dynamic model of microalgal cultures was presented in Chapter 6, Eq. 6.1. For brevity, it can be summarized as:

$$\frac{d\xi}{dt} = \psi(\xi, u, k) \quad (7.5)$$

with ξ being the vector of state variables, u the vector containing the inlet and outlet flowrates, and k the model parameters.

The objective of the optimization is to find the optimal feeding strategy, u^* , for a given culture time, t_f , and initial conditions, $\xi(t_0)$, that maximizes the selected productivity function. Mathematically, this can be written as:

$$u^* = \arg \max_u \mathbb{P}(u, \xi(t_0), k, t_f) \quad (7.6)$$

The feasible solution space is constrained by the finite volume of the bioreactor (V_{Reactor}). At any given time, the reaction volume, $V(t)$, can be calculated as:

$$V(t) = V(t_0) + \int_{t_0}^t u dt + \sum_{i=1}^M f_{o,i} \quad (7.7)$$

where M is the number of samples being removed up to time t , and $f_{o,i}$ is the volume or flowrate of each sample removed.

Then, the optimization problem in Eq. 7.6 is subject to:

$$\max\{V(t)\} < V_{\text{Reactor}} \quad (7.8)$$

7.2.2 Implementation

The optimization of fed-batch bioprocesses is usually performed run-to-run. That is, the optimal feeding profile is calculated by solving the optimization problem and this calculated profile is then implemented for all the batch duration. After completion of the batch, process data is analyzed and the optimal feeding profile is adjusted for the next batch. This approach will be hereinafter referred as Open-loop optimal feeding trajectory, for short Open-loop OFT.

An alternative approach is to update the optimal feeding profile as soon as new process data is available. This is achieved by implementing an adaptive optimization, in which model parameters are re-estimated based on the newly available data. The optimization problem is subsequently solved for the new set of model parameters, using as initial conditions the current estimated or

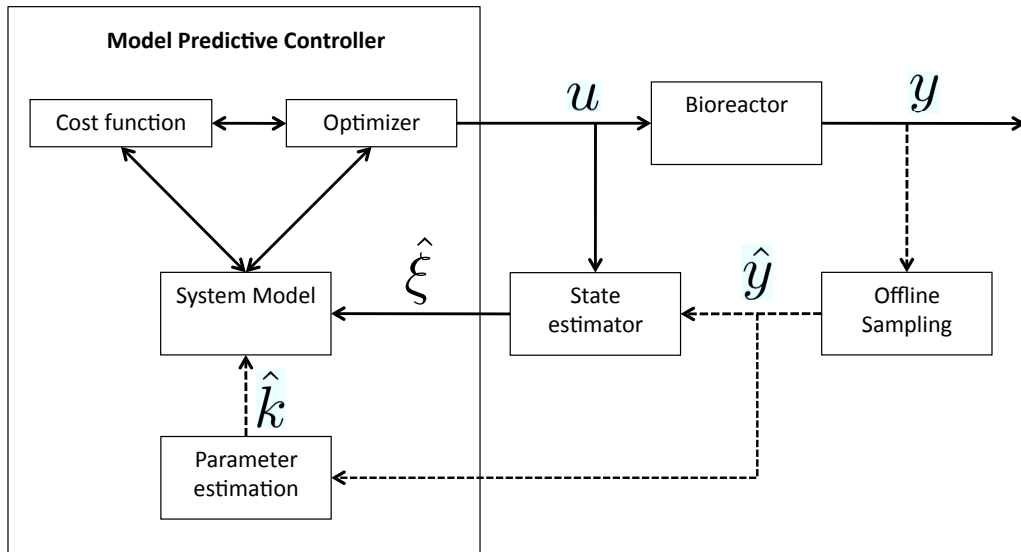


Figure 7.3: Flow diagram for the Adaptive Model Predictive Control optimization approach used. u is the flow-rate profile to be implemented in the bioreactor, y is a vector containing the true value of all the process outputs (biomass, glucose, and oil concentration, and \hat{y} are the estimated values of the process output. Biomass productivity, \mathbb{P}_x , was used as the cost function to be optimized.

measured state variables. At each iteration in the optimization loop the time horizon shrinks as the batch approaches the predefined final culture time. A schematic of the adaptive optimization approach is presented in Fig. 7.3.

To solve this optimization problem, PatternSearch (MATLAB[®], Mathworks Inc.) was used. In the PatternSearch algorithm, a mesh is defined over the feasible solution space and the cost function is evaluated at the nodes of the mesh. The evaluation poll moves through the mesh in the direction that decreases the objective function, while the mesh is continuously refined in order to identify the optimum solution (Audet and Dennis, 2006).

Non-optimal fed-batch culture (Pseudo-random binary sequence feeding - PRBS)

A non-optimal fed-batch run was performed as a base-line culture starting with a medium composition equal to that of Medium B4-Fe (see Table 3.1). Nutrients were supplemented along the run in two independent streams. The first contained only glycine, while the second stream contained glucose and all the other trace minerals present in Medium B4-Fe. The two streams were fed to the reactor following a pseudo-random profile as shown in Fig. 7.4.

Open-loop optimal feeding trajectory (OFT) culture

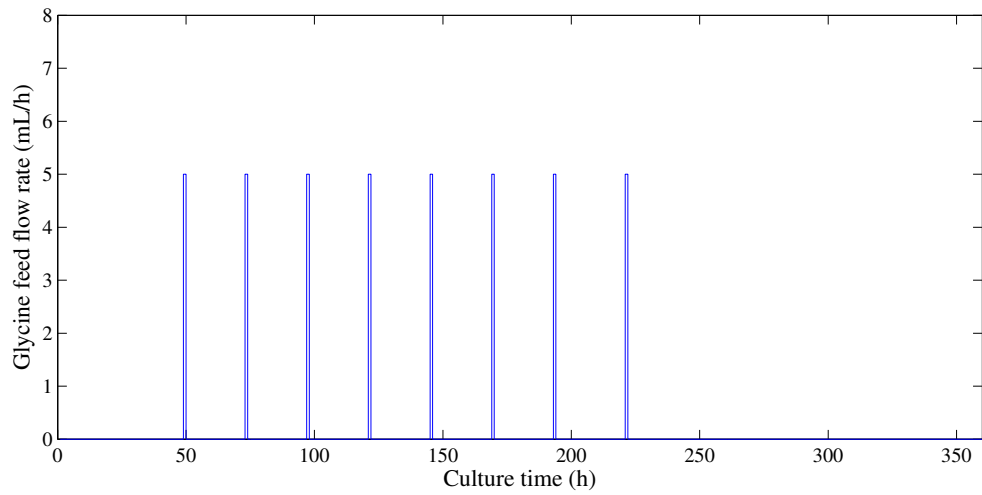
In a first attempt to optimize the biomass productivity of heterotrophic fed-batch microalgal cultures, the trajectories of the flow rate of the two substrate feeds were parameterized in order to reduce the computational complexity of the optimization problem. The glycine feed was allowed to follow a log-normal function:

$$u_1 = f_1^i = \frac{a_1}{t} \exp \left[\frac{(\ln(t) - a_2)^2}{a_3} \right] \quad (7.9)$$

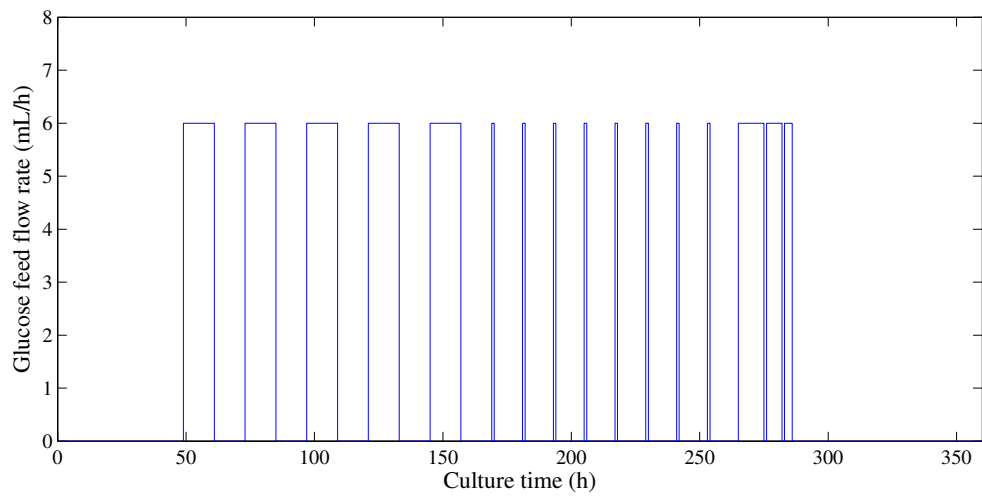
For the glucose-rich feed an exponential profile was selected:

$$u_2 = f_2^i = a_4 \exp(a_5 t) \quad (7.10)$$

The optimal values of the parametric coefficients (a_i) were estimated using PatternSearch. The continuous feeding profiles calculated with the optimal parametric coefficients were further discretized to allow their implementation as set-points in the bioreactor control system. The discretized optimal feeding trajectories are shown in Fig. 7.5, together with the final feeding flowrates as implemented.



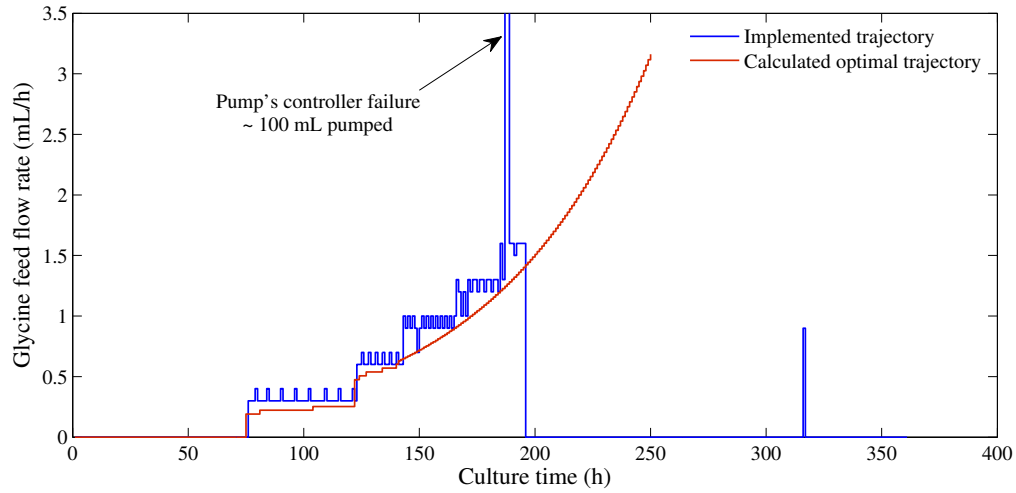
(a) Glycine-rich feed



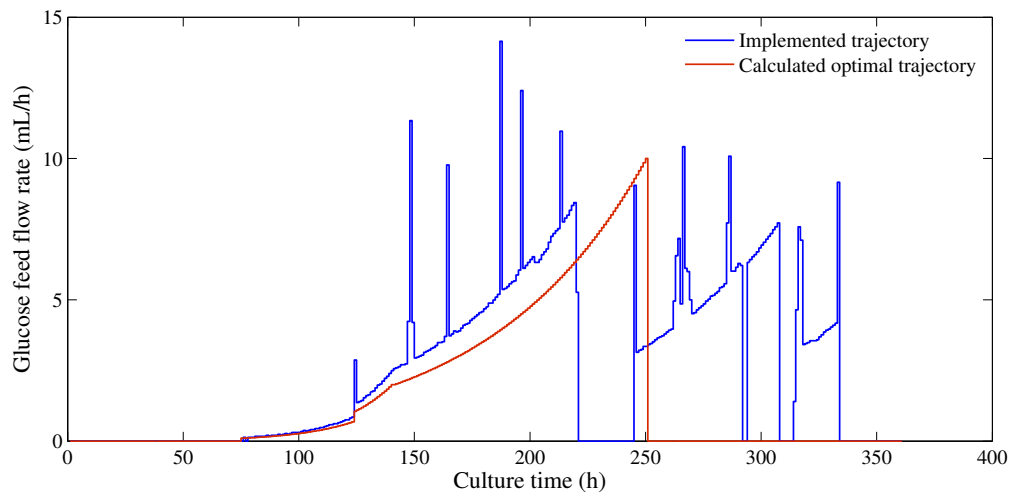
(b) Glucose-rich feed

Figure 7.4: Feeding flowrates for the pseudo-random binary sequence (PRBS) fed-batch culture of *A. protothecoides*.

7.2. Optimal feeding strategy for glucose-fed microalgal fed-batch cultures



(a) Glycine-rich feed



(b) Glucose-rich feed

Figure 7.5: Feeding flowrates for the open-loop optimal feeding trajectory (OFT) fed-batch culture of *A. protothecoides*.

From Fig. 7.5, it can be seen that there was a mismatch between the calculated and the implemented feeding trajectories. In general the implemented flowrate was higher than the calculated one, as there was a delay between the time the stop signal was sent to the pump and the time at which the pump was fully stopped. Moreover, the glycine feed pump failed to stop at around 186 h and approximately 100 mL of glycine-rich feed were pumped into the reactor. For this reason, glycine feeding was completely stopped after 196 h, as there was already an excess of nitrogen in the culture. Between 221 h and 244 h, glucose feeding was suspended due to intensive foaming and the inability to sustain a non-zero oxygen level in the culture. Glucose feeding was later restarted, but at a lower rate than predicted from the optimization. A detailed description of this experimental run is presented in Appendix B.1

Adaptive model predictive control culture

Given that the estimated parameter values might not be valid whenever there are significant changes in the conditions under which the bioreactor is operated, it might be necessary to update the parameter estimates during a given run. This is particularly true in lumped phenomenological models, as the one used in this work, in which model parameters do not represent a unique physical phenomenon but the aggregate result of several interacting phenomena. In adaptive model predictive control (MPC) the optimal feeding trajectories are computed at the start of the culture and recalculated as soon as new process information is available. In this way, the possibility of plant-model mismatch is reduced.

In the implementation of the adaptive MPC, the feeding trajectories, u , were parameterized as constant piece-wise functions, with a fixed flow-rate for every 12 h interval. The optimal feeding trajectories, u^* , were calculated from the

7.2. Optimal feeding strategy for glucose-fed microalgal fed-batch cultures

start of the culture, t_0 , until a predetermined fixed time horizon, t_H :

$$u^* = \{u_{t_0}, u_{t_1}, u_{t_2}, \dots, u_{t_H}\} = f(\hat{k}, \xi(t_0)) \quad (7.11)$$

Samples were collected every 4 h and analyzed for biomass and glucose concentration. These experimental measurements were then used to re-estimate the model parameters, \hat{k} , and to estimate the states trajectories from the start of the culture, t_0 , up to the current culture time, t_S . In the experimental run presented here, model parameters were updated approximately every 24–48 h. The optimal feeding flowrate trajectories were subsequently calculated from the current culture time until the fixed end of the culture:

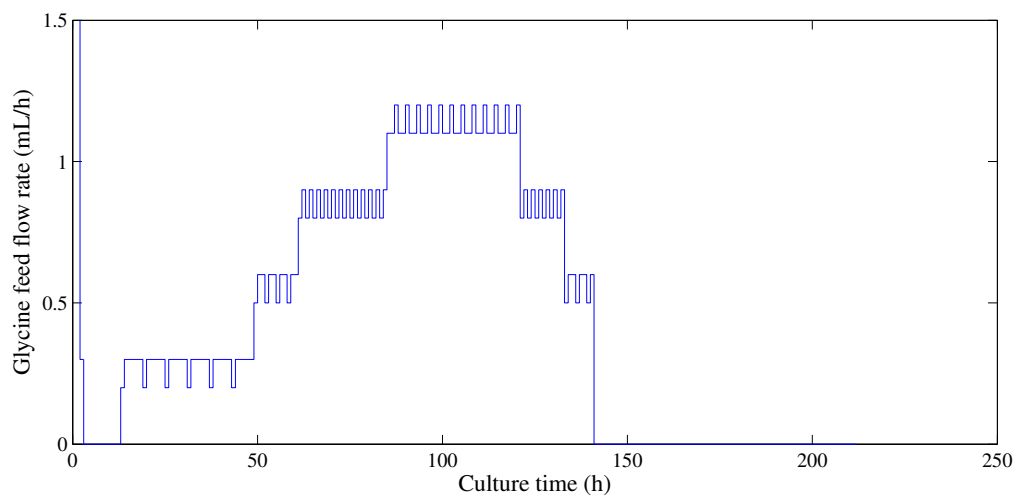
$$u^* = \{u_{t_S}, u_{t_{S+1}}, u_{t_{S+2}}, \dots, u_{t_H}\} = f(\hat{k}, \xi(t_0 \rightarrow t_S)) \quad (7.12)$$

The flowrate profiles of the two feeding streams, as implemented in the adaptive optimal culture, are shown in Fig. 7.6.

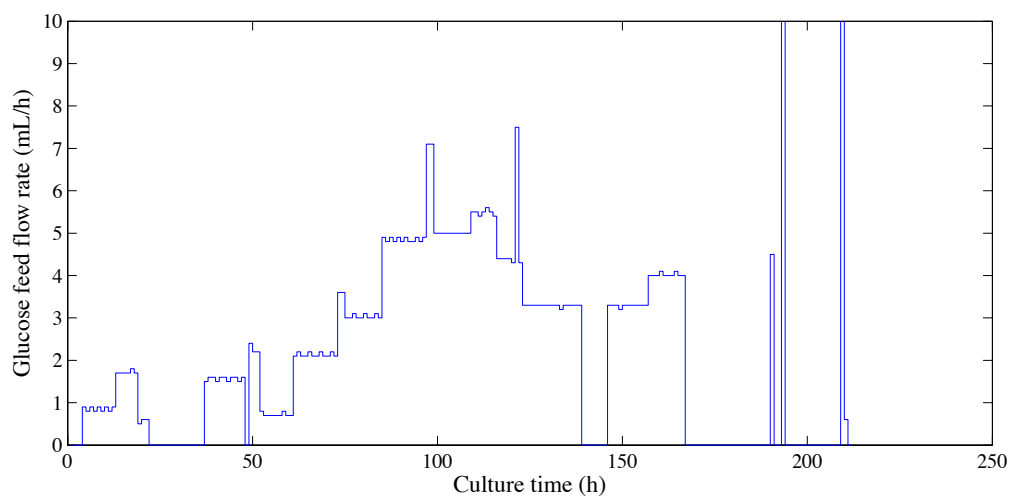
7.2.3 Comparison

The growth curves for the three fed-batch runs described in the previous section are shown in Fig. 7.7. For comparison purposes the growth curve of a batch run is also included. The implementation of the proposed optimization strategies produced a significant increase in biomass production, from 20 g/L in 350 h for the PRBS fed-batch run, to 98 g/L in the Open-loop OFT, and to 144 g/L after only 210 h in the Adaptive MPC run.

The observed increase in cell density, and the reduction in culture time, translates into a substantial enhancement in biomass productivity. Fig. 7.8 shows the average and maximum biomass productivity observed in the three fed-batch runs of *A. protothecoides*, and in the reference batch culture. Average



(a) Glycine-rich feed



(b) Glucose-rich feed

Figure 7.6: Feeding flowrates for the adaptive MPC fed-batch culture of *A. protothecoides*.

7.2. Optimal feeding strategy for glucose-fed microalgal fed-batch cultures

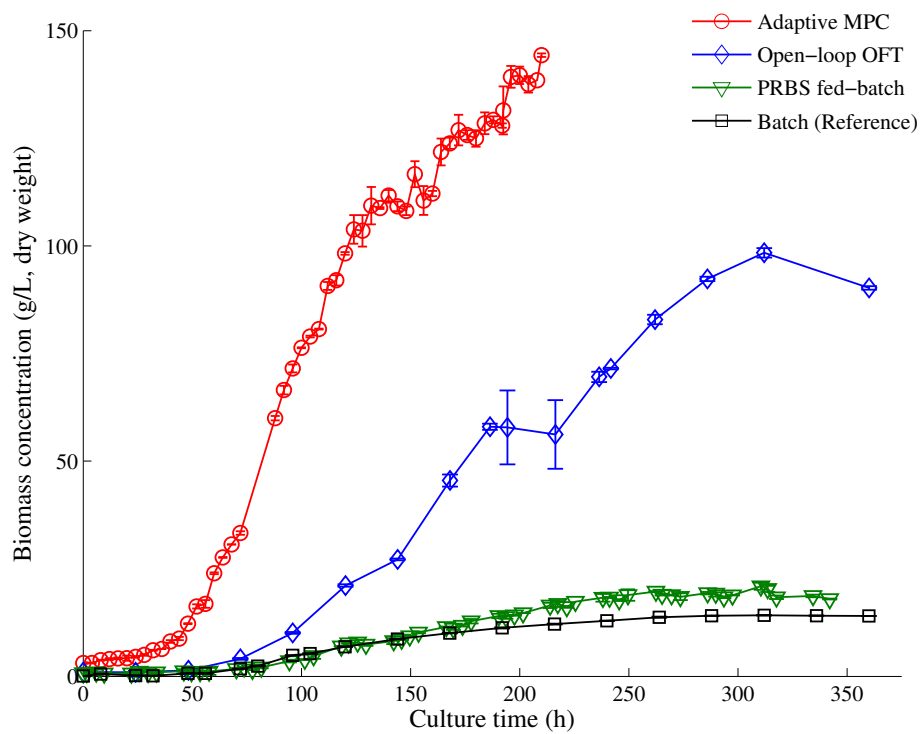


Figure 7.7: Increased biomass concentration as a result of the proposed optimization strategy.

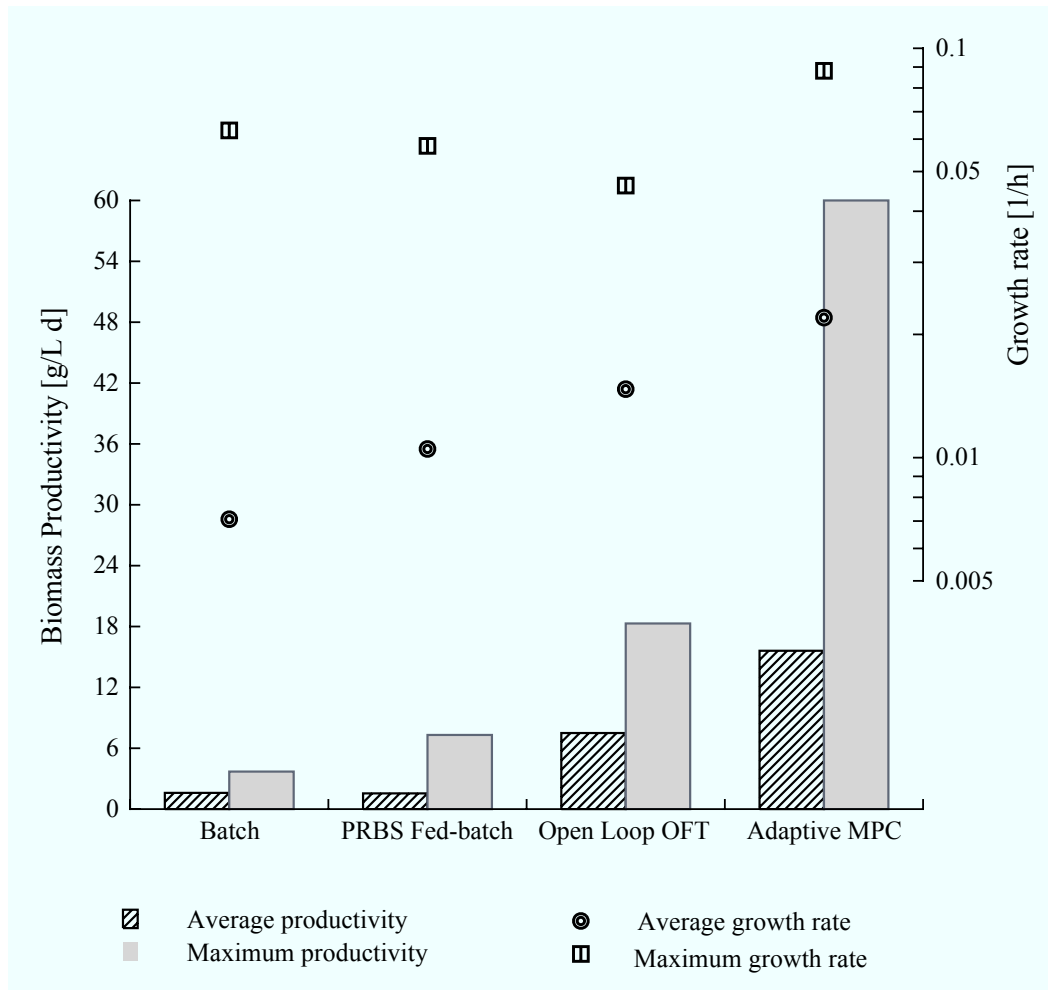


Figure 7.8: Biomass productivity and growth rate for different culture strategies. The optimized fed-batch cultures (open-loop OFT and adaptive MPC) provided a substantial increase in productivity with respect to the batch and the unoptimized fed-batch cultures.

productivity was calculated for the full duration of the batch, while the maximum productivity corresponds to the observed one during the exponential growth phase. In summary, there was a 10-fold increase in the average productivity and a 16-fold increase in the maximum biomass productivity as a result of the proposed optimization strategy.

7.2. Optimal feeding strategy for glucose-fed microalgal fed-batch cultures

Biomass productivity can be increased either by augmenting the growth rate or by extending the time in which cells are growing at their maximum rate. To explore which one of these possibilities was responsible for the observed increased productivity, the average and maximum growth rates were calculated and reported in Fig. 7.8. While there was a significant increase in the average growth rate going from the batch culture to the optimized Adaptive MPC fed-batch, the maximum observed growth rate remained around the same value ($0.05 - 0.09 \text{ h}^{-1}$). This implies that the observed growth rate during the exponential growth phase was nearly independent of the cultivation strategy selected. This observation is relevant for experimental design as it shows that batch cultures are a valid tool for the screening of algal strains and process conditions.

The reported enhancement in the biomass productivity highlights the success of the proposed optimization strategy. However, given that biodiesel is one of the most promising products to be derived from microalgae, it is desirable to also increase the lipid productivity in algal cultures. A greater biomass productivity is not necessarily expected to translate into an increment in lipid productivity. In fact, it is widely known that lipids are accumulated in algal cells as a result of a growth limiting stressor. Therefore, it is expected that conditions that favour growth will be deleterious to lipid accumulation. Fig. 7.9 shows the oil content and the apparent lipid production rate for the Adaptive MPC run. Lipid content decreased in the first 88 hours of the culture as a result of the unbalance between growth rate and oil production rate. After 88 h, however, lipid content steadily increased and stabilized, after 150 h, between 50 and 60%.

The increment in lipid content in the algal cells during exponential growth phase is in apparent contradiction with the fact that lipid accumulation is

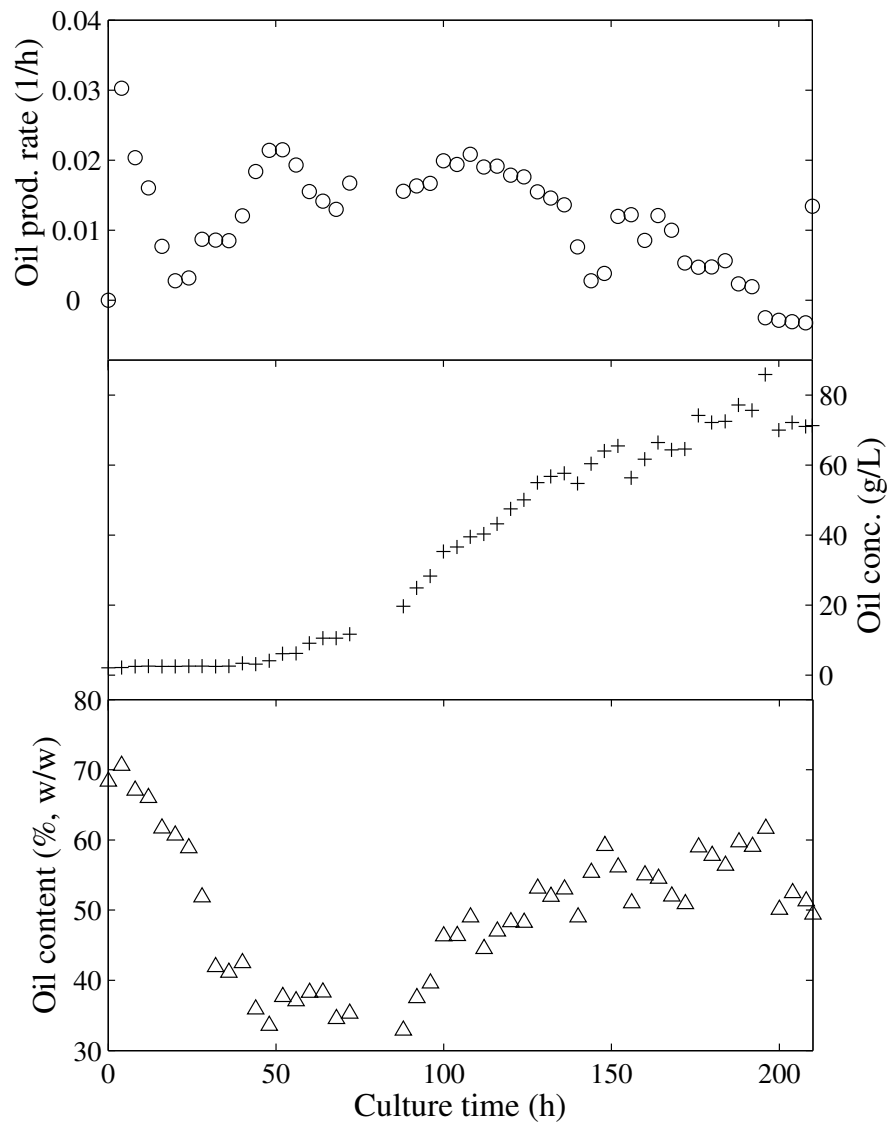


Figure 7.9: Lipid content and apparent lipid production rate in an Adaptive MPC fed-batch culture of *A. protothecoides*

7.2. Optimal feeding strategy for glucose-fed microalgal fed-batch cultures

triggered by a condition that limits growth in the cells. This contradiction is only apparent as nitrogen deficiency is indeed limiting growth rate, given that the increased biomass productivity was achieved while maintaining nitrogen deficient conditions. To verify that nitrogen limiting conditions were indeed maintained along the entire culture, the total molar ratio of carbon to nitrogen in the culture media was calculated and plotted in Fig. 7.10 against the Redfield ratio (C:N = 106:16).

The high biomass productivity achieved while sustaining nitrogen-limiting conditions in the culture resulted in a substantial surge in lipid productivity, as shown in Fig. 7.11. The maximum lipid productivity of the optimized adaptive MPC fed-batch culture was significantly higher than for the other cultures, and even higher than the reported productivity for other algal species. The maximum productivity (20.16 g/L·d) is six times higher than the highest value previously achieved in *A. protothecoides* (3.32 g/L·d, Table 7.1). The average

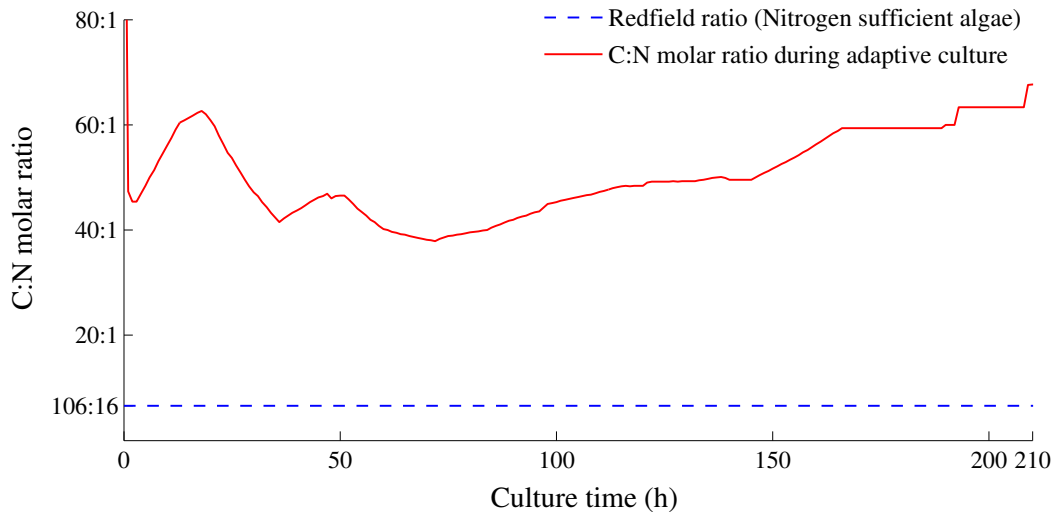


Figure 7.10: Carbon to nitrogen (C:N) molar ratio during the Adaptive MPC fed-batch culture. The Redfield ratio (C:N = 106:16) is indicated as reference of a nitrogen-sufficient culture.

lipid productivity, for all the batch duration, in the optimized culture was 10.32 g/L·d, which is still 3.1 times the previous maximum value. Furthermore, the maximum recorded lipid productivity was 75% of the maximum predicted productivity in continuous cultures. Clearly, the proposed optimization strategy greatly enhanced the lipid production capabilities of *A. protothecoides*.

The resultant high lipid productivity of the optimized *A. protothecoides* culture is significant, even compared with classic oleaginous microorganisms. In Table 7.2, the oil content at the end of the culture and the lipid productivity is

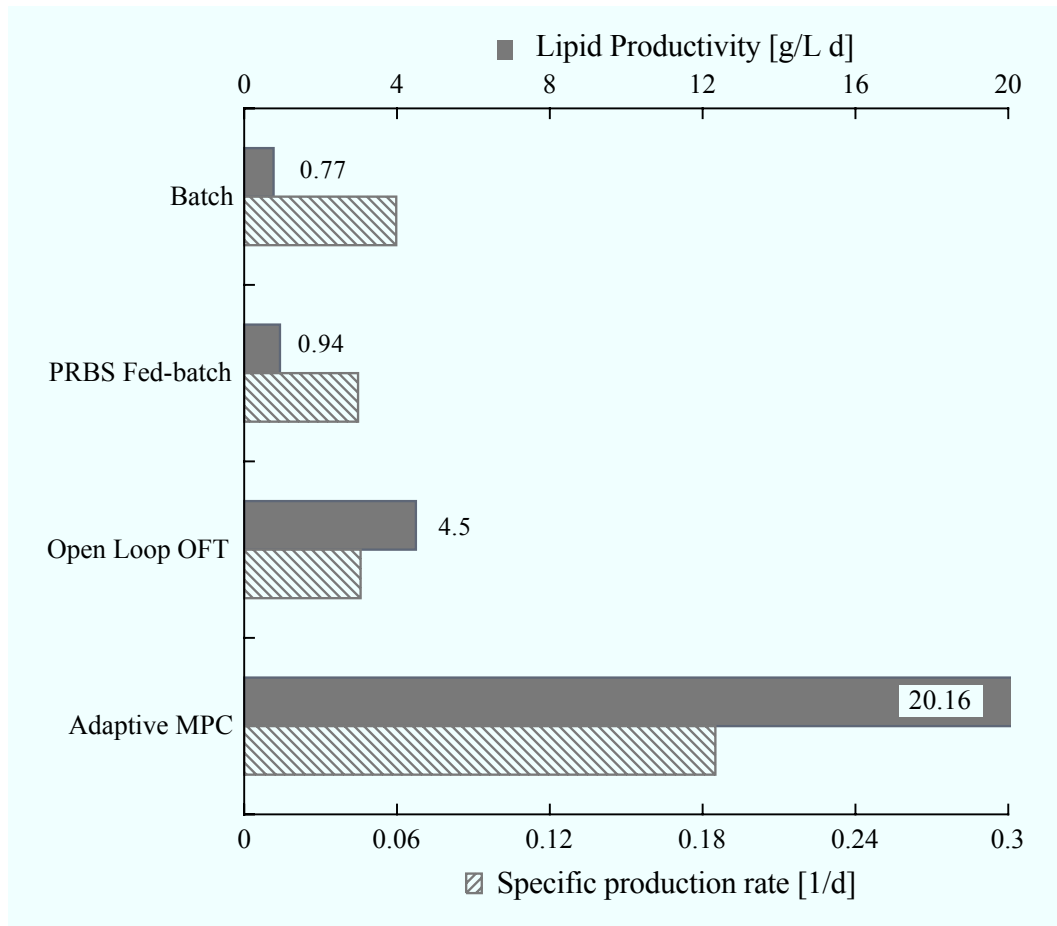


Figure 7.11: Maximum lipid productivity and specific lipid production rate for different *A. protothecoides* cultures.

7.2. Optimal feeding strategy for glucose-fed microalgal fed-batch cultures

reported for several microalga, yeast, and mold species growing heterotrophically on glucose. The productivity of the model-based optimized culture of *A. protothecoides* was 3 – 6 times higher than the productivity of the improved fed-batch reported by Xiong et al. (2008). Moreover, the maximum measured oil productivity was larger than that of *R. toruloides* and *C. curvatus*, which are two of the most productive oleaginous yeasts used for the production of single cell oils. The optimized culture of the green microalgae *A. protothecoides* also outcompeted the heterotrophic cultures of filamentous fungi and bacteria in terms of productivity.

Table 7.2: Lipid content and lipid productivity, \mathbb{P} , of *A. protothecoides* and other selected oleaginous microorganisms growing on glucose.

Species	Lipid content, %	\mathbb{P} [g/L·h]	References ^d
Microalgae			
<i>Auxenochlorella protothecoides</i>	49.4	0.43 - 0.84 ^a	This work
<i>Auxenochlorella protothecoides</i>	50.3	0.14	1
<i>Chlorella vulgaris</i>	9.7	0.12	2
<i>Schizochytrium sp. G13/2S</i>	30	0.096	3
Yeast			
<i>Rhodospiridium toruloides</i>	67.5	0.54	4
<i>Lipomyces starkeyi</i>	56.0	0.04	5
	–	0.60 ^b	5
<i>Cryptococcus curvatus</i>	82.7	0.47	6
Filamentous fungi			
<i>Mortierella ramanniana</i>	67.7	0.17	7
<i>Cunninghamella echinulata</i>	26.9	0.07	5
Bacteria			
<i>Rhodococcus opacus</i> PD630	38.4	0.171	8
<i>E. coli</i> , genetically engineered	25.4 ^c	0.246 ^c	9

^a The lower value reported corresponds to the average lipid productivity, and the higher value is the average productivity during the exponential growth phase (88 - 132 h)

^b Ethanol was used as the organic substrate.

^c Lipid content expressed as ethyl ester content in the cells.

^d Reference key: 1. Xiong et al. (2008); 2. Doucha and Lívanský (2011); 3. Ganuza and Izquierdo (2007); 4. Li et al. (2007b); 5. Kosa and Ragauskas (2011); 6. Zhang et al. (2011); 7. Hiruta et al. (1997); 8. Kurosawa et al. (2010); 9. Elbahloul and Steinbuechel (2010).

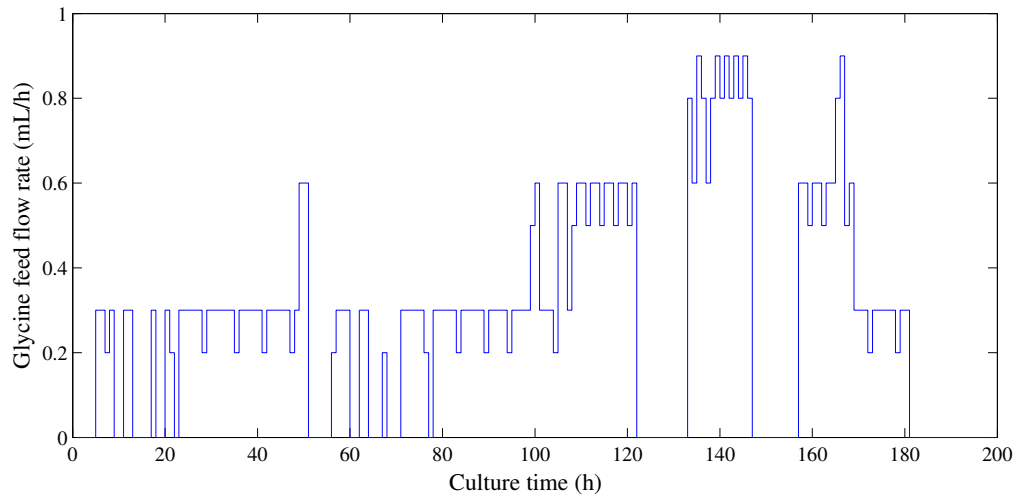
7.3 Optimization of glycerol-fed cultures

The production cost of glucose-fed algal cultures is greatly affected by the high price of sugar. Process optimization, in terms of production cost, can be achieved by replacing glucose with a low-priced carbon source. One possible alternative is glycerol, which is a by-product of biodiesel and oleochemicals production. The increasing expansion in the production capacity of biodiesel has driven down the market value of glycerol, making it an attractive and economical alternative carbon source. In this section, the fed-batch cultivation of the green microalgae *A. protothecoides*, using glycerol as the carbon source, is presented.

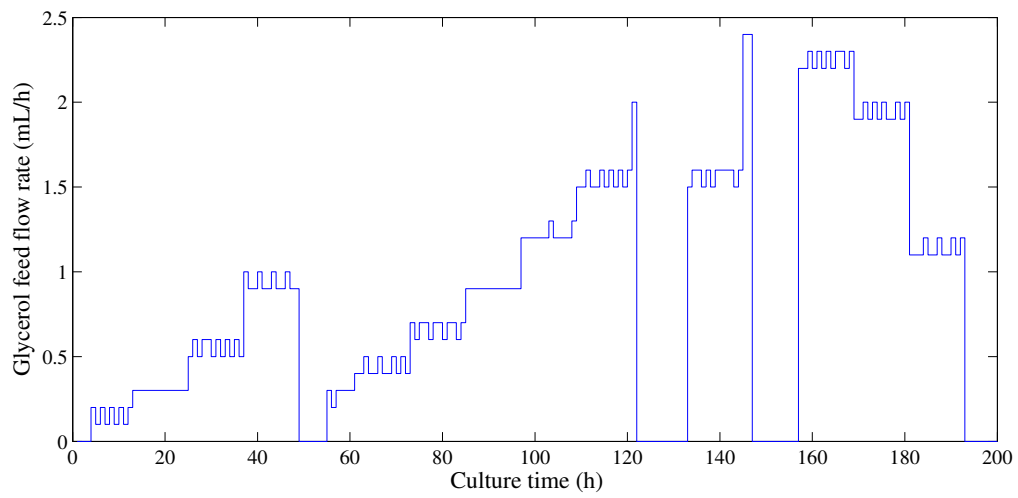
7.3.1 Culture conditions

The fresh water microalga *A. protothecoides* was cultured as previously described for glucose-fed cultures. The start-up medium was B4-Fe (Table 3.1) supplemented with glycerol at a concentration of 10 g/L, and glycine at 0.1 g/L. Glycine was used as the sole nitrogen source and was intermittently fed into the reactor as a 150 g/L aqueous solution. A glycerol-rich feed was formulated to contain not just glycerol but also all the other trace elements required for algal growth. The composition of the glycerol-rich feed is shown in Table 7.3.

The feeding strategy was calculated in order to maximize the biomass productivity in the culture, using the adaptive scheme reported in Fig. 7.3. The initial parameter values were set equal to the values estimated for glucose-fed cultures, and were adjusted after 48 h, 120 h, and 144 h. The adjustment in the parameter values resulted in a corresponding modification of the feeding strategy. The feeding profiles followed in the glycerol-fed culture are shown in Fig. 7.12.



(a) Glycine-rich feed



(b) Glycerol-rich feed

Figure 7.12: Feeding flowrates for the glycerol-fed culture of *A. protothecoides*.

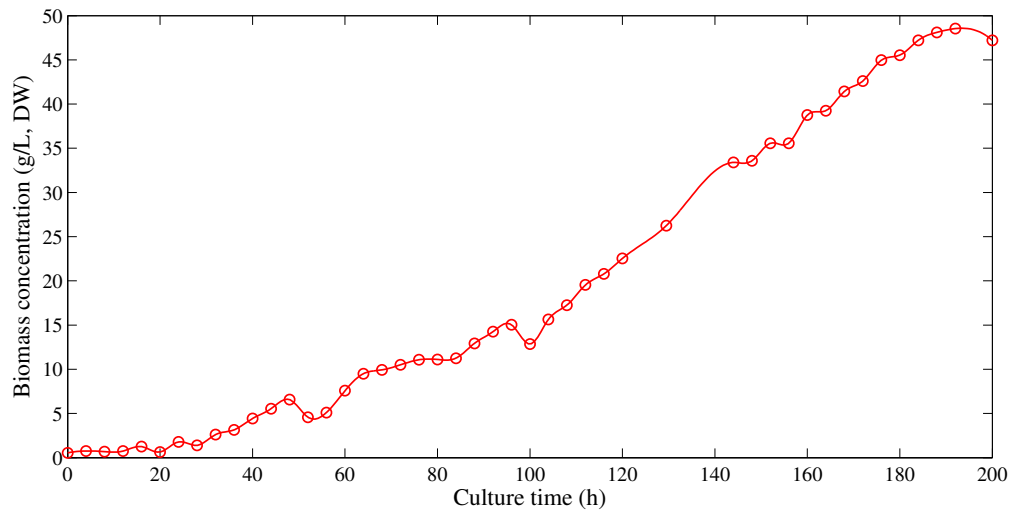
Table 7.3: Composition of glycerol-rich feed.

Component	Concentration	Units
Glycerol ($C_3H_8O_3$)	1123	g/L
Potassium phosphate monobasic (KH_2PO_4)	50	g/L
Magnesium sulfate ($MgSO_4 \cdot 7H_2O$)	32	g/L
Iron sulfate ($FeSO_4 \cdot 7H_2O$)	1.272	g/L
di-sodium EDTA	1.696	g/L
Thiamine hydrochloride	1.06	g/L
Calcium chloride ($CaCl_2 \cdot 2H_2O$)	0.260	g/L
Boric Acid (H_3BO_3)	0.3074	g/L
Manganese chloride ($MnCl_2 \cdot 4H_2O$)	0.1908	g/L
Zinc sulfate ($ZnSO_4 \cdot 7H_2O$)	23.32	mg/L
Cooper sulfate ($CuSO_4 \cdot 5H_2O$)	8.48	mg/L
Sodium Molybdate ($MoNa_2O_4 \cdot 2H_2O$)	3.207	mg/L

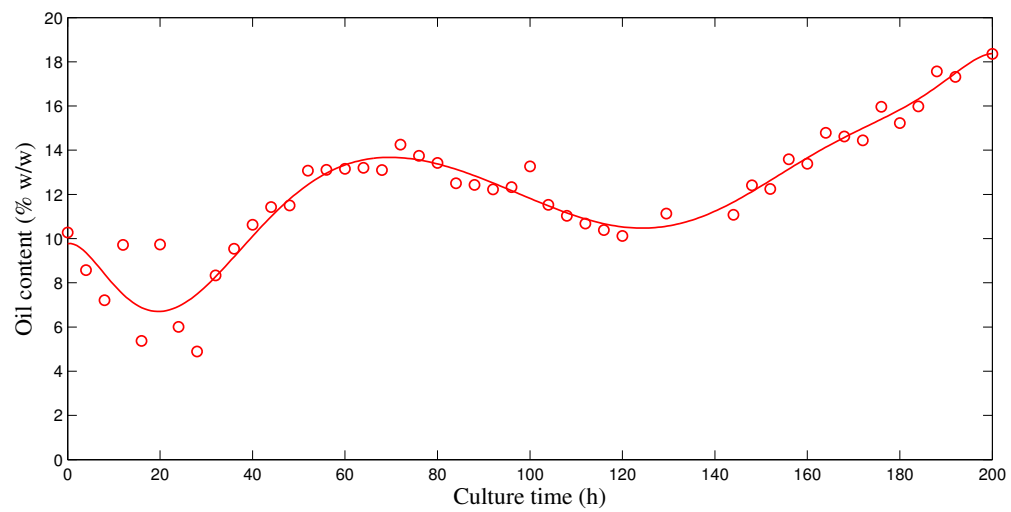
7.3.2 Effect of glycerol on growth and oil production

A. protothecoides was able to use glycerol to fuel their metabolism and growth. The growth curve for the glycerol fed-batch experiment is shown in Fig. 7.13. Cell density increased from 0.5357 g/L to 47.2 g/L in 200 h, corresponding to an average productivity of 5.6 g/L-d, and an average doubling time of 31 h. The maximum productivity was 16.7 g/L-d, achieved at approximately 100 – 108 h, while the minimum doubling time was 10.5 h. The biomass productivity in the glycerol-fed Adaptive MPC run was lower than in the Adaptive MPC glucose-fed run, but it was comparable to the average and maximum productivities for the Open-loop MPC run.

The average observed specific growth rate in the glycerol-fed culture was 0.022 h^{-1} and the maximum growth rate was 0.084 h^{-1} . Interestingly, the observed maximum growth rate was in the same range of observed growth rate for glucose cultures. This indicates that there is a potential to bring the



(a) Biomass concentration



(b) Intracellular oil content

Figure 7.13: Biomass and oil content profiles of a glycerol-fed culture of *A. protothecoides*.

biomass productivity of glycerol-fed microalgal cultures to a similar level of that achieved in glucose-fed cultures.

Oil production, on the other hand, was significantly reduced when glycerol was used as carbon source. Initial oil content was approximately 10.3%(w/w) and increased to 18.4%(w/w) after 200 h. The average lipid productivity was 1.0 g/L·d and the maximum was 2.3 g/L·d, these values are one order of magnitude lower than those achieved during the glucose-fed culture. Whether the reduction in lipid production was due to particular metabolic response to glycerol or due to a non-optimal medium composition was not investigated in this work.

7.3.3 A second stage to boost oil production

Physical or temporal separation of growth and oil production in microalgal cultures has been suggested as a possibility to optimize overall process performance. This idea arises naturally as the two processes are not fully correlated as previously shown. Chi et al. (2009) reported the use of this approach to increase the production of docosahexaenoic acid (DHA) in *S. limacinum*; in a first stage, process conditions were optimized in order to increase cell numbers, while in a second stage culture conditions were modified to induce lipid accumulation.

To explore the potential of this idea in *A. protothecoides* cultures, glucose was fed to the bioreactor after completion of the Adaptive MPC glycerol-grown culture. In this way, the glycerol-fed phase can be considered as a biomass production stage, while the glucose-fed phase will correspond to a lipid accumulation phase.

Glucose was pumped into the bioreactor as a concentrated aqueous solution (800 g/L) following the flowrate profile indicated in Fig. 7.14. No other

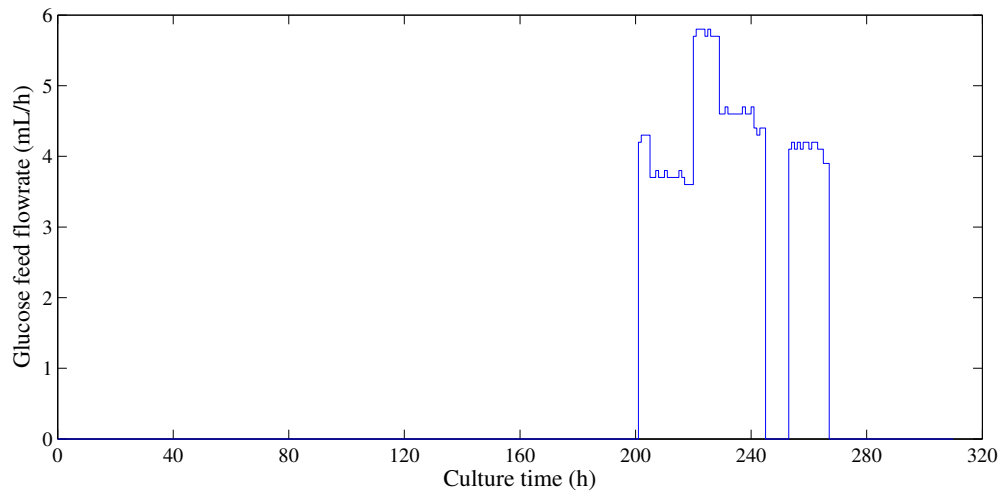


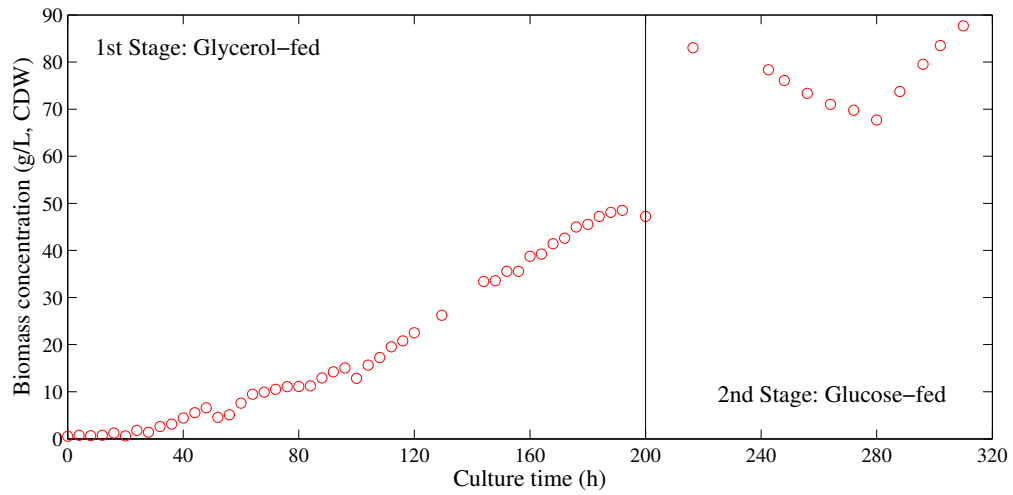
Figure 7.14: Glucose feeding flowrate for the two-stages culture of *A. protothecoides*.

nutrients were supplemented during this second culture stage.

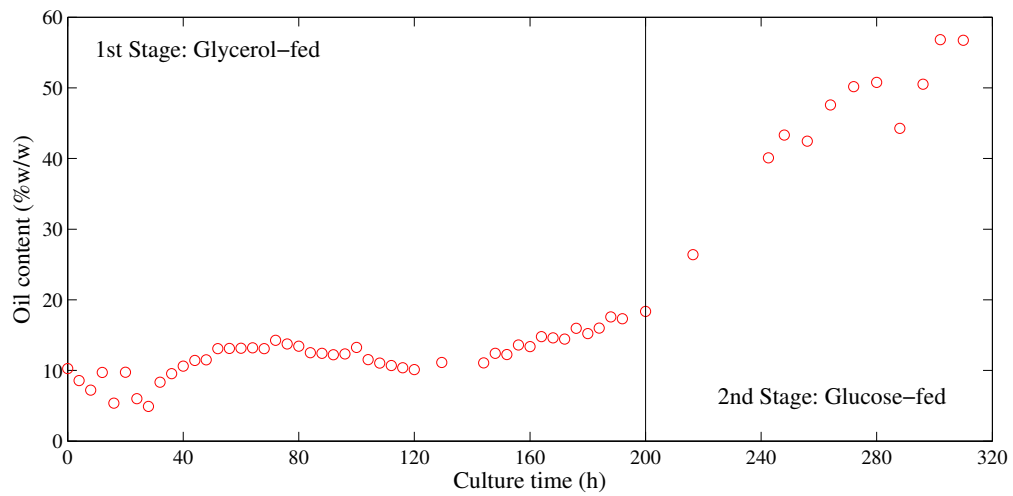
The measured increase in total biomass concentration and oil content in the cells is shown in Fig. 7.15, where the concentration profiles for the precedent 200 h of cultures is shown as a reference. Due to a generalized and recurrent power failure in the building at the end of the glycerol feeding phase, the autosampler system was rendered inoperative. Consequently, it was not possible to automatically collect samples during the initial part of the glucose-fed stage. The failure in autosampler was corrected at 248 h, after which sampling frequency was resumed to 8 h.

As shown in Fig. 7.15(a), there was a significant increase in the total biomass concentration after the glucose feeding started. In the first 16 h of glucose feeding, the biomass concentration increased 75%, from 47 g/L to 83 g/L. This corresponds to a doubling time of 20.2 h and a productivity of 52 g/L·d. After this initial surge in productivity, however, there was a reduction in the glucose consumption and growth rate. As a result, glucose accumulated in the

7.3. Optimization of glycerol-fed cultures



(a) Biomass concentration



(b) Intracellular oil content

Figure 7.15: Biomass and oil content profiles of the two-stages culture of *A. protothecoides*.

culture media reaching a concentration of 35 g/L at 242.5 h, and 56 g/L at 272 h. This in turn, resulted in a reduction in the biomass concentration due to the dilution of the reaction broth.

Oil content in the cells, on the other hand, steadily increase from 18.3%w/w at the start of the glucose feeding (200 h) to 56.7%w/w at 310 h. This resulted in an initial (and maximum) lipid productivity of 19.3 g/L·d, and an average lipid productivity equal to 9.0 g/L·d. That is, the maximum lipid productivity in the second stage of the culture was equal to 96% of the maximum lipid productivity observed in the Adaptive MPC glucose-fed culture, while the average lipid productivity was 87% of the observed average value in the Adaptive MPC culture. The results obtained in this two-stages experiment are remarkable, specially considering that culture conditions were not optimal.

Under optimal conditions, it is expected that biomass productivity will be maximized in the first stage by operating the culture at an average growth rate close to 0.084 h^{-1} , the maximum value observed in the first stage of this experiment. In the second stage, it has been shown that an oil productivity greater than $0.8 \text{ g/L}\cdot\text{h}$ is feasible.

7.3.4 The yield of glucose and glycerol cultures

In the previous sections it has been shown that the cell density and productivity of microalgal cultures can be increased by manipulating the feeding profiles into the bioreactor. In this section, the substrate to product yield is compared for the previously presented runs.

To properly estimate the yields from substrate to biomass and from substrate to lipids, the reactor operating volume was corrected at each time to account for the evaporation losses (F_{loss}) and for the dilution due to the pumping of

the feeds (F_{feeds}) and base (F_{base}) and acid (F_{acid}) solutions .

A dilution factor $D(t)$ was calculated at each time t as follows:

$$D(t) = \frac{D(t-1) \cdot V(t)}{V(t) - F_{loss}(\Delta t) + F_{base}(\Delta t) + F_{acid}(\Delta t) + F_{feeds}(\Delta t)} \quad (7.13)$$

where $F(\Delta t)$ indicates the cumulative flow between time t and $t - 1$. The dilution factor was applied to the measured biomass concentration in order to estimate the total amount of biomass produced between times t and $t - 1$.

The carbon substrate to biomass yield ($Y_{x/s}$) was:

- Glucose (Adaptive MPC): $Y_{x/s} = 0.542$ g/g
- Glycerol (Two-stages): $Y_{x/s} = 0.332$ g/g
- Glucose (Two-stages): $Y_{x/s} = 0.470$ g/g

The lower yield of glycerol cultures, compared to that of glucose cultures, signifies that glycerol is less bioavailable to algae. The carbon content of each substrate is similar (approximately 40%w/w), which implies that more carbon in the glycerol-fed culture was loss as CO_2 than in the glucose-fed cultures. Further research is required to establish if this is a general characteristic of glycerol-fed microalgal cultures, or if the observed result was due to the specific (suboptimal) conditions of the glycerol experiment reported here.

The observed carbon substrate to oil yield ($Y_{p/s}$) was:

- Glucose (Adaptive MPC): $Y_{p/s} = 0.267$ g/g
- Glycerol (Two-stages): $Y_{p/s} = 0.0612$ g/g
- Glucose (Two-stages): $Y_{p/s} = 0.347$ g/g

In order to compare the overall efficiency of converting glucose or glycerol into lipids, carbon base yields were calculated assuming that all the oil was in the form of oleic acid triglyceride ($C_{57}H_{104}O_6$). In this case the corresponding carbon base yields ($Y_{p/s}^C$) were:

- Glucose (Adaptive MPC): $Y_{p/s}^C = 0.516$ g/g
- Glycerol (Two-stages): $Y_{p/s}^C = 0.121$ g/g
- Glucose (Two-stages): $Y_{p/s}^C = 0.670$ g/g

This implies that, in the single stage Adaptive MPC run, 51.6% of the carbon was accumulated as TAGs, whereas in the two-stage culture 67% of the glucose fed was converted into TAGs. In other words, there was a 30% improvement in the yield of glucose into lipids. Given the high commercial value of glucose, the reported finding is significant as it provides the possibility of using the higher cost substrate more efficiently.

7.4 Characterization of algal oil as a source for biodiesel production

The extracted oil was characterized in order to determine its lipid profile, and suitability as a biodiesel feedstock. HPLC analysis of the algal lipids revealed that the hexane-extracted oil was in the form of nearly 100% triglycerides. There were traces (below the limit of quantitation) of sterol esters and/or phosphatidylcholine. Free fatty acids and other lipid classes were not detected.

The fatty acid profile of the algal oil was determined by gas chromatography and is reported in Table 7.4. Interestingly, there was not a significant variation in oil composition between the two glucose-fed optimal fed-batch runs, even

though there was a 4-fold increase in lipid productivity between the Open-loop OFT run and the Adaptive MPC run. On the other hand, the relative content of long chain saturated fatty acids decreased from 49.1% in the batch run to around 14% for the two optimal runs, and to 5% for the two-stages culture.

Highly unsaturated and very long chain fatty acids were only produced in significant amounts in the two runs with the lowest productivity (Batch and reference fed-batch). From Fig. 7.7, it can be noticed that both the batch and the reference fed-batch runs underwent a relatively long stationary phase, while the two optimal runs were finished during or just after the exponential phase. This suggests that the oil profile of *A. protothecoides* is basically constant during exponential growth, while elongation and excessive accumulation of saturated fatty acids occur during the stationary phase.

Interestingly, there was a significant amount of DHA measured in the two-stages culture. Given that DHA was not detected in the two optimal glucose fed runs, it could be suggested that the production of DHA in the two stages culture was induced by glycerol. It could be possible that a higher amount (as percentage content) of DHA was present by the end of the first stage of the culture. However, this was not investigated in this report.

In Table 7.4, it is also reported the degree of unsaturation (DU) of the oil, as defined by Ramos et al. (2009):

$$\text{DU} = (\text{monounsaturated, w\%}) + 2 \cdot (\text{polyunsaturated, w\%}) \quad (7.14)$$

The DU of an oil used as feedstock for biodiesel production determines the cetane number (CN) and the iodine value (IV) of the final biodiesel product (Ramos et al., 2009). For DU values lesser than 137, the biodiesel produced is expected to meet the European Standard (UNE-EN 14214).

Table 7.4: Fatty acid profile, % w, of *A. protothecoides* for different fed-batch cultures of *A. protothecoides*

Fatty Acid		Batch	PRBS	Fed-batch	Open-loop	OFT	Adaptive MPC	Two-stages
Myristic	C14:0	2.31	1.39	0.84	0.86	—	—	
Palmitic	C16:0	26.20	14.30	12.68	12.89	—	—	
Palmitoleic	C16:1	0.80	0.20	0.59	0.58	0.73	—	
Stearic	C18:0	17.58	6.87	—	—	4.43	—	
Oleic	C18:1	47.61	70.17	58.82	57.64	70.42	—	
Linoleic	C18:2	0.83	4.30	24.95	25.56	22.24	—	
Linolenic	C18:3	0.05	0.31	2.11	2.18	1.51	—	
Stearidonic	C18:4	1.35	0.29	—	—	—	—	
Arachidic	C20:0	1.35	0.46	—	0.24	0.33	—	
Behenic	C22:0	0.14	0.10	—	0.05	0.10	—	
Erucic	C22:1	0.13	0.10	—	—	—	—	
DHA	C22:6	0.13	0.04	—	—	0.24	—	
Lignoceric	C24:0	0.20	—	—	—	—	—	
Hexacosanoic	C26:0	1.29	1.46	—	—	—	—	
DJ ^a		53.3	80.4	113.5	113.7	119.13	—	
Saturated		49.1	24.6	13.5	14.1	4.9	—	
Monounsaturated		48.5	70.5	59.4	58.2	71.1	—	
Polysaturated		2.4	4.9	27.1	27.7	24.0	—	

^a Degree of unsaturation

7.4. Characterization of algal oil as a source for biodiesel production

The DU for the algal oil extracted from the two optimal runs was 113.5–113.7, similar to that of corn and high oleic sunflower oil. The content of saturated, monounsaturated, and polyunsaturated fatty acids was also similar to that of corn, high oleic sunflower, and rapeseed oils. For this range of composition, the expected cold filter plugging point (CFPP) is below -12°C .

The high content of saturated fatty acids in the batch and reference fed-batch cultures, however, causes the CFPP of the biodiesel produced from these two oils to be higher than 0°C . That is, when grown at lower rate and reduced productivity, the oil accumulated by *A. protothecoides* might not be suitable for biodiesel production. Fast algal growth promotes the production and accumulation of oil with a better quality as a biodiesel precursor. That is, the enhanced lipid productivity comes associated with an increased product quality.

This page intentionally left blank

8

Feasibility evaluation of microalgal oil production

The economic feasibility of algal bioprocesses is affected by the substrate to product yield, the volumetric productivity, and the cost of the feedstock, as well as by the cost of processing and product recovery. Photoautotrophic algal growth processes have negligible feedstock costs, but they are still economically unfeasible due to the very low productivities and the high product recovery costs. Heterotrophic bioreactor-based microalgal cultures, on the other hand, offer the possibility of increased lipid production and ease of process scale-up, intensification, and control as shown in the preceding chapters.

A heterotrophic microalgal process for the production of biodiesel can be evaluated both in terms of the land required for feedstock production, as well as the final production costs. A sustainable biodiesel production process based on heterotrophic microalgae requires that the land required for feedstock

production be minimized, such that there is not an excessive competition for cropland for food. For a long term viability, it is also necessary that production costs be reduced while keeping a positive cash flow.

In this chapter, the land requirements and oil production costs are estimated based on the productivities and cell density reported in Chapter 7 for the optimized heterotrophic algal cultures. All cost values presented are in 2010 U.S. dollars, unless otherwise indicated.

8.1 Land requirement for biodiesel production from microalgae

Microalgae can be cultured heterotrophically using a wide variety of organic carbon substrates, ranging from simple carbohydrates to organic acids, to complex substrates. Even though it is possible to grow microalgae on agricultural wastes and cellulosic materials, in this evaluation it is assumed that microalgae grow on hexoses or glycerol. In this sense, the present evaluation is fully based on the experimental results presented in Chapter 7. Nonetheless, the utilization of a different, more favourable, substrate may reduce the land requirements.

8.1.1 Substrates for heterotrophic microalgal growth

Four different sugar crops were considered as potential feedstock for the microalgal heterotrophic cultivation based on their current availability in North America: sugar beets, sugarcane, corn, and red winter wheat. Sugar beet is a plant whose root contains a high concentration of sucrose. It is cultivated in temperate weathers, mainly in Europe, eastern U.S.A and Canada, Chile and Japan. The sugar content in sugar beets is usually between 15 – 20% in

weight. The yield and production cost of sugar from sugar beets is reported in Fig. 8.1.

Sugarcane is a perennial grass that grows in warm temperate to tropical weathers. In North America, it is grown in southern United States, Hawaii, and Mexico. Sugar content in sugarcane is approximately 10 % in weight. The yield and production cost of sugar from sugarcane is reported in Fig. 8.2.

Maize, or corn, is an annual grass that is extensively cultivated in the Americas. Maize seeds are rich in starch from where sugar is obtained by hydrolysis. Maize is used for the production of sweeteners, ethanol for biofuel, and animal meals. The yield and production cost of sugar from corn is reported in Fig. 8.3.

Soft red winter wheat is a variety of wheat characterized for its lower protein content. It is planted in late autumn and sprouts before freezing occurs, remaining dormant until the spring. It is harvested in early July. This characteristic make it an ideal crop for high latitude areas. Soft red winter wheat contains on average 64% of starch in the whole grain. The average historical yields and farm prices for soft red winter wheat in the United States is presented in Fig. 8.4.

As can be seen from Figs. 8.1 – 8.4, sugar beet crops have the highest yield of sugar per hectare, while the sugar from maize has the lowest production cost. The significantly lower cost of sugar from maize is due to the credits that are built into the corn price. Each bushel of maize (25.4 kg) produces on average 15 kg of sweeteners (glucose and fructose), 0.7 L of corn oil, 5.2 kg of gluten feed, and 1.4 kg of gluten meal. The application of similar credits for the other two crops under consideration may reduce their relative cost.

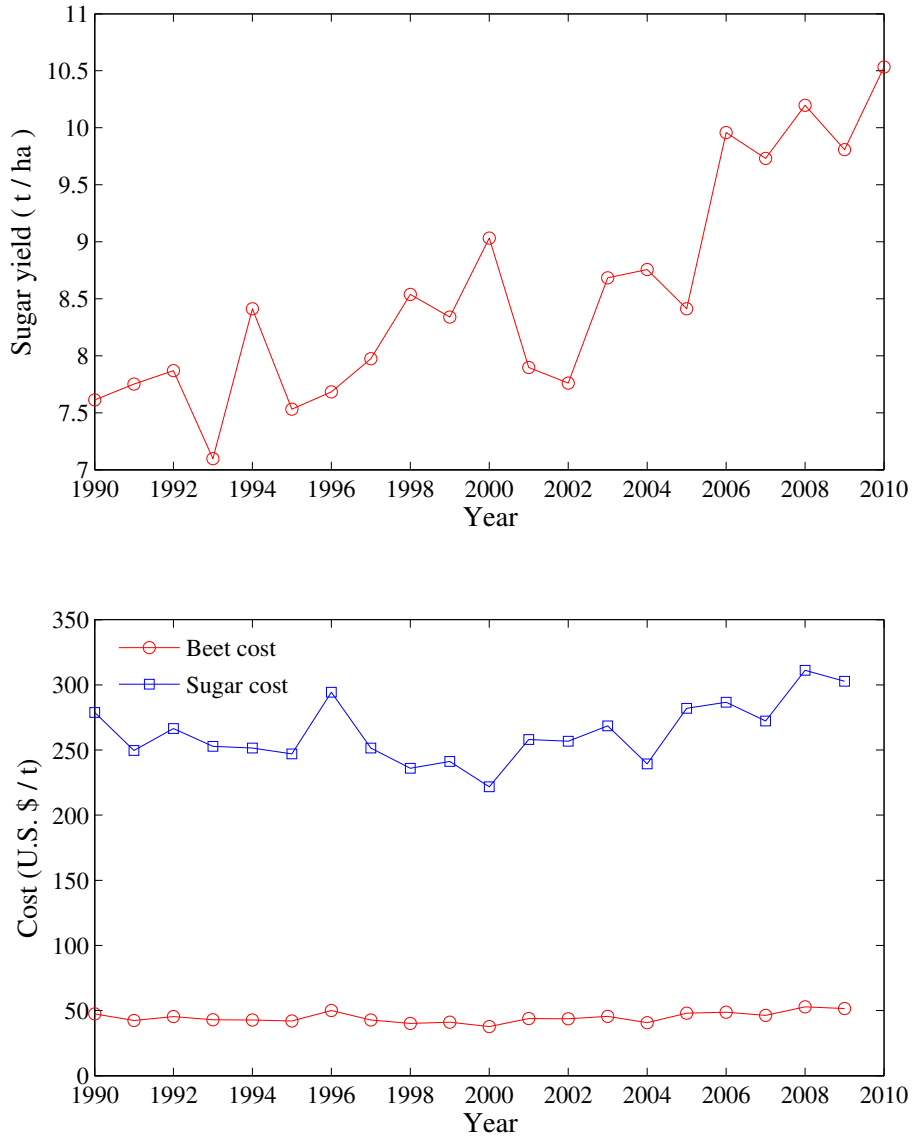


Figure 8.1: Historical yield and production cost of sugar beet crops in U.S. Sugar yield was calculated considering a 17% recoverable sugar content in the beets.

8.1. Land requirement for biodiesel production from microalgae

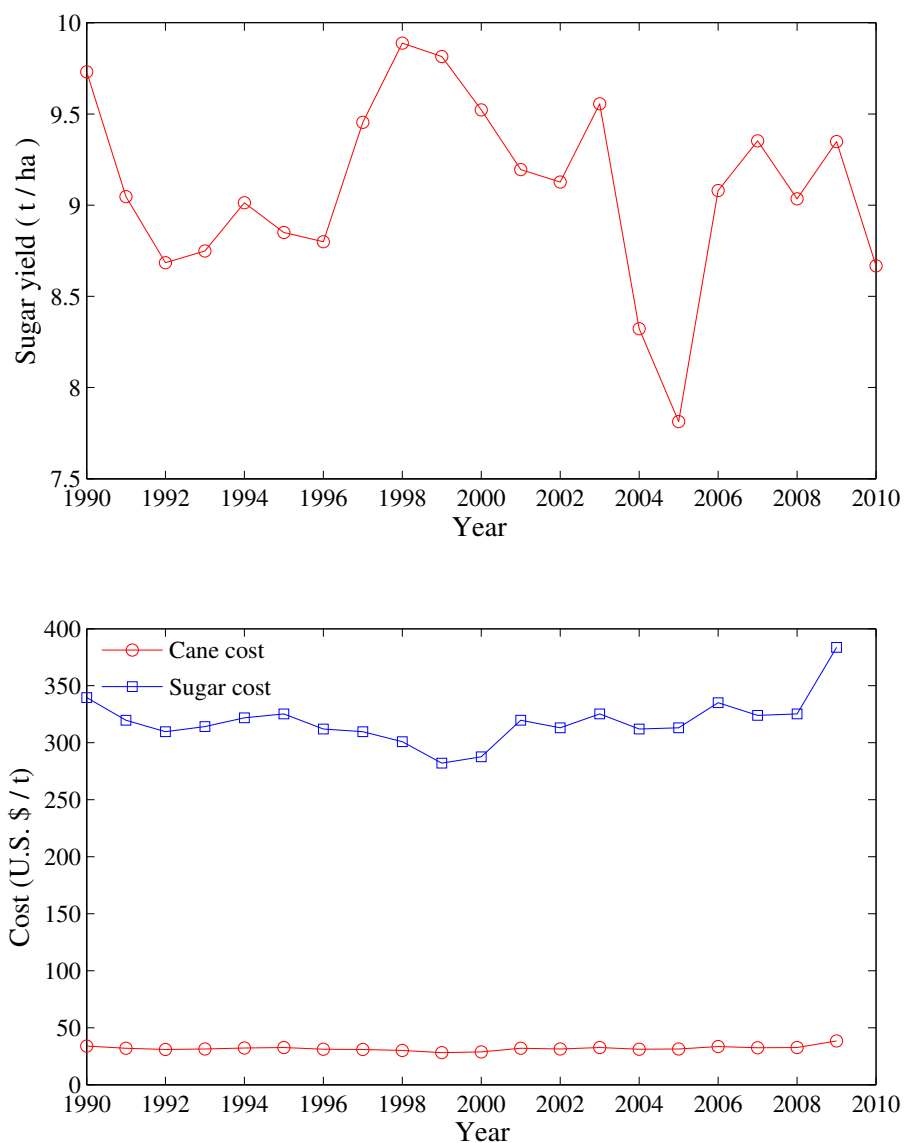


Figure 8.2: Historical yield and production cost of sugarcane crops in U.S. Reported prices are the national average for the continental United States and Hawaii. The reported yield excludes the cane harvested for seeding.

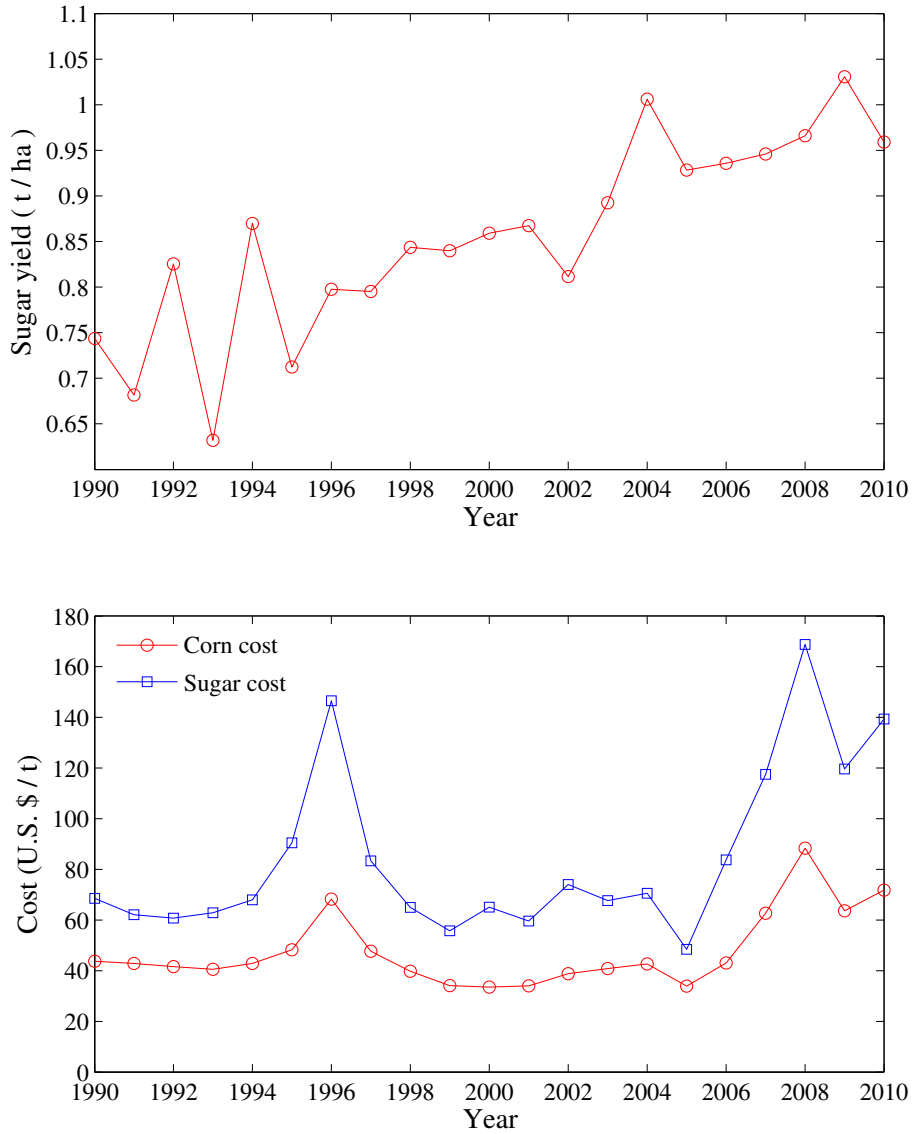


Figure 8.3: Historical yield and production cost of maize crops in U.S. Maize cost are the average midwest country elevator producer bid prices and do not include transportation costs. Sugar cost represents the cost for wet-millers after applying the price credits for corn-oil, gluten feed, and gluten meal.

8.1. Land requirement for biodiesel production from microalgae

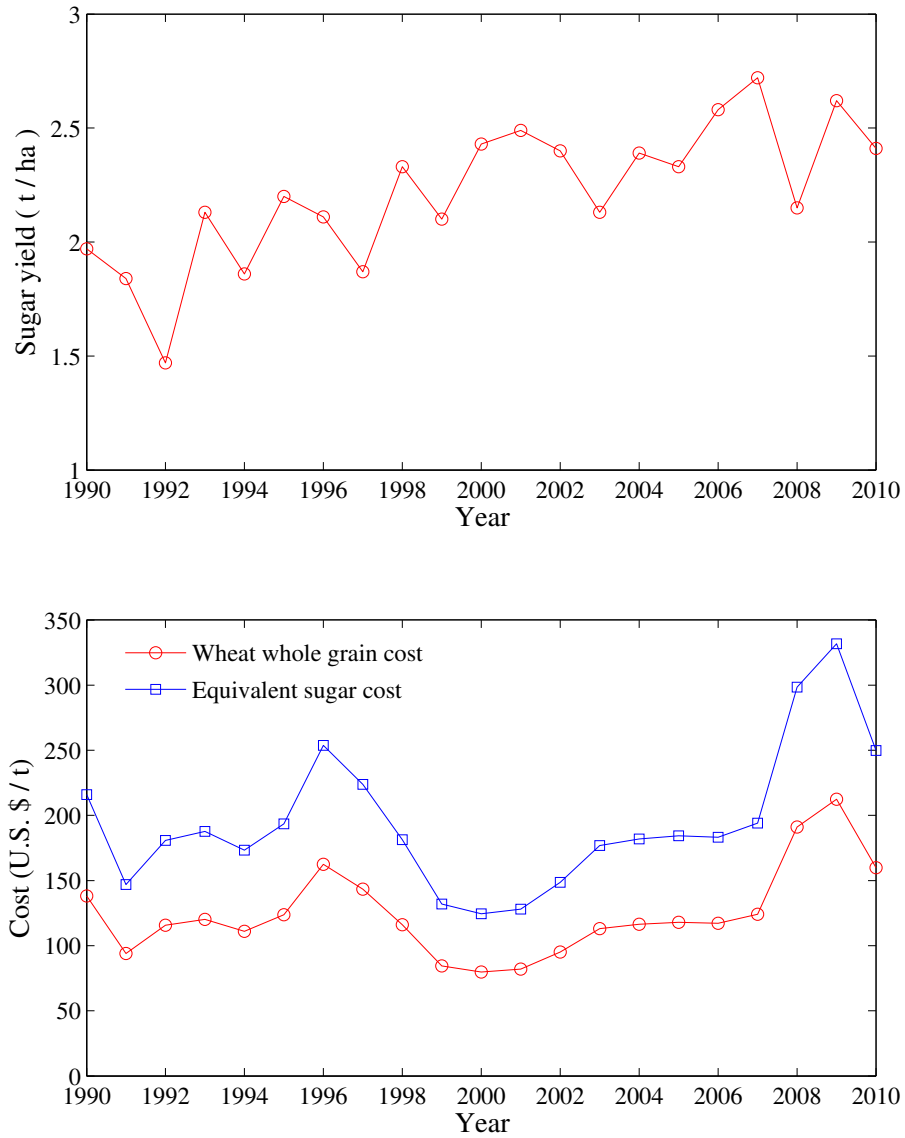


Figure 8.4: Historical yield and average farm price of soft red winter wheat crop in U.S.

8.1.2 Substrate to product yield scenarios

Two different scenarios were considered based on whether algae are cultured in a single stage process or in a two-stage culture. In the first scenario, microalgae are assumed to grow on a single sugar with the same yield as in the optimized glucose culture ($Y_{\text{oil/sugar}} = 0.267$ g/g), as reported in Section 7.3.4.

For the second scenario, it is assumed that in the first stage microalgae are grown on glycerol and in a second stage they are grown on a simple sugar. The glycerol is assumed to be derived from the trans-esterification of oils for biodiesel production and therefore no land is needed for glycerol production. The yield of oil from sugar for this second scenario is assumed to be equal to that reported in Section 7.3.4 for the second stage of the two-stage glycerol/glucose culture ($Y_{\text{oil/sugar}} = 0.347$ g/g).

8.1.3 Algal oil yield per hectare of sugar crop

The average sugar yield per hectare of sugar crop and the corresponding algal oil yield, after conversion of the sugar feedstock, is reported in Table 8.1. The sugar yield for each crop was linearly extrapolated for 2011 from the historical data reported in Figs. 8.1 – 8.4. Sugar beets offer the highest sugar yield per hectare and therefore the land requirement will be minimized if sugar beets are used as the feedstock for heterotrophic microalgal biofuel production. Therefore, for temperate regions such as Canada, it is recommended to use sugar beet as the crop of choice for the heterotrophic cultivation of microalgae.

8.1.4 Land requirements for biodiesel production

For 2012, the biodiesel target in Canada has been mandated at 2% (B2). In United States, the target for the year 2020 is 20% of biofuel content, equivalent

8.1. Land requirement for biodiesel production from microalgae

Table 8.1: Annual yield of sugar crops in North-America, and expected oil yield for the heterotrophic cultivation of microalgae.

Crop	Sugar yield (t/ha) ^a	Oil yield (kg/ha)	
		One-stage ^b	Two-stage ^c
Sugarcane	9.0	2400	3119
Sugar beets	10.0	2667	3465
Corn	1.0	267	347
Red winter wheat	2.34	624	811

^a Assumed yields correspond to the linear fit projection at 2011 of the historical yield values from 1990 – 2010.

^b In the one-stage scenario, microalgae are grown using the sugars derived from the indicated crops as the only carbon source.

^c In the two-stage scenario glycerol is used in the first stage to support algal biomass production, and in the second stage a hexose is used for production of oil.

to B20. To satisfy the biodiesel demand generated to comply a B2 target in Canada, it would be necessary to produce 638 million litres of biodiesel in 2011 (equivalent to 587000 tonnes).

In Table 8.2, the average and maximum oil yield per hectare per year is reported for different oleaginous crops and for two of the combined sugar crop/microalgal conversion alternatives presented in Table 8.1. The land required to satisfy the expected biodiesel demand is also reported in Table 8.2. The reported area requirement was calculated using the average crop yield. The indicated cost for the different vegetable oils correspond to the forecasted price of the unrefined oils for the period 2010–2011. The cost for the algal oil are estimated values at 2010 and correspond to the price of the oil that makes the return on equity equal 0% (see details in Section 8.4).

The maximum oil yield for the heterotrophic conversion of sugar beets into

Table 8.2: Oil yield, cost, and required land to satisfy the biodiesel demand to comply with a B2 (2% biodiesel) target, for different oleaginous crops

Crop	Oil yield (L/ha·year)	Cost (U.S.\$/L) ^d	Land required for B2 kha % Cropland ^e	References ^f
Soybean ^a	563 – 611	1.04 – 1.13	1133	2.7 [1]
Sunflower ^a	761 – 827	1.48 – 1.56	838	2.0 [2]
Canola ^b	790 – 1110	1.18 – 1.26	808	1.9 [3]
Sugar beets/Microalgae	3766 – 5725	0.86 – 1.24	169	0.4 (This work)
Wheat/Microalgae	882 – 987	0.75 – 1.07	723	1.7 (This work)
Olive	1212			[4]
Jatropha ^c	1728 – 1892			[5, 6]
Oil Palm ^c	3935 – 5950			[7, 8]

^a Lower yield value corresponds to the average yield for the period 2002 – 2010. Higher value is the highest yield reported over the same period.

^b Lower value corresponds to the average crop yield for the year 2006. Higher value is the predicted yield for the year 2015.

^c Lower value is the yield reported in the first reference indicated; higher value is the one reported by the second reference.

^d Forecasted price of crude vegetable oil for the 2010 – 2011 period (USDA, 2011).

^e Percentage of Canada's crop land, estimated at 41.6 million hectares.

^f Reference key: 1. USDA (2011); 2. N.S.A. (2010); 3. J.C.C.C. (2009); 4. Chisti (2007); 5. Gui et al. (2008); 6. Chisti (2007); 7. Sumathi et al. (2008); 8. Chisti (2007).

oil by *A. protothecoides* was calculated assuming a maximum sugar yield of 15.2 t/ha. This value is the average of the highest crop yields obtained in the United States from 2002 – 2010, based on state crop yield averages.

As per Table 8.2, it can be seen that none of the temperate weather crops considered will require an excessive amount of crop land in order to satisfy the expected biodiesel demand once the government target for B2 enters in effect. However, in the long-term, with a projected target of B20 expected for 2020, the pressure for crop-land will increase. For a B20 scenario the land requirement for producing sugar beets for biofuel conversion using microalgae will represent 4.1% of the existing arable land in Canada. For the other crops, the land requirement in a B20 scenario will be between 17 – 27% of the arable land. Therefore, using sugar beets as the carbon source for heterotrophic algal cultivation is the best alternative in order to guarantee long-term sustainability.

8.2 Estimation of production and capital costs

For the estimation of the production cost it is considered that the heterotrophic production of microalgal oil operates as an independent facility, acquiring the sugar feedstock from the market and selling the algal oil to biodiesel producers. As such, the resulting costs or credits that can arise from a combined facility are not considered in the analysis.

8.2.1 Organic carbon substrate cost

In 2010, the average production cost of sugar beets was \$51.5/t, and that of sugar beet sugar was \$302.8/t. As a reference, it can be noted that the average bulk price for refined sugar was \$584.2/t and that of raw sugar was

\$463.3/t. With a yield ranging from 0.2667 g/g to 0.3465 g/g, and assuming an oil density equal to 0.92 kg/L, the cost of the carbon source per unit of product will range from \$1.04/L to \$0.80/L if sugar beets are used as the carbon feedstock. For other carbon feedstocks, the historical prices are reported in Figs. 8.1(b), 8.2(b), 8.3(b), and 8.4(b).

8.2.2 Other nutrients cost

Besides the carbon source, algae requires trace minerals and a nitrogen source to support their growth. Li et al. (2007a) estimated that the cost of inorganic chemicals for the formulation of the algal growth media represented a cost of 7 cents per litre of oil. This value is used here for estimation purposes.

8.2.3 Oil extraction

Electromechanical extraction has been proposed to cost-effectively recover oil from microalgal cells. Hebner (2010) has estimated the cost of electromechanical extraction at \$0.04 – 0.26 per gallon of oil (Schlesinger et al., 2011), based on an initial algal concentration of 10 % in the algal slurry, with a 20 % oil content in the cells.

Previously, Benemann and Oswald (1993) estimated the extraction cost to be as high as \$0.22/L. In this case, traditional mechanical and solvent extraction technologies were considered. The value reported by Benemann and Oswald (1993) is used here as the maximum expected extraction cost. This value corrected at 2010 dollars is \$0.33/L.

8.2.4 Capital cost

Alabi et al. (2009) estimated that the capital cost for a microalgal heterotrophic

production system with a nominal reactor capacity of 1200 m³ was \$2,800,000. Two different scenarios are considered for the productivity of the system. In the first, scenario the productivity is considered to be equal to the average productivity of the optimized culture reported in Chapter 7, 10.32 g/L · d. The second, optimistic scenario consider that the plant will operate at the maximum productivity achieved in the optimized culture, 20.16 g/L · d. Assuming that the plant will be in operation for 300 days in a year, then the output of a 1200 m³ plant will be 4,040,000 L/year for the low productivity scenario and 7,890,000 L/year for the high productivity scenario.

In this study, a nominal plant capacity of 25 million litres of algal oil is used for the economic evaluation. The capital cost estimated by Alabi et al. (2009) is taken as a reference value with a scale factor of 0.6. The cost of the 25 million litres plant is estimated using the following relation:

$$\text{Capital_cost} = \text{Capital_cost}_{\text{ref}} \left(\frac{\text{Capacity}}{\text{Capacity}_{\text{ref}}} \right)^{0.6} \quad (8.1)$$

For the economic evaluation it is further assumed a 50% leverage, 15 years of capital life, and a 6.5 % interest rate with a straight line amortization. Income tax rate is fixed at 34%.

8.2.5 Labour cost

Alabi et al. (2009) assumed that a staff of 10 employes, with two administrative and four shifts of two operators, is required for operating the heterotrophic microalgal plant considered in their report. The total labour cost in this case was considered to an average of \$40,000 per employee, or \$400,000 in total.

8.3 Valuation of algal byproducts

Oil content in the algal biomass is near 50 % in weight, implying that 50 % of the algal biomass will be a residue or a by-product. The residual algal biomass could be commercialized as a substitute or a supplement for animal nutrition. Nitrogen starved algal cells usually have a final nitrogen content ranging from 1 - 2 %. To convert from nitrogen content to protein content in the algal meal a factor between 5.26 to 7.69 is normally used (FAO, 2002). Therefore the expected protein content of the residual algal meal, after oil extraction, is 10.5 - 30.8 %.

The expected protein content in the algal biomass is lower than that of soybean meal (48 %) or fish meal (60 %) and consequently the algal meal could not be used as a direct substitute for them. Nonetheless, algal biomass have been shown to have important benefits in animal nutrition and aquaculture (Pulz and Gross, 2004), and therefore it is feasible to commercialize it as a supplement with an equal or higher value than either soybean meal or fish meal.

In Fig. 8.5, the price of fishmeal and soybean meal is reported from 1990 to 2010. It can be observed that while the price of soybean meal has remained stable between \$200 and \$300 dollars per ton, fish meal price has spiked in recent years.

Even though production of fish-meal has remained stable in the last years, the continuous increase in fish meal demand has resulted in sharp increases in the fish meal price. The current price of fish meal can be considered unsustainable in the long-term and a more realistic price of \$600/t, 2002 – 2005 price, should be expected if the supply of fish meal increases as a result of a surge in algal biomass availability.

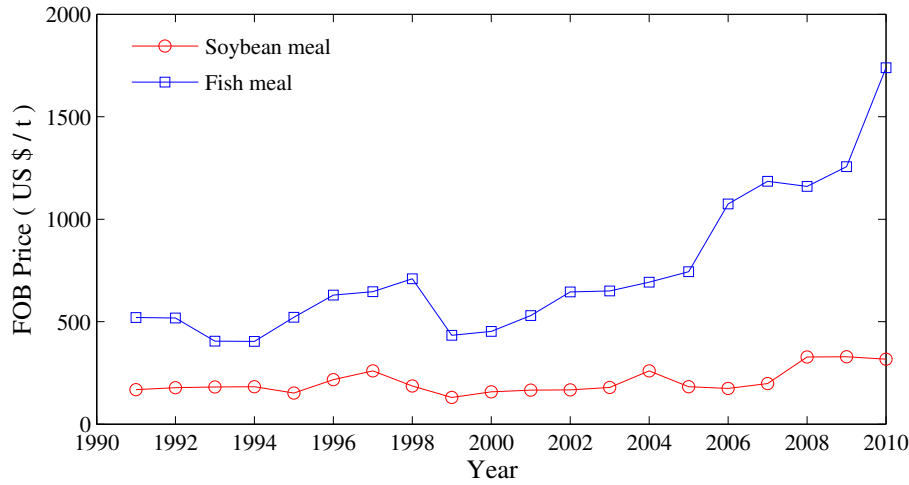


Figure 8.5: Historical FOB price of fish meal and soybean meal.

8.4 Economic evaluation

In Table 8.3, the income statement for a plant with nominal production capacity equal to 25 million litres per year is presented. Four different scenarios are summarized, depending on the yield and productivity achieved in the large scale operation. In Table 8.3, algal oil was priced at \$1.1 per litre which correspond to the forecasted price of soybean oil for 2011. Algal meal was priced at \$0.3/kg, and the sugar feedstock was priced at \$302/t. For maintenance a 4% of the capital cost was allocated annually, and 1% of the capital cost was assumed as overhead.

The earnings before interests, depreciation, taxes, and amortization (EBITDA) is presented together with the expected net income and the return on assets (ROA) and return on equity (ROE). EBITDA is used as a measure of profitability and general financial performance. The ROE is a measure of how profitably the shareholders money is employed, while the ROA measures how efficiently the assets are used.

Table 8.3: Estimated production cost of microalgal oil, in million of 2010 U.S. dollars, for a plant with nominal capacity of 25 million litres per year. The reported nominal oil cost corresponds to the sale price to achieve net income equal zero.

	Scenario			
Productivity	Low	Low	High	High
Yield	Low	High	Low	High
Capital	7.53	7.53	5.04	5.04
Revenues				
Algal oil	23.10	23.10	23.10	23.10
Algal meal	5.80	5.80	5.80	5.80
Operating expenses				
Materials	30.34	22.75	30.34	22.75
Labor	0.40	0.40	0.40	0.40
Maintenance	0.30	0.30	0.20	0.20
Overhead	0.08	0.08	0.05	0.05
EBIDTA	-2.22	5.37	-2.09	5.50
Net income	-1.96	3.05	-1.71	3.30
Return on assets (ROA)	-26%	41%	-34%	65%
Return on equity (ROE)	-52%	81%	-68%	131%
Nominal oil cost (US\$/L)	1.24	0.88	1.22	0.86

From Table 8.3, it can be concluded that in order to generate a positive cash flow it is essential to achieve a high yield in the conversion from sugar to oil. Alternatively, a lower cost carbon source could be used to reduce the total production cost. In Fig. 8.6, the sensitivity of the ROA and ROE to the cost of the sugar feedstock is presented. There is a substantial improvement in profitability as the cost of the feedstock is reduced. Sugar beets cost can be reduced if credits were applied for the production of sugar beet byproducts, such as molasses and biomass.

Profitability is also dependent on the cost of the oil extraction. The sensitivity of the ROA and ROE to the extraction cost is reported in Fig. 8.7. There is an opportunity to improve the process' economic performance by using low cost oil extraction technologies or algal strains with weaker cell walls.

The sensitivity of the ROA and ROE to the price of algal meal and algal oil is presented in Figs. 8.8 and 8.9, respectively. A higher valuation for the algal meal has a very significant impact on profitability. Given the current price and trend of fish meal, there is a clear incentive to try to commercialize the algal meal as a partial replacement of fish meal.

In Fig. 8.9, it can be seen that the profitability of algal oil production increases if the oil is sold at a higher price than soy bean oil. Considering the fatty acid profile of the algal oil there is a potential to commercialize it for higher value applications. In that case, however, the production volumes will be reduced, affecting the capital cost estimates.

Considering the production cost, and the potential credit for by-products sales, the optimized heterotrophic algal oil production process provides a reasonably priced alternative to fossil fuels, while minimizing the requirement for agricultural land.

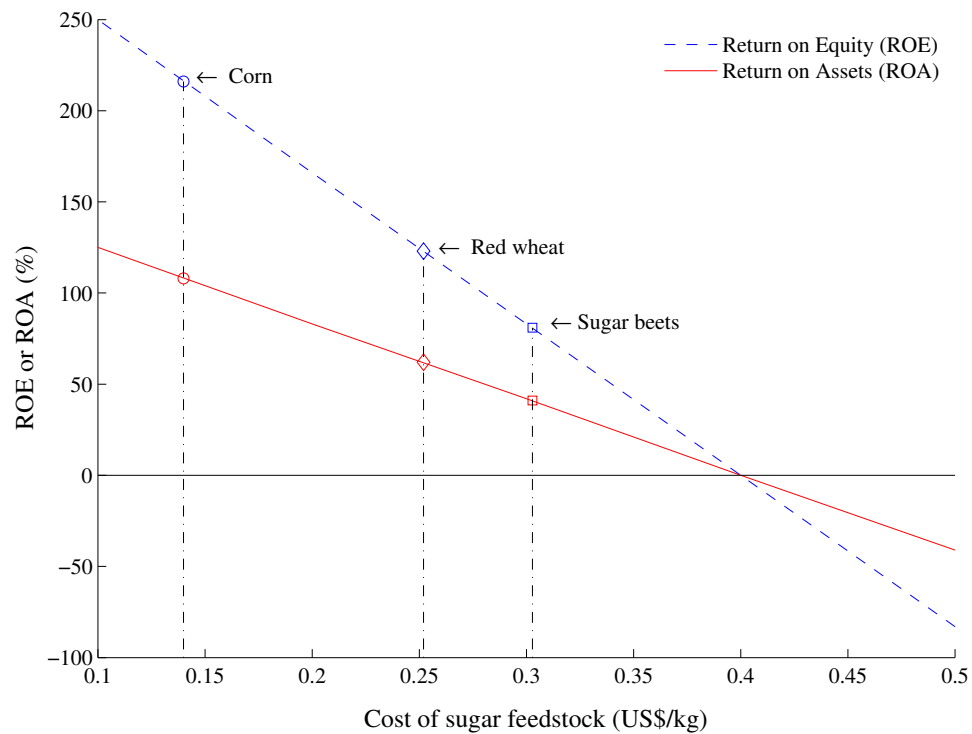


Figure 8.6: Sensitivity of the return on assets (ROA) and return on equity (ROE) indicators to the cost of the sugar feedstock. All other costs were kept the same as for the low productivity/high yield scenario reported in Table 8.3. As a reference, the production cost of sugar from different sugar crops is indicated.

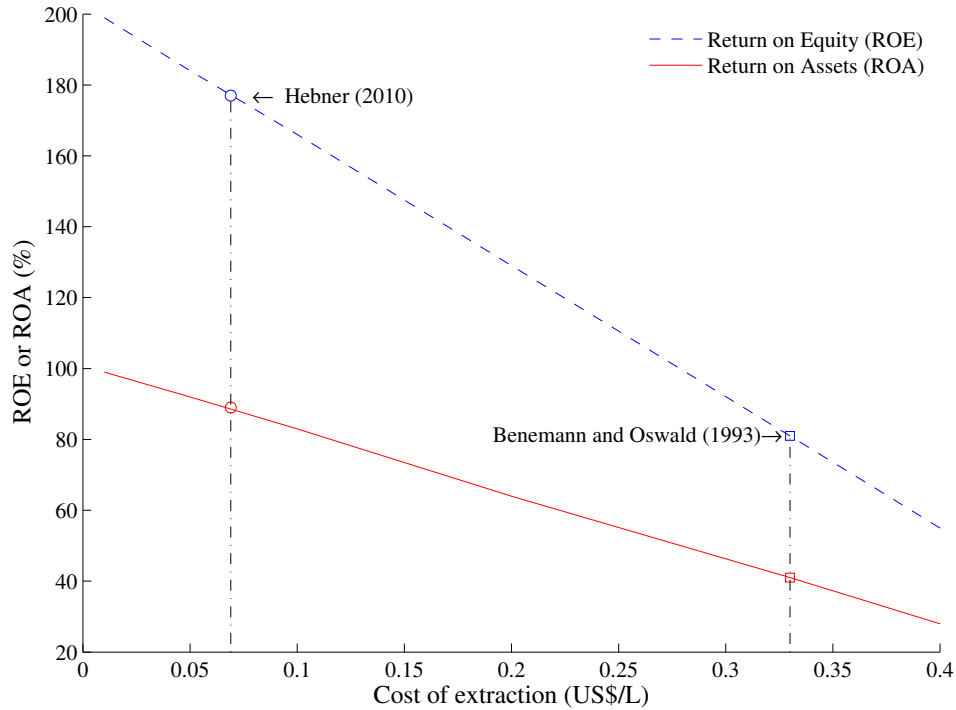


Figure 8.7: Sensitivity of the return on assets (ROA) and return on equity (ROE) indicators to the extraction cost of algal oil. All other costs were kept the same as for the low productivity/high yield scenario reported in Table 8.3. For reference, the estimated extraction cost reported by Benemann and Oswald (1993) has been corrected to 2010 dollars and included in the figure, together with the extraction cost reported for the electromechanical extraction proposed by Hebner (Hebner, 2010; Schlesinger et al., 2011).

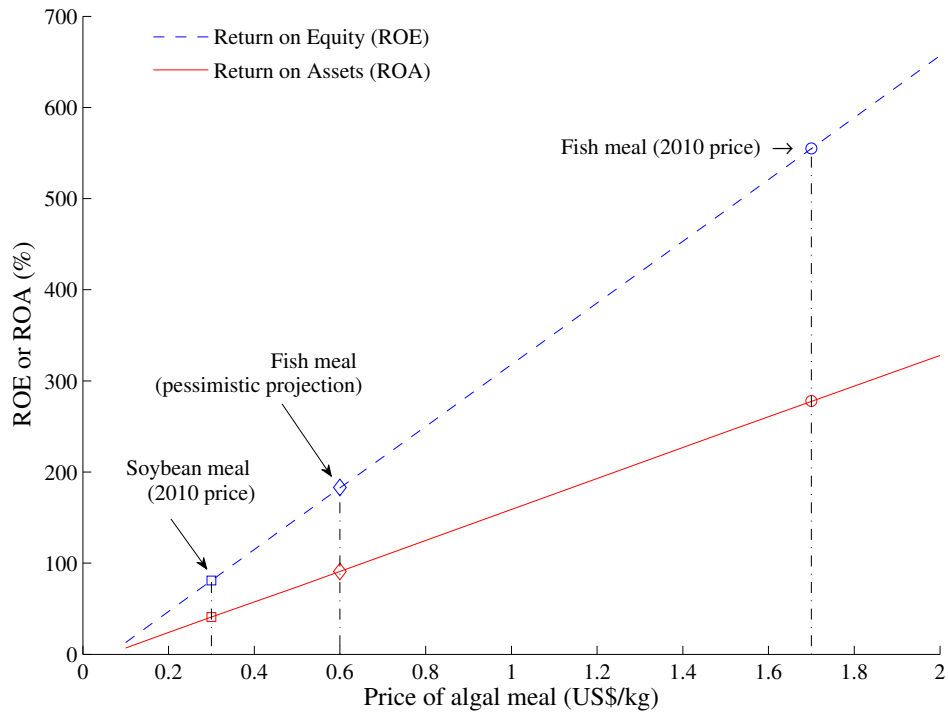


Figure 8.8: Sensitivity of the return on assets (ROA) and return on equity (ROE) indicators to the selling price of algal meal. All other costs were kept the same as for the low productivity/high yield scenario reported in Table 8.3. As a reference, the average 2010 - 2011 FOB price for soybean meal and fish meal is indicated. A pessimistic projection for the fish meal price is also presented for comparison.

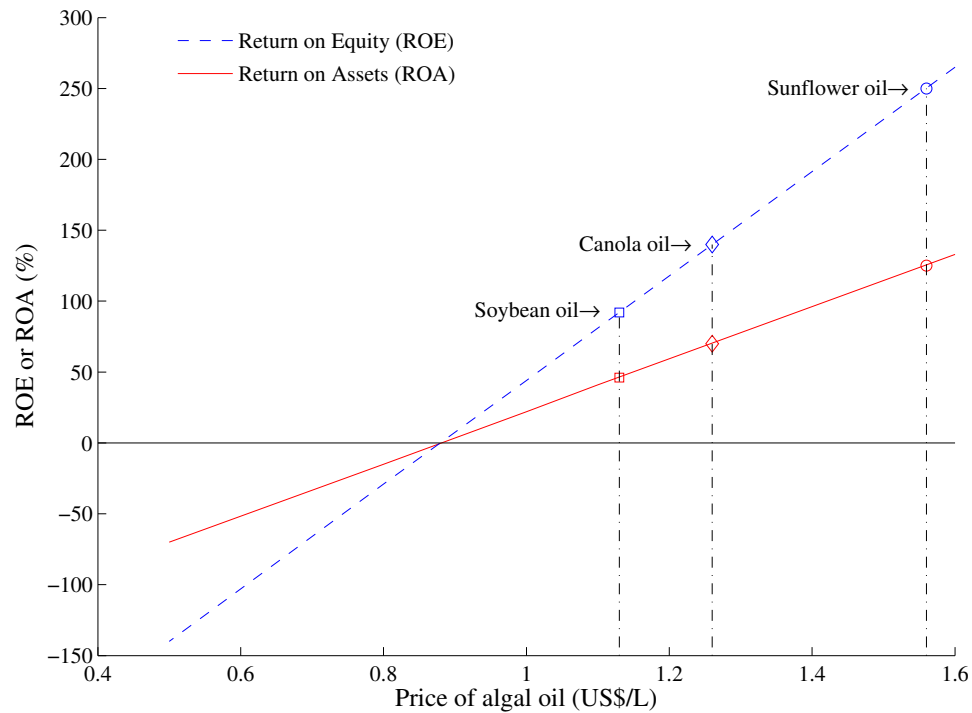


Figure 8.9: Sensitivity of the return on assets (ROA) and return on equity (ROE) indicators to the selling price of algal oil. All other costs were kept the same as for the low productivity/high yield scenario reported in Table 8.3. As a reference, the average 2010 - 2011 price for soybean oil, canola oil, and sunflower oil is indicated.

This page intentionally left blank

9

Conclusions and Recommendations

9.1 Conclusions

The biomass and lipid productivities of heterotrophic microalgal cultures can be increased by regulating the nitrogen availability to the cells as well as the carbon to nitrogen ratio. Biomass productivity in the optimized culture reached a maximum of 60 g/L·d and an average value of 15.6 g/L·d. For this optimized culture, maximum lipid productivity was 20.2 g/L·d, with an average value of 10.3 g/L·d. The lipid productivity in optimized heterotrophic microalgal cultures was shown to exceed the values previously reported for other heterotrophic oleaginous microbes.

The importance of nitrogen in the production and accumulation of neutral lipids in microalgae is widely recognized, but not so well understood. In this research, it was found that the relationship of cell growth and lipid production

with respect to the concentration of nitrogen is not linear in nature. At extreme nitrogen deficient conditions, cells grow slowly but continue synthesizing lipids, resulting in an enhanced lipid content. At nitrogen sufficient conditions cellular growth outpaces lipid production resulting in a reduced lipid content. At intermediate nitrogen deficient conditions, however, cell growth rate reaches a maximum without compromising the lipid content in the cells, resulting in an increased lipid productivity.

A characteristic behaviour of microalgal cells is their great capacity to uptake nitrogen, as well as other limiting nutrients, from the media and to store it intracellularly. Whenever there is a supply of nitrogen in the culture media, the nitrogen pool in the cells will surge. Changes in the cell physiology occur when the intracellular nitrogen concentration increases. Readily apparent physiological changes include change in pigmentation, excretion of red pigments, and increased foaming in the culture. It is expected that these physiological changes are accompanied with variations in the cell metabolism. If the nitrogen supply is limited and temporary then the changes the cells incurred will have to be reversed, generating a cost to the cells in terms of substrate utilization, affecting the yield and growth rate. A mathematical expression was proposed to account for the inhibitory effects that large surges in the intracellular nitrogen pool have on growth rate. This expression was incorporated in a first principles model to describe the nutrient uptake, growth, and oil production in microalgae. The proposed model was able to capture the macroscopic behaviour of algal cultures and was shown to have good prediction capabilities.

The maximum growth rate in microalgal cultures, measured during the exponential growth phase, remained relatively constant independently of whether the culture was performed in batch or fed-batch mode. There was however,

a significant difference between the average and the maximum growth rate. The final aim of the different optimization strategies is to lead the average growth rate to converge with the maximum growth rate. Batch cultures, therefore, provide a simple and reliable way of estimating the upper limit for the optimization target.

Fed-batch microalgal cultures were conducted in a single-stage mode and a two-stage mode. In the single stage case, glucose was used as the single carbon source supporting both growth and oil production. For the single stage culture, different optimization strategies were evaluated. The adaptive model based optimization shown a significantly better performance than the open loop strategy. It is expected that a full feedback model predictive control strategy will have the potential to further increase the productivity of the algal cultures.

To enable the use of feedback control, it is desirable to have a sensor for monitoring the nutrient concentration as well as the product concentration. It has been shown that Raman spectroscopy can provide a good estimate of glucose and biomass concentration as well as the neutral lipid content in the cells.

In the two-stage culture, algal cells were fed initially with glycerol and in the second phase glucose was added to the culture. The experiment conducted in a two-stage mode exhibited an increased yield in the conversion from sugar to oil compared to the single-stage culture. This was due to the use of glycerol in the first stage, which promoted cell growth but not lipid production. Furthermore, a faster production and accumulation of lipids was observed at the start of the second stage, indicating that glycerol conditioned the cells to a status in which glucose can quickly and efficiently be converted into lipids.

The fatty acid profile of the algal oil extracted from the cells cultured under the optimized conditions indicated that the algal is a suitable feedstock

for biodiesel production. Fast growth and increased lipid productivity were associated with an increased lipid quality.

The economic evaluation showed that the production cost for heterotrophic microalgal oil will range from \$0.86 to \$1.24 US\$/L, with the potential to lowering this cost by using cheaper carbon substrates or by applying credits to the oil whenever other by-products are commercialized.

9.2 Future research directions

Even though the idea of using microalgae for the production of biofuels dates back to the early 1950's, several political, scientific, and economic factors have hindered the realization of this idea. As such, the field of microalgal biotechnology is still in its infancy, and therefore there are plenty of opportunities for improvement. In the following paragraphs, a quick overview of several potential avenues of research, identified during the course of this thesis, are presented.

9.2.1 Adaptive optimization with Raman-enabled feedback control

The Raman-based sensor developed to monitor the biomass, glucose and oil concentration can be integrated into the optimization strategy, acting as an on-line measuring device. This arrangement will allow the implementation of different feedback control schemes.

To better study the effect carbon substrate concentration has on the overall lipid production and cell growth rates, a series of fed-batch experiments should be conducted at constant carbon substrate concentration. Feedback control using the Raman sensor will allow to run the reactor at a fixed substrate

concentration. The use of the Raman sensor, perhaps in combination with a windows moving average algorithm to reduce the noise in the estimated values, will potentially facilitate the discrimination among the different kinetic models for the production of oil.

9.2.2 Optimization of process conditions

In this thesis, the focus was restricted to identifying the effect that the concentration of the main nutrients has on the growth and production rate of microalgae. Several other process variables, however, were kept at fixed values taken from other references. Further research should explore the effect of temperature, pH, pO_2 , and osmotic pressure, and determine either the optimal fixed values or functional relationships of the growth and lipid production rate with respect to the aforementioned variables.

9.2.3 Controlling the fatty acid profile

Given the importance of the fatty acid profile in the quality of the biodiesel product, or any other application for the algal oil, the next logical step in the modelling of algal oil production is to incorporate in the model the effect the different process conditions have over the production and consumption of each individual fatty acid.

Lipid production can be modelled as the coupling of few series of reactions that generate all the fatty acids found in the cells: de-novo synthesis, elongation, and denaturation. A mechanistic model can be proposed starting with the current understanding of these reactions, and moving to close any gap that results between model prediction and experimental observations.

Experiments can be conducted in order to determine the fatty acid profile at

different culture times, or at varying concentrations of nutrients. These experimental measurements can be later used for model selection and calibration.

9.2.4 Population based modelling

Even though the model proposed in this thesis was successful at describing the important characteristics of the bulk dynamics of microalgal cultures, allowing a substantial increase in biomass and oil productivity, there are still several observations that remain unexplained. Batch to batch variability is a the defining characteristic of biological cultures. Cultures performed under seemingly identical conditions may produce totally different results. It is possible that this variability is due to differences in the cell distribution. In particular, cell populations with a multimodal distribution can be identical when compared using a bulk measurement, such as dry weight, total cell volume, or cell number, but have completely different behaviours due to differences in the cell distribution.

In the fed-batch cultures presented in this thesis, bimodal distributions were observed in the algal population, as shown in Fig. 9.1. In this case, a bimodal distribution emerged from a cell population with a single mode in their size distribution after the addition of glucose to the culture. This indicates that a fraction of the cells were in a more favourable status to initiate growth and oil accumulation.

As mentioned before, multimodality may help to explain some of the variability observed in cell cultures, and therefore a population based model has the potential to allow the construction of control tools to better reduce or eliminate such variations.

Future research should focus on determining the factors that induce the onset of bimodal/multimodal cell distribution from unimodal distributions in algal

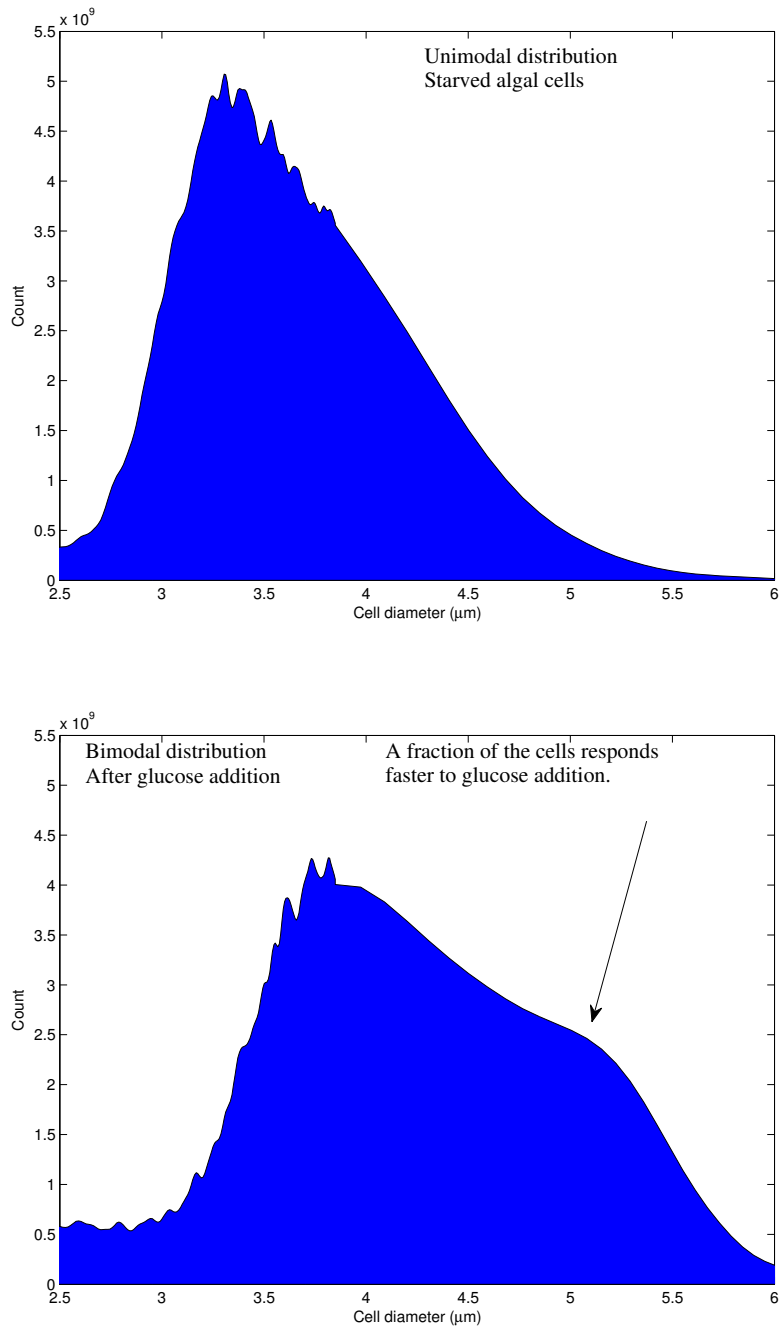


Figure 9.1: Size distribution of a microalgal population in a heterotrophic culture. 9.1(a) Unimodal distribution carbon and nitrogen starved cells. 9.1(b) A bimodal distribution appeared after the addition of glucose.

populations. It is also necessary to evaluate how the transitions between different cell cycle stages are regulated and what is the effect of growth promoters and inhibitors on microalgae at the different stages of the cell cycle. The final objective must be to propose a mathematical description capable of explaining the onset of multimodality observed in microalgal cultures.

9.2.5 Optimization of culture conditions for harvesting

As presented in Chapter 8, oil extraction from the microalgal biomass represents the second highest production cost after the feedstock cost. To increase the efficiency of the extraction process it is desirable to guarantee that all the cells that are subject to lipid extraction contains the maximum amount of lipids. In practice, however, there is a distribution in the cell population, as shown in Fig. 9.1. As such, some cells are very rich in oil, indeed lighter than water, while other cells are leaner in oil, and heavier than water.

It is be desirable to have a better understanding of the factors controlling when and how the cells become fat, and to design the process in such a way than only the fat-rich cells get skimmed while allowing the leaner cells to continue growing and accumulating oil.

For the purpose of skimming the fat-rich cells, air assisted flotation (i.e. Froth flotation) may prove to be useful. Due to the differences in cell size and cell density between fat and lean cells, it is expected that large lipid-rich cells will float faster than young lean cells.

References

- Aaronson, S., Dubinsky, Z., 1982. Mass production of microalgae. *Cell. Mol. Life Sci.* 38 (1), 36–40.
<http://dx.doi.org/10.1007/BF01944523>
- Abbas, A., Josefson, M., Abrahamsson, K., 2011. Characterization and mapping of carotenoids in the algae *Dunaliella* and *Phaeodactylum* using Raman and target orthogonal partial least squares. *Chemometrics Intellig. Lab. Syst.* 107 (1), 174–177.
<http://dx.doi.org/10.1016/j.chemolab.2011.03.004>
- Afseth, N. K., Segtnan, V. H., Wold, J. P., 2006. Raman spectra of biological samples: A study of preprocessing methods. *Appl. Spectrosc.* 60 (12), 1358–1367.
<http://www.opticsinfobase.org/abstract.cfm?URI=as-60-12-1358>
- Ahmad, I., Hellebust, J. A., 1990. Regulation of chloroplast development by nitrogen source and growth conditions in a *Chlorella protothecoides* strain. *Plant Physiol.* 94 (3), 944–949.
<http://www.jstor.org/stable/4273185>
- Alabi, A. O., Tampier, M., Bibeau, E., 2009. Microalgae technologies and processes for biofuels/bioenergy production in British Columbia. Tech. rep., The British Columbia Innovation Council.
http://www.bcic.ca/images/stories/publications/lifesciences/microalgae_report.pdf

-
- Andersen, R. A., 1992. Diversity of eukaryotic algae. *Biodivers. Conserv.* 1 (4), 267–292.
<http://dx.doi.org/10.1007/BF00693765>
- Antizar-Ladislao, B., Turrion-Gomez, J. L., 2008. Second-generation biofuels and local bioenergy systems. *Biofuels, Bioproducts and Biorefining* 2 (5), 455–469.
<http://dx.doi.org/10.1002/bbb.97>
- Arnold, S., Gaensakoo, R., Harvey, L., McNeil, B., 2002. Use of at-line and in-situ near-infrared spectroscopy to monitor biomass in an industrial fed-batch *Escherichia coli* process. *Biotechnol. Bioeng.* 80 (4), 405–413.
<http://dx.doi.org/10.1002/bit.10383>
- Arnon, D. I., 1938. Microelements in culture-solution experiments with higher plants. *Botanical Society of America* 25 (5), 322–325.
<http://www.jstor.org/stable/2436754>
- Audet, C., Dennis, J. E., 2006. Mesh adaptive direct search algorithms for constrained optimization. *SIAM J. Optim.* 17, 188–217.
<http://dx.doi.org/10.1137/040603371>
- Becker, T., Breithaupt, D., Doelle, H. W., Fiechter, A., Schlegel, G., Shimizu, S., Yamada, H., 2009. Biotechnology, 5. Monitoring and modeling of bioprocesses. In: *Ullmann's Encyclopedia of Industrial Chemistry*. Wiley-VCH Verlag GmbH & Co. KGaA.
http://dx.doi.org/10.1002/14356007.n04_n05
- Behrens, P. W., Kyle, D. J., 1996. Microalgae as a source of fatty acids. *Journal of Food Lipids* 3 (4), 259–272.
<http://dx.doi.org/10.1111/j.1745-4522.1996.tb00073.x>
- Bellgardt, K.-H., 2000. Bioprocess models. In: Schugerl, K., Bellgardt, K.-H. (Eds.), *Bioreaction Engineering: Modelling and Control*. Springer, Ch. 2, pp. 44–105.

- Benemann, J. R., Oswald, W., 1993. Systems and economic analysis of microalgae ponds for conversion of CO₂ to biomass. Tech. Rep. CONF-9409207-2, Department of Energy.
<http://dx.doi.org/10.2172/29423>
- Bessou, C., Ferchaud, F., Gabrielle, B., Mary, B., 2011. Biofuels, greenhouse gases and climate change. In: Lichtfouse, E., Hamelin, M., Navarrete, M., Debaeke, P. (Eds.), Sustainable Agriculture. Vol. 2. Springer Netherlands, pp. 365–468.
http://dx.doi.org/10.1007/978-94-007-0394-0_20
- Bhattacharya, D., Medlin, Linda, 1998. Algal phylogeny and the origin of land plants. *Plant Physiol.* 116 (1), 9–15.
<http://dx.doi.org/10.1104/pp.116.1.9>
- Blanco, M., Peinado, A., Mas, J., 2006. Monitoring alcoholic fermentation by joint use of soft and hard modelling methods. *Anal. Chim. Acta* 556 (2), 364–373.
<http://dx.doi.org/10.1016/j.aca.2005.09.066>
- Brennan, L., Owende, P., 2010. Biofuels from microalgae—a review of technologies for production, processing, and extractions of biofuels and co-products. *Renew. Sustainable Energy Rev.* 14 (2), 557–577.
<http://dx.doi.org/10.1016/j.rser.2009.10.009>
- Cannizzaro, C., Rhiel, M., Marison, I., von Stockar, U., 2003. On-line monitoring of *Phaffia rhodozyma* fed-batch process with in situ dispersive Raman spectroscopy. *Biotechnol. Bioeng.* 83 (6), 668–680.
<http://dx.doi.org/10.1002/bit.10698>
- Caperon, J., Meyer, J., 1972. Nitrogen-limited growth of marine phytoplankton—II. Uptake kinetics and their role in nutrient limited growth of phytoplankton. *Deep. Sea Res. Oceanogr. Abstr.* 19 (9), 619–632.
[http://dx.doi.org/10.1016/0011-7471\(72\)90090-3](http://dx.doi.org/10.1016/0011-7471(72)90090-3)

-
- Carlsson, A. S., van Beilen, J. B., Moller, R., Clayton, D., 2007. Micro- and Macro-Algae: Utility for Industrial Applications. CPL Press, Berks, UK.
<http://epobio.net/pdfs/0709AquaticReport.pdf>
- C.C.C., 2009. Annual report. Tech. rep., Canola Council of Canada, 400-167 Lombard Ave., Winnipeg, MB.
- Chaudhuri, T. K., Spencer, R. P., 1968. Amino acid uptake in *Acetabularia*. *Protoplasma* 66 (1), 255–259.
<http://dx.doi.org/10.1007/BF01252536>
- Chen, F., Johns, M., 1991. Effect of C/N ratio and aeration on the fatty acid composition of heterotrophic *Chlorella sorokiniana*. *J. Appl. Phycol.* 3 (3), 203–209.
<http://dx.doi.org/10.1007/BF00003578>
- Chen, W., Zhang, C., Song, L., Sommerfeld, M., Hu, Q., 2009. A high throughput Nile Red method for quantitative measurement of neutral lipids in microalgae. *J. Microbiol. Methods* 77 (1), 41–47.
<http://dx.doi.org/10.1016/j.mimet.2009.01.001>
- Cheng, Y., Lu, Y., Gao, C., Wu, Q., 2009. Alga-based biodiesel production and optimization using sugar cane as the feedstock. *Energy Fuels* 23 (8), 4166–4173.
<http://dx.doi.org/10.1021/ef9003818>
- Chi, Z., Liu, Y., Frear, C., Chen, S., 2009. Study of a two-stage growth of DHA-producing marine algae *Schizochytrium limacinum* SR21 with shifting dissolved oxygen level. *Appl. Microbiol. Biotechnol.* 81 (6), 1141–1148.
<http://dx.doi.org/10.1007/s00253-008-1740-7>
- Chisti, Y., 2007. Biodiesel from microalgae. *Biotechnol. Adv.* 25, 294–306.
<http://dx.doi.org/10.1016/j.biotechadv.2007.02.001>
- Cho, B.-H., Komor, E., 1985. The amino acid transport systems of the autotrophically grown green alga *Chlorella*. *Biochim. Biophys. Acta*,

- Biomembr. 821 (3), 384–392.
[http://dx.doi.org/10.1016/0005-2736\(85\)90042-2](http://dx.doi.org/10.1016/0005-2736(85)90042-2)
- Clementsich, F., Bayer, K., 2006. Improvement of bioprocess monitoring: development of novel concepts. *Microbial Cell Factories* 5 (19).
<http://dx.doi.org/10.1186/1475-2859-5-19>
- Cooper, M. S., Hardin, W. R., Petersen, T. W., Cattolico, R. A., 2010. Visualizing “green oil” in live algal cells. *J. Biosci. Bioeng.* 109 (2), 198–201.
<http://dx.doi.org/10.1016/j.jbiosc.2009.08.004>
- Davidson, K., Cunningham, A., 1996. Accounting for nutrient processing time in mathematical models of phytoplankton growth. *Limnol. Oceanogr.* 41 (4), 779–783.
<http://www.jstor.org/stable/2838735>
- Demirbas, M. F., 2011. Biofuels from algae for sustainable development. *Applied Energy* 88 (10), 3473–3480.
<http://dx.doi.org/10.1016/j.apenergy.2011.01.059>
- Dortch, Q., Clayton, J. R., Thoresen, S. S., Ahmed, S. I., 1984. Species differences in accumulation of nitrogen pools in phytoplankton. *Mar. Biol.* 81 (3), 237–250.
<http://dx.doi.org/10.1007/BF00393218>
- Doucha, J., Lívanský, K., 2011. Production of high-density *Chlorella* culture grown in fermenters. *J. Appl. Phycol.*, 1–910.1007/s10811-010-9643-2.
<http://dx.doi.org/10.1007/s10811-010-9643-2>
- Droop, M. R., 1968. Vitamin B12 and marine ecology. iv. the kinetics of uptake, growth and inhibition in *Monochrysis Lutheri*. *J. Mar. Biol. Assoc. U.K.* 48 (03), 689–733.
<http://dx.doi.org/10.1017/S0025315400019238>

-
- Droop, M. R., 1973. Some thoughts on nutrient limitation in algae. *J. Phycol.* 9, 264–272.
<http://dx.doi.org/10.1111/j.1529-8817.1973.tb04092.x>
- Elbahloul, Y., Steinbuchel, A., 2010. Pilot-scale production of fatty acid ethyl esters by an engineered *Escherichia coli* strain harboring the p(microdiesel) plasmid. *Appl. Environ. Microbiol.* 76 (13), 4560–4565.
<http://aem.asm.org/cgi/content/abstract/76/13/4560>
- Elsley, D., Jameson, D., Raleigh, B., Cooney, M. J., 2007. Fluorescent measurement of microalgal neutral lipids. *J. Microbiol. Methods* 68 (3), 639–642.
<http://dx.doi.org/10.1016/j.mimet.2006.11.008>
- FAO, 2002. Food energy – methods of analysis and conversion factors. FAO Food and Nutrition Paper 77, Food and Agriculture Organization of the United Nations.
<ftp://ftp.fao.org/docrep/fao/006/y5022e/y5022e00.pdf>
- FDA, 2004. Guidance for industry PAT - a framework for innovative pharmaceutical development, manufacturing, and quality assurance. Tech. rep., Center of Drug Evaluation and Research, Food and Drug Administration. <http://www.fda.gov/downloads/Drugs/GuidanceComplianceRegulatoryInformation/Guidances/ucm070305.pdf>
- Flynn, K. J., 2001. A mechanistic model for describing dynamic multi-nutrient, light, temperature interactions in phytoplankton. *J. Plankton Res.* 23 (9), 977–997.
<http://dx.doi.org/10.1093/plankt/23.9.977>
- Flynn, K. J., 2003. Modelling multi-nutrient interactions in phytoplankton; balancing simplicity and realism. *Prog. Oceanogr.* 56, 249–279.
[http://dx.doi.org/10.1016/S0079-6611\(03\)00006-5](http://dx.doi.org/10.1016/S0079-6611(03)00006-5)

- Fowler, S. D., Brown, W. J., Warfel, J., Greenspan, P., 1987. Use of Nile Red for the rapid in situ quantitation of lipids on thin-layer chromatograms. *J. Lipid Res.* 28 (10), 1225–1232.
<http://www.jlcr.org/content/28/10/1225.abstract>
- Friedman, M., 2004. Applications of the Ninhydrin reaction for analysis of amino acids, peptides, and proteins to agricultural and biomedical sciences. *J. Agric. Food Chem.* 52 (3), 385–406.
<http://dx.doi.org/10.1021/jf030490p>
- Ganuza, E., Izquierdo, M., 2007. Lipid accumulation in *Schizochytrium* G13/2S produced in continuous culture. *Appl. Microbiol. Biotechnol.* 76, 985–990.
<http://dx.doi.org/10.1007/s00253-007-1019-4>
- Gerpen, J. V., Shanks, B., Pruszko, R., Clements, D., Knothe, G., 2004. Biodiesel production technology. Subcontractor Report NREL/SR-510-36244, National Renewable Energy Laboratory, 1617 Cole Boulevard, Golden, Colorado.
<http://dx.doi.org/10.2172/15008801>
- Giles, J., Gilmore, D., Denton, M., 1999. Quantitative analysis using Raman spectroscopy without spectral standardization. *Journal of Raman Spectroscopy* 30, 767–771.
[http://dx.doi.org/10.1002/\(SICI\)1097-4555\(199909\)30:9<767::AID-JRS447>3.0.CO;2-J](http://dx.doi.org/10.1002/(SICI)1097-4555(199909)30:9<767::AID-JRS447>3.0.CO;2-J)
- Gocze, P. M., Freeman, D. A., 1994. Factors underlying the variability of lipid droplet fluorescence in MA-10 leydig tumor cells. *Cytometry* 17 (2), 151–158.
<http://dx.doi.org/10.1002/cyto.990170207>
- Gomy, C., Jouan, M., Dao, N., 1988. Methode d'analyse quantitative par spectrometrie Raman-laser associee aux fibres optiques pour le suivi d'une fermentation alcoolique. *Anal. Chim. Acta* 215, 211–221.
[http://dx.doi.org/10.1016/S0003-2670\(00\)85279-4](http://dx.doi.org/10.1016/S0003-2670(00)85279-4)

-
- Goodacre, R., 2003. Explanatory analysis of spectroscopic data using machine learning of simple, interpretable rules. *Vibrational Spectroscopy* 32 (1), 33–45.
[http://dx.doi.org/10.1016/S0924-2031\(03\)00045-6](http://dx.doi.org/10.1016/S0924-2031(03)00045-6)
- Greenspan, P., Fowler, S. D., 1985. Spectrofluorometric studies of the lipid probe, Nile Red. *J. Lipid Res.* 26 (7), 781–789.
<http://www.jlrr.org/content/26/7/781.abstract>
- Griffiths, M., Harrison, S., 2009. Lipid productivity as a key characteristic for choosing algal species for biodiesel production. *J. Appl. Phycol.* 21 (5), 493–507.
<http://dx.doi.org/10.1007/s10811-008-9392-7>
- Gui, M. M., Lee, K. T., Bhatia, S., 2008. Feasibility of edible oil vs. non-edible oil vs. waste edible oil as biodiesel feedstock. *Energy* 33 (11), 1646–1653.
<http://dx.doi.org/10.1016/j.energy.2008.06.002>
- Guiry, M., Guiry, G., 2005. Algaebase. world-wide electronic publication, National University of Ireland, Galway.
<http://www.algaebase.org>
- Gurden, S., Westerhuis, J., Smilde, A., 2002. Monitoring of batch processes using spectroscopy. *AIChE Journal* 48 (10), 2283–2297.
<http://dx.doi.org/10.1002/aic.690481018>
- Hebner, R., 2010. Electromechanical algae oil extraction, electronic presentation. Center for Electromechanics, University of Texas.
<http://www.cleantx.org/archives/archives/November/AlgaeOilExtractionCleanTXHebner.ppt>
- Hein, M., Pedersen, M. F., Sand-Jensen, K., 1995. Size-dependent nitrogen uptake in micro- and macroalgae. *Mar. Ecol. Prog. Ser.* 118, 247–253.
<http://www.int-res.com/articles/meps/118/m118p247.pdf>
- Hiruta, O., Yamamura, K., Takebe, H., Futamura, T., Inuma, K., Tanaka, H., 1997. Application of maxblend fermentor for microbial processes. *J. Ferment.*

- Bioeng. 83 (1), 79 – 86.
[http://dx.doi.org/10.1016/S0922-338X\(97\)87331-X](http://dx.doi.org/10.1016/S0922-338X(97)87331-X)
- Hsieh, C.-H., Wu, W.-T., 2009. Cultivation of microalgae for oil production with a cultivation strategy of urea limitation. *Bioresour. Technol.* 100 (17), 3921–3926.
<http://dx.doi.org/10.1016/j.biortech.2009.03.019>
- Hu, Q., Sommerfeld, M., Jarbis, E., Ghirardi, M., Posewitz, M., Seibert, M., Darzins, A., 2008. Microalgal triacylglycerols as feedstocks for biofuel production: perspectives and advances. *Plant J.* 54 (4), 621–639.
<http://dx.doi.org/10.1111/j.1365-313X.2008.03492.x>
- Huang, G.-H., Chen, G., Chen, F., 2009. Rapid screening method for lipid production in alga based on Nile red fluorescence. *Biomass Bioenergy* 33 (10), 1386–1392.
<http://dx.doi.org/10.1016/j.biombioe.2009.05.022>
- Huang, Y., Beal, C., Cai, W., Ruoff, R., Terentjev, E., 2010. Micro-Raman spectroscopy of algae: Composition analysis and fluorescence background behavior. *Biotechnol. Bioeng.* 105 (5), 889–898.
<http://dx.doi.org/10.1002/bit.22617>
- Huppe, H., Turpin, D., 1994. Integration of carbon and nitrogen metabolism in plant and algal cells. *Annu. Rev. Plant Physiol. Plant Mol. Biol.* 45, 577–607.
<http://dx.doi.org/10.1146/annurev.pp.45.060194.003045>
- Inokuchia, R., Kumab, K.-I., Miyatab, T., Okada, M., 2002. Nitrogen-assimilating enzymes in land plants and algae: phylogenetic and physiological perspectives. *Physiol. Plant.* 116, 1–11.
<http://dx.doi.org/10.1034/j.1399-3054.2002.1160101.x>
- Jannasch, H. W., Egli, T., 1993. Microbial growth kinetics: a historical perspective. *Antonie Van Leeuwenhoek* 63, 213–224.
<http://dx.doi.org/10.1007/BF00871219>

-
- Jarvis, R., Goodacre, R., 2005. Genetic algorithm optimization for pre-processing and variable selection of spectroscopic data. *Bioinformatics* 21 (7), 860–868.
<http://dx.doi.org/10.1093/bioinformatics/bti102>
- Junker, B., Wang, H., 2006. Bioprocess monitoring and computer control: Key roots of the current PAT initiative. *Biotechnol. Bioeng.* 95 (2), 226–261.
<http://dx.doi.org/10.1002/bit.21087>
- Kinast, J., March 2003. Production of biodiesels from multiple feedstocks and properties of biodiesels and biodiesel/diesel blends. Subcontractor Report NREL/SR-510-31460, National Renewable Energy Laboratory, 1617 Cole Boulevard, Golden, Colorado.
<http://dx.doi.org/10.2172/15003582>
- Kosa, M., Ragauskas, A. J., 2011. Lipids from heterotrophic microbes: advances in metabolism research. *Trends Biotechnol.* 29 (2), 53–61.
<http://dx.doi.org/10.1016/j.tibtech.2010.11.002>
- Kurosawa, K., Boccazzi, P., de Almeida, N. M., Sinskey, A. J., 2010. High-cell-density batch fermentation of *Rhodococcus opacus* PD630 using a high glucose concentration for triacylglycerol production. *J. Biotechnol.* 147 (3–4), 212–218.
<http://dx.doi.org/10.1016/j.jbiotec.2010.04.003>
- Leadbeater, B. S. C., 2006. The 'Droop Equation' – Michael Droop and the legacy of the 'Cell-Quota Model' of phytoplankton growth. *Protist* 157 (3), 345–358.
<http://dx.doi.org/10.1016/j.protis.2006.05.009>
- Lee, H., Boccazzi, P., Gorret, N., Rama, R., Sinskey, A., 2004. In situ bioprocess monitoring of *Escherichia coli* bioreactions using Raman spectroscopy. *Vibrational Spectroscopy* 35, 131–137.
<http://dx.doi.org/10.1016/j.vibspec.2003.12.015>

- Lee, S., Yoon, B.-D., Oh, H.-M., 1998. Rapid method for the determination of lipid from the green alga *Botryococcus braunii*. *Biotechnol. Tech.* 12 (7), 553–556.
<http://dx.doi.org/10.1023/A:1008811716448>
- Lehman, J. T., Botkin, D. B., Likens, G. E., 1975. The assumptions and rationales of a computer model of phytoplankton population dynamics. *Limnol. Oceanogr.* 20 (3), 343–378.
<http://www.jstor.org/stable/2835195>
- Lewis, L. A., McCourt, R. M., 2004. Green algae and the origin of land plants. *Am. J. Bot.* 91 (10), 1535–1556.
<http://dx.doi.org/10.3732/ajb.91.10.1535>
- Li, X., Xu, H., Wu, Q., 2007a. Large-scale biodiesel production from microalga *Chlorella protothecoides* through heterotrophic cultivation in bioreactors. *Biotechnol. Bioeng.* 98 (4), 764–771.
<http://dx.doi.org/10.1002/bit.21489>
- Li, Y., Horsman, M., Wang, B., Wu, N., Lan, C., 2008. Effects of nitrogen sources on cell growth and lipid accumulation of green alga *Neochloris oleoabundans*. *Appl. Microbiol. Biotechnol.* 81 (4), 629–636.
<http://dx.doi.org/10.1007/s00253-008-1681-1>
- Li, Y., Zhao, Z. K., Bai, F., 2007b. High-density cultivation of oleaginous yeast *Rhodospiridium toruloides* y4 in fed-batch culture. *Enzyme Microb. Technol.* 41 (3), 312–317.
<http://dx.doi.org/10.1016/j.enzmictec.2007.02.008>
- Liang, Y., Sarkany, N., Cui, Y., 2009. Biomass and lipid productivities of *Chlorella vulgaris* under autotrophic, heterotrophic and mixotrophic growth conditions. *Biotechnol. Lett.* 31 (7), 1043–1049.
<http://dx.doi.org/10.1007/s10529-009-9975-7>
- Liu, J., Huang, J., Sun, Z., Zhong, Y., Jiang, Y., Chen, F., 2011. Differential lipid and fatty acid profiles of photoautotrophic and heterotrophic *Chlorella*

-
- zofingiensis*: Assessment of algal oils for biodiesel production. *Bioresour. Technol.* 102 (1), 106–110.
<http://dx.doi.org/10.1016/j.biortech.2010.06.017>
- Ma, F., Hanna, M. A., 1999. Biodiesel production: a review. *Bioresour. Technol.* 70 (1), 1–15.
[http://dx.doi.org/10.1016/S0960-8524\(99\)00025-5](http://dx.doi.org/10.1016/S0960-8524(99)00025-5)
- Macaloney, G., Draper, I., Preston, J., Anderson, K., Rollins, M., Thompson, B., Hall, J., McNeil, B., 1996. At-line control and fault analysis in an industrial high cell density *Escherichia coli* fermentation, using NIR spectroscopy. *Transactions of the Institution of Chemical Engineers* 74 (C), 212–220.
<http://dx.doi.org/10.1205/096030896531217>
- Mandalam, R. K., Palsson, B., 1998. Elemental balancing of biomass and medium composition enhances growth capacity in high-density *Chlorella vulgaris* cultures. *Biotechnol. Bioeng.* 59 (5), 605–611.
[http://dx.doi.org/10.1002/\(SICI\)1097-0290\(19980905\)59:5<605::AID-BIT11>3.0.CO;2-8](http://dx.doi.org/10.1002/(SICI)1097-0290(19980905)59:5<605::AID-BIT11>3.0.CO;2-8)
- Mandenius, C.-F., 2004. Recent developments in the monitoring, modeling and control of biological production systems. *Bioprocess Biosystems Eng.* 26, 347–351.
<http://dx.doi.org/10.1007/s00449-004-0383-z>
- Marsili-Libelli, S., Guerrizio, S., Checchi, N., 2003. Confidence regions of estimated parameters for ecological systems. *Ecol. Model.* 165 (2-3), 127–146.
[http://dx.doi.org/10.1016/S0304-3800\(03\)00068-1](http://dx.doi.org/10.1016/S0304-3800(03)00068-1)
- Masarovicova, E., Kralova, K., Pesko, M., 2009. Energetic plants - cost and benefit. *Ecological Chemistry and Engineering S - Chemia I Inzynieria Ekologiczna S* 16 (3), 263–276.
[http://tchie.uni.opole.pl/freeECE/S_16_3/Masarovicova_16\(3\).pdf](http://tchie.uni.opole.pl/freeECE/S_16_3/Masarovicova_16(3).pdf)

- McCormick, R., Williams, A., Ireland, J., Brimhall, M., Hayes, R., 2006. Effects of biodiesel blends on vehicle emissions. Milestone Report 540-40554, National Renewable Energy Laboratory.
<http://dx.doi.org/10.2172/894987>
- McGovern, A., Broadhurst, D., Taylor, J., Kaderbhai, N., Winson, M., Small, D., Rowland, J., Kell, D., Goodacre, R., 2002. Monitoring of complex industrial bioprocesses for metabolite concentrations using modern spectroscopies and machine learning: Application to gibberellic acid production. *Biotechnol. Bioeng.* 78 (5), 527–538.
<http://dx.doi.org/10.1002/bit.10226>
- Meyer, H., 1957. The ninhydrin reaction and its analytical applications. *Biochem. J.* 67 (2), 333–340.
<http://www.biochemj.org/bj/067/bj0670333.htm>
- Miao, X., Wu, Q., 2006. Biodiesel production from heterotrophic microalgal oil. *Bioresour. Technol.* 97 (6), 841–846.
<http://dx.doi.org/10.1016/j.biortech.2005.04.008>
- Miao, X., Wu, Q., Yang, C., 2004. Fast pyrolysis of microalgae to produce renewable fuels. *Journal of Analytical and Applied Pyrolysis* 71, 855–863.
<http://dx.doi.org/10.1016/j.jaap.2003.11.004>
- Miyoshi, Y., 1972. Mechanical properties of *Chlorella* cell walls as determined by the suspension method. *J. Plant Res.* 85 (1), 59–70.
<http://dx.doi.org/10.1007/BF02489201>
- Naik, S. N., Goud, V. V., Rout, P. K., Dalai, A. K., 2010. Production of first and second generation biofuels: A comprehensive review. *Renew. Sustainable Energy Rev.* 14 (2), 578–597.
<http://dx.doi.org/10.1016/j.rser.2009.10.003>
- Naumann, D., Helm, D., Labischinski, H., 1991. Microbiological characterizations by FT-IR spectroscopy. *Nature* 351, 81–82.
<http://dx.doi.org/10.1038/351081a0>

-
- Ning, Y.-C., 2005. Structural Identification of Organic Compounds with Spectroscopic Techniques. Wiley-VCH Verlag GmbH & Co. KGaA.
- N.S.A., 2010. U.S. Sunflower crop quality report. Tech. rep., National Sunflower Association, 2401 46th Ave. S.E. Ste. 206, Mandan, ND.
- Olaizola, M., 2003. Commercial development of microalgal biotechnology: from the test tube to the marketplace. *Biomol. Eng.* 20 (4-6), 459–466.
[http://dx.doi.org/10.1016/S1389-0344\(03\)00076-5](http://dx.doi.org/10.1016/S1389-0344(03)00076-5)
- Pernet, F., Tremblay, R., 2003. Effect of ultrasonication and grinding on the determination of lipid class content of microalgae harvested on filters. *Lipids* 38 (11), 1191–1195.
<http://dx.doi.org/10.1007/s11745-003-1178-6>
- Piedras, P., Aguilar, M., Pineda, M., 1998. Uptake and metabolism of allantoin and allantoate by cells of *Chlamydomonas reinhardtii* (Chlorophyceae). *Eur. J. Phycol.* 33 (1), 57–64.
http://journals.cambridge.org/article_S0967026298001528
- Piorreck, M., Baasch, K.-H., Pohl, P., 1984. Biomass production, total protein, chlorophylls, lipids and fatty acids of freshwater green and blue-green algae under different nitrogen regimes. *Phytochemistry* 23 (2), 207–216.
[http://dx.doi.org/10.1016/S0031-9422\(00\)80304-0](http://dx.doi.org/10.1016/S0031-9422(00)80304-0)
- Pulz, O., Gross, W., 2004. Valuable products from biotechnology of microalgae. *Appl. Microbiol. Biotechnol.* 65 (6), 635–648.
<http://dx.doi.org/10.1007/s00253-004-1647-x>
- Ramos, M. J., Fernández, C. M., Casas, A., Rodríguez, L., Pérez, A., 2009. Influence of fatty acid composition of raw materials on biodiesel properties. *Bioresour. Technol.* 100 (1), 261 – 268.
<http://dx.doi.org/10.1016/j.biortech.2008.06.039>
- Ricketts, T. R., 1988. Homeostasis in nitrogenous uptake/assimilation by the green alga *Platymonas (Tetraselmis) striata* (Prasinophyceae). *Ann. Bot.*

- 61 (4), 451–458.
<http://aob.oxfordjournals.org/content/61/4/451>
- Rodolfi, L., Zittelli, G. C., Bassi, N., Padovani, G., Biondi, N., Bonini, G., Tredici, M. R., 2009. Microalgae for oil: Strain selection, induction of lipid synthesis and outdoor mass cultivation in a low-cost photobioreactor. *Biotechnol. Bioeng.* 102 (1), 100–112.
<http://dx.doi.org/10.1002/bit.22033>
- Schlesinger, A., Eisenstadt, D., Einbinder, S., Gressel, J., 2011. Method and system for efficient harvesting of microalgae and cyanobacteria. United States Patent Application. US 2011/0081706 A1.
- Shaw, A., Kaderbhai, N., Jones, A., Woodward, A., Goodacre, R., Rowlan, J., Kell, D., 1999. Noninvasive, on-line monitoring of the biotransformation by yeast of glucose to ethanol using dispersive Raman spectroscopy and chemometrics. *Appl. Spectrosc.* 53 (11), 1419–1428.
<http://www.opticsinfobase.org/abstract.cfm?URI=as-53-11-1419>
- Shaw, A., Winson, M., Woodward, A., McGovern, A., Davey, H., Kaderbhai, N., Broadhurst, D., Gilbert, R., Taylor, J., Timmins, É., Goodacre, R., Kell, D., 2000. Rapid analysis of high-dimensional bioprocesses using multivariate spectroscopies and advanced chemometrics. *Advances in Biochemical Engineering/Biotechnology* 66, 83–113.
http://dx.doi.org/10.1007/3-540-48773-5_3
- Sheehan, J., Dunahay, T., Benemann, J., Roessler, P., 1998. A look back at the U.S. department of energy's aquatic species program - biodiesel from algae. Close-Out Report NREL/TP-580-24190, National Renewable Energy Laboratory, 1617 Cole Boulevard Golden, Colorado 80401-3393.
<http://dx.doi.org/10.2172/15003040>
- Shi, X.-M., Zhang, X.-W., Chen, F., 2000. Heterotrophic production of biomass and lutein by *Chlorella protothecoides* on various nitrogen sources. *Enzyme Microb. Technol.* 27 (3-5), 312–318.
[http://dx.doi.org/10.1016/S0141-0229\(00\)00208-8](http://dx.doi.org/10.1016/S0141-0229(00)00208-8)

-
- Shihira-Ishikawa, I., Hase, E., 1964. Nutritional control of cell pigmentation in *Chlorella protothecoides* with special reference to the degeneration of chloroplast induced by glucose. *Plant Cell Physiol.* 5, 227–240.
<http://pcp.oxfordjournals.org/content/5/2/227>
- Shope, T., Vickers, T., Mann, C., 1987. The direct analysis of fermentation products by Raman spectroscopy. *Appl. Spectrosc.* 41 (5), 908–912.
<http://www.opticsinfobase.org/abstract.cfm?URI=as-41-5-908>
- Singh, J., Gu, S., 2010. Commercialization potential of microalgae for biofuels production. *Renew. Sustainable Energy Rev.* 14 (9), 2596–2610.
<http://dx.doi.org/10.1016/j.rser.2010.06.014>
- Sivakesava, S., Irudayaraj, J., Demirci, A., 2001. Monitoring a bioprocess for ethanol production using FT-MIR and FT-Raman spectroscopy. *Journal of Industrial Microbiology and Biotechnology* 26 (4), 185–190.
<http://dx.doi.org/10.1038/sj.jim.7000124>
- Sommer, U., 1991. A comparison of the Droop and the Monod models of nutrient limited growth applied to natural populations of phytoplankton. *Funct. Ecol.* 5 (4), 535–544.
<http://www.jstor.org/stable/2389636>
- Sørensen, G., Sørensen, K. B., Hansen, H. O., Nygaard, S. D., 2011. Fuel for the future: Development of new fuels, e.g. biofuels. In: Whitby, C., Skovhus, T. L. (Eds.), *Applied Microbiology and Molecular Biology in Oilfield Systems*. Springer Netherlands, pp. 219–228.
http://dx.doi.org/10.1007/978-90-481-9252-6_26
- Spolaore, P., Joannis-Cassan, C., Duran, E., Isambert, A., 2006. Commercial applications of microalgae. *J. Biosci. Bioeng.* 101 (2), 87–96.
<http://dx.doi.org/10.1263/jbb.101.87>
- Sumathi, S., Chai, S. P., Mohamed, A. R., 2008. Utilization of oil palm as a source of renewable energy in malaysia. *Renew. Sustainable Energy Rev.*

- 12 (9), 2404–2421.
<http://dx.doi.org/10.1016/j.rser.2007.06.006>
- Surisetty, K., Hoz Siegler, H. D. I., McCaffrey, W. C., Ben-Zvi, A., 2010. Robust modeling of a microalgal heterotrophic fed-batch bioreactor. *Chem. Eng. Sci.* 65 (19), 5402–5410.
<http://dx.doi.org/10.1016/j.ces.2010.06.008>
- Tett, P., Droop, M., 1988. Cell quota models and planktonic primary production. In: Wimpenny, J. W. (Ed.), *Handbook of Laboratory Model Systems for Microbial Ecosystems*. Vol. II. CRC Press, Boca Raton, FL, US, Ch. 7, pp. 177–223.
- Tyler, A. C., McGlathery, K. J., Macko, S. A., 2005. Uptake of urea and amino acids by the macroalgae *Ulva lactuca* (Chlorophyta) and *Gracilaria vermiculophylla* (Rhodophyta). *Mar. Ecol. Prog. Ser.* 294, 161–172.
<http://www.int-res.com/articles/meps2005/294/m294p161.pdf>
- USDA, 2011. Economics, statistics, and market information system. Tech. rep., United States Department of Agriculture.
- USEPA, 2002. A comprehensive analysis of biodiesel impacts on exhaust emissions. Draft Technical Report EPA420-P-02-001, United States Environmental Protection Agency.
- Vaidyanathan, S., Macaloney, G., Vaughan, J., McNeil, B., Harvey, L. M., 1999. Monitoring of submerged bioprocesses. *Crit. Rev. Biotechnol.* 19 (4), 277–316.
<http://dx.doi.org/10.1080/0738-859991229161>
- Weldy, C. S., Huesemann, M., 2007. Lipid production by *Dunaliella salina* in batch culture: effects of nitrogen limitation and light intensity. *USDOE J. Undergrad. Res.* 7 (1), 115–122.
- Wen, Z. Y., Chen, F., 2001. A perfusion–cell bleeding culture strategy for enhancing the productivity of eicosapentaenoic acid by *Nitzschia laevis*.

-
- Appl. Microbiol. Biotechnol. 57 (3), 316–322.
<http://dx.doi.org/10.1007/s002530100786>
- Wen, Z.-Y., Chen, F., 2003. Heterotrophic production of eicosapentaenoic acid by microalgae. Biotechnol. Adv. 21 (4), 273–294.
[http://dx.doi.org/10.1016/S0734-9750\(03\)00051-X](http://dx.doi.org/10.1016/S0734-9750(03)00051-X)
- Wu, H., Volponi, J. V., Singh, S., 2010. Single-cell diesel mining on microalgae: Direct and quantitative monitoring of microalgal oil production in vivo by Raman spectroscopy. Biophys. J. 98 (3, Supplement 1), 744a–744a.
<http://dx.doi.org/10.1016/j.bpj.2009.12.4080>
- Wu, Z.-Y., Shi, C.-L., Shi, X.-M., 2007. Modeling of lutein production by heterotrophic *Chlorella* in batch and fed-batch cultures. World Journal of Microbiology and Biotechnology 23 (9), 1233–1238.
<http://dx.doi.org/10.1007/s11274-007-9354-2>
- Xiong, W., Li, X., Xiang, J., Wu, Q., 2008. High-density fermentation of microalga *Chlorella protothecoides* in bioreactor for microbio-diesel production. Appl. Microbiol. Biotechnol. 78 (1), 29–36.
<http://dx.doi.org/10.1007/s00253-007-1285-1>
- Xiong, W., Liu, L., Wu, C., Yang, C., Wu, Q., 2010. ¹³C-Tracer and gas chromatography-mass spectrometry analyses reveal metabolic flux distribution in the oleaginous microalga *Chlorella protothecoides*. Plant Physiol. 154 (2), 1001–1011.
<http://dx.doi.org/10.1104/pp.110.158956>
- Xu, H., Miao, X., Wu, Q., 2006. High quality biodiesel production from a microalga *Chlorella protothecoides* by heterotrophic growth in fermenters. J. Biotechnol. 126 (4), 499–507.
<http://dx.doi.org/10.1016/j.jbiotec.2006.05.002>
- Xu, Y., Ford, J., Mann, C., Vickers, T., 1997. Raman measurement of glucose in bioreactors materials. SPIE 2976, 10–19.
<http://dx.doi.org/10.1117/12.275527>

- Zhang, J., Fang, X., Zhu, X.-L., Li, Y., Xu, H.-P., Zhao, B.-F., Chen, L., Zhang, X.-D., 2011. Microbial lipid production by the oleaginous yeast *Cryptococcus curvatus* O3 grown in fed-batch culture. *Biomass Bioenergy* 35 (5), 1906–1911.
<http://dx.doi.org/10.1016/j.biombioe.2011.01.024>

This page intentionally left blank



Experimental Protocols

A.1 Fluorometric Quantification of Neutral Lipids

Materials

1. Fluorescence multi-well plate reader (Fluoroskan)
2. Multi-well plate with round bottom (COSTAR 96, black)
3. Nile red staining solution, 10 $\mu\text{g}/\text{mL}$ in ethanol (Alcohol Reagent grade)
4. 30% v/v ethanol aqueous solution (Alcohol Reagent grade)
5. Micro-pipettes: 2 – 20 μL and 20 – 200 μL
6. Volumetric flasks (10 mL)
7. Analytical balance with a precision at ± 0.1 mg

Preparation of the Nile red solution

1. Weight 10 mg of Nile red in a weighing tray.
2. Transfer the Nile red to a 10 mL volumetric flask. If necessary, wash the weighing tray with ethanol and transfer the ethanol to the volumetric flask.
3. Complete the volume of the volumetric flask up to the indicate level line (10 mL) using ethanol (Alcohol Reagent grade).
4. Label this solution as *Solution A (1000 $\mu\text{g/mL}$)*.
5. With a micro-pipette take a 100 μL aliquote of *Solution A* and transfer it to a 10 mL volumetric flask.
6. Using ethanol (Alcohol Reagent grade) complete the volume to 10 mL.
7. Label this solution as *Nile Red - Working Solution (10 $\mu\text{g/mL}$)*.
8. Store both solutions (Solution A and the Working Solution) at 4 °C, protected from the light in an amber container or covered with foil paper.

Preparation of the ethanol aqueous solution

1. In a clean glass container, add 30 mL of ethanol (Alcohol Reagent grade).
2. Add 70 mL of reversed osmosis water (MilliQ).
3. Label container as *30% v/v Ethanol - Working Solution*.
4. Store solution at 4 °C.

Sample preparation

For each sample, it is necessary to perform enough replicates in order to get a statistically significant estimation of the sample mean, and variance. A minimum of three replicates must be run, though five (5) is the recommended number of replicates.

1. Prepare the algae sample at a concentration of 5 g/L.
2. Add 10 μL of algal sample to a well.
3. Add 10 μL of the *Nile Red - Working Solution*.
4. Add 80 μL of the *30% v/v Ethanol - Working Solution*.

Standard preparation

For proper interpretation of the fluorometric results it is recommended that for each plate that is run, a two-point calibration be performed. The standards should correspond to algal samples of known lipid content, and should undergo the same processing as the samples to measure. It is desirable that the selected standards have a concentration range that cover the expected lipid content of the samples under analysis.

1. Prepare the algae standards at a concentration of 5 g/L
2. Add 10 μL of algal sample to a well
3. Add 10 μL of Nile red solution
4. Add 80 μL of the 30% v/v ethanol solution

Fluorescence measurement

1. Start-up the fluorescence (Fluoroskan) reader

2. Introduce plate

3. Select Algae cycle:
 - a. Shake at 1200 rpm, orbit 3 mm, for 30 s

 - b. Incubate at 40°C for 10 min

 - c. Shake at 1200 rpm, orbit 3 mm, for 30 s

 - d. Record fluorescence, Excitation at 530 nm, Emission at 604 nm

4. Convert fluorescent measurement to oil percentage using the results from the internal standards.

A.2 Gravimetric Quantification of Neutral Lipids

Materials

1. Ceramic mortar and pestle.
2. Small centrifugation glass tubes (10 – 15 mL) with screw Teflon-lined caps.
3. Small (4mL) tubes, pre-weighed with cap-on.
4. Pasteur glass pipettes
5. Hexanes mixtures (Technical grade)
6. Analytical balance with a precision at ± 0.1 mg

Precautions before start

1. Hexane solvent must be distilled before use to ensure no residues are dissolved in it.
2. Keep a working amount, approximately 50 – 100 mL, of hexane in a clean container.
3. Do not pipette hexane directly from the storage jar as this might contaminate all the hexane in it.
4. Always handle the hexane jar (4 L) in the fume hood.
5. All materials must be thoroughly cleaned and washed with hexane before use.

Procedure

1. Weigh 50 mg (approx) of dried algae directly in a weighting paper. Record the actual weight. To ensure accurate weight, check scale to see that it is centered.
2. Transfer algae sample to the mortar.
3. Grind cells for 5 minutes to ensure cell walls are thoroughly broken. It is a better to start with a gentle grinding, sliding the pestle against the wall of the mortar, and gradually increase the strength and pace of grinding. If tired, take a rest, but consider the resting time so the total grinding time is kept constant.
4. Add 1 mL of hexane to the mortar, and with the pestle dissolve (homogenize) the algae debris.
5. Using a Pasteur pipette, transfer the hexane and cell debris to the centrifugation tube.
6. Wash the mortar with hexane and transfer the solvent to the centrifuge tube, repeat until the mortar and pestle are free of cell debris.
7. Centrifuge at 3000 rpm, 4°C, for 10 minutes.
8. With a clean Pasteur pipette, recover the oil-hexane mixture from the clear upper layer, and transfer to the pre-weighted tube.
9. Add 3 mL of fresh hexane to the centrifuge tube and shake vigorously for 5 minutes.
10. Repeat steps 7-8.

A.2. Gravimetric Quantification of Neutral Lipids

11. Let solvent to evaporate and weight the tube containing the oil to calculate oil content. To speed up the evaporation you can flush your tubes with nitrogen or air.

Note: when the above procedure is followed, the expected error is $\pm 0.4\%$ w/w.

This page intentionally left blank

B

Fed-batch cultures of *A. protothecoides*

B.1 Open-loop optimal run

The open-loop optimal run was performed with the aim of reaching a very high cell density. The start-up medium contained glucose ($\text{C}_6\text{H}_{12}\text{O}_6$, 20 g/L), glycine ($\text{NH}_2\text{CH}_2\text{COOH}$, 0.2 g/L), thiamine hydrochloride (20 $\mu\text{g/L}$), K_2HPO_4 (0.6 g/L), KH_2PO_4 (1.4 g/L), $\text{FeSO}_4 \cdot 7 \text{H}_2\text{O}$ (0.024 g/L), $\text{CaCl}_2 \cdot 2 \text{H}_2\text{O}$ (0.01 g/L), $\text{MgSO}_4 \cdot 7 \text{H}_2\text{O}$ (0.6 g/L), $\text{MnCl}_2 \cdot 4 \text{H}_2\text{O}$ (3.6 mg/L), $\text{ZnSO}_4 \cdot 7 \text{H}_2\text{O}$ (0.44 mg/L), $\text{CuSO}_4 \cdot 5 \text{H}_2\text{O}$ (3.9 mg/L), H_3BO_3 (5.8 mg/L), and $\text{Na}_2\text{MoO}_4 \cdot 5 \text{H}_2\text{O}$ (0.08 mg/L),

Feed 1 (Nitrogen source) consisted of an aqueous solution of glycine, at 100 g/L, and Feed 2 contained the carbon source and the trace nutrients. Feed 2 contained glucose ($\text{C}_6\text{H}_{12}\text{O}_6$, 900 g/L), $\text{FeSO}_4 \cdot 7 \text{H}_2\text{O}$ (0.72 g/L), $\text{MgSO}_4 \cdot 7 \text{H}_2\text{O}$ (18 g/L), $\text{MnCl}_2 \cdot 4 \text{H}_2\text{O}$ (108 mg/L), $\text{ZnSO}_4 \cdot 7 \text{H}_2\text{O}$ (13.2 mg/L), $\text{CuSO}_4 \cdot 5 \text{H}_2\text{O}$

(4.8 mg/L), H_3BO_3 (174 mg/L), $\text{Na}_2\text{MoO}_4 \cdot 5 \text{H}_2\text{O}$ (1.8 mg/L), and thiamine hydrochloride (600 $\mu\text{g/L}$).

The temperature in the reactor was controlled using an electrical heating jacket without providing any cooling. Temperature set-point was established at 25 °C. The dissolved oxygen concentration was fixed at 30% of the saturation value at 25 °C. pH was controlled around 6.2 using K_2HPO_4 (1 M) as base and KH_2PO_4 (1 M) as acid. The ester-base antifoam O-30 was used to avoid excessive foaming in the system.

B.1.1 Results

The flowrates of the two feeds and the acid and base solutions are shown in Table B.1 together with the hourly average values for temperature, pH, and dissolved oxygen concentration. The measured biomass concentration is presented in Table B.2.

Table B.1: Flow rate and process conditions for the Open-Loop MPC culture

Time (h)	Acid (mL/h)	Base (mL/h)	Feed 2 (mL/h)	Feed 1 (mL/h)	Temp. (C)	pH (-)	DO (%)
0	0	0	0	0	25.0	6.23	100.1
1	0	0	0	0	25.0	6.21	99.5
2	0.59	0	0	0	25.0	6.21	98.8
3	0.25	0	0	0	25.0	6.21	99.1
4	0.04	0	0	0	25.0	6.21	98.7
5	0	0	0	0	25.0	6.20	98.6
6	0	0	0	0	25.0	6.20	99.0
7	0	0.01	0	0	25.0	6.19	98.9
8	0	0.25	0	0	25.0	6.19	99.0
9	0	1.17	0	0	25.0	6.19	98.8
10	0	0.57	0	0	25.0	6.19	98.9
11	0	1.15	0	0	25.0	6.19	99.0
12	0	0.58	0	0	25.0	6.19	98.9
13	0	0.64	0	0	25.0	6.19	98.9
14	0	0.49	0	0	25.0	6.19	99.0
15	0	0.63	0	0	25.0	6.19	99.1
16	0	0.16	0	0	25.0	6.19	99.3
17	0	1.04	0	0	25.0	6.19	99.2
18	0	0.59	0	0	25.0	6.19	99.2
19	0	1.02	0	0	25.0	6.19	99.1
20	0	0.77	0	0	25.0	6.19	99.3

Continued on Next Page...

B.1. Open-loop optimal run

Table B.1 – Continued

Time (h)	Acid (mL/h)	Base (mL/h)	Feed 2 (mL/h)	Feed 1 (mL/h)	Temp. (C)	pH (-)	DO (%)
21	0	1.00	0	0	25.0	6.19	99.2
22	0	0.43	0	0	25.0	6.19	99.2
23	0	0.81	0	0	25.0	6.19	99.3
24	0	0.17	0	0	25.0	6.19	100.0
25	0	0.05	0	0	25.0	6.19	100.1
26	0	0.13	0	0	25.0	6.19	100.2
27	0	0.67	0	0	25.0	6.19	100.4
28	0	0.13	0	0	25.0	6.19	100.4
29	0	0.26	0	0	25.0	6.19	99.2
30	0	0.50	0	0	25.0	6.19	100.5
31	0	0.48	0	0	25.0	6.19	100.5
32	0	0.48	0	0	25.0	6.19	100.5
33	0	0.44	0	0	25.0	6.19	100.6
34	0	0.76	0	0	25.0	6.19	100.5
35	0	0.89	0	0	25.0	6.19	100.6
36	0	0.43	0	0	25.0	6.19	100.5
37	0	0.52	0	0	25.0	6.19	100.4
38	0	0.45	0	0	25.0	6.19	100.4
39	0	0.32	0	0	25.0	6.19	100.4
40	0	0.54	0	0	25.0	6.19	100.3
41	0	0.34	0	0	25.0	6.19	100.3
42	0	0.34	0	0	25.0	6.19	100.2
43	0	0.35	0	0	25.0	6.19	100.0
44	0	0.69	0	0	25.0	6.19	99.9
45	0	0.63	0	0	25.0	6.19	99.7
46	0	0.28	0	0	25.0	6.19	99.3
47	11.36	0.01	0	0	25.0	6.21	99.1
48	0	0	0	0	25.0	6.20	99.3
49	0	0	0	0	25.0	6.20	99.0
50	0	0	0	0	25.0	6.20	98.7
51	0	0.01	0	0	25.0	6.20	98.3
52	0	0.14	0	0	25.0	6.19	98.1
53	0	0.68	0	0	25.0	6.19	97.8
54	0	0.51	0	0	25.0	6.19	97.4
55	0	0.78	0	0	25.0	6.19	97.1
56	0	0.79	0	0	25.0	6.19	96.5
57	0	0.66	0	0	25.0	6.19	96.0
58	0	0.63	0	0	25.0	6.19	95.4
59	0	0.47	0	0	25.0	6.19	94.8
60	0	0.38	0	0	25.0	6.19	94.2
61	0	0.47	0	0	25.0	6.19	92.9
62	0	0.40	0	0	25.0	6.19	89.4
63	0	0.48	0	0	25.0	6.19	87.4
64	0	0.53	0	0	25.0	6.19	85.5
65	0	0.52	0	0	25.0	6.19	83.1
66	0	0.59	0	0	25.0	6.19	81.0
67	0	0.54	0	0	25.0	6.19	79.4
68	0	0.68	0	0	25.0	6.19	78.2
69	0	0.34	0	0	25.0	6.19	77.8
70	0	0.75	0	0	25.0	6.19	76.5
71	0	0.63	0	0	25.0	6.19	76.0
72	0	0.86	0	0	25.0	6.19	75.1
73	0	0.51	0	0	25.0	6.19	74.6
74	0	0.13	0	0	25.0	6.19	75.6
75	0	0.37	0	0	25.0	6.19	76.0
76	0	0.88	0.1	0.3	25.0	6.19	71.7

Continued on Next Page...

Table B.1 – Continued

Time (h)	Acid (mL/h)	Base (mL/h)	Feed 2 (mL/h)	Feed 1 (mL/h)	Temp. (C)	pH (-)	DO (%)
77	0	0.33	0	0.3	25.0	6.19	66.3
78	0	0.01	0.1	0.3	25.0	6.20	67.1
79	0	0.01	0.1	0.4	25.0	6.20	65.2
80	0	0.01	0.1	0.3	25.0	6.20	63.7
81	0	0.01	0.2	0.3	25.0	6.20	61.8
82	0	0	0.2	0.3	25.0	6.20	60.4
83	0	0.01	0.2	0.3	25.0	6.20	59.9
84	0	0.02	0.2	0.4	25.0	6.19	57.7
85	0	0.25	0.2	0.3	25.0	6.19	56.8
86	0	0.22	0.2	0.3	25.0	6.19	55.4
87	0	0.62	0.2	0.3	25.0	6.19	54.3
88	0	0.39	0.2	0.3	25.0	6.19	52.6
89	0	0.06	0.2	0.3	25.0	6.19	52.3
90	0	0.34	0.2	0.4	25.0	6.19	52.2
91	0	0.38	0.2	0.3	25.0	6.19	51.4
92	0	0.19	0.2	0.3	25.0	6.19	51.4
93	0	0.24	0.2	0.3	25.0	6.19	51.5
94	0	0.06	0.3	0.3	25.0	6.19	50.2
95	0	0.13	0.2	0.3	25.0	6.19	48.8
96	0	0.23	0.3	0.4	25.0	6.19	47.2
97	0	0.03	0.3	0.3	25.0	6.20	46.1
98	0	0.04	0.3	0.3	25.0	6.19	43.4
99	0	0.22	0.3	0.3	25.0	6.19	39.7
100	0	0.39	0.3	0.3	25.0	6.19	36.1
101	0	0.14	0.3	0.3	25.0	6.19	32.5
102	0	0.42	0.4	0.4	25.0	6.19	30.1
103	0	0.25	0.3	0.3	25.0	6.19	29.7
104	0	0.29	0.4	0.3	25.0	6.19	29.7
105	0	0.63	0.4	0.3	25.0	6.19	29.7
106	0	0.38	0.4	0.3	25.0	6.19	29.6
107	0	0.04	0.4	0.3	25.0	6.19	30.9
108	0	0.31	0.4	0.3	25.0	6.19	31.2
109	0	0.74	0.5	0.4	25.0	6.19	32.9
110	0	0.43	0.5	0.3	25.0	6.19	33.4
111	0	0.38	0.5	0.3	25.0	6.19	32.9
112	0	0.31	0.5	0.3	25.0	6.19	32.7
113	0	0.48	0.6	0.3	25.0	6.20	32.2
114	0	0.33	0.6	0.3	25.0	6.19	31.5
115	0	0.52	0.6	0.4	25.0	6.19	31.1
116	0	1.03	0.6	0.3	25.0	6.19	30.8
117	0	4.40	0.6	0.3	25.0	6.19	30.4
118	0	0.24	0.7	0.3	25.0	6.19	30.2
119	0	0.30	0.7	0.3	25.0	6.19	30.1
120	0	0.36	0.8	0.3	25.0	6.19	30.1
121	1.09	0.14	0.8	0.4	25.0	6.20	31.3
122	1.26	0.84	0.8	0.3	25.0	6.20	30.7
123	1.28	1.03	0.9	0.6	25.0	6.20	30.6
124	0.91	3.17	2.9	0.6	25.0	6.19	29.0
125	1.49	0.71	1.4	0.7	25.0	6.20	31.2
126	1.67	1.06	1.4	0.6	25.0	6.20	30.5
127	1.55	1.42	1.4	0.6	25.0	6.20	30.7
128	2.37	1.78	1.5	0.7	25.0	6.20	31.2
129	2.35	2.24	1.6	0.6	25.0	6.20	31.4
130	2.43	2.20	1.6	0.6	25.0	6.20	31.4
131	2.53	2.51	1.7	0.7	25.0	6.20	31.4
132	3.08	2.48	1.8	0.6	25.0	6.20	31.5

Continued on Next Page...

B.1. Open-loop optimal run

Table B.1 – Continued

Time (h)	Acid (mL/h)	Base (mL/h)	Feed 2 (mL/h)	Feed 1 (mL/h)	Temp. (C)	pH (-)	DO (%)
133	2.38	2.63	1.9	0.6	25.0	6.20	31.0
134	2.56	2.84	2.0	0.7	25.1	6.20	30.8
135	2.09	2.78	2.0	0.6	25.0	6.20	31.0
136	1.66	2.92	2.1	0.6	25.1	6.20	30.5
137	3.13	3.27	2.2	0.7	25.0	6.20	30.5
138	1.59	2.50	2.3	0.6	25.0	6.20	30.5
139	1.17	2.94	2.4	0.6	25.0	6.20	29.7
140	1.16	2.82	2.5	0.7	25.0	6.20	29.7
141	0.74	2.44	2.6	0.6	25.0	6.20	30.1
142	0.86	2.94	2.6	0.6	25.1	6.20	29.6
143	0.60	2.90	2.6	1.0	25.0	6.20	30.0
144	0.29	2.86	2.7	0.9	25.0	6.20	30.5
145	0.16	2.89	2.7	1.0	25.1	6.20	29.9
146	0.37	3.45	2.7	0.9	25.0	6.20	29.5
147	0.08	2.77	4.2	1.0	25.0	6.20	28.4
148	0	3.11	11.3	0.9	25.3	6.19	31.7
149	0	1.67	4.2	0.7	25.5	6.19	30.0
150	0	2.17	2.9	0.9	25.5	6.19	30.0
151	0	1.59	3.0	1.0	25.5	6.19	30.0
152	0	2.33	3.0	0.9	25.4	6.19	30.0
153	0	1.31	3.0	1.0	25.4	6.19	30.3
154	0.01	1.87	3.1	0.9	25.4	6.20	30.7
155	0.06	1.00	3.2	1.0	25.3	6.20	30.8
156	0.04	1.34	3.2	0.9	25.2	6.20	30.9
157	0.63	1.94	3.3	1.0	25.2	6.20	30.9
158	1.05	2.75	3.3	0.9	25.2	6.20	31.1
159	1.11	1.67	3.4	1.0	25.1	6.20	31.2
160	2.10	1.78	3.5	0.9	25.1	6.20	31.0
161	0.71	1.38	3.5	1.0	25.0	6.20	31.2
162	3.15	3.05	3.5	0.9	25.0	6.20	31.1
163	0.48	3.41	3.7	1.0	25.0	6.20	28.8
164	0	2.46	9.8	0.9	25.6	6.19	31.4
165	0	2.10	3.7	1.0	25.9	6.19	29.8
166	0	1.78	3.8	1.3	26.2	6.19	29.8
167	0	2.22	3.9	1.2	26.5	6.19	29.6
168	0	0.28	3.9	1.0	26.8	6.19	30.9
169	0.73	4.07	3.9	1.2	27.0	6.20	25.5
170	0.01	0.00	4.0	1.0	27.3	6.20	32.3
171	0	4.43	4.1	1.3	27.5	6.19	30.0
172	0	0.27	4.1	1.2	27.7	6.19	29.9
173	0	0.42	4.2	1.3	27.8	6.19	29.9
174	0	3.79	4.3	1.3	27.9	6.19	30.0
175	0	0	4.3	1.2	27.9	6.20	30.0
176	0	0	4.4	1.3	28.1	6.20	29.9
177	0	0	4.5	1.3	28.2	6.20	29.9
178	0.02	0.01	4.5	1.2	28.2	6.20	30.7
179	3.60	0	4.6	1.3	28.0	6.21	30.0
180	2.75	0	4.7	1.3	27.8	6.20	30.1
181	4.68	0.42	4.7	1.2	27.6	6.20	30.0
182	2.93	0.28	4.9	1.3	27.3	6.20	30.0
183	3.68	0.03	4.9	1.3	27.1	6.20	29.9
184	4.92	0.01	5.0	1.2	27.0	6.20	29.9
185	8.23	3.83	5.1	1.6	27.0	6.20	30.1
186	0.99	0	5.2	1.3	27.0	6.21	29.9
187	14.44	24.73	14.1	60.9	27.3	6.20	18.3
188	86.43	11.28	5.4	26.8	27.7	6.23	29.5

Continued on Next Page...

Table B.1 – Continued

Time (h)	Acid (mL/h)	Base (mL/h)	Feed 2 (mL/h)	Feed 1 (mL/h)	Temp. (C)	pH (-)	DO (%)
189	0	31.97	5.4	1.6	27.2	6.17	0.1
190	0	22.85	5.5	1.6	26.9	6.18	0.6
191	0	15.71	5.6	1.5	26.8	6.18	1.3
192	0	97.33	5.6	1.6	26.9	6.17	2.0
193	0	123.78	5.7	1.6	27.2	6.14	2.6
194	0	0	5.9	1.6	27.6	6.13	3.4
195	0.02	0	6.0	1.6	28.2	6.17	4.1
196	1.26	0	12.4	0	28.0	6.21	4.0
197	0	0	6.1	0	27.0	6.19	4.0
198	0	0	6.2	0	26.1	6.19	4.3
199	0	0	6.3	0	25.6	6.19	4.5
200	0	0	6.4	0	25.2	6.20	4.7
201	0	0	6.5	0	25.0	6.22	4.9
202	0	0	6.3	0	24.9	6.24	5.1
203	0	0	6.3	0	25.0	6.27	5.5
204	0	0	6.4	0	25.2	6.29	5.8
205	0	0	6.6	0	25.4	6.28	6.1
206	0	0	6.7	0	25.6	6.26	6.3
207	0	0	6.8	0	26.0	6.24	6.6
208	0	0	7.0	0	26.4	6.21	7.0
209	0	0	7.2	0	26.9	6.19	7.7
210	0	0	7.3	0	27.5	6.18	14.7
211	0	0	7.4	0	28.0	6.18	28.4
212	0	0	7.5	0	27.9	6.18	6.4
213	0	0	11.0	0	27.3	6.18	3.4
214	0	0	7.8	0	27.2	6.18	3.8
215	0	0	7.9	0	27.3	6.19	4.7
216	0	0	8.0	0	27.7	6.21	5.4
217	0	0	8.2	0	27.3	6.18	4.9
218	0	0	8.3	0	27.1	6.18	5.1
219	0	0	8.4	0	27.0	6.19	5.5
220	0	0	5.3	0	27.3	6.21	6.0
221	0	0	0	0	27.0	6.20	5.6
222	0	0	0	0	26.4	6.18	5.4
223	0	0	0	0	26.1	6.19	5.5
224	0	0	0	0	25.9	6.19	5.7
225	0	0	0	0	26.0	6.21	6.0
226	0	0	0	0	26.3	6.22	7.1
227	0	0	0	0	26.7	6.21	17.1
228	0	0	0	0	27.0	6.19	20.5
229	0	0	0	0	27.2	6.16	23.6
230	0	0	0	0	27.4	6.14	27.9
231	0	0	0	0	27.5	6.12	34.4
232	0	0	0	0	27.6	6.09	30.4
233	0	0	0	0	27.7	6.07	30.5
234	0	0	0	0	27.8	6.05	34.0
235	0	0	0	0	27.8	6.04	47.4
236	0	0	0	0	27.9	6.02	62.2
237	0	0	0	0	27.6	6.00	49.3
238	0	0	0	0	27.1	5.93	0.0
239	0	0	0	0	27.0	5.86	0.0
240	0	0	0	0	27.4	5.83	0.0
241	0	0	0	0	28.2	5.86	1.7
242	0	0	0	0	28.9	5.95	26.4
243	0	0	0	0	29.4	6.02	33.1
244	0	0	0	0	29.6	6.06	29.2

Continued on Next Page...

B.1. Open-loop optimal run

Table B.1 – Continued

Time (h)	Acid (mL/h)	Base (mL/h)	Feed 2 (mL/h)	Feed 1 (mL/h)	Temp. (C)	pH (-)	DO (%)
245	0	0	9.1	0	29.7	6.07	30.7
246	0	0	3.1	0	29.8	6.06	30.2
247	0	0	3.2	0	29.8	6.06	30.0
248	0	0	3.2	0	29.8	6.07	30.1
249	0	0	3.3	0	29.8	6.06	30.2
250	0	0	3.3	0	29.8	6.06	30.1
251	0	0	3.4	0	29.8	6.06	30.1
252	0	0	3.5	0	29.7	6.07	30.4
253	0	0	3.5	0	29.3	6.08	30.1
254	0	0	3.6	0	28.7	6.10	30.5
255	0	0	3.7	0	28.1	6.12	30.2
256	0	0	3.7	0	27.5	6.14	30.8
257	0	0	3.7	0	27.1	6.16	30.7
258	0	0	3.8	0	26.7	6.17	30.5
259	0	0	3.9	0	26.4	6.19	30.9
260	0	0	3.9	0	26.2	6.20	30.5
261	0	0	4.0	0	26.0	6.21	30.8
262	0	0	5.0	0	25.9	6.22	30.3
263	0	0	6.6	0	26.1	6.23	29.5
264	0	0	7.2	0	26.4	6.23	31.6
265	0	0	4.9	0	26.5	6.22	30.9
266	0	0	10.4	0	26.7	6.23	29.5
267	0	0	6.1	0	26.9	6.22	30.5
268	0	0	6.0	0	27.3	6.21	31.0
269	0	0	5.0	0	27.6	6.18	30.0
270	0	0	4.5	0	27.8	6.17	30.0
271	0	0	4.5	0	27.9	6.16	30.0
272	0	0	4.6	0	28.0	6.15	30.0
273	0	0	4.7	0	28.0	6.14	30.0
274	0	0	4.8	0	28.0	6.14	30.0
275	0	0	4.9	0	28.1	6.13	30.0
276	0	0	5.0	0	28.1	6.12	30.0
277	0	0	5.0	0	28.1	6.12	30.0
278	0	0	5.1	0	28.1	6.11	30.0
279	0	0	5.2	0	28.0	6.11	30.0
280	0	0	5.2	0	27.9	6.11	30.0
281	0	0	5.3	0	27.8	6.11	30.2
282	0	0	5.4	0	27.5	6.12	30.1
283	0	0	5.5	0	27.3	6.13	30.2
284	0	0	5.6	0	27.4	6.13	30.4
285	0	0	7.7	0	27.3	6.14	30.2
286	0	0	10.1	0	27.3	6.13	30.1
287	0	0	6.0	0	27.5	6.13	30.2
288	0	0	6.0	0	27.5	6.13	30.3
289	0	0	6.1	0	27.5	6.12	30.8
290	0	0	6.3	0	27.5	6.12	31.1
291	0	0	6.2	0	27.4	6.11	31.0
292	0	0	0	0	27.2	6.11	31.8
293	0	0	0	0	27.1	6.11	30.7
294	0	0	6.3	0	26.9	6.11	30.3
295	0	0	6.4	0	26.7	6.11	30.0
296	0	0	6.5	0	26.4	6.11	30.1
297	0	0	6.6	0	26.2	6.11	30.0
298	0	0	6.7	0	26.1	6.10	30.0
299	0	0	6.8	0	25.9	6.10	30.1
300	0	0	6.9	0	25.8	6.10	30.1

Continued on Next Page...

Table B.1 – Continued

Time (h)	Acid (mL/h)	Base (mL/h)	Feed 2 (mL/h)	Feed 1 (mL/h)	Temp. (C)	pH (-)	DO (%)
301	0	0	7.0	0	25.6	6.10	30.0
302	0	0	7.1	0	25.5	6.09	30.1
303	0	0	7.2	0	25.4	6.09	30.1
304	0	0	7.3	0	25.2	6.08	30.0
305	0	0	7.5	0	25.1	6.08	29.9
306	0	0	7.6	0	25.0	6.08	30.1
307	0	0	7.7	0	25.0	6.07	30.0
308	0	0	0	0	25.0	6.06	30.1
309	0	0	0	0	25.0	6.06	31.5
310	0	0	0	0	25.0	6.06	43.1
311	0	0	0	0	25.1	6.05	31.1
312	0	0	0	0	25.2	6.04	31.2
313	0	0	0	0	25.3	6.04	31.4
314	0	0	1.4	0	25.4	6.03	31.4
315	0	0	4.6	0	25.5	6.03	31.3
316	0.07	0	7.6	0.9	25.6	6.02	31.7
317	0	0	7.1	0	25.7	6.02	31.7
318	0	0	3.4	0	25.7	6.01	31.2
319	0	0	3.5	0	25.6	6.01	31.3
320	0	0	3.5	0	25.5	6.01	31.1
321	0	0	3.6	0	25.3	6.00	30.2
322	0	0	3.6	0	25.2	6.00	30.1
323	0	0	3.6	0	25.1	6.00	30.0
324	0	0	3.6	0	25.0	6.00	30.0
325	0	0	3.7	0	24.9	6.00	30.0
326	0	0	3.8	0	25.0	6.00	29.9
327	0	0	3.9	0	25.0	5.99	30.0
328	0	0	3.9	0	25.0	5.99	30.1
329	0	0	4.0	0	25.0	5.99	30.0
330	0	0	4.0	0	25.0	5.98	30.1
331	0	0	4.1	0	25.0	5.98	30.1
332	0	0	4.2	0	25.0	5.98	29.9
333	0	0	9.2	0	25.0	5.97	30.0
334	0	0	0	0	25.0	5.96	30.2
335	0	0	0	0	25.0	5.96	30.0
336	0	0	0	0	25.0	5.95	30.1
337	0	0	0	0	25.0	5.96	30.1
338	0	0	0	0	25.0	5.96	29.9
339	0	0	0	0	25.0	5.96	29.9
340	0	0	0	0	25.0	5.96	29.9
341	0	0	0	0	25.0	5.95	30.1
342	0	0	0	0	25.0	5.95	29.9
343	0	0	0	0	25.0	5.95	30.0
344	0	0	0	0	25.0	5.95	30.0
345	0	0	0	0	25.0	5.95	30.1
346	0	0	0	0	25.0	5.94	30.0
347	0	0	0	0	25.0	5.94	30.1
348	0	0	0	0	25.0	5.94	30.1
349	0	0	0	0	25.0	5.94	30.2
350	0	0	0	0	25.0	5.93	30.0
351	0	0	0	0	25.0	5.93	30.2
352	0	0	0	0	25.0	5.92	30.2
353	0	0	0	0	25.0	5.92	36.8
354	0	0	0	0	25.0	5.92	37.0
355	0	0	0	0	25.0	5.91	40.3
356	0	0	0	0	25.0	5.91	46.4

Continued on Next Page...

Table B.1 – Continued

Time (h)	Acid (mL/h)	Base (mL/h)	Feed 2 (mL/h)	Feed 1 (mL/h)	Temp. (C)	pH (-)	DO (%)
357	0	0	0	0	25.0	5.90	62.9
358	0	0	0	0	25.0	5.91	86.1
359	0	0	0	0	25.0	5.94	18.5
360	0	0	0	0	25.0	5.96	32.1

Table B.2: Biomass concentration for the Open-Loop MPC culture

Time (h)	Biomass (g/L)	
	Average	Std. dev.
0	1.0	-
24.1	1.0	0.15
48.2	1.4	0.05
72.0	4.1	0.10
96.0	10.1	0.10
120.2	21.1	0.15
144.1	27.1	0.10
168.1	45.5	0.71
186.4	58.0	0.35
194.4	57.8	4.29
216.3	56.2	3.99
236.4	69.6	0.61
241.8	71.5	0.10
262.0	82.9	0.56
286.0	92.3	0.25
312.1	98.4	0.56
360.2	90.2	0.20

B.1.2 Important observations

1. Between 120 h and 150 h, the temperature and the dissolved oxygen concentration oscillated around their corresponding set points. Dissolved oxygen concentration frequently reached zero. This may help to explain the slower growth rate during this period.
2. At 160 h, the reaction temperature rose up to 28 °C (after pure oxygen addition started), and then decreased until 27 °C. Temperature remained out of control until 330 h.
3. At 186.2 h, there was a failure in the loop controlling Feed-Pump 1. As a

result, approximately 100 mL of feed 1 were pump into the reactor with a subsequent loss of control in the process variables (pH, DO).

4. The addition of enriched air (or pure oxygen) improved the growth rate. The resulting higher metabolic activity, however, increased culture temperature. During this run, the bioreactor did not have cooling capabilities, and therefore temperature went out of control.
5. The addition of antifoam O-30 completely eliminated the foam. The antifoam effect last for about one day and after that more antifoam had to be added to the reaction media. The dissolved oxygen concentration, however, appeared to be affected by the antifoam addition.

B.2 Adaptive model predictive control run for maximum biomass

The adaptive model predictive control culture was carried out in a stirred tank bioreactor as described in Chapter 3. The start-up medium was formulated according to Medium B4-Fe, as shown in Table 3.1, supplemented with glycine (0.4 g/L) and glucose (30 g/L).

Nutrients were added to the culture in a fed-batch mode with two independent feeds. The nitrogen rich feed (Feed 1) consisted of an aqueous solution of glycine (150 g/L). The carbon rich feed (Feed 2) contained KH_2PO_4 (50 g/L), $\text{MgSO}_4 \cdot 7\text{H}_2\text{O}$ (32 g/L), $\text{FeSO}_4 \cdot 7\text{H}_2\text{O}$ (1.27 g/L), disodium salt of EDTA (1.7 g/L), H_3BO_3 (0.31 g/L), $\text{CaCl}_2 \cdot 2\text{H}_2\text{O}$ (0.26 g/L), $\text{MnCl}_2 \cdot 4\text{H}_2\text{O}$ (0.2 g/L), $\text{ZnSO}_4 \cdot 7\text{H}_2\text{O}$ (23.3 mg/L), $\text{CuSO}_4 \cdot 5\text{H}_2\text{O}$ (8.5 mg/L), $\text{Na}_2\text{MoO}_4 \cdot 5\text{H}_2\text{O}$ (3.2 mg/L), thiamine hydrochloride (1.06 mg/L), and glucose (900 g/L).

The pH was controlled around 6.2 using a 500 g/L solution of K_2HPO_4 as base and a 200 g/L aqueous solution of KH_2PO_4 as acid. The dissolved oxygen concentration (DO) was controlled around 50% of the saturation value by bubbling air enriched with oxygen at the bottom of the reactor vessel.

B.2.1 Results

The flow-rates of all the gas and liquid streams as well as the hourly average process measurements are presented in Table B.3. The reported volume was calculated from the initial medium and inoculum volumes, accounting the

B.2. Adaptive model predictive control run for maximum biomass

amount of liquid added to the reactor and discounting the volume removed for each sample and the losses for evaporation (assumed proportional to the gas flowrate). The experimental measurements for biomass concentration, glucose concentration, and intracellular lipid content is presented in Table B.4.

Table B.3: Flow rate and process conditions for the Adaptive MPC culture

Time (h)	Air (mL/h)	O2 (mL/h)	Acid (mL/h)	Base (mL/h)	Feed 2 (mL/h)	Feed 1 (mL/h)	Volume (mL)	Temp. (C)	pH (-)	DO (%)
0	0	0	0	0	0	0	768.0	25.1	6.15	91.8
1	300	0	0	0.1	0	4.9	760.4	25.1	6.20	59.7
2	0	0	0	0.4	0	0.3	761.1	25.1	6.19	50.6
3	100	0	0	0	0	0	761.1	25.0	6.20	50.6
4	0	0	0	0.3	0.9	0	762.3	25.4	6.19	50.3
5	0	0	0	0.1	0.8	0	750.6	25.1	6.19	50.2
6	0	0	0	0.1	0.9	0	751.6	25.1	6.19	50.2
7	100	0	0	0.3	0.8	0	752.7	25.1	6.19	50.1
8	0	0	0	0.2	0.9	0	753.8	25.1	6.19	50.1
9	0	0	0	0.3	0.8	0	742.3	25.1	6.19	50.3
10	0	0	0	0.4	0.9	0	743.6	25.1	6.19	50.2
11	0	0	0	0.2	0.8	0	744.6	25.1	6.19	50.3
12	100	0	0	0.3	0.9	0	745.8	25.0	6.19	50.3
13	0	0	0	0.3	1.7	0.2	735.4	25.1	6.19	50.5
14	0	0	0	0.2	1.7	0.3	737.6	25.0	6.19	50.4
15	0	0	0	0.4	1.7	0.3	740.0	25.0	6.19	50.3
16	100	0	0	0.3	1.7	0.3	742.3	25.1	6.19	50.4
17	0	0	0	0.2	1.8	0.3	732.0	25.1	6.19	50.3
18	0	0	0	0.3	1.7	0.3	734.3	25.1	6.19	50.3
19	0	0	0	0.1	0.5	0.2	735.1	25.1	6.19	50.3
20	100	0	0	0.4	0.6	0.3	736.4	25.1	6.19	50.1
21	0	0	0	0.2	0.6	0.3	724.9	25.1	6.19	50.0
22	0	0	0	0.3	0	0.3	725.5	25.1	6.19	50.0
23	100	0	0	0	0	0.3	725.8	25.0	6.19	50.0
24	100	0	0	0.2	0	0.3	726.3	25.0	6.19	50.0
25	0	0	0.1	0	0	0.2	714.0	25.1	6.20	49.9
26	100	0	6.1	0	0	0.3	720.4	25.1	6.24	49.9
27	100	0	0.1	0	0	0.3	720.8	25.2	6.23	49.9
28	200	0	0.3	0	0	0.3	721.4	25.2	6.23	49.8
29	500	0	0.9	0	0	0.3	710.0	25.2	6.23	49.1
30	1300	0	0.1	0	0	0.3	710.4	25.2	6.23	48.3
31	1800	200	0	0	0	0.2	710.5	25.2	6.22	46.5
32	1800	600	0	0	0	0.3	710.8	25.2	6.22	44.5
33	1800	1300	0	0	0	0.3	698.5	25.2	6.22	42.5
34	1900	2000	0	0	0	0.3	698.7	25.1	6.21	40.6
35	1800	3000	0	0	0	0.3	698.9	25.1	6.21	38.8
36	1800	3000	0	0	0	0.3	699.1	25.1	6.20	38.1
37	1800	3000	0	0	1.5	0.2	688.2	25.1	6.20	38.1
38	1800	3000	0	0	1.6	0.3	690.0	25.1	6.19	37.7
39	1800	2900	0	0	1.6	0.3	691.8	25.2	6.17	37.0
40	1800	3000	0	0.5	1.5	0.3	694.0	25.2	6.17	33.2
41	1800	2500	0	0.4	1.6	0.3	683.7	25.2	6.17	31.9
42	500	4000	0	0.5	1.6	0.3	686.0	25.2	6.17	70.6
43	500	4800	0	0.3	1.5	0.2	687.9	25.3	6.17	74.5
44	400	4200	0	0.4	1.6	0.3	690.1	25.2	6.17	42.4
45	600	5800	0	0.1	1.6	0.3	679.4	25.0	6.17	40.2

Continued on Next Page...

Table B.3 – Continued

Time (h)	Air (mL/h)	O2 (mL/h)	Acid (mL/h)	Base (mL/h)	Feed 2 (mL/h)	Feed 1 (mL/h)	Volume (mL)	Temp. (C)	pH (-)	DO (%)
46	600	6300	1.6	0.1	1.5	0.3	682.8	25.1	6.19	50.9
47	700	2800	9.7	0	1.6	0.3	694.4	25.1	6.23	91.3
48	1100	3500	0	0	0	0.3	694.6	25.1	6.22	32.6
49	700	3300	0.2	0	2.4	0.5	685.0	25.2	6.23	53.8
50	600	2200	0.5	0	2.2	0.6	688.3	25.3	6.23	93.3
51	600	1200	0.1	0	2.2	0.6	691.2	25.4	6.23	59.5
52	600	1000	0.1	0	0.8	0.5	692.5	25.3	6.22	50.0
53	600	1100	0	0	0.7	0.6	681.2	25.4	6.21	49.8
54	600	1000	0	0	0.7	0.6	682.5	25.4	6.20	49.9
55	600	1100	0	0	0.7	0.5	683.7	25.5	6.19	50.3
56	600	1100	0	0	0.7	0.6	684.9	25.6	6.18	50.0
57	600	1200	0	0.6	0.7	0.6	674.2	25.6	6.17	49.9
58	600	1100	0	0.1	0.8	0.5	675.6	25.6	6.17	49.9
59	600	1200	0	0.2	0.7	0.6	677.1	25.6	6.17	50.1
60	600	1100	0	0.2	0.7	0.6	678.5	25.5	6.17	50.4
61	600	1400	0	0.3	2.1	0.8	669.1	25.5	6.17	50.0
62	600	1300	0	0.3	2.2	0.9	672.5	25.6	6.17	49.9
63	600	1500	0	0.2	2.1	0.8	675.5	25.7	6.18	49.6
64	700	1700	0	0.2	2.1	0.9	678.7	25.8	6.18	49.4
65	600	2500	0	0.2	2.2	0.8	669.2	25.9	6.18	48.6
66	600	2800	0	0.1	2.1	0.9	672.3	25.7	6.19	50.1
67	600	2600	1.1	0	2.1	0.8	676.2	25.4	6.22	49.9
68	600	2800	5.5	0	2.2	0.9	684.8	25.6	6.22	50.0
69	600	2600	0.2	0.2	2.1	0.8	675.4	25.9	6.19	51.2
70	600	2900	0	0.6	2.1	0.9	679.0	26.2	6.19	48.9
71	600	3300	0	0.5	2.2	0.8	682.4	26.5	6.18	49.7
72	600	3300	0	0.5	2.1	0.9	685.9	26.9	6.19	49.9
73	600	3300	0	0.4	3.6	0.8	678.0	27.3	6.18	51.0
74	600	3400	0	0.6	3.6	0.9	683.0	27.7	6.18	49.8
75	600	3200	0	0.4	3	0.8	687.2	28.0	6.19	49.6
76	600	3100	0	0.2	3	0.9	691.2	28.0	6.19	50.1
77	500	3600	0	0.3	3.1	0.8	695.4	27.4	6.19	49.8
78	600	3400	0	0.2	3	0.9	699.4	27.2	6.19	49.9
79	500	3500	0	0.2	3	0.8	703.3	27.2	6.19	49.4
80	600	3600	0	0.4	3.1	0.9	707.7	27.5	6.19	49.7
81	500	3700	0	0.5	3	0.8	711.9	27.7	6.19	50.7
82	600	3700	0	0.4	3	0.9	716.1	28.0	6.19	50.0
83	500	3800	0	0.3	3.1	0.8	720.3	28.2	6.19	49.6
84	600	4000	0.1	0.3	3	0.9	724.5	28.3	6.20	49.6
85	500	4700	0.1	0.9	4.9	1.1	731.4	28.5	6.18	49.5
86	600	4800	0	0.6	4.8	1.1	737.8	29.1	6.18	49.7
87	500	5300	0	0.5	4.9	1.2	744.3	29.5	6.18	49.8
88	600	5800	0	0.5	4.8	1.1	750.6	29.7	6.17	49.0
89	500	6400	0	0.7	4.9	1.1	744.6	29.6	6.17	51.2
90	600	6300	0	0.3	4.8	1.2	750.8	29.2	6.17	49.5
91	500	8300	0	0	4.9	1.1	756.7	27.8	6.18	34.4
92	600	4100	0	0	4.8	1.1	762.5	26.9	6.19	48.8
93	500	3700	0	0	4.8	1.2	755.8	26.6	6.20	50.1
94	600	3700	0	0	4.9	1.1	761.8	26.4	6.19	51.7
95	500	4100	0	0	4.8	1.1	767.6	26.3	6.18	48.0
96	600	4200	0	0.2	4.9	1.2	773.8	26.1	6.17	50.2
97	500	3900	0	0.3	7.1	1.1	769.6	26.0	6.17	48.8
98	600	3800	0	0.7	7.1	1.1	778.5	26.0	6.17	49.4
99	500	4000	0	0.5	5	1.2	785.1	26.1	6.17	49.2
100	600	4000	0	0.4	5	1.1	791.5	26.1	6.17	49.7
101	500	4400	0	0.4	5	1.1	785.4	26.1	6.17	55.2

Continued on Next Page...

B.2. Adaptive model predictive control run for maximum biomass

Table B.3 – Continued

Time (h)	Air (mL/h)	O2 (mL/h)	Acid (mL/h)	Base (mL/h)	Feed 2 (mL/h)	Feed 1 (mL/h)	Volume (mL)	Temp. (C)	pH (-)	DO (%)
102	600	4100	0	0.6	5	1.2	792.1	26.2	6.17	50.3
103	500	4100	0	0.4	5	1.1	798.5	26.2	6.17	49.9
104	600	4400	0	0.5	5	1.1	805.0	26.3	6.17	49.8
105	500	4500	0	0.3	5	1.2	798.9	26.1	6.17	55.7
106	600	4500	0	0.6	5	1.1	805.5	26.2	6.17	49.3
107	500	4400	0	0.5	5	1.1	812.0	26.2	6.17	49.4
108	500	4500	0	0.4	5	1.2	818.5	26.1	6.17	49.9
109	600	5000	0	0.3	5.5	1.1	812.7	25.9	6.17	57.5
110	500	4800	0	0.6	5.5	1.1	819.8	25.8	6.17	49.4
111	600	5100	0	0.4	5.4	1.2	826.8	25.7	6.17	49.6
112	500	5300	0	0.3	5.5	1.1	833.6	25.6	6.17	49.3
113	600	5800	0	0.4	5.6	1.1	828.0	25.5	6.17	56.3
114	500	5900	0	0.5	5.5	1.2	835.1	25.7	6.17	48.3
115	600	5900	0	0.6	5.4	1.1	842.1	25.8	6.17	50.1
116	500	6000	0	0.5	4.4	1.1	848.0	25.9	6.17	51.5
117	600	6700	0	0.2	4.4	1.2	841.0	25.7	6.17	52.4
118	500	6300	0	0.5	4.4	1.1	846.9	25.4	6.17	56.3
119	600	5800	0	0.7	4.4	1.1	853.0	25.7	6.17	49.0
120	500	5800	0	0.6	4.3	1.2	859.0	25.9	6.17	50.4
121	600	6200	0	0.4	7.5	0.8	855.0	25.8	6.17	59.2
122	500	5600	0	0.7	4.3	0.9	860.8	25.8	6.17	50.6
123	600	5700	0	0.5	3.3	0.8	865.3	25.8	6.17	47.3
124	500	6000	0	0.6	3.3	0.9	870.0	25.8	6.17	54.1
125	600	6600	0	0	3.3	0.8	861.4	25.7	6.18	57.1
126	500	5800	0	0.2	3.3	0.9	865.7	25.5	6.17	49.7
127	600	6100	0	0.7	3.3	0.8	870.4	25.4	6.17	51.4
128	500	6500	0	0.3	3.3	0.9	874.8	25.2	6.17	51.9
129	600	7400	0	0	3.3	0.8	866.2	25.0	6.18	60.5
130	500	6200	0	0.6	3.3	0.9	870.9	25.1	6.17	49.9
131	600	6600	0	0.7	3.3	0.8	875.6	25.1	6.17	53.4
132	500	6800	0	0.4	3.3	0.9	880.0	25.0	6.17	53.2
133	600	7600	0	0.2	3.2	0.5	871.2	25.2	6.17	63.1
134	500	6100	0	0.3	3.3	0.6	875.3	25.0	6.17	48.0
135	600	6200	0	0.8	3.3	0.6	879.9	25.0	6.16	48.2
136	500	6600	0	0.6	3.3	0.5	884.2	25.0	6.17	49.8
137	600	8400	0	0.1	3.3	0.6	875.4	25.2	6.17	48.5
138	500	8900	0	0.6	3.3	0.6	879.8	25.0	6.17	33.4
139	600	8900	0	0.2	0	0.5	880.3	25.0	6.17	43.2
140	500	8800	0.3	0	0	0.6	881.1	25.0	6.18	45.6
141	600	4400	1.3	0	0	0	869.7	25.0	6.21	81.3
142	500	5100	0	0	0	0	869.6	25.2	6.20	49.3
143	600	4600	1	0	0	0	870.5	25.1	6.20	59.1
144	500	3900	0	0	0	0	870.5	25.0	6.20	58.2
145	600	3100	0	0	0	0	857.8	25.0	6.21	55.8
146	500	2900	0	0	3.3	0	861.1	25.0	6.20	52.1
147	600	2900	0	0	3.3	0	864.3	25.0	6.18	49.6
148	500	3200	0	0.3	3.3	0	867.9	25.0	6.17	47.0
149	600	3200	0	0	3.2	0	858.4	25.0	6.17	55.6
150	500	2700	0	0.4	3.3	0	862.0	25.0	6.17	49.0
151	600	2700	0	0.6	3.3	0	865.9	25.0	6.17	50.7
152	500	2900	0	0.5	3.3	0	869.6	25.0	6.17	49.9
153	600	3700	0	0.4	3.3	0	860.7	25.0	6.17	59.3
154	500	3000	0	0.8	3.3	0	864.7	25.1	6.17	48.6
155	600	3100	0	0.5	3.3	0	868.5	25.1	6.17	48.1
156	500	3200	0	0.4	3.3	0	872.1	25.1	6.17	49.5
157	600	4100	0	0.3	4	0	863.7	25.1	6.17	60.4

Continued on Next Page...

Table B.3 – Continued

Time (h)	Air (mL/h)	O2 (mL/h)	Acid (mL/h)	Base (mL/h)	Feed 2 (mL/h)	Feed 1 (mL/h)	Volume (mL)	Temp. (C)	pH (-)	DO (%)
158	500	2800	0	0.7	4	0	868.4	25.1	6.17	51.7
159	600	2800	0	0.6	4	0	872.9	25.1	6.17	50.1
160	500	3400	0	0.4	4.1	0	877.4	25.1	6.17	47.4
161	4800	6000	0	0.3	4	0	868.9	25.1	6.17	39.6
162	2200	6000	0	0.5	4	0	873.3	25.1	6.17	50.6
163	1300	6000	0	0.3	4	0	877.4	25.1	6.17	52.7
164	1200	6000	0	1.2	4.1	0	882.6	25.1	6.18	50.4
165	1700	5900	0	0	4	0	873.9	25.1	6.20	57.2
166	14100	6000	0	0	4	0	877.6	25.1	6.20	80.9
167	9200	6000	0.5	0.3	0	0	878.2	25.1	6.21	81.2
168	8400	6000	0	0	0	0	877.9	25.1	6.21	80.6
169	8400	6000	0	0	0	0	865.1	25.1	6.21	79.6
170	8400	6000	0	0	0	0	864.9	25.1	6.21	77.0
171	8400	6000	0	0	0	0	864.6	25.1	6.21	75.1
172	8400	6000	0	0	0	0	864.4	25.1	6.21	76.3
173	8400	6000	0	0	0	0	851.6	25.1	6.21	78.2
174	8400	5900	0	0	0	0	851.4	25.1	6.22	78.1
175	8400	6000	0	0	0	0	851.1	25.1	6.21	73.9
176	8400	6000	0	0	0	0	850.9	25.1	6.21	75.3
177	8400	6000	0	0	0	0	838.1	25.1	6.20	83.2
178	8400	6000	0	0	0	0	837.9	25.1	6.20	83.5
179	8400	6000	0	0	0	0	837.6	25.1	6.19	83.6
180	8300	6000	0	0	0	0	837.4	25.1	6.19	85.0
181	8400	5900	0	0	0	0	824.6	25.1	6.19	87.9
182	8300	6100	0	0	0	0	824.4	25.1	6.18	88.1
183	8400	6000	0	0	0	0	824.1	25.1	6.18	91.1
184	8300	6000	0	0	0	0	823.9	25.1	6.18	92.3
185	8400	6100	0	0	0	0	811.1	25.1	6.19	89.7
186	8300	6000	0	0	0	0	810.8	25.1	6.19	93.4
187	8400	6100	0	0	0	0	810.6	25.1	6.20	94.5
188	8300	6000	0	0	0	0	810.4	25.1	6.20	95.9
189	8400	6100	0	0	0	0	797.6	25.1	6.21	97.1
190	6700	6000	0	0	4.5	0	801.9	25.1	6.20	100.8
191	6100	6000	0	0.1	0	0	801.8	25.1	6.18	90.2
192	6000	6100	0	0.5	0	0	802.1	25.1	6.17	87.7
193	6000	6000	0	0.5	26.1	0	815.9	25.1	6.17	90.7
194	6100	6100	0	0	0	0	803.1	25.1	6.18	94.2
195	6000	6000	0	0	0	0	802.9	25.1	6.17	92.5
196	6000	6000	0	0.1	0	0	802.8	25.1	6.17	88.7
197	5900	6100	0	0	0	0	790.0	25.1	6.17	99.7
198	5900	6000	0	0.3	0	0	790.1	25.1	6.17	100.6
199	6000	6100	0	0.2	0	0	790.2	25.1	6.17	100.1
200	5900	6000	0	0.2	0	0	790.2	25.1	6.17	100.3
201	5900	6100	0	0.1	0	0	777.5	25.1	6.17	108.0
202	6000	6000	0	0.3	0	0	777.6	25.1	6.17	108.4
203	5900	6000	0	0.1	0	0	777.5	25.1	6.17	109.6
204	5900	5900	0	0	0	0	777.3	25.0	6.18	117.1
205	6000	6000	0	0	0	0	764.5	25.1	6.19	217.0
206	5900	5900	0	0	0	0	764.3	25.1	6.19	253.9
207	5900	5900	0	0	0	0	764.2	25.0	6.19	260.7
208	5900	6000	0	0	0	0	764.0	25.0	6.20	267.4
209	6000	5900	0	0	33.4	0	784.6	25.1	6.21	272.2
210	5900	5900	0	0	0.6	0	785.0	25.1	6.21	245.0
211	5900	6000	0	0	0	0	772.2	24.9	6.21	240.2
212	6000	5900	0	0	0	0	772.0	24.9	6.20	256.1

B.2. Adaptive model predictive control run for maximum biomass

Table B.4: Experimental measurements for the Adaptive MPC culture

Time (h)	Biomass (g/L)		Glucose (g/L)		Oil content (%w/w)	
	Average	Std. dev.	Average	Std. dev.	Average	Std. dev.
0	3.1	0.10	18.6	0.35	68.4	1.0
4	3.1	0.05	18.6	0.11	70.6	1.8
8	3.7	0.05	21.8	0.04	67.1	4.1
12	4.0	0.10	24.9	0.02	66.0	1.2
16	4.1	0.10	31.3	0.09	61.7	2.8
20	4.2	0.30	36.3	0.06	60.7	1.4
24	4.5	0.10	36.2	0.05	58.8	1.4
28	5.0	0.10	35.0	0.04	51.9	1.5
32	6.0	0.05	33.1	0.09	41.9	0.5
36	6.4	0.00	31.4	0.02	41.1	2.9
40	8.1	0.15	29.2	0.04	42.5	1.8
44	8.8	0.20	25.5	0.06	35.9	0.8
48	12.3	0.05	20.0	0.14	33.6	1.6
52	16.3	0.25	12.3	0.07	37.7	2.1
56	16.8	0.45	6.2	0.13	37.1	1.8
60	23.9	0.10	0.1	0.00	38.3	1.3
64	27.6	0.05	0.1	0.00	38.3	2.9
68	30.6	0.00	0.1	0.01	34.5	4.3
72	33.3	0.20	2.1	0.01	35.3	1.2
88	60.0	0.25	0.2	0.00	32.9	0.6
92	66.5	0.51	1.3	0.01	37.5	1.1
96	71.5	0.45	5.3	0.15	39.6	2.1
100	76.3	0.05	13.0	0.03	46.3	2.7
104	78.9	0.10	16.2	0.20	46.4	1.4
108	80.7	0.05	19.5	0.36	49.0	1.5
112	90.7	0.45	26.6	0.24	44.5	3.7
116	92.0	0.61	30.4	0.00	47.0	1.3
120	98.3	0.15	35.0	0.15	48.3	3.4
124	103.8	1.67	37.1	0.11	48.2	0.5
128	103.5	1.82	37.9	0.03	53.1	5.0
132	109.3	2.17	39.1	0.13	51.9	3.5
136	108.8	0.10	40.0	0.11	53.0	3.7
140	111.7	0.66	34.4	0.02	49.0	1.6
144	109.2	0.56	20.2	0.02	55.3	2.7
148	108.1	0.51	19.5	0.26	59.2	6.4
152	116.6	1.52	24.4	0.53	56.1	3.0
156	110.5	1.67	27.2	0.13	51.0	4.3
160	112.1	0.30	34.1	0.98	55.0	1.7
164	121.8	1.57	45.6	0.17	54.5	3.3
168	123.8	0.66	44.5	0.19	52.0	6.7
172	126.9	1.77	34.7	0.19	50.9	1.1
176	125.8	0.56	26.0	0.63	59.0	1.7
180	125.0	0.96	17.6	0.06	57.8	2.3
184	128.5	1.26	10.2	0.37	56.4	2.8
188	129.3	0.40	1.7	0.04	59.7	4.2
192	128.0	0.25	2.3	0.39	59.1	13.5
192.5	131.5	2.78	15.4	0.25	54.1	7.7
196	139.3	1.26	8.4	0.51	61.7	11.3
200	139.6	1.01	3.6	0.05	50.1	0.0
204	137.5	0.96	0.2	0.07	52.4	1.3
208	138.5	0.00	0.2	0.21	51.3	1.0
210	144.3	0.20	0.4	0.14	49.4	3.1

B.3 Two-stage culture with glycerol/glucose feeding

The start-up medium was formulated according to Medium B4-Fe, as shown in Table 3.1, supplemented with glycine (0.4 g/L) and glycerol (10 g/L).

Nutrients were added to the culture in a fed-batch mode with two independent feeds. The nitrogen rich feed (Feed 1) consisted of an aqueous solution of glycine (150 g/L). The carbon rich feed (Feed 2a) contained KH_2PO_4 (50 g/L), $\text{MgSO}_4 \cdot 7\text{H}_2\text{O}$ (32 g/L), $\text{FeSO}_4 \cdot 7\text{H}_2\text{O}$ (1.27 g/L), disodium salt of EDTA (1.7 g/L), H_3BO_3 (0.31 g/L), $\text{CaCl}_2 \cdot 2\text{H}_2\text{O}$ (0.26 g/L), $\text{MnCl}_2 \cdot 4\text{H}_2\text{O}$ (0.2 g/L), $\text{ZnSO}_4 \cdot 7\text{H}_2\text{O}$ (23.3 mg/L), $\text{CuSO}_4 \cdot 5\text{H}_2\text{O}$ (8.5 mg/L), thiamine hydrochloride (1.06 mg/L), $\text{Na}_2\text{MoO}_4 \cdot 5\text{H}_2\text{O}$ (3.2 mg/L), and glycerols (1123 g/L). Another carbon rich feed (Feed 2b), used during the fattening stage (second stage), was formulated to contain only glucose at a concentration of 800 g/L.

The pH was controlled around 6.2 using a 500 g/L solution of K_2HPO_4 as base and a 200 g/L aqueous solution of KH_2PO_4 as acid. The dissolved oxygen concentration (DO) was controlled around 50% of the saturation value by bubbling air enriched with oxygen at the bottom of the reactor vessel.

B.3.1 Results

The flow-rates of all the gas and liquid streams as well as the hourly average process measurements are presented in Table B.5. The reported volume was calculated from the initial medium and inoculum volumes, accounting the amount of liquid added to the reactor and discounting the volume removed for each sample and the losses for evaporation (assumed proportional to the gas flowrate). The experimental measurements for biomass, glucose, and glycerol concentration are presented in Table B.6, as well as the intracellular neutral lipid content.

B.3. Two-stage culture with glycerol/glucose feeding

Table B.5: Flow rate and process conditions for the two-stage culture

Time (h)	Air (mL/h)	O ₂ (mL/h)	Acid (mL/h)	Base (mL/h)	Feed 2a (mL/h)	Feed 2b (mL/h)	Feed 1 (mL/h)	Volume (mL)	Temp. (C)	pH (-)	DO (%)
0	0	0	0	0	0	0	0	1104	24.99	6.17	52.62
1	200	0	0	0	0	0	0	1104	24.99	6.17	50.00
2	200	0	0	0	0	0	0	1104	24.99	6.17	49.56
3	200	0	0	0	0	0	0	1104	24.99	6.17	50.16
4	300	0	0	0.1	0	0.2	0	1092	24.99	6.17	49.98
5	400	0	0	0	0	0.1	0.3	1092	24.99	6.18	50.03
6	400	0	0	0	0	0.2	0.3	1093	24.99	6.18	50.06
7	300	0	0	0	0	0.1	0.2	1093	24.99	6.18	49.71
8	500	0	0	0	0	0.2	0.3	1081	24.99	6.18	50.25
9	400	0	0	0	0	0.1	0	1081	24.99	6.19	49.76
10	500	0	0	0	0	0.2	0	1081	24.99	6.20	50.08
11	700	0	0	0	0	0.1	0.3	1082	24.99	6.20	49.92
12	800	0	0	0	0	0.2	0.3	1070	24.99	6.21	50.08
13	800	0	0	0	0	0.3	0	1070	24.99	6.21	49.49
14	800	0	0	0	0	0.3	0	1070	24.99	6.22	49.89
15	1100	0	0	0	0	0.3	0	1070	24.99	6.21	49.18
16	1800	0	0	0	0	0.3	0	1058	24.99	6.21	48.82
17	3300	0	0	0	0	0.3	0.3	1059	24.99	6.21	48.31
18	3400	0	0	0	0	0.3	0	1059	24.99	6.21	49.51
19	4100	0	0	0	0	0.3	0	1059	24.99	6.21	48.65
20	5700	0	0	0	0	0.3	0.3	1047	24.99	6.21	47.90
21	6500	0	0	0	0	0.3	0.2	1047	24.99	6.21	49.58
22	6400	0	0	0	0	0.3	0	1048	24.99	6.21	49.58
23	7400	0	0	0	0	0.3	0.3	1048	24.99	6.20	49.85
24	7000	0	0	0	0	0.3	0.3	1036	24.99	6.20	49.98
25	7300	0	0	0	0	0.5	0.3	1037	24.99	6.20	49.57
26	7900	0	0	0	0	0.6	0.3	1037	24.99	6.20	48.88
27	8700	0	0	0	0	0.5	0.3	1038	24.99	6.20	49.04
28	9700	0	0	0	0	0.6	0.2	1026	24.99	6.20	48.44
29	10500	0	0	0	0	0.6	0.3	1027	24.99	6.19	49.13
30	11300	0	0	0	0	0.5	0.3	1028	24.99	6.19	48.55
31	12300	0	0	0	0	0.6	0.3	1028	24.99	6.18	48.83
32	14300	0	0	0	0	0.5	0.3	1016	24.99	6.18	49.32
33	14800	0	0	0	0	0.6	0.3	1017	24.99	6.17	50.01
34	17700	0	0	0	0	0.5	0.3	1017	24.99	6.17	51.97
35	18000	0	0	0.2	0	0.6	0.2	1018	24.99	6.17	52.45
36	18000	100	0	0.2	0	0.5	0.3	1006	24.99	6.17	51.12
37	18000	0	0	0.3	0	1	0.3	1008	24.99	6.17	50.57
38	18100	100	0	0.3	0	0.9	0.3	1009	24.99	6.17	49.64
39	18000	100	0	0.1	0	0.9	0.3	1010	25.00	6.17	49.99
40	18000	200	0	0.1	0	1	0.3	998	24.99	6.17	49.84
41	18000	200	0	0.1	0	0.9	0.2	999	25.00	6.17	49.76
42	18000	300	0	0.1	0	0.9	0.3	1000	25.00	6.17	49.45
43	18000	400	0	0.1	0	1	0.3	1001	25.00	6.17	49.57
44	18000	600	0	0.1	0	0.9	0.3	990	25.00	6.17	48.94
45	18100	700	0	0	0	0.9	0.3	991	25.00	6.18	49.66
46	18000	600	0	0	0	1	0.3	992	25.00	6.17	50.05
47	18000	800	0	0.1	0	0.9	0.2	993	25.00	6.17	49.43
48	18000	900	0	0.1	0	0.9	0.3	981	25.00	6.18	49.43
49	18000	700	0	0	0	0	0.6	981	25.00	6.18	52.60
50	18000	600	0	0	0	0	0.6	982	25.00	6.20	48.92
51	18100	500	0	0	0	0	0	981	25.00	6.22	50.91
52	18000	400	0.1	0	0	0	0	968	25.00	6.23	50.45
53	18000	400	0	0	0	0	0	968	25.00	6.23	50.64

Continued on Next Page...

Table B.5 – Continued

Time (h)	Air (mL/h)	O2 (mL/h)	Acid (mL/h)	Base (mL/h)	Feed 2a (mL/h)	Feed 2b (mL/h)	Feed 1 (mL/h)	Volume (mL)	Temp. (C)	pH (-)	DO (%)
54	18000	200	0	0	0	0	0	968	25.00	6.23	50.71
55	18000	200	0	0	0	0.3	0	968	25.00	6.22	50.16
56	18000	400	0	0	0	0.2	0.2	955	25.00	6.20	49.27
57	18100	600	0	0	0	0.3	0.3	956	25.00	6.20	48.80
58	18000	800	0	0	0	0.3	0.3	956	25.00	6.20	49.62
59	18000	700	0	0	0	0.3	0.3	956	25.00	6.21	49.48
60	18000	600	0	0	0	0.3	0	944	25.00	6.22	50.97
61	18000	600	0	0	0	0.4	0	944	25.00	6.22	50.62
62	18000	700	0	0	0	0.4	0.3	944	25.00	6.20	49.15
63	18100	900	0	0	0	0.5	0.3	945	25.00	6.20	48.95
64	18000	700	0	0	0	0.4	0	932	25.00	6.22	50.86
65	18000	700	0	0	0	0.4	0	932	25.00	6.22	50.47
66	18000	400	0	0	0	0.5	0	933	25.00	6.22	51.68
67	18000	700	0	0	0	0.4	0.2	933	25.00	6.20	48.22
68	18000	600	0	0	0	0.4	0	920	25.00	6.21	50.94
69	18000	600	0	0	0	0.5	0	921	25.00	6.22	50.35
70	18100	300	0	0	0	0.4	0	921	25.00	6.22	51.53
71	18000	500	0	0	0	0.5	0.3	921	25.00	6.20	49.09
72	18000	900	0	0	0	0.4	0.3	909	25.00	6.19	50.82
73	18000	1300	0	0	0	0.7	0.3	910	25.00	6.19	47.60
74	18000	1400	0	0	0	0.6	0.3	910	25.08	6.20	50.37
75	18000	1500	0	0	0	0.7	0.3	911	25.00	6.19	49.55
76	18100	1700	0	0	0	0.7	0.2	899	25.00	6.19	49.27
77	18000	1500	0	0	0	0.6	0	899	25.00	6.20	50.52
78	18000	1700	0	0	0	0.7	0.3	900	25.00	6.19	49.84
79	18000	1700	0	0	0	0.7	0.3	901	25.00	6.19	49.93
80	18000	1800	0	0	0	0.6	0.3	889	25.00	6.18	49.44
81	18000	2300	0	0	0	0.7	0.3	889	25.01	6.18	48.60
82	17800	2200	0	0.1	0	0.7	0.3	890	25.00	6.18	50.76
83	17500	2200	0	0.3	0	0.6	0.2	891	25.01	6.18	49.54
84	17600	2400	0	0	0	0.7	0.3	879	25.01	6.18	49.59
85	17600	2700	0	0	0	0.9	0.3	880	25.00	6.18	48.71
86	17600	2600	0	0.1	0	0.9	0.3	881	25.00	6.18	51.26
87	17500	2500	0	0.1	0	0.9	0.3	882	25.00	6.18	49.75
88	17600	2600	0	0	0	0.9	0.3	870	25.00	6.19	49.81
89	17600	3000	0	0	0	0.9	0.2	871	25.00	6.18	48.67
90	17600	2800	0	0	0	0.9	0.3	872	25.00	6.18	51.03
91	17600	2900	0	0.1	0	0.9	0.3	873	25.00	6.18	49.32
92	17500	3100	0	0	0	0.9	0.3	861	25.00	6.18	49.23
93	17600	3500	0	0.2	0	0.9	0.3	862	25.00	6.20	49.02
94	17600	3500	0	0	0	0.9	0.2	863	25.00	6.21	50.30
95	17600	3400	0	0	0	0.9	0.3	864	25.00	6.20	49.69
96	17500	4000	0	0	0	0.9	0.3	852	25.00	6.19	47.97
97	17600	4400	0	0.2	0	1.2	0.3	853	25.00	6.19	50.69
98	17600	3600	0	0	0	1.2	0.3	854	25.00	6.19	51.54
99	17600	4400	0.4	0.1	0	1.2	0.5	856	25.00	6.18	46.89
100	17500	5500	0	0	0	1.2	0.6	845	25.00	6.19	42.82
101	17600	6000	0	0	0	1.2	0.3	846	25.01	6.19	38.96
102	17600	6000	0	0	0	1.2	0.3	847	25.01	6.20	40.03
103	17600	6000	0	0	0	1.3	0.3	849	25.01	6.19	39.02
104	17500	6000	0	0	0	1.2	0.2	837	25.01	6.18	36.41
105	17600	6000	0	0.2	0	1.2	0.6	839	25.01	6.19	24.33
106	17600	6000	0	0	0	1.2	0.6	840	25.01	6.20	20.22
107	17600	6000	0	0	0	1.2	0.3	841	25.01	6.21	22.93
108	17500	6100	0	0	0	1.3	0.5	830	25.01	6.19	16.78
109	17600	6000	0	0	0	1.5	0.6	832	25.01	6.18	18.45

Continued on Next Page...

B.3. Two-stage culture with glycerol/glucose feeding

Table B.5 – Continued

Time (h)	Air (mL/h)	O2 (mL/h)	Acid (mL/h)	Base (mL/h)	Feed 2a (mL/h)	Feed 2b (mL/h)	Feed 1 (mL/h)	Volume (mL)	Temp. (C)	pH (-)	DO (%)
110	17600	6000	0	0.1	0	1.5	0.6	834	25.01	6.18	16.81
111	17600	6100	0.2	0.3	0	1.6	0.5	836	25.01	6.19	17.17
112	17600	6000	0.8	0	0	1.5	0.6	826	25.01	6.23	17.09
113	17500	6100	0	0	0	1.5	0.6	828	25.01	6.22	15.14
114	17600	6000	0	0	0	1.6	0.5	829	25.01	6.21	16.08
115	17600	6100	0	0	0	1.5	0.6	831	25.01	6.21	13.54
116	17600	6000	0	0	0	1.6	0.6	820	25.01	6.21	11.80
117	17500	6000	0	0	0	1.5	0.5	822	25.01	6.20	13.92
118	17600	6100	0	0	0	1.6	0.6	824	25.01	6.19	15.31
119	17600	6000	0	0	0	1.5	0.6	825	25.01	6.18	13.29
120	17600	7500	0	0.1	0	1.6	0.5	815	25.01	6.17	35.01
121	17500	8900	6.1	0.5	0	2	0.6	823	25.01	6.21	39.75
122	13000	6100	12.4	1.1	0	0	0	837	25.01	6.19	58.49
123	12300	5200	0	0.5	0	0	0	837	25.01	6.21	50.21
124	12300	5100	0	0	0	0	0	837	25.01	6.23	49.45
125	12400	5300	0	0	0	0	0	836	25.01	6.22	49.12
126	12300	5800	0	0	0	0	0	836	25.01	6.22	49.68
127	12300	5400	0	0	0	0	0	836	25.01	6.22	51.59
128	12300	4700	0	0	0	0	0	835	25.01	6.21	52.03
129	12300	4200	0	0	0	0	0	835	25.01	6.21	50.16
130	12300	3700	0	0	0	0	0	822	25.01	6.22	52.68
131	12300	3100	0	0	0	0	0	822	25.01	6.22	50.04
132	12300	3000	0	0	0	0	0	822	25.00	6.21	50.61
133	12300	4800	0	0	0	1.5	0.8	824	25.01	6.18	47.10
134	12300	5600	0	0	0	1.6	0.6	826	25.01	6.18	49.20
135	12300	6300	0	0	0	1.6	0.9	828	25.01	6.18	47.70
136	12300	7400	0	0	0	1.5	0.8	830	25.01	6.18	47.94
137	12300	7900	0	0	0	1.6	0.6	832	25.01	6.17	46.88
138	12300	8500	0	0.7	0	1.5	0.8	835	25.01	6.18	36.29
139	12300	8700	0	0	0	1.6	0.9	837	25.01	6.20	38.36
140	12300	8900	0	0	0	1.6	0.8	839	25.01	6.20	32.43
141	12300	9000	0	0	0	1.6	0.9	841	25.01	6.19	26.90
142	12300	9000	0	0	0	1.6	0.8	843	25.01	6.19	24.08
143	12300	9000	0	0	0	1.5	0.9	845	25.02	6.19	26.69
144	9700	8800	0	0	0	1.6	0.8	835	25.02	6.18	37.42
145	8800	8400	0	0	0	2.4	0.9	838	25.02	6.18	39.43
146	8800	8900	0	0	0	2.4	0.8	841	25.03	6.18	35.01
147	8700	8500	0	0	0	0	0	840	25.03	6.18	52.42
148	8800	8300	0	0	0	0	0	827	25.04	6.20	49.25
149	8800	6800	0	0	0	0	0	827	25.04	6.19	53.96
150	8800	7200	0	0	0	0	0	827	25.03	6.18	47.62
151	8800	7600	0	0	0	0	0	827	25.03	6.18	50.35
152	8800	6900	0	0	0	0	0	814	25.04	6.18	52.71
153	8800	5000	0	0	0	0	0	814	25.04	6.19	53.00
154	8800	5100	0	0	0	0	0	813	25.04	6.19	49.63
155	8700	5000	0	0	0	0	0	813	25.03	6.19	50.13
156	8800	4800	0	0	0	0	0	800	25.03	6.19	51.77
157	8800	4800	0.6	1	0	2.2	0.6	805	25.04	6.19	50.56
158	8800	5400	5.6	0	0	2.2	0.6	813	25.04	6.24	48.51
159	8800	6500	3.5	0	0	2.3	0.5	819	25.04	6.23	48.25
160	8800	7200	0.1	0	0	2.2	0.6	809	25.04	6.23	48.35
161	8800	7000	0	0	0	2.3	0.6	811	25.05	6.22	50.81
162	8800	8100	0	0	0	2.2	0.5	814	25.05	6.21	44.37
163	8800	8300	0	0	0	2.3	0.6	817	25.06	6.20	43.05
164	8700	8800	0	0	0	2.2	0.6	806	25.06	6.20	39.21
165	8800	8400	0	0	0	2.3	0.8	809	25.08	6.18	39.85

Continued on Next Page...

Table B.5 – Continued

Time (h)	Air (mL/h)	O2 (mL/h)	Acid (mL/h)	Base (mL/h)	Feed 2a (mL/h)	Feed 2b (mL/h)	Feed 1 (mL/h)	Volume (mL)	Temp. (C)	pH (-)	DO (%)
166	8800	8600	0	0.1	0	2.3	0.9	812	25.06	6.18	35.51
167	8800	8800	0	0	0	2.2	0.5	815	25.07	6.18	33.19
168	8800	8800	0	0	0	2.3	0.6	805	25.08	6.18	33.52
169	8800	8500	0	0	0	1.9	0.3	807	25.08	6.18	49.18
170	8800	8600	0.7	0	0	1.9	0.3	809	25.09	6.18	46.30
171	8800	8700	0	0.6	0	2	0.3	812	25.08	6.18	45.62
172	8700	8700	0	0	0	1.9	0.2	801	25.08	6.22	43.86
173	8800	8600	0	0	0	2	0.3	803	25.08	6.21	45.31
174	8800	8700	0	0	0	1.9	0.3	805	25.07	6.20	42.66
175	8800	8800	0	0	0	2	0.3	807	25.07	6.19	44.31
176	8800	8400	0	0	0	1.9	0.3	796	25.08	6.18	49.43
177	8800	7600	0	0.1	0	1.9	0.3	798	25.10	6.17	52.43
178	8800	7200	0	0	0	2	0.2	800	25.10	6.17	49.98
179	8800	6800	0	0.7	0	1.9	0.3	803	25.12	6.18	51.14
180	8800	7200	0	0	0	2	0.3	793	25.11	6.21	48.21
181	8700	5800	0	0	0	1.1	0	793	25.10	6.22	53.00
182	8800	5500	0	0	0	1.1	0	794	25.11	6.22	51.13
183	8800	5000	0	0	0	1.1	0	795	25.11	6.21	51.44
184	8800	4400	0	0	0	1.2	0	784	25.11	6.21	51.54
185	8800	3600	0	0	0	1.1	0	784	25.13	6.21	51.45
186	8800	3500	0	0	0	1.1	0	785	25.13	6.20	50.56
187	8800	3000	0	0	0	1.2	0	786	25.13	6.20	51.37
188	8800	2600	0	0	0	1.1	0	775	25.13	6.20	50.23
189	8700	2600	0	0	0	1.1	0	776	25.15	6.19	50.72
190	8800	2200	0	0	0	1.2	0	777	25.12	6.19	50.54
191	8800	2200	0	0	0	1.1	0	778	25.10	6.18	50.75
192	8800	1800	0	0	0	1.2	0	766	25.07	6.18	50.65
193	6400	1000	0	0.5	0	0	0	766	25.10	6.16	40.49
194	7800	1800	0	0	0	0	0	766	25.09	6.14	45.03
195	8800	1400	0	0	0	0	0	766	25.04	6.16	50.69
196	8800	1300	0	0	0	0	0	766	25.05	6.17	50.48
197	8800	1100	0	0	0	0	0	766	25.05	6.18	50.09
198	8700	1300	0	0	0	0	0	766	25.05	6.18	49.87
199	8800	1300	0	0	0	0	0	765	25.04	6.18	49.96
200	8800	3400	0	0	0	0	0	693	25.04	6.18	47.24
201	8800	4100	5.5	2.3	4.2	0	0	704	25.18	6.20	43.51
202	8800	7400	0	0	4.3	0	0	708	25.29	6.36	37.18
203	8800	8500	0	0	4.3	0	0	713	25.41	6.37	30.91
204	8800	8800	0	0	4.3	0	0	717	25.56	6.30	10.01
205	8800	8800	0	0	3.7	0	0	720	25.60	6.26	25.09
206	8800	8800	0	0	3.7	0	0	723	25.50	6.25	38.88
207	8700	8800	13.3	0	3.8	0	0	740	25.46	6.23	29.08
208	8800	8800	0	0	3.7	0	0	744	25.43	6.20	12.78
209	8800	8800	0	0.9	3.7	0	0	748	25.38	6.17	14.47
210	8800	8700	0.3	0	3.8	0	0	752	25.37	6.19	11.99
211	8800	8800	3.8	2.4	3.7	0	0	761	25.38	6.19	15.88
212	8800	8800	0	0	3.7	0	0	765	25.41	6.34	21.61
213	8800	8800	0	0	3.7	0	0	768	25.44	6.30	22.26
214	8800	8800	0	0	3.7	0	0	772	25.44	6.27	22.73
215	8700	8700	42.8	0	3.8	0	0	818	25.40	6.24	25.59
216	8800	8800	0.2	0	3.7	0	0	809	25.43	6.21	25.19
217	8800	8800	0	0.1	3.6	0	0	812	25.42	6.19	22.08
218	8800	8800	0	0	3.6	0	0	816	25.35	6.19	19.86
219	6400	8800	11.1	0	3.6	0	0	830	25.34	6.18	38.74
220	5300	8000	8.2	0	5.7	0	0	844	25.34	6.22	32.24
221	5300	7900	0	0	5.8	0	0	849	25.32	6.19	53.33

Continued on Next Page...

B.3. Two-stage culture with glycerol/glucose feeding

Table B.5 – Continued

Time (h)	Air (mL/h)	O2 (mL/h)	Acid (mL/h)	Base (mL/h)	Feed 2a (mL/h)	Feed 2b (mL/h)	Feed 1 (mL/h)	Volume (mL)	Temp. (C)	pH (-)	DO (%)
222	5200	7200	0	3.7	5.8	0	0	859	25.27	6.17	31.09
223	5300	8800	31.9	1.5	5.8	0	0	898	25.29	6.25	15.21
224	5300	8800	0	6.8	5.7	0	0	910	25.24	6.16	4.60
225	5300	8800	26.9	0	5.8	0	0	943	25.18	6.24	0.67
226	5200	8800	0	10.1	5.7	0	0	958	25.15	6.17	0.00
227	5300	8700	21.4	0	5.7	0	0	985	25.19	6.24	0.00
228	5300	8800	0	9.6	5.7	0	0	1000	25.19	6.16	0.00
229	5300	8800	38.9	0	4.6	0	0	1043	25.25	6.25	0.00
230	5200	8800	0	0	4.6	0	0	1048	25.37	6.21	0.01
231	5300	6600	16	0	4.7	0	0	1068	25.32	6.24	55.21
232	5300	3700	0	0	4.6	0	0	1073	25.17	6.22	47.80
233	5200	6800	0	0	4.6	0	0	1077	25.15	6.21	42.93
234	5300	7900	0	0	4.6	0	0	1082	25.14	6.21	49.58
235	5300	7500	0	0	4.6	0	0	1086	25.13	6.20	51.40
236	5300	7600	0	0	4.6	0	0	1090	25.12	6.19	48.52
237	5200	8600	0	0	4.7	0	0	1095	25.12	6.18	38.07
238	5300	8800	0	0	4.6	0	0	1099	25.12	6.17	25.56
239	5300	8800	0	4.2	4.6	0	0	1108	25.12	6.16	18.47
240	5300	8800	0	0	4.7	0	0	1112	25.12	6.19	19.42
241	5200	8800	0	0	4.4	0	0	1116	25.12	6.19	21.33
242	5300	8800	0	0	4.3	0	0	1120	25.11	6.18	21.29
243	5300	5000	0	0	4.4	0	0	1112	25.11	6.18	51.31
244	5300	7400	0	0.7	4.4	0	0	1117	25.12	6.17	19.36
245	5200	8800	0	2	0	0	0	1119	25.12	6.18	12.19
246	5300	8800	0	0	0	0	0	1119	25.10	6.18	2.74
247	5300	8700	0	14.2	0	0	0	1133	25.09	6.16	40.07
248	5200	3800	4.9	0	0	0	0	1125	25.19	6.31	65.82
249	5300	2600	0	0	0	0	0	1125	25.11	6.34	48.04
250	5300	6500	0	0	0	0	0	1124	25.10	6.33	30.98
251	5300	8800	0	0	0	0	0	1124	25.08	6.28	0.00
252	5200	8800	0	0	0	0	0	1124	25.07	6.23	0.00
253	5300	8800	0	0	4.1	0	0	1128	25.04	6.19	0.00
254	5300	8800	0	3.1	4.2	0	0	1135	25.04	6.17	0.00
255	5300	8800	0	6.1	4.1	0	0	1145	25.05	6.20	0.00
256	5200	8700	0	0	4.2	0	0	1136	25.05	6.23	0.00
257	5300	8800	0	0	4.1	0	0	1140	25.05	6.23	0.00
258	5300	8800	0	0	4.2	0	0	1144	25.04	6.23	0.00
259	5200	8800	0	0	4.2	0	0	1148	25.03	6.22	0.00
260	5300	8800	0	0	4.1	0	0	1152	25.03	6.21	0.00
261	5300	8800	0	0	4.2	0	0	1156	25.03	6.21	0.00
262	5300	8800	0	0	4.2	0	0	1160	25.03	6.20	0.00
263	5200	8800	0	0	4.1	0	0	1164	25.03	6.19	0.00
264	5300	8800	0	0	4.1	0	0	1155	25.03	6.19	0.00
265	5300	8300	0	0	3.9	0	0	1159	25.04	6.19	71.32
266	5300	4400	0	0	3.9	0	0	1163	25.05	6.21	54.83
267	5200	5600	0	0	0	0	0	1162	25.04	6.21	45.41
268	5300	5600	0	0	0	0	0	1162	25.04	6.22	51.99
269	5300	5400	0	0	0	0	0	1162	25.04	6.22	48.26
270	5200	6600	0	0	0	0	0	1162	25.03	6.22	47.01
271	5300	7600	0	0	0	0	0	1162	25.04	6.23	47.75
272	5300	8500	0	0	0	0	0	1149	25.04	6.24	46.67
273	5300	4500	0	0	0	0	0	1149	25.04	6.26	62.61
274	5200	4100	0	0	0	0	0	1149	25.04	6.28	46.24
275	5300	2100	3	0	0	0	0	1151	25.04	6.30	59.91
276	5300	900	0	0	0	0	0	1151	25.04	6.32	49.90
277	5300	2800	0	0	0	0	0	1151	25.04	6.34	40.77

Continued on Next Page...

Table B.5 – Continued

Time (h)	Air (mL/h)	O2 (mL/h)	Acid (mL/h)	Base (mL/h)	Feed 2a (mL/h)	Feed 2b (mL/h)	Feed 1 (mL/h)	Volume (mL)	Temp. (C)	pH (-)	DO (%)
278	5200	5800	0	0	0	0	0	1151	25.03	6.36	48.86
279	5300	1900	0	0	0	0	0	1151	25.01	6.37	61.63
280	5300	1700	0	0	0	0	0	1138	25.01	6.37	40.82
281	5300	7600	0	0	0	0	0	1138	25.01	6.36	31.03
282	5200	8800	0	0	0	0	0	1138	25.01	6.36	27.98
283	5300	8700	0	0	0	0	0	1138	25.01	6.36	23.73
284	5300	8800	0	0	0	0	0	1137	25.01	6.36	19.51
285	5200	8800	0	0	0	0	0	1137	25.02	6.36	15.87
286	5300	8800	0	0	0	0	0	1137	25.02	6.36	10.48
287	5300	8800	0	0	0	0	0	1137	25.02	6.36	7.85
288	5300	8800	0	0	0	0	0	1124	25.02	6.36	5.03
289	5200	4400	0	0	0	0	0	1124	25.02	6.36	57.66
290	5300	2600	2.5	0	0	0	0	1126	25.02	6.36	50.30
291	5300	2700	0	0	0	0	0	1126	25.02	6.36	49.81
292	5300	2600	0	0	0	0	0	1126	25.03	6.36	49.44
293	5200	2600	0	0	0	0	0	1126	25.03	6.36	49.14
294	5300	3200	0	0	0	0	0	1126	25.02	6.35	48.45
295	5300	3500	0	0	0	0	0	1125	25.02	6.35	50.07
296	5200	3500	0	0	0	0	0	1113	25.02	6.35	50.19
297	5300	3300	0	0	0	0	0	1113	25.02	6.34	50.76
298	5300	2600	0	0	0	0	0	1112	25.02	6.34	50.55
299	5300	2700	0	0	0	0	0	1112	25.02	6.33	49.52
300	5200	3300	0	0	0	0	0	1112	25.02	6.33	49.49
301	5300	3600	0	0	0	0	0	1112	25.02	6.32	48.30
302	5300	4000	0	0	0	0	0	1099	25.01	6.31	48.49
303	5200	5000	0	0	0	0	0	1099	25.02	6.31	47.70
304	5300	5600	0	0	0	0	0	1099	25.02	6.30	48.52
305	5300	6200	0	0	0	0	0	1099	25.02	6.30	50.12
306	5300	5800	0	0	0	0	0	1099	25.02	6.29	50.74
307	5200	5200	0	0	0	0	0	1098	25.02	6.29	51.59
308	5300	5200	0	0	0	0	0	1098	25.03	6.28	50.17
309	5300	4900	0	0	0	0	0	1098	25.03	6.27	50.49
310	5300	4800	0	0	0	0	0	1085	25.04	6.27	49.33

Table B.6: Experimental measurements for the two-stage culture

Time (h)	Biomass (g/L)		Glycerol (g/L)		Glucose (g/L)		Oil content (%w/w)	
	Average	Std. dev.	Average	Std. dev.	Average	Std. dev.	Average	Std. dev.
0	0.5	0.05	11.5	0.02	0.0	0	10.3	0.8
4	0.7	0.05	11.2	0.02	0.0	0	8.6	0.3
8	0.7	0.05	11.0	0.03	0.0	0	7.2	0.6
12	0.7	0.05	11.3	0.03	0.0	0	9.7	0.5
16	1.2	0.05	11.8	0.01	0.0	0	5.4	0.2
20	0.6	0.00	11.6	0.30	0.0	0	9.7	1.0
24	1.8	0.00	12.1	0.03	0.0	0	6.0	0.3
28	1.4	0.05	13.1	0.00	0.0	0	4.9	0.1
32	2.6	0.05	13.8	0.00	0.0	0	8.3	0.9
36	3.1	0.10	14.0	0.02	0.0	0	9.5	0.3
40	4.4	0.10	15.3	0.04	0.0	0	10.6	0.2
44	5.5	0.05	16.4	0.03	0.0	0	11.4	1.0

Continued on Next Page...

B.3. Two-stage culture with glycerol/glucose feeding

Table B.6 – Continued

Time (h)	Biomass (g/L)		Glycerol (g/L)		Glucose (g/L)		Oil content (%w/w)	
	Average	Std. dev.	Average	Std. dev.	Average	Std. dev.	Average	Std. dev.
48	6.6	0.10	17.0	0.01	0.0	0	11.5	1.0
52	4.6	0.00	14.4	0.01	0.0	0	13.1	0.4
56	5.1	0.05	13.2	0.03	0.0	0	13.1	0.4
60	7.6	0.00	12.2	0.02	0.0	0	13.2	0.6
64	9.5	0.00	11.8	0.00	0.0	0	13.2	0.9
68	9.9	0.00	11.4	0.01	0.0	0	13.1	0.7
72	10.5	0.40	11.0	0.01	0.0	0	14.3	0.6
76	11.1	0.10	10.9	0.00	0.0	0	13.7	0.8
80	11.1	0.15	11.5	0.02	0.0	0	13.4	0.7
84	11.3	0.15	11.4	0.02	0.0	0	12.5	0.8
88	12.9	0.51	12.2	0.10	0.0	0	12.4	0.5
92	14.3	0.05	12.7	0.01	0.0	0	12.2	0.7
96	15.0	0.05	13.1	0.01	0.0	0	12.3	0.3
100	12.9	0.20	14.1	0.01	0.0	0	13.3	0.3
104	15.6	0.10	15.8	0.01	0.0	0	11.5	0.8
108	17.3	0.05	17.2	0.00	0.0	0	11.0	0.4
112	19.5	0.45	19.9	0.01	0.0	0	10.7	0.3
116	20.8	0.20	22.2	0.07	0.0	0	10.4	0.4
120	22.5	0.25	24.7	0.01	0.0	0	10.1	0.4
129.5	26.3	0.45	16.4	0.05	0.0	0	11.1	0.5
144	33.4	0.96	17.4	0.05	0.0	0	11.1	0.3
148	33.6	0.10	16.5	0.06	0.0	0	12.4	0.3
152	35.6	0.20	11.3	0.03	0.0	0	12.2	0.7
156	35.6	0.10	5.9	0.00	0.0	0	13.6	0.3
160	38.8	0.56	9.1	0.06	0.0	0	13.4	0.3
164	39.3	0.05	12.4	0.04	0.0	0	14.8	1.0
168	41.4	0.10	15.4	0.03	0.0	0	14.6	0.7
172	42.6	0.25	17.5	0.01	0.0	0	14.4	0.4
176	45.0	0.15	20.0	0.05	0.0	0	16.0	0.6
180	45.5	0.05	22.0	0.15	0.0	0	15.2	0.7
184	47.2	0.30	21.1	0.02	0.0	0	16.0	0.5
188	48.1	0.05	21.5	0.02	0.0	0	17.6	0.7
192	48.5	0.25	22.6	0.01	0.0	0	17.3	0.3
200	47.2	1.72	15.3	0.06	0.2	0.02	18.4	1.3
216.4	83.0	0.56	0.5	0.14	0.2	0.05	26.4	1.4
242.5	78.4	0.91	0.0	0.00	35.6	0.08	40.1	2.6
248	76.1	1.21	0.6	0.25	29.9	0.17	43.3	1.4
256	73.4	0.30	0.4	0.42	33.2	0.14	42.4	1.4
264	71.0	0.20	0.0	0.00	54.5	0.02	47.6	1.6
272	69.8	0.61	0.3	0.49	57.0	0.07	50.2	3.5
280	67.7	0.71	0.0	0.00	51.3	0.01	50.8	0.9
288	73.8	0.66	0.0	0.00	39.7	0.06	44.3	1.3
296	79.5	0.25	0.0	0.00	13.3	NaN	50.5	1.9
302	83.5	0.30	0.0	0.00	6.3	NaN	56.8	5.1
310	87.7	0.56	0.0	0.00	0.0	NaN	56.7	2.6

B.3.2 Important observations

1. A glycerol-rich feed was pumped into the reactor during the first 200 hours.
2. At 201 h, the glycerol-rich feed was replaced by a glucose feed.
3. 60 mL of culture were withdrawn at time = 200 h.
4. The power supply to the building failed repeatedly around 194 – 196 h. As a result of this power failure the autosampler got stuck and no sample was collected (automatically) afterwards.
5. The autosampler was fixed and re-started after 248 h.

C

Matlab scripts

This appendix contains the MATLAB implementation of the numerical methods used in this work for parameter estimation, model prediction, and optimization, as well as several routines for data processing.

C.1 Simulation of batch and fed-batch cultures

Code listing C.1: Dynamic model of microalgal batch cultures

```
1 function df = Batch(t, x, k)
2 %-----%
3 % Dynamic model for algal growth in Batch Cultures %
4 %-----%
5 %           States %
6 %-----%
7 %   x(1) = s1 = Glycine concentration (g/L) %
8 %   x(2) = s2 = Glucose concentration (g/L) %
9 %   x(3) = x = Active biomass concentration (g/L) %
10 %   x(4) = p = Oil body concentration (g/L) %
11 %   x(5) = q = Intracellular Nitrogen concentration (g/L) %
12 %-----%
13 %           Parameters %
14 %-----%
15 %   k(1) = Ysx = yield substrate to biomass = 1 / Yxs
```

```

16 % k(2) = Ysp = yield substrate to product (oil)
17 % k(3) = Yqx = yield nitrogen (in quota) to biomass
18 % k(4) = km = maintenance constant
19 % k(5) = mu_max
20 % k(6) = k_c
21 % k(7) = k_q
22 % k(8) = rho_max
23 % k(9) = k_rho
24 % k(10) = pi_max
25 % k(11) = k_pi
26 % k(12) = Ypx
27 % k(13) = Kinh (glucose)
28 % k(14) = 1 / Kinh (nitrogen)
29 %-----%
30 %           Kinetic expressions           %
31 %-----%
32
33 q = x(5) / (x(3) + x(4) +x(5));
34 p = x(4) / (x(3) + x(4) +x(5));
35
36 rC = x(2) / (k(6) + x(2) + (((x(2))^2)/k(13)));
37
38 if t > 0
39     rN = q * exp((-k(14)*x(6)/t)) / (k(7) + q);
40 else
41     rN = 0;
42 end
43
44 r_mu = k(5) * rC * rN;
45
46 if x(1) >0
47     r_rho = k(8) * x(1) / (k(9) + x(1));
48 else
49     r_rho = 0;
50 end
51
52 r_pi = (1 - p) * (k(10) * x(2) / (k(11) + x(2)));
53
54 df = [ -r_rho*x(3,1);
55         -(k(1,1)*r_mu*x(3,1) - (k(4,1)*x(3,1)) - (k(2,1)*r_pi*x(3,1)));
56         r_mu * x(3,1);
57         r_pi * x(3,1) - (k(12)*r_mu*x(3,1));
58         (0.18658 * r_rho * x(3,1)) - (k(3,1)*r_mu*x(3,1));
59         q];

```

C.1. Simulation of batch and fed-batch cultures

Code listing C.2: Dynamic model of microalgal fedbatch cultures

```

1 function df = FedBatch(t, x, k, f)
2 %-----%
3 %           States
4 %-----%
5 %   x(1) = s1 = Glycine concentration (g/L)           %
6 %   x(2) = s2 = Glucose concentration (g/L)           %
7 %   x(3) = x = Active biomass concentration (g/L)     %
8 %   x(4) = p = Oil body concentration (g/L)           %
9 %   x(5) = q = Intracellular Nitrogen concentration (g/L) %
10 %-----%
11 %           Parameters
12 %-----%
13 %   k(1) = Ysx = yield substrate to biomass = 1 / Yxs
14 %   k(2) = Ysp = yield substrate to product (oil)
15 %   k(3) = Yqx = yield nitrogen (in quota) to biomass
16 %   k(4) = km = maintenance constant
17 %   k(5) = mu_max
18 %   k(6) = k_c
19 %   k(7) = k_q
20 %   k(8) = rho_max
21 %   k(9) = k_rho
22 %   k(10) = pi_max
23 %   k(11) = k_pi
24 %   k(12) = Yxp
25 %   k(13) = Kinh (glucose)
26 %   k(14) = 1 / Kinh (nitrogen)
27 %-----%
28 %           Feed rate
29 %-----%
30 %   u(1) = f(floor(t)+1, 1)/1000; % Glycine feed
31 %   u(2) = f(floor(t)+1, 2)/1000; % Glucose feed
32 %   u(3) = f(floor(t)+1, 3)/1000; % Output flowrate
33 %   u(4) = 150; % Glycine concentration in F1
34 %   u(5) = 900; % Glucose concentration in F2
35 %   D = (u(1) + u(2))/x(7);
36 %-----%
37 %           Kinetic expressions
38 %-----%
39
40 %   q = x(5) / (x(3) + x(4) + x(5));
41 %   p = x(4) / (x(3) + x(4) + x(5));
42
43 %   rC = x(2) / (k(6) + x(2) + ((x(2))^2)/k(13));
44
45 %   if t > 0
46 %       rN = q * exp(-(k(14)*x(6)/t)) / (k(7) + q);
47 %   else
48 %       rN = 0;
49 %   end
50
51 %   r_mu = max(0, k(5) * rC * rN); % Assume interacting kinetic model
52
53 %   r_rho = k(8) * x(1) / (k(9) + x(1));
54
55 %   r_pi = (k(10) * x(2) / (k(11) + x(2)));
56

```

```

57 %-----%
58 %           differential equations           %
59 %-----%
60
61 df = [(-r_rho*x(3,1)  +(u(4)*u(1)/x(7,1))  -(x(1,1)*D));
62        (-k(1,1)*r_mu*x(3,1) - (k(4,1)*x(3,1) - (k(2,1)*r_pi*x(3,1))...
63        + (u(5)*u(2)/x(7,1)) - (x(2,1)*D));
64        (r_mu * x(3,1) -(x(3,1)*D));
65        (r_pi * x(3,1) - (k(12)*r_mu*x(3,1) - (x(4,1)*D));
66        ((0.18658 * r_rho * x(3,1)) - (k(3,1)*r_mu*x(3,1) - (x(5,1)*D));
67        q;
68        ((x(7,1)*D) - u(3))];
69
70 %-----%
71 %   By: Hector De la Hoz Sieglar   (c) 2008-2011   %
72 %-----%

```

C.2 Estimation of model parameter values and confidence analysis

Code listing C.3: Residual error for a given set of model parameters

```

1  function Error = ErrP(k)
2
3      options = odeset('RelTol', 2.3e-14);
4
5      % Ensure that only positive values are passed to the function
6      k = (k + abs(k))/2;    % Negative values are converted to zero
7
8      % Model parameters are scalated to the proper values required
9      k(3,1) = k(3,1)/100;
10     k(7,1) = k(7,1)/100;
11     k(12,1) = k(12,1)/100;
12     k(4,1) = k(4,1)/24;
13     k(5,1) = k(5,1)/24;
14     k(8,1) = k(8,1)/24;
15     k(10,1) = k(10,1)/24;
16
17     ErrDat = zeros(11,1);
18
19     % Parallel for loop can be replaced for a classic for loop if
20     % parallel functionality is missed.
21     parfor j2=1:11
22         ErrDat(j2) = myErrJ(j2,k, options);
23     end
24
25     % Total residual error (for all datasets)
26     Error = sum(ErrDat);
27
28     % Compare if the current parameter set provides a better WSSE than the

```

C.2. Estimation of model parameter values and confidence analysis

```
29 % previous best paramter set.
30 load Temporal
31 if BestFcn > Error
32     BestFcn = Error;
33     kn = k;
34     save('Temporal.mat', 'kn', 'BestFcn');
35 end
36
37 function ErrJ = myErrJ(j, kf, options)
38
39     ErrJ = 0;
40
41     % Loading dataset
42     DataFile = ['Set-', int2str(j)]; % Non smoothed
43     % DataFile = ['smSet-', int2str(j)]; % SMOOTHED
44     load(DataFile);
45
46     % Specifying additional initial conditions
47     IniCond(5,1) = IniCond(5,1) - (IniCond(3,1) * kf(3,1));
48     IniCond(6,1)=0.015;
49
50     % Solving ODE system with RK 4th order
51     [T, x] = ode45(@(t,x) Batch(t,x,kf), Tsol, IniCond, options);
52
53     % Calculating the output variables
54     y(:,1) = x(:,3) + x(:,4) + x(:,5);
55     y(:,2) = x(:,2);
56     y(:,3) = 100 * (x(:,5) + (kf(3,1) * x(:,3))) ./ y(:,1);
57     y(:,4) = 100 * x(:,4) ./ y(:,1);
58
59     % Handling missing data and specifying the weight matrix
60     % yhat = yhat-sm; %SMOOTHED
61     % w_inv = ones(15,4)*diag(1 ./w-sm); %SMOOTHED
62     w_inv = 1 ./w; %Non smoothed
63
64     w_inv(isnan(yhat))=0;
65     w_inv(isnan(w_inv))=0;
66     yhat(isnan(yhat))=0;
67
68
69     % Computing the residual error (WSSE)
70     for i = 1:4
71         ErrJ = ErrJ + ((yhat(:,i) - y(:,i)))' * diag(w_inv(:,i)) * ...
72             (yhat(:,i) - y(:,i)))/1000;
73     end
```

C.2.1 Optimization of model parameter values

Code listing C.4: BFGS method for optimization

```
1 %-----%
2 %           Broyden-Fletcher-Goldfarb-Shano Optimization Method           %
3 %-----%
4 % This function optimize a multivariable function using the Golden      %
5 % Section line search, and the BFGS method.                             %
6 %-----%
7 % Inputs:   number of parameters (p)                                   %
8 % Outputs:  optimum input (f), cost function (J), states profile (x).    %
9 %-----%
10
11 function [f, J] = minBFGS(MyFun,ko)
12
13 % Function to be minimized ----- %
14 %       MyFun = 'OptFun';          %
15 %-----%
16
17 %----- Variable initialization -----%
18 p = length(ko);
19 phi = (1 + sqrt(5))/2;           % Golden Ratio
20 B = eye(p,p);
21 sk = zeros(p,1);
22 yk = zeros(p,1);
23 f = ko;
24 %-----%
25 %               ***   Main Routine   ***                               %
26 %-----%
27
28 tic
29 alpha = 0.001;
30 gradxo = gradF(MyFun, f);
31 Iter = 0;
32 Tol = 100;
33
34 while (Tol>1e-5) && (Iter<500)
35     pk = -B\gradxo;
36
37 %-----%
38 %               Line Search                                           %
39 %-----%
40     fGRs(1) = feval(MyFun,f);
41     GRs(1) = 0;
42     GRs(3) = alpha;
43     fGRs(3) = feval(MyFun,f + (GRs(3)*pk));
44
45     if fGRs(3) > fGRs(1)
46         while fGRs(3) > fGRs(1)
47             GRs(4) = GRs(3);
48             fGRs(4) = fGRs(3);
49             GRs(3) = (1/phi) * GRs(4);
50             fGRs(3) = feval(MyFun,f + (GRs(3)*pk));
51         end
52     else
```

C.2. Estimation of model parameter values and confidence analysis

```

53     GRs(4) = alpha*phi;
54     fGRs(4) = feval(MyFun,f + (GRs(4)*pk));
55     while fGRs(4) < fGRs(3)
56         GRs(3) = GRs(4);
57         fGRs(3) = fGRs(4);
58         GRs(4) = phi * GRs(4);
59         fGRs(4) = feval(MyFun,f + (GRs(4)*pk));
60     end
61 end
62
63 GRs(2) = GRs(4)*(1-(1/phi));
64 fGRs(2) = feval(MyFun,f + (GRs(2)*pk));
65
66 while abs((fGRs(4) - fGRs(1))/min(fGRs)) > 0.05
67     if fGRs(2) > fGRs(3)
68         GRs(1) = GRs(2);
69         GRs(2) = GRs(3);
70         GRs(3) = GRs(4)/phi;
71         fGRs(1) = fGRs(2);
72         fGRs(2) = fGRs(3);
73         fGRs(3) = feval(MyFun,f + (GRs(3)*pk));
74     else
75         GRs(4) = GRs(3);
76         GRs(3) = GRs(2);
77         GRs(2) = GRs(4)*(1-(1/phi));
78         fGRs(4) = fGRs(3);
79         fGRs(3) = fGRs(2);
80         fGRs(2) = feval(MyFun,f + (GRs(2)*pk));
81     end
82 end
83 %-----%
84 %                               New Optimum Estimate                               %
85 %-----%
86
87     fi = f + (0.5 * (GRs(3) + GRs(2)) * pk);
88
89     gradxp = gradF(MyFun, fi);
90
91     sk = fi - f;
92     yk = gradxp - gradxo;
93
94     B = B - ((B*sk)*(B*sk)')/(sk'*B*sk) + ((yk*yk')/(yk'*sk));
95
96     Tol = norm(sk,'inf');
97
98     f = fi;
99     gradxo = gradxp;
100     Iter = Iter +1;
101
102 end
103 toc
104
105 J = feval(MyFun, f);
106
107 disp('Number of iterations:');
108 disp(Iter);
109 disp('Final tolerance:');
110 disp(Tol);
111 disp('Optimum control input');

```

```

112 disp(f);
113 disp('Optimum cost function');
114 disp(J);
115
116 save('Optimum.mat','f','J')
117
118 %-----%
119 %   By: Hector De la Hoz Siegler (c) 2007-2011   %
120 %-----%

```

Code listing C.5: Numerical estimation of the gradient

```

1 %-----%
2 %           Gradient of a multivariable function           %
3 %-----%
4 %   Gradient is calculated using centered finite differences %
5 %-----%
6
7 function GradX = gradF(MyFun, X)
8
9 n=length(X);
10
11 GradX = zeros(n,1);
12
13 for i = 1:n
14     if X(i) == 0
15         h = 1/10000;
16     else
17         h = X(i)/10000;
18     end
19     Hx = X;
20     Hx(i)=X(i)+h;
21     yp = feval(MyFun, Hx);
22     Hx(i)=X(i)-h;
23     ym = feval(MyFun, Hx);
24     GradX(i) = (yp - ym)/(2 * h);
25 end
26
27 %-----%
28 %   By: Hector De la Hoz Siegler (c) 2007-2011   %
29 %-----%

```

Code listing C.6: Pattern search function call for parameter estimation

```

1 function [x,fval,exitflag,output] = PatSearch(x0,lb,ub)
2
3 % Estimate the value of model parameters x, through Pattern Search
4
5 options = psoptimset; % Start with the default options
6
7 % Modify options setting
8 options = psoptimset(options,'PollingOrder', 'Random');

```

C.2. Estimation of model parameter values and confidence analysis

```
9 options = psoptimset(options, 'SearchMethod', @MADSPositiveBasisNp1);
10 options = psoptimset(options, 'CompleteSearch', 'on');
11 options = psoptimset(options, 'Display', 'off');
12 options = psoptimset(options, 'OutputFcns', { [] });
13 options = psoptimset(options, 'PlotFcns', { @psplotbestf });
14
15 [x,fval,exitflag,output] = ...
16 patternsearch(@ErrP,x0,[],[],[],[],lb,ub,[],options);
```

C.2.2 Numerical estimation of the covariance matrix of parameter estimates

Code listing C.7: Numerical approximation of the Hessian matrix

```
1 function H = coHessian(INI, khat)
2
3 %-----%
4 % Covariance Hessian Matrix Computation %
5 % Method from: Marsili et al, 2003. %
6 % INI : Initial step size %
7 % khat : Estimated parameter vector %
8 % (c)Hector De la Hoz Siegler %
9 %-----%
10
11
12 % Step for calculation of finite differences is
13 % recalculated at each iteration.
14 % Global error of the method is O(h)6
15
16 nk = length(khat);
17
18 iter = 1;
19 eta(iter) = 1;
20 g(iter)=INI;
21 Hb = eye(nk);
22 tol = 1e-6;
23 IterMax = 200;
24 step = 1;
25 H = zeros(nk,nk);
26
27 d= zeros(nk,1);
28 while (eta(iter) > tol) && (iter < IterMax)
29
30 for h=1:nk
31     if khat(h) ≠ 0
32         d(h) = khat(h)/g(iter);
33     else
34         d(h) = tol;
35     end
36 end
37
38 for i = 1:nk
```

```

39 for j = 1:nk
40     if i == j
41         H(i,i) = Emm(khat, i, d(i));
42     elseif j > i
43         E = Emi_nj(khat, i, j, d(i), d(j));
44         H(i,j) = (1/8100)*(1/(d(i)*d(j)))* ((256*E(1,5)) - ...
45             (256*E(1,6)) - (40*E(1,3)) + (40*E(1,4)) + E(1,1) - E(1,2)) ...
46             - ((256*E(2,5)) - (256*E(2,6)) - (40*E(2,3)) + (40*E(2,4)) ...
47             + E(2,1) - E(2,2)) - ((10240*E(3,5)) - (10240*E(3,6)) - ...
48             (1600*E(3,3)) + (1600*E(3,4)) + (40*E(3,1)) - (40*E(3,2))) ...
49             + ((10240*E(4,5)) - (10240*E(4,6)) - (1600*E(4,3)) + ...
50             (1600*E(4,4)) + (40*E(4,1)) - (40*E(4,2))) + ((65536*E(5,5)) ...
51             - (65536*E(5,6)) - (10240*E(5,3)) + (10240*E(5,4)) + ...
52             (256*E(5,1)) - (256*E(5,2))) - ((65536*E(6,5)) - ...
53             (65536*E(6,6)) - (10240*E(6,3)) + (10240*E(6,4)) + ...
54             (256*E(6,1)) - (256*E(6,2))));
55     else
56         H(i,j) = H(j,i); % Hessian is symmetric
57     end
58 end
59 end
60
61     g(iter + 1) = g(iter) + step;
62     eta(iter + 1) = norm(Hb-H, inf);
63     Hb = H;
64     iter = iter + 1;
65
66 end
67
68 save('HessHat', 'H');

```

Code listing C.8: Second derivative for symmetric elements

```

1 function H = Emm(khat, i, di)
2
3     k = khat;
4
5     k(i) = khat(i) + di;
6     Ep = ErrP(k);
7
8     k(i) = khat(i) - di;
9     Em = ErrP(k);
10
11     En = ErrP(khat);
12
13     w1 = (Ep - (2 * En) + Em)/(di ^ 2);
14
15     k(i) = khat(i) + (di / 2);
16     Ep = ErrP(k);
17
18     k(i) = khat(i) - (di / 2);
19     Em = ErrP(k);
20
21     w2 = (Ep - (2 * En) + Em)/((di / 2) ^ 2);
22     H = ((4 * w2) - w1) / 3;

```

C.2. Estimation of model parameter values and confidence analysis

Code listing C.9: Second derivative for asymmetric elements

```
1 function E = Emi_nj(khat, i, j, di, dj)
2
3     k = khat;
4
5     k(j) = khat(j) + dj;
6
7     k(i) = khat(i) + di;
8     E(1,1) = ErrP(k);
9
10    k(i) = khat(i) - di;
11    E(2,1) = ErrP(k);
12
13    k(i) = khat(i) + (di / 2);
14    E(3,1) = ErrP(k);
15
16    k(i) = khat(i) - (di / 2);
17    E(4,1) = ErrP(k);
18
19    k(i) = khat(i) + (di / 4);
20    E(5,1) = ErrP(k);
21
22    k(i) = khat(i) - (di / 4);
23    E(6,1) = ErrP(k);
24
25    %-----
26
27    k(j) = khat(j) - dj;
28
29    k(i) = khat(i) + di;
30    E(1,2) = ErrP(k);
31
32    k(i) = khat(i) - di;
33    E(2,2) = ErrP(k);
34
35    k(i) = khat(i) + (di / 2);
36    E(3,2) = ErrP(k);
37
38    k(i) = khat(i) - (di / 2);
39    E(4,2) = ErrP(k);
40
41    k(i) = khat(i) + (di / 4);
42    E(5,2) = ErrP(k);
43
44    k(i) = khat(i) - (di / 4);
45    E(6,2) = ErrP(k);
46
47    %-----
48
49    k(j) = khat(j) + (dj / 2);
50
51    k(i) = khat(i) + di;
52    E(1,3) = ErrP(k);
53
54    k(i) = khat(i) - di;
55    E(2,3) = ErrP(k);
56
```

```

57     k(i) = khat(i) + (di / 2);
58     E(3,3) = ErrP(k);
59
60     k(i) = khat(i) - (di / 2);
61     E(4,3) = ErrP(k);
62
63     k(i) = khat(i) + (di / 4);
64     E(5,3) = ErrP(k);
65
66     k(i) = khat(i) - (di / 4);
67     E(6,3) = ErrP(k);
68
69     %-----
70
71     k(j) = khat(j) - (dj / 2);
72
73     k(i) = khat(i) + di;
74     E(1,4) = ErrP(k);
75
76     k(i) = khat(i) - di;
77     E(2,4) = ErrP(k);
78
79     k(i) = khat(i) + (di / 2);
80     E(3,4) = ErrP(k);
81
82     k(i) = khat(i) - (di / 2);
83     E(4,4) = ErrP(k);
84
85     k(i) = khat(i) + (di / 4);
86     E(5,4) = ErrP(k);
87
88     k(i) = khat(i) - (di / 4);
89     E(6,4) = ErrP(k);
90
91     %-----
92
93     k(j) = khat(j) + (dj / 4);
94
95     k(i) = khat(i) + di;
96     E(1,5) = ErrP(k);
97
98     k(i) = khat(i) - di;
99     E(2,5) = ErrP(k);
100
101     k(i) = khat(i) + (di / 2);
102     E(3,5) = ErrP(k);
103
104     k(i) = khat(i) - (di / 2);
105     E(4,5) = ErrP(k);
106
107     k(i) = khat(i) + (di / 4);
108     E(5,5) = ErrP(k);
109
110     k(i) = khat(i) - (di / 4);
111     E(6,5) = ErrP(k);
112
113     %-----
114
115     k(j) = khat(j) - (dj / 4);

```

C.2. Estimation of model parameter values and confidence analysis

```
116
117     k(i) = khat(i) + di;
118     E(1,6) = ErrP(k);
119
120     k(i) = khat(i) - di;
121     E(2,6) = ErrP(k);
122
123     k(i) = khat(i) + (di / 2);
124     E(3,6) = ErrP(k);
125
126     k(i) = khat(i) - (di / 2);
127     E(4,6) = ErrP(k);
128
129     k(i) = khat(i) + (di / 4);
130     E(5,6) = ErrP(k);
131
132     k(i) = khat(i) - (di / 4);
133     E(6,6) = ErrP(k);
```

C.2.3 Confidence intervals and confidence regions

Code listing C.10: Preparation of matrices for generating confidence regions

```
1 function PlotConfidence(H, N, np, Ph, Eph, Conf, model)
2
3 %-----%
4 % Plot confidence regions for parameter estimation %
5 % H : Hessian Matrix for Covariance estimation %
6 % N : Number of experimental data points %
7 % np : Number of parameters %
8 % ph : Estimated parameters %
9 % Eph : Error residual for the estimated set of parameters %
10 % Conf : Confidence level %
11 % model: String with model name (used for placing labels) %
12 % (c)Hector De la Hoz Siegler %
13 %-----%
14
15 Area = 0;
16 AvArea = [];
17
18 Wf = Ph;
19 Wr = [];
20 Wl = [];
21
22 for i=1:np
23     Wl = [Wl Wf];
24     Wr = [Wr; Wf'];
25 end
26
27 for k = 1:max(size(Conf))
28     A = ((N - np)/np) * (1/(2 * Eph * finv(1-Conf(k), np, N-np))) * H;
29     Ascale = Wl .* A .* Wr;
30     for i = 1:np
```

```

31     for j = 1:np
32         if j > i
33             A22 = [Ascale(i,i) Ascale(i,j); Ascale(j,i) Ascale(j,j)];
34             [Areai] = Ellip2Plot (A22, [1 1], i, j, model);
35             if k == 1
36                 Area = Area + Areai;
37                 AvArea = [AvArea Areai];
38             end
39         end
40     end
41 end
42 end
43
44 [-, Da] = eig(Ascale);
45 ev = diag(Da);
46 la = 1./ sqrt(ev);
47 MagConf = norm(la);
48
49 % Individual parameters confidence interval (Student's T distribution)
50 Ch = 2 * Eph * inv(H)/(N - np);
51 factor = tinv(1-(Conf(1)/2),N-np);
52 for k=1:np
53     Δ = factor * (Ch(k,k))^(0.5);
54     Pbound(k,1) = Ph(k) - Δ; % Lower bound
55     Pbound(k,2) = Ph(k) + Δ; % Upper bound
56 end
57
58 disp('Individual confidence limits for alpha =')
59 disp(Conf(1))
60 disp(' ')
61 disp(Pbound)
62
63 disp('Total area enclosed for confidence regions')
64 disp(' ')
65 disp(Area)
66
67 disp('Average area enclosed for confidence regions')
68 disp(' ')
69 disp(mean(AvArea))
70
71 Lema = ['Norm of semiaxes of the confidence hyperellipsoid, d = ', ...
72     num2str(np)];
73 disp(Lema)
74 disp(MagConf)

```

Code listing C.11: Generation of an ellipse from a symmetric 2x2 matrix

```

1 function [Area] = Ellip2Plot (K, Xo, i, j, model)
2
3 %-----%
4 % This function generates a plot of a 2 x 2 matrix %
5 % % %
6 % The plot is centered around Xo %
7 % K is a 2x2 matrix %
8 % i, j, and model are used to label the axis of %
9 % the plot. (c) Hector De la Hoz Siegler %

```

C.2. Estimation of model parameter values and confidence analysis

```

10 %-----%
11
12 [V,D] = eig(K);
13 ev = diag(D);
14
15 figure(i*100 + j)
16 set(gcf, 'Position', [759 257 441 427])
17 hold on
18
19 if min(ev)> 0    % Matrix represents an ellipse
20
21     l = 1./sqrt(ev);
22     Area = l(1)*l(2)*pi();
23     W = V * l/sqrt(D);
24
25     t = linspace(0,2*pi,1000);
26     % Zm = linspace(1000,1000,1000);
27
28     plot((Xo(1) + W(1,1) .* cos(t) + W(1,2) .* sin(t)), (Xo(2) ...
29           + W(2,1) .* cos(t) + W(2,2) .* sin(t)), '-k', 'LineWidth',2);
30
31 else    % Confidence region is not an ellipse
32
33     af = num2str(K(1,1));
34     bf = num2str(K(2,1));
35     cf = num2str(K(2,2));
36     Xof1 = num2str(Xo(1));
37     Xof2 = num2str(Xo(2));
38
39     f = inline( [af '(x -' Xof1 ')^2 + 2*' bf '(x -' ...
40               Xof1 ')*(y -' Xof2 ') + ' cf '(y -' Xof2 ')^2 - 1'], 'x', 'y');
41
42     implot(f, [-1 3 -1 3], 100)
43     Area = -1;
44 end
45
46 set(gca, 'FontSize', 18, 'FontName', 'Times')
47 LabelX = myLabel(model, i);
48 LabelY = myLabel(model, j);
49 xlabel(LabelX, 'FontName', 'Times', 'FontSize', 20)
50 ylabel(LabelY, 'FontName', 'Times', 'FontSize', 20)
51 axis equal
52 ylim([0.5 1.5])
53 hold off
54 axis equal
55 ylim([0 2])
56 xlim([0 2])
57 set(gca, 'OuterPosition', [0.065 0.12 0.97 0.9])
58 set(gca, 'Position', [0.2 0.2 0.75 0.75])
59
60
61 function axLabel = myLabel(MyModel, ix)
62
63 switch MyModel
64     case 'Final'
65         switch ix
66             case 1
67                 axLabel = 'Y_{x/s} / Y^{*}_{x/s}';
68             case 2

```

```

69         axLabel = 'Y_{p/s} / Y^{*}_{p/s}';
70     case 3
71         axLabel = 'Y_{x/q} / Y^{*}_{x/q}';
72     case 4
73         axLabel = 'k_m / k^{*_m}';
74     case 5
75         axLabel = '\mu_m / \mu^{*_m}';
76     case 6
77         axLabel = 'K_{s_2} / K^{*_s_2}';
78     case 7
79         axLabel = 'K_{q} / K^{*_q}';
80     case 8
81         axLabel = '\rho_m / \rho^{*_m}';
82     case 9
83         axLabel = 'K_{s_1} / K^{*_s_1}';
84     case 10
85         axLabel = '\pi_m / \pi^{*_m}';
86     case 11
87         axLabel = 'K_{s_2}^{\pi} / K_{s_2}^{\pi*}';
88     case 12
89         axLabel = 'Y_{x/p} / Y^{*_x/p}';
90     case 13
91         axLabel = 'K_{i2} / K^{*_i2}';
92     case 14
93         axLabel = 'K_{i1} / K^{*_i1}';
94     otherwise
95         axLabel = 'Check Model';
96     end
97 otherwise
98     axLabel = num2str(ix);
99 end

```

Code listing C.12: Generation of a plot from any implicit function

```

1 function implot(fun,rangexy,ngrid)
2
3 %-----%
4 % Implicit plot function - A.Jutan UWO 2-2-98 ajutan@julian.uwo.ca %
5 % %
6 % fun is 'inline' function f(x,y)=0 %
7 % rangexy =[xmin,xmax,ymin,ymax] %
8 % range over which x and y is plotted default(-2*pi,2*pi) %
9 % ngrid is the number of grid points used to calculate the plot, %
10 % Start with course grid (ngrid =20) and then use finer grid %
11 % default ngrid=50 %
12 %-----%
13
14 if nargin == 1 ;% grid value and ranges not specified
15     rangexy=[-2*pi,2*pi,-2*pi,2*pi];
16     ngrid=50;
17 end
18
19 if nargin == 2; % grid value not specified
20     ngrid=50;
21 end
22

```

C.3. Determination of optimal feeding profiles to fed-batch cultures

```
23 % get 2-D grid for x and y
24 xm=linspace(rangexy(1),rangexy(2),ngrid);
25 ym=linspace(rangexy(3),rangexy(4),ngrid);
26 [x,y]=meshgrid(xm,ym);
27
28 % vectorize the inline function to handle vectors of x y
29 fvector=vectorize(fun);
30
31 %calculate with feval-this works if fvector is an m file too
32 fvalues=feval(fvector,x,y);
33
34 % plot single contour at f(x,y)=0, blue lines
35 contour(x,y,fvalues,[0,0],'b-');
36 xlabel('x');ylabel('y');
37 grid
```

C.3 Determination of optimal feeding profiles to fed-batch cultures

Code listing C.13: Pattern search calling function

```
1 function [x,fval,exitflag,output] = OptFlow(x0, fm1, tml, k)
2
3 % tml: current culture time
4 % fm1: flowrate (per hour) as implemented up to time tml
5 % k: current estimated value of model parameters
6
7 lb = zeros(length(x0),1);
8 ub = ones(length(x0),1);
9
10 % Optimizer options
11 options = psoptimset;
12 options = psoptimset(options,'InitialMeshSize', 0.1);
13 options = psoptimset(options,'PollMethod', 'MADSPositiveBasis2N');
14 options = psoptimset(options,'PollingOrder', 'Success');
15 options = psoptimset(options,'SearchMethod', @GPSPositiveBasisNp1);
16 options = psoptimset(options,'CompleteSearch', 'on');
17 options = psoptimset(options,'Display', 'iter');
18 options = psoptimset(options,'OutputFcns', { [] });
19 options = psoptimset(options,'PlotFcns', { @psplotbestf @psplotbestx });
20 options = psoptimset(options,'Vectorized', 'off');
21 options = psoptimset(options,'UseParallel', 'always');
22
23 [x,fval,exitflag,output] = ...
24 patternsearch(@(p) SolBatch(p, fm1, tml, k), x0, [], [], [], [], lb, ub, [], options);
```

Code listing C.14: Determination of culture productivity

```

1 function MyObj = SolBatch(p, fml, tml, k, varargin)
2
3 % p: normalized flow rate vector
4 % tml: current culture time
5 % fml: flowrate (per hour) as implemented up to time tml
6 % k: current estimated value of model parameters
7
8 optargin = size(varargin,2);
9 if optargin == 1
10     PlotMe = varargin{1}; % Do plot Solution
11     LINEPLOT = '-k';
12 elseif optargin == 2
13     PlotMe = varargin{1};
14     LINEPLOT = varargin{2};
15 else
16     PlotMe = 0; % Do not plot Solution
17 end
18
19 Tcult = 192; % Scheduled culture time
20 Tmax = Tcult - tml; % Remaining Culture time in hours
21 TimeStep = 2*Tmax/length(p);
22
23 fmin=zeros(length(p),1);
24 fmax=[0.5*ones(length(p)/2,1); 10*ones(length(p)/2,1)] ;
25 p = fmin + p.*(fmax - fmin);
26
27 % Initial Conditions for current batch
28 iniBiomass = 2;
29 IniCond = [0.1; % Glycine
30            20; % Glucose
31            (1 - 0.35 - 0.01)*iniBiomass; % Biomass
32            0.35*iniBiomass; % Oil
33            0.01*iniBiomass; % Cellular quota
34            0.01; % Past quota
35            0.72]; % Volume (L)
36 IniCond(5,1) = max(0,IniCond(5,1) - (IniCond(3,1) * k(3,1)));
37
38 SampleVol = 12.6; %Sample volume (estimated)
39
40 t = linspace(0,tml+Tmax,tml+Tmax+1)';
41 for i = 1:length(p)/2
42     f(TimeStep*(i-1)+1:(TimeStep)*i, 1) = p(i) * ones(TimeStep,1);
43     f(TimeStep*(i-1)+1:(TimeStep)*i, 2) = p((length(p)/2)+i) *...
44         ones(TimeStep,1);
45     f(TimeStep*(i-1)+1:(TimeStep)*i, 3) = p(i) * zeros(TimeStep,1);
46     f(TimeStep*(i-1)+1, 3) = SampleVol;
47     f(TimeStep*(i-1)+1+4, 3) = SampleVol;
48     f(TimeStep*(i-1)+1+8, 3) = SampleVol;
49 end
50 f(Tmax+1,:) = f(Tmax,:);
51
52 f = [fml ; f]; % Ensemble together previous and future flowrates
53
54 % Solve ODE system
55 options = odeset('RelTol', 2.3e-14);
56 [T, x] = ode45(@(t,x) FedBatch(t,x,k,f), t, IniCond, options);

```

C.3. Determination of optimal feeding profiles to fed-batch cultures

```

57
58
59 %% - Output Calculation
60 y(:,1) = x(:,3) + x(:,4) + x(:,5);           % Biomass
61 y(:,2) = x(:,2);                             % Glucose
62 y(:,3) = (x(:,5) + (k(3,1) * x(:,3))) ./ y(:,1); % Nitrogen Quota
63 y(:,4) = x(:,4) ./ y(:,1);                   % Oil
64 y(:,5) = x(:,1);                             % Glycine
65
66
67 Poil = x(Tcult + 1, 4) / Tcult;               % Oil productivity
68 Pbio = y(Tcult + 1, 1) / Tcult;               % Biomass productivity
69
70 % Select which variable to optimize
71 MyObj = - Pbio;
72
73
74 %% - Plot subroutines
75
76 if PlotMe == 1
77
78     q = x(:,5) ./ (x(:,3) + x(:,4) + x(:,5));
79     r_mu = k(5) * (q.*exp(-(k(14)*x(:,6)./T))) ./ (k(7) + q)) .* ...
80         (x(:,2) ./ (k(6) + x(:,2) + ((x(:,2)).^2)/k(13)))) ;
81
82     figure(984);
83
84     subplot(2,3,1); hold on
85     title('Biomass Profile'); plot(T, y(:,1), LINEPLOT);
86     ylabel('TSS(g/L)'); hold off
87
88     subplot(2,3,2); hold on
89     title('Glycine Profile'); plot(T, y(:,5), LINEPLOT);
90     ylabel('Glycine(g/L)'); hold off
91
92     subplot(2,3,3); hold on
93     title('Glucose Profile'); plot(T, y(:,2), LINEPLOT);
94     ylabel('Glucose(g/L)'); hold off
95
96     subplot(2,3,4); hold on
97     title('Cell quota Profile'); plot(T, y(:,3), LINEPLOT);
98     ylabel('g of Nitrogen / g of biomass'); hold off
99
100    subplot(2,3,5); hold on
101    title('Oil Profile'); plot(T, y(:,4), LINEPLOT);
102    ylabel('g of oil / g of biomass'); hold off
103
104    subplot(2,3,6); hold on
105    title('Volume'); plot(T, 1000*x(:,7), LINEPLOT);
106    ylabel('mL'); hold off
107
108    figure(985); hold on
109    plot(T, r_mu,LINEPLOT);
110    hold off
111 end

```

Code listing C.15: Feeding rate and set points to implement in the culture

```

1 function [F1 F2] = Flow_R10(p)
2
3     % Scheduled culture time in hours
4     Tmax = 192;
5
6     TimeStep = 2*Tmax/length(p);
7     fmin=zeros(length(p),1);
8     fmax=[0.5*ones(length(p)/2,1); 10*ones(length(p)/2,1)] ;
9
10    % Scale normalized flow to mL/h
11    p = fmin + p.*(fmax - fmin);
12
13    % Distribute flow on a per hour basis
14    for i = 1:length(p)/2
15        f(TimeStep*(i-1)+1:(TimeStep)*i, 1) = p(i) * ones(TimeStep,1);
16        f(TimeStep*(i-1)+1:(TimeStep)*i, 2) = p((length(p)/2)+i) * ...
17            ones(TimeStep,1);
18        f(TimeStep*(i-1)+1:(TimeStep)*i, 3) = p(i) * zeros(TimeStep,1);
19    end
20
21    % Nitrogen substrate flow rate
22    F1(:,2) = f(:,1); % Flow rate in mL/h
23    F1(:,1) = round(F1(:,2) / (1.700878103/60)); % Seconds pump is ON
24
25    % Carbon substrate flow rate
26    F2(:,4) = f(:,2); % flow rate in mL/h
27    F2(:,2) = 20; % Pump set point (%)
28    F2(1:100,2) = 10; % Pump set point (%)
29    F2(:,3) = 2.096666666666666e-03; % Pump flow rate at 10%
30    % Seconds pump must be ON
31    F2(:,1) = (round(F2(:,4) ./ F2(:,3))) ./ (F2(:,2)/10);

```

C.4 Cell count

Code listing C.16: Data reading from .Z2 file

```

1 function [dilF,sVol,binDiam,binHeight,TL,TU>TotalCount,aboveCount]...
2     = CellCounter(filename)
3
4 % ----- %
5 % filename = Name of '#Z2' file %
6 % dilF     = Dilution factor   %
7 % sVol     = Sample volume (most of the time 500 uL) %
8 % binDiam  = Diameter bins     %
9 % binHeight = Height bins      %
10 % ----- %
11
12 %% open the file for reading
13 fid = fopen(filename);
14
15 %% Get first strings
16 aWord = fscanf(fid,'%s \n', 1) ;
17
18 %% Read number of bins
19 while ~(strcmp(aWord,'nBins='));
20     aWord = fscanf(fid,'%s', 1) ;
21 end
22 nBins = fscanf(fid,'%d',1);
23 binHeight = zeros(nBins,1);
24 binDiam = zeros(nBins,1);
25
26 %% Read dilution factor
27 while ~(strcmp(aWord,'DilF='));
28     aWord = fscanf(fid,'%s', 1) ;
29 end
30 dilF = fscanf(fid,'%d',1);
31
32 %% Read Sample Volume
33 while ~(strcmp(aWord,'AnalyticVol='));
34     aWord = fscanf(fid,'%s', 1) ;
35 end
36 sVol = fscanf(fid,'%d',1);
37
38 %% Read Total Count and limits
39 while (length(aWord) < 15);
40     aWord = fscanf(fid,'%s', 1) ;
41 end
42
43 while ((strcmp(aWord(1:6),'ThCnts')) || (strcmp(aWord(2:7),'ThCnts')));
44     v = strread(aWord,'%s','delimiter',' ');
45     w = strread(char(v(1,1)), '%s', 'delimiter', '=');
46     TL = w(2,1);
47     TotalCount = v(2,1);
48     TU = v(3,1);
49     aboveCount = v(4,1);
50     aWord = fscanf(fid,'%s', 1) ;
51 end

```

```

52
53 %% Read bin diameters
54 while ~( strcmp( aWord, '#Bindiam' ) );
55     aWord = fscanf( fid, '%s', 1 ) ;
56 end
57 for i = 1 : nBins+1
58     binDiam(i,1) = fscanf(fid, '%g', 1);
59 end
60
61 %% Read bin heights
62 aWord = fscanf( fid, '%s \n', 1) ;
63 while ~( strcmp( aWord, '#Binheight' ) );
64     aWord = fscanf( fid, '%s', 1 ) ;
65 end
66 for i = 1 : nBins+1
67     binHeight(i,1) = fscanf(fid, '%g', 1);
68 end
69
70 %% Close the file
71 fclose(fid);
72
73 %% Apply dilution factor to bin heights
74 binHeight = binHeight * dilF *(1000 / sVol);
75 TotalCount = str2double(cell2mat(TotalCount)) * dilF *(1000 / sVol);
76 aboveCount = str2double(cell2mat(aboveCount)) * dilF *(1000 / sVol);

```

D

Routines and functions for OPC in Visual Basic

Code listing D.1: Main routine for the OPC client

```
1 Attribute VB.Name = "General"
2 Option Explicit
3
4 Public mNode As Node
5 Public mItem As ListItem
6 Public fMainForm As WSform
7 Public m_myForms() As frmSubstrate1
8
9 Global ServerAddress As String, ServerName As String
10 Global ItemsGroup1() As String
11 Global gr1Values() As Variant
12 Global gr1Times() As Date
13 Global gr1Qualities() As Long
14 Global gr1ServerID() As Long
15 Global UpdateRate As Long
16 Global ItemsGroup3() As String, ItemsGroup2() As String
17
18 Global db As Database
19 Global FlagWrite As Integer
20 Global boolSaveOK As Boolean
21
22 Dim Tags() As String
23 Dim CountTags() As Integer
```

```

24 Dim OPCDA As New OPCDataAccess
25
26 Sub Main()
27
28     frmSplash.Show
29     Set fMainForm = New WSform
30     Load fMainForm
31     Unload frmSplash
32     fMainForm.Show
33
34 End Sub
35
36 Function ShowServers(IPServer As String)
37
38     Dim dummyServer As OPCServer
39     Dim Servers As Variant
40     Dim cntServers As Integer
41
42     'create a dummy server object
43     Set dummyServer = New OPCServer
44
45     'returns all available servers
46     Servers = dummyServer.GetOPCServers(IPServer)
47
48     OpcExp.ServerList.Clear
49
50     'display server names
51     For cntServers = LBound(Servers) To UBound(Servers)
52         OpcExp.ServerList.AddItem Servers(cntServers)
53     Next cntServers
54
55 End Function
56
57
58 Function ConnectServer(ServerName As String, ServerIP As String)
59
60     Set OPCDA = New OPCDataAccess
61     If OPCDA.Connect(ServerName, ServerIP, Tags, CountTags) = False Then
62         MsgBox "Connect Error"
63         Exit Function
64     End If
65
66 End Function
67
68 Function DisconnectServer()
69
70     Set OPCDA = Nothing
71
72 End Function
73
74 Sub ShowTags(NodeID As Integer)
75
76     Dim ItmX As ListItem
77     Dim LimSup As Integer, LimInf As Integer, i As Integer
78
79     LimInf = CountTags(NodeID)
80
81     If CountTags(NodeID + 1) <> 0 Then
82         LimSup = CountTags(NodeID + 1)

```

```

83     Else
84         LimSup = CountTags(NodeID + 2)
85     End If
86
87     OpcExp.LvwTags.ColumnHeaders.Item(1).Text = "Tags in " _
88         & CStr(OpcExp.TreeView1.Nodes.Item(NodeID).FullPath)
89
90     For i = LimInf To LimSup - 1
91         Set ItmX = OpcExp.LvwTags.ListItems.Add(, , Tags(1, i))
92         ItmX.Tag = Tags(2, i)
93     Next i
94
95 End Sub
96
97 Sub InfoTag(TagID As Integer)
98
99     OpcExp.ReadOption(CInt(Tags(3, TagID)) - 1).Value = True
100    OpcExp.chkWrite.Value = CInt(Tags(4, TagID))
101
102 End Sub
103
104 Sub ModifyTagsMatrix(TagID As Integer, Index As Integer, Opt As Integer)
105
106     Select Case Opt
107         Case 1 'Modify read properties
108             Tags(3, TagID) = Index + 1
109         Case 2 'Modify write properties
110             Tags(4, TagID) = Index
111     End Select
112
113
114 End Sub
115
116 Sub OrderGroups()
117
118     Dim i As Integer, j As Integer
119     Dim i1 As Integer, i2 As Integer, i3 As Integer
120
121     i1 = 1
122     i2 = 1
123     i3 = 1
124
125     ReDim ItemsGroup1(1 To 4, 1 To 1) As String
126     ReDim ItemsGroup2(1 To 4, 1 To 1) As String
127     ReDim ItemsGroup3(1 To 4, 1 To 1) As String
128
129     For i = 1 To UBound(Tags, 2)
130         If Tags(3, i) = CStr(1) Then 'Group 1
131             For j = 1 To 4
132                 ItemsGroup1(j, i1) = Tags(j, i)
133             Next j
134             i1 = i1 + 1
135             ReDim Preserve ItemsGroup1(1 To 4, 1 To i1) As String
136
137         ElseIf Tags(3, i) = CStr(2) Then 'Group 2
138             For j = 1 To 4
139                 ItemsGroup2(j, i2) = Tags(j, i)
140             Next j
141             i2 = i2 + 1

```

```

142         ReDim Preserve ItemsGroup2(1 To 4, 1 To i2) As String
143     End If
144
145     If Tags(4, i) = CStr(1) Then 'Group 3
146         For j = 1 To 4
147             ItemsGroup3(j, i3) = Tags(j, i)
148         Next j
149         i3 = i3 + 1
150         ReDim Preserve ItemsGroup3(1 To 4, 1 To i3) As String
151     End If
152
153     Next i
154
155     If i1 > 1 Then ReDim Preserve ItemsGroup1(1 To 4, 1 To i1 - 1) As String
156     If i2 > 1 Then ReDim Preserve ItemsGroup2(1 To 4, 1 To i2 - 1) As String
157     If i3 > 1 Then ReDim Preserve ItemsGroup3(1 To 4, 1 To i3 - 1) As String
158
159 End Sub
160
161 Sub CreateReadGroup()
162
163     UpdateRate = Val(frmOPCws.txtUpRate.Text)
164     OPCDA.AddGroup UpdateRate
165
166 End Sub
167
168 Sub DeactivateGroup()
169
170     OPCDA.StopGroupRead 'UpdateRate
171
172 End Sub
173
174 Sub ActivateGroup()
175
176     OPCDA.ReStartGroupRead 'UpdateRate
177
178 End Sub
179
180 Sub AsynWrite(xNumber As Integer, xHandles() As Long, xValues() As Variant)
181
182     OPCDA.ASynchronWrite xNumber, xHandles, xValues
183
184 End Sub

```

Code listing D.2: Class definition for OPC data access

```

1 VERSION 1.0 CLASS
2 BEGIN
3     MultiUse = -1 'True
4     Persistable = 0 'NotPersistable
5     DataBindingBehavior = 0 'vbNone
6     DataSourceBehavior = 0 'vbNone
7     MTSTransactionMode = 0 'NotAnMTSObject
8 END
9 Attribute VB.Name = "OPCDataAccess"
10 Attribute VB.GlobalNamespace = False

```

```

11 Attribute VB.Creatable = True
12 Attribute VB.PredeclaredId = False
13 Attribute VB.Exposed = False
14 Option Explicit
15
16 'OPC arrays indices must start with 1
17 Option Base 1
18
19 'OPC Server Object (Events optional)
20 Dim WithEvents MyServer As OPCServer
21 Attribute MyServer.VB.VarHelpID = -1
22
23 'OPC Group Collection (Events optional)
24 Dim WithEvents MyGroups As OPCGroups
25 Attribute MyGroups.VB.VarHelpID = -1
26
27 'OPC Group Object
28 Dim WithEvents MyGroup As OPCGroup
29 Attribute MyGroup.VB.VarHelpID = -1
30
31 Dim WithEvents GrpSyncr As OPCGroup 'Read sync
32 Attribute GrpSyncr.VB.VarHelpID = -1
33 Dim WithEvents GrpAsync As OPCGroup 'Read async
34 Attribute GrpAsync.VB.VarHelpID = -1
35 Dim WithEvents GrpWrite As OPCGroup 'Write setpoints
36 Attribute GrpWrite.VB.VarHelpID = -1
37
38 Dim MyBrowser As OPCBrowser
39
40 Dim nrItems As Integer
41 Dim MyItems As OPCItems 'OPC Item Collection Object
42 Dim MyItem As OPCItem 'OPC Item Object
43 Dim ItemsID() As String 'fully qualified items
44
45 Dim ClientHandles() As Long
46
47 Dim ServerHandles() As Long 'must be a dynamic array
48 Dim ServerErrors() As Long 'must be a dynamic array
49
50 Dim TransactionID As Long
51 Dim CancelID As Long
52
53 Function Connect(ServerName As String, ServerNode As String, -
54                 TagsMatrix() As String, NodeCount() As Integer)
55
56     Dim vName As Variant, vName1 As Variant
57     Dim FQID As Variant, vName2 As Variant
58     Dim i As Integer, j As Integer, k As Integer
59
60     On Error GoTo ConnectError
61
62     Set MyServer = New OPCServer
63     MyServer.Connect ServerName, ServerNode 'connection is risky
64     Connect = True
65
66     Set MyBrowser = MyServer.CreateBrowser
67     MyBrowser.ShowBranches 'show the branches
68
69     i = 0

```

```

70     j = 0
71     k = 0
72
73     ReDim NodeCount(1 To 1) As Integer
74
75     'TagMatrix stores information of all the tags in the current server
76     ReDim TagsMatrix(1 To 4, 1 To 1) As String
77
78     For Each vName In MyBrowser
79
80         Set mNode = OpcExp.TreeView1.Nodes.Add(, , , vName)
81         i = i + 1
82         j = j + 1
83         mNode.Tag = j
84         mNode.Expanded = True
85         MyBrowser.MoveDown vName
86         MyBrowser.ShowBranches
87
88         For Each vName1 In MyBrowser
89
90             Set mNode = OpcExp.TreeView1.Nodes.Add(i, tvwChild, , vName1)
91             j = j + 1
92             mNode.Tag = j
93
94             ReDim Preserve NodeCount(1 To j) As Integer
95             NodeCount(j) = k + 1
96
97             MyBrowser.MoveDown vName1
98             MyBrowser.ShowLeafs
99
100            For Each vName2 In MyBrowser
101                FQID = MyBrowser.GetItemID(vName2)
102                k = k + 1
103                TagsMatrix(1, k) = vName2
104                TagsMatrix(2, k) = FQID
105                TagsMatrix(3, k) = "3"
106                TagsMatrix(4, k) = "0"
107                ReDim Preserve TagsMatrix(4, UBound(TagsMatrix, 2) + 1) -
108                    As String
109            Next vName2
110
111            MyBrowser.MoveUp
112
113        Next vName1
114
115        MyBrowser.MoveUp
116
117    Next vName
118
119    ReDim Preserve NodeCount(1 To j + 1) As Integer
120    NodeCount(j) = k
121
122    Exit Function
123
124 ConnectError:
125     MsgBox Err.Number & ": " & Err.Description
126
127     Err.Clear
128     Connect = False

```

```

129
130 End Function
131
132 Function AvlbTags(TagsMatrix() As String)
133
134     Dim FQID As Variant, vName As Variant
135     Dim vName1 As Variant, vName2 As Variant
136     Dim k As Integer
137
138     MyBrowser.ShowBranches           'show the branches
139     k = 0
140
141     For Each vName In MyBrowser
142
143         MyBrowser.MoveDown vName
144         MyBrowser.ShowBranches
145
146         For Each vName1 In MyBrowser
147
148             MyBrowser.MoveDown vName1
149             MyBrowser.ShowLeafs
150
151             For Each vName2 In MyBrowser
152
153                 FQID = MyBrowser.GetItemID(vName2)
154                 k = k + 1
155                 TagsMatrix(k, 1) = vName2
156                 TagsMatrix(k, 2) = FQID
157                 TagsMatrix(k, 3) = "3"
158                 TagsMatrix(k, 4) = "0"
159
160             Next vName2
161
162             MyBrowser.MoveUp
163
164         Next vName1
165
166         MyBrowser.MoveUp
167
168     Next vName
169
170 End Function
171
172 Function AddGroup(UpdateRate As Long)
173
174     Set MyGroups = MyServer.OPCGroups   'create groups collection
175
176     MyGroups.DefaultGroupUpdateRate = UpdateRate
177
178     'add group, name private
179     Set GrpAsync = MyGroups.Add("GrpAsyncRead")
180
181     'define the OPCItems of Group
182     Set MyItems = GrpAsync.OPCItems
183
184     Dim i As Integer
185     Dim x As Integer
186     Dim FQItemIDs() As String
187

```

```

188     nrItems = UBound(ItemsGroup1, 1)
189
190     If nrItems = 0 Then
191         MsgBox "No Items for the Reading Group"
192         Exit Function
193     End If
194
195     ReDim FQItemIDs(1 To nrItems) As String
196     ReDim ClientHandles(1 To nrItems) As Long
197
198     ReDim grlServerID(1 To nrItems) As Long
199     ReDim grlValues(1 To nrItems) As Variant
200     ReDim grlTimes(1 To nrItems) As Date
201     ReDim grlQualities(1 To nrItems) As Long
202
203
204     For i = 1 To nrItems
205         FQItemIDs(i) = ItemsGroup1(i, 2)
206         ClientHandles(i) = 100 + i
207     Next i
208
209     MyItems.AddItem nrItems, FQItemIDs, ClientHandles, -
210         ServerHandles, ServerErrors
211
212     For i = 1 To nrItems
213
214         frmOPCws.LvwRead.ListItems.Item(i).SubItems(5) = ServerHandles(i)
215         frmOPCws.LvwRead.ListItems.Item(i).SubItems(6) = ClientHandles(i)
216         grlServerID(i) = ServerHandles(i)
217
218     Next i
219
220     GrpAsync.ClientHandle = 1
221     GrpAsync.IsActive = True
222     GrpAsync.IsSubscribed = True
223
224 End Function
225
226 Private Sub GrpAsync_DataChange(ByVal TransID As Long, -
227     ByVal nrItems As Long, ClntHndls() As Long, ItemValues() As Variant, -
228     Qualities() As Long, TimeStamps() As Date)
229
230     Dim cntItems As Integer
231
232     On Error GoTo ErrorHndl
233
234     For cntItems = LBound(ClntHndls) To UBound(ClntHndls) ' index 1..n
235
236         frmOPCws.LvwRead.ListItems.Item(ClntHndls(cntItems) - 100) -
237             .SubItems(2) = ItemValues(cntItems)
238         frmOPCws.LvwRead.ListItems.Item(ClntHndls(cntItems) - 100) -
239             .SubItems(4) = DateAdd("h", 0, TimeStamps(cntItems))
240         frmOPCws.LvwRead.ListItems.Item(ClntHndls(cntItems) - 100) -
241             .SubItems(3) = Qualities(cntItems)
242         grlValues(ClntHndls(cntItems) - 100) = ItemValues(cntItems)
243         grlTimes(ClntHndls(cntItems) - 100) = -
244             DateAdd("h", 0, TimeStamps(cntItems))
245         grlQualities(ClntHndls(cntItems) - 100) = Qualities(cntItems)
246

```

```

247     Next cntItems
248
249     Exit Sub
250
251 ErrorHndl:
252     Select Case Err.Number
253     Case 13 ' Error from the OPC Server
254         If Left(CStr(ItemValues(cntItems)), 5) = "Error" Then
255             Dim ErrCode As String
256
257             ErrCode = Hex(CLng(Right(CStr(ItemValues(cntItems)), 11)))
258
259             MsgBox "The OPC server has reported an error" & vbCr & vbCr -
260                 & "ClientID of error variable: " & ClntHndls(cntItems) -
261                 & vbCr & "Error Code:" & ErrCode & vbCr & vbCr & -
262                 "Check OPC DA Handbook for reference", vbExclamation
263         End If
264         Resume Next
265     Case Else
266         MsgBox Err.Number & ": " & Err.Description, vbExclamation
267     End Select
268
269 End Sub
270
271 Private Sub MyServer.ServerShutDown(ByVal reason As String)
272
273     MsgBox "my OPC Server " & MyServer.ServerName & " quit"
274
275 End Sub
276
277 Sub ServerShutDown()
278
279     Dim dummyServer As OPCServer
280     Dim Servers As Variant           'this is an array of strings
281     Dim cntServers As Integer
282
283     Set MyGroup = Nothing           'creates a dummy server object
284     Set MyGroups = Nothing         'returns all available servers
285     Set MyServer = Nothing
286
287 End Sub
288
289 Sub StopGroupRead()
290
291     GrpAsync.IsSubscribed = False
292     GrpAsync.IsActive = False
293
294 End Sub
295
296 Sub ReStartGroupRead()
297
298     GrpAsync.IsActive = True
299     GrpAsync.IsSubscribed = True
300
301 End Sub
302
303 Function ASynchronWrite(x As Integer, ServerHandle() As Long, -
304                         Value() As Variant)
305     'x = How many tags to write in current transaction

```

```

306     'ServerHandle() = vector with the serverhandles of items to write
307     'Value() = vector with the values to be written
308
309     'passing the value to be written
310     GrpAsync.AsyncWrite x, ServerHandle, Value, ServerErrors, -
311                     TransactionID, CancelID
312
313 End Function
314
315 Private Sub GrpAsync.AsyncWriteComplete(ByVal TransactionID As Long, -
316     ByVal NumItems As Long, ClientHandles() As Long, Errors() As Long)
317
318     ' When FlagWrite is 0 a message of completion is shown
319     If FlagWrite = 0 Then
320         MsgBox ("Async Write Complete")
321     End If
322
323 End Sub

```

Code listing D.3: Functions for saving OPC readings in historian database

```

1 Attribute VB_Name = "DataBaseOPC"
2 Option Explicit
3
4 Private Declare Function Beep Lib "kernel32" -
5     (ByVal dwFreq As Long, ByVal dwDuration As Long) As Long
6
7 Dim HistorianTitle As String
8 Dim T As String, TabName As String
9 Dim Response As String
10
11 Sub doBeepNow()
12     Beep 500, 100
13 End Sub
14
15 Sub OPCCreateDB()
16
17     Dim i As Integer
18
19     On Error GoTo DialogCancel
20
21     With fMainForm.dlgCommonDialog
22         .CancelError = True
23         .FileName = "*.mdb"
24         .DialogTitle = "Create a New Database"
25         .Filter = "Access Database File (*.mdb)|*.mdb"
26         .InitDir = "c:\DataOPC\ "
27         .ShowOpen
28         T = Dir("C:\DataOPC\ " & .FileTitle)
29         If Len(T) <> 0 Then
30             Response = MsgBox("File already exists, erase?", -
31                 vbQuestion + vbYesNo, "File Already Exists")
32             If Response = vbYes Then
33                 Kill .FileName
34             End If
35

```

```

36         If Response = vbNo Then
37             MsgBox "Operation cancelled"
38             Exit Sub
39         End If
40     End If
41     HistorianTitle = .FileName
42 End With
43
44 'Create the database
45 Set db = DBEngine(0).CreateDatabase(HistorianTitle, -
46                                     dbLangGeneral, dbVersion30)
47
48 'Define a variable as a tabledef object
49 Dim TblDef As TableDef
50
51 Set TblDef = db.CreateTableDef("MasterTable")
52 'Create fields within the table
53 With TblDef
54     .Fields.Append .CreateField("Variable", dbText, 50)
55     .Fields.Append .CreateField("FQID", dbText, 50)
56     .Fields.Append .CreateField("ServerID", dbLong)
57     .Fields.Append .CreateField("ClientID", dbLong)
58     .Fields.Append .CreateField("TableName", dbText, 10)
59     db.TableDefs.Append TblDef 'Append the table to the database
60 End With
61
62 For i = 1 To UBound(ItemsGroup1, 1)
63     'Create table in the database
64     TabName = "Table10" + CStr(i)
65     Set TblDef = db.CreateTableDef(TabName)
66     'Create fields within the table
67     With TblDef
68         .Fields.Append .CreateField("TimeStamp", dbDate)
69         .Fields.Append .CreateField("Value", dbSingle)
70         .Fields.Append .CreateField("Quality", dbSingle)
71         db.TableDefs.Append TblDef 'Append the table to the database
72     End With
73 Next i
74
75 Dim rsRecord As Variant
76 Set rsRecord = db.OpenRecordset("MasterTable", dbOpenDynaset)
77
78 For i = 1 To UBound(ItemsGroup1, 1)
79     With rsRecord
80         .AddNew
81         !Variable = ItemsGroup1(i, 1)
82         !FQID = ItemsGroup1(i, 2)
83         !ServerID = grlServerID(i)
84         !ClientID = 100 + i
85         !TableName = "Table10" + CStr(i)
86         .Update
87         .Bookmark = .LastModified
88     End With
89 Next i
90
91 rsRecord.Close
92 Set rsRecord = Nothing
93 Exit Sub
94

```

```

95 DialogCancel:
96     MsgBox Err.Number & ": " & Err.Description
97     MsgBox "Operation cancelled"
98
99 End Sub
100
101 Sub SaveOPCDataDB()
102     Dim rsRecord As Variant
103     Dim i As Integer
104
105     For i = 1 To UBound(ItemsGroup1, 1)
106         TabName = "Table10" + CStr(i)
107         Set rsRecord = db.OpenRecordset(TabName, dbOpenDynaset)
108         With rsRecord
109             .AddNew
110             !TimeStamp = gr1Times(i)
111             !Value = gr1Values(i)
112             !Quality = gr1Qualities(i)
113             .Update
114             .Bookmark = .LastModified
115         End With
116         rsRecord.Close
117     Next i
118
119     Set rsRecord = Nothing
120     Beep 500, 100
121
122 End Sub

```

Code listing D.4: General functions for handling client files

```

1 Attribute VB_Name = "FileSave"
2 Option Explicit
3
4 Dim objXML As MSXML2.DOMDocument
5 Dim strXML As String
6
7 Type rcdSetup
8     rcItemsGroup1(1 To 20, 1 To 4) As String * 50
9     rcServerAddress As String
10    rcServerName As String
11    rcUpdateRate As String
12    rcItems As Integer
13 End Type
14
15 Sub LoadXML(xmlFileName As String)
16
17     Dim objElem As MSXML2.IXMLDOMElement
18     Dim xmlItems As MSXML2.IXMLDOMNodeList
19     Dim itemCount As Integer, i As Integer
20
21     Set objXML = New MSXML2.DOMDocument
22
23     'Open XML file - to replace by filename from common dialog
24     objXML.Load (xmlFileName)
25

```

```

26 'Get HOST IP
27 Set objElem = objXML.selectSingleNode("Session/Hostname")
28 If Not objElem Is Nothing Then
29     ServerAddress = objElem.getAttribute("RemoteHost")
30 End If
31
32 'Get server name
33 Set objElem = objXML.selectSingleNode("Session/Hostname/Server")
34 If Not objElem Is Nothing Then
35     ServerName = objElem.getAttribute("Name")
36 End If
37
38
39 'Get Update rate
40 Set objElem = objXML.selectSingleNode("Session/Hostname/Server/Group")
41 If Not objElem Is Nothing Then
42     UpdateRate = Val(objElem.getAttribute("ReqUpdateRate"))
43     ItemCount = Val(objElem.getAttribute("ItemCount"))
44 End If
45
46 ReDim ItemsGroup1(1 To ItemCount, 1 To 4) As String
47
48 'Get item list
49 Set xmlItems = objXML.selectNodes("Session/Hostname/Server/Group/Item")
50 i = 1
51 For Each objElem In xmlItems
52     ItemsGroup1(i, 2) = objElem.Text
53     ItemsGroup1(i, 1) = objElem.Text
54     i = i + 1
55 Next
56
57 End Sub
58
59 Sub Save.File(FileName As String)
60
61     Dim FileNum As Integer
62     Dim RecLength As Long
63     Dim CurrentFile As rcdSetup
64     Dim i As Integer, j As Integer
65
66     RecLength = LenB(CurrentFile)
67     FileNum = FreeFile
68     Open FileName For Random As FileNum Len = RecLength
69
70     For i = 1 To UBound(ItemsGroup1, 1)
71         For j = 1 To 4
72             CurrentFile.rcItemsGroup1(i, j) = ItemsGroup1(i, j)
73         Next j
74     Next i
75
76     CurrentFile.rcServerAddress = ServerAddress
77     CurrentFile.rcServerName = ServerName
78     CurrentFile.rcUpdateRate = UpdateRate
79     CurrentFile.rcItems = UBound(ItemsGroup1, 1)
80
81     Put #FileNum, , CurrentFile
82
83 End Sub
84

```

```

85 Sub Open_File(fileName As String)
86
87     Dim FileNum As Integer, RecLength As Long
88     Dim CurrentFile As rcdSetup
89
90     Dim j As Integer, i As Integer
91
92     On Error GoTo Error_Handler
93
94     RecLength = LenB(CurrentFile) ' 16636 V10
95     FileNum = FreeFile
96     Open fileName For Random As FileNum Len = RecLength
97     Get #FileNum, , CurrentFile
98     ReDim ItemsGroup1(1 To CurrentFile.rcItems, 1 To 4) As String
99
100    For i = 1 To CurrentFile.rcItems
101        For j = 1 To 4
102            ItemsGroup1(i, j) = CurrentFile.rcItemsGroup1(i, j)
103        Next j
104    Next i
105
106    ServerAddress = CurrentFile.rcServerAddress
107    ServerName = CurrentFile.rcServerName
108    UpdateRate = CurrentFile.rcUpdateRate
109
110    Exit Sub
111 Error_Handler:
112
113 End Sub
114
115 Sub SaveCurrentData(SubsA As String, pH As String, pO2 As String, -
116     Temp As String, Stirr As String, O2 As String, Glycine As String, -
117     Acid As String, Base As String, UpdateTime As String, -
118     sFileName As String)
119
120     Dim hFile As Long
121     hFile = FreeFile
122     Open sFileName For Output As #hFile
123     Print #hFile, "SubsA=" & SubsA
124     Print #hFile, "pH=" & pH
125     Print #hFile, "pO2=" & pO2
126     Print #hFile, "Temp=" & Temp
127     Print #hFile, "Stirr=" & Stirr
128     Print #hFile, "O2=" & O2
129     Print #hFile, "Glycine=" & Glycine
130     Print #hFile, "Acid=" & Acid
131     Print #hFile, "Base=" & Base
132     Print #hFile, "Update=" & UpdateTime
133     Close #hFile
134
135 End Sub

```

Code listing D.5: Interface between Matlab and the OPC client

```
1 Attribute VB.Name = "MatlabConnect"
2 Option Explicit
3 Option Base 1
4
5 Dim MatLab As Object
6 Dim AppMatlab As MLab.MLab
7
8 Public Sub Call_MFile(MatLabDir As String, -
9     MatlabFunc As String, TerminalSource As Integer)
10
11     Dim i As Integer
12     Dim Result As String
13     Dim aReal(1, 1) As Double
14     Dim tempImag(1, 1) As Double
15     Dim MatLabString As String
16     Dim xHandles() As Long
17     Dim xValues() As Variant, Counter As Integer
18
19     Set MatLab = CreateObject("Matlab.Application")
20
21     MatLabString = MatLabDir
22     MatLabString = "cd '" + MatLabString + "'"
23     Result = MatLab.Execute(MatLabString)
24
25     i = m_myForms(TerminalSource).Tag
26
27     For i = 1 To m_myForms(TerminalSource).LvwMatlab.ListItems.Count
28         aReal(1, 1) = gr1Values(m_myForms(TerminalSource). -
29             LvwMatlab.ListItems.Item(i).Tag)
30         Call MatLab.PutFullMatrix(m_myForms(TerminalSource). -
31             LvwMatlab.ListItems.Item(i).Text, "base", aReal, tempImag)
32     Next i
33
34     'Current counter value
35     aReal(1, 1) = CDBl(m_myForms(TerminalSource).Label11.Caption)
36     Call MatLab.PutFullMatrix(m_myForms(TerminalSource).Text2.Text, -
37         "base", aReal, tempImag)
38
39     MatLabString = MatlabFunc
40     Result = MatLab.Execute(MatLabString)
41
42     ReDim xValues(1 To m_myForms(TerminalSource).LvwSP.ListItems.Count) -
43         As Variant
44     ReDim xHandles(1 To m_myForms(TerminalSource).LvwSP.ListItems.Count) -
45         As Long
46
47     For i = 1 To m_myForms(TerminalSource).LvwSP.ListItems.Count
48         Call MatLab.GetFullMatrix(m_myForms(TerminalSource). -
49             LvwSP.ListItems.Item(i).Text, "base", aReal, tempImag)
50
51         'assign aReal to some variable
52         xValues(i) = aReal(1, 1)
53         '—> Get serverhandle
54         xHandles(i) = gr1ServerID(m_myForms(TerminalSource). -
55             LvwSP.ListItems.Item(i).Tag)
56     Counter = Counter + 1
```

```
57     Next i
58
59     Call MatLab.GetFullMatrix(m.myForms(TerminalSource).Text3.Text, -
60                               "base", aReal, tempImag)
61     m.myForms(TerminalSource).Label20.Caption = CStr(aReal(1, 1))
62
63     Call MatLab.GetFullMatrix(m.myForms(TerminalSource).Text4.Text, -
64                               "base", aReal, tempImag)
65     m.myForms(TerminalSource).Label22.Caption = CStr(aReal(1, 1))
66     m.myForms(TerminalSource).timePump.Enabled = True
67     FlagWrite = 1
68     Call AsynWrite(Counter, xHandles, xValues)
69
70 End Sub
```